
CONTROLLED FABRICATION AND OPTIMISATION OF CROSSLINKED GRAPHENE OXIDE MEMBRANES FOR ENHANCED WATER PURIFICATION PERFORMANCE



A thesis submitted to the School of Engineering and Faculty of Science at the University of East Anglia (UEA) in partial fulfilment of the requirements for the degree of Doctor of Philosophy in Engineering.

VEPIKA KANDJOU

June 2020

© This copy of the thesis has been supplied on condition that anyone who consults it is understood to recognise that its copyright rests with the author and that use of any information derived therefrom must be in accordance with current UK Copyright Law. In addition, any quotation or extract must include full attribution.



In loving memory of my father Ruueza Kandjou (1947 – 2016) and my grand uncle

Tarakaija Johannes Lesetlhe (1927 – 2019). Forever in our hearts!

DECLARATION OF ORIGINALITY

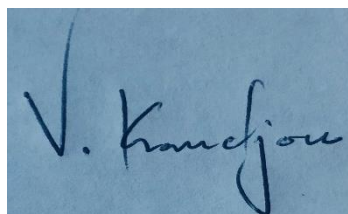
I hereby declare that the work presented in this thesis was composed and written by myself. Information derived from published and unpublished sources has been rightly acknowledged in the thesis and relevant references have been provided.

VEPIKA KANDJOU

University of East Anglia (UEA)

June 2020

Signature

A blue rectangular stamp containing a handwritten signature in black ink. The signature appears to be 'V. Kandjou' written in a cursive style.

ABSTRACT

“Nothing in life is to be feared, it is only to be understood. Now is time to understand more so that we may fear less.”

MARIE CURIE, (1867-1934)

Graphene Oxide (GO) is an equitable next generation membrane material and significant graphene alternative owing to its large-scale production scalability specifically and physicochemical characteristics. The use of GO as a water purification and desalination membrane was first demonstrated by Nair et al in 2012. As such, its feasibility as a nanofiltration separation membrane material is still in its primary usage hence the need for optimisations, modifications and understanding of its permeation mechanisms.

Major limitations in the use of GO as a separation membrane material include the widening of the membrane interlayer spacing (pore-gap) during operation and poor membrane stability. This doctoral research in consequence looked into the use of different crosslinkers to enhance the performance and stability of GO membranes through both inter and intralayer crosslinking. Successively, p-Phenylenediamine, 1,3,5-triazine – 2,4,6 triamine (melamine) and polyethyleneimine were systematically introduced onto the GO nanosheets via the dip-assisted layer-by-layer method to fabricate crosslinked GO membranes.

Principally, the feasibility of the use of the aforementioned crosslinkers in interconnecting GO nanosheets and fabricating thin-films/membranes via the layer by layer assembly method was explored. The nature of interaction between GO and the crosslinkers was analysed and subsequently crosslinked thin films were fabricated to demonstrate the control of key characteristics like thickness. Respective

characterizations were undertaken, proving successful thin-film assembly. Following thin film fabrication, the thesis goes on to look into the nanofiltration performance of respective membranes assembled on poly (acrylonitrile) and polycarbonate substrates. The impact of crosslinking in enhancing performance was apparent. Successively, the impact of the physicochemical properties of GO, specifically its lateral size and surface chemistry onto the nanofiltration performance of the crosslinked membranes was studied. Ultimately, GO and crosslinker concentration alteration on membrane nanofiltration performance was analysed. These were optimisation stages where the aim was to determine the optimum lateral-size of GO nanosheets and concentration effects in membrane stability and performance.

Access Condition and Agreement

Each deposit in UEA Digital Repository is protected by copyright and other intellectual property rights, and duplication or sale of all or part of any of the Data Collections is not permitted, except that material may be duplicated by you for your research use or for educational purposes in electronic or print form. You must obtain permission from the copyright holder, usually the author, for any other use. Exceptions only apply where a deposit may be explicitly provided under a stated licence, such as a Creative Commons licence or Open Government licence.

Electronic or print copies may not be offered, whether for sale or otherwise to anyone, unless explicitly stated under a Creative Commons or Open Government license. Unauthorised reproduction, editing or reformatting for resale purposes is explicitly prohibited (except where approved by the copyright holder themselves) and UEA reserves the right to take immediate 'take down' action on behalf of the copyright and/or rights holder if this Access condition of the UEA Digital Repository is breached. Any material in this database has been supplied on the understanding that it is copyright material and that no quotation from the material may be published without proper acknowledgement.

ACKNOWLEDGEMENTS

*“I am a part of all that I have met
Yet all experience is an arch wherethro’
Gleams that untraveled world whose margins fades
Forever and forever when I move...”*

ALFRED, LORD TENNYSON; ULYSSES (1809 – 1892)

TO GOD BE THE GLORY.

In no way I would have completed this work on my own despite my name alone appearing on its forefront. This is a sincere appreciation to all those who played a part both directly and indirectly.

My sincerest gratitude goes to my primary supervisor Dr Sonia Melendi-Espina. She made the hard days bearable and the good days, even greater. Great appreciation to her for having the patience, constant support and immense knowledge contribution to the development of this thesis. It has been a privilege being one of her students and I am forever indebted to her encouragement and believe in my capability as a researcher. For that, I cannot thank her enough. Great acknowledgements also go to Dr Andrew Mayes, his contribution was significant, first for allowing us to carry out initial experiments in his lab and knowledge contribution to the research, especially the proof of interactions between GO and crosslinkers.

To Dr Ana Matilde Perez Mas, I am grateful for her support and great advice on having consistency and control over my data. Her contribution to the optimization of the fabrication of the membranes is greatly appreciated. Special thanks also go to the members of the *Melendi-Espina Lab Group*, Dr Miguel Hernaez, Dr Beatriz Acevedo-Munoz and Dr Pedro Sanchez their contribution to my development as a researcher

and help with the fabrication and characterizations of the thin films is highly appreciated.

Sincere acknowledgements go to the Masturd Seed Chapel International Church in Norwich, Pastor Joel, Emmanuel, Jesse Annan, Nii Noye, Naomi Akor and the rest of the brethren. Appreciations for providing a home and spiritual nourishment to me during some of the hardest days of my life. Gratitude to Ben Marshall at the Student Wellbeing Centre, the counselling he provided saved me from the ravages of depression. Further thanks to my fellow postgraduate researchers, Moses Bosire, Rebecca Hill, Aruna Kumari and Chengyang Liu for their constant encouragement. I wish them greatness in their future endeavours.

Heartfelt gratitude to the Botswana Government's Ministry of Tertiary Education, Research, Science and Technology and the Top Achievers Scholarship for offering the studentship that enabled the carrying out of this work. Great indebtedness to the taxpayers of my beautiful nation, Botswana. May God bless our country!

Lastly, I am forever beholden to my family, my mother, brothers and sisters, despite them not being physical present; their absence was never felt as they provided a hand and a shoulder to lean on during the hard times and a cheer on during the great times. For that I am grateful. Special thanks to my brother and guardian Moses Ndiriva Kandjou for the upbringing and tough love sometimes, his contribution to my arrival this far has been immense.

To Vetu Kaotozu, appreciations to her for comforting me through my breakdowns and cheered me through my breakthroughs. Bless your heart dear.

LIST OF PUBLICATIONS AND INTERNATIONAL CONFERENCE PRESENTATIONS

PEER REVIEWED PUBLICATIONS

1. **Kandjou V**, Hernaez M, Acevedo B, Melendi-Espina S, Interfacial crosslinked controlled thickness graphene oxide thin films by means of dip-assisted layer by layer assembly, *Progress in Organic Coatings Journal* 137 (2019) 105345, [doi:10.1016/j.porgcoat.2019.105345](https://doi.org/10.1016/j.porgcoat.2019.105345)
2. **Kandjou V**, Perez-Mas AM, Acevedo B, Hernaez M, Mayes AG, Melendi-Espina S, Enhanced covalent p-phenylenediamine crosslinked graphene oxide membranes: towards superior contaminant removal from wastewaters and improved membrane reusability, *Journal of Hazardous Materials* 380 (2019) 120840, doi.org/10.1016/j.jhazmat.2019.120840
3. **Kandjou V**, Gonzalez Z, Acevedo B, Munuera JM, Paredes JI and Sonia Melendi-Espina S, The impact of Graphene Oxide's physicochemical characteristics on the performance of crosslinked nanofiltration membranes, *Surfaces and Interfaces Journal* (2020) (**Manuscript Under Review**)
4. **Kandjou V**, Maria D. C, Melendi-Espina S, Optimising the fabrication concentration of layer by layer crosslinked graphene oxide membranes: enhancing membrane material conservation, *Separation and Purification Technology Journal* (2020) (***Final Stages of Submission***)

INTERNATIONAL CONFERENCE PRESENTATIONS AND PROCEEDINGS

1. The World Conference on Carbon, “The fabrication and characterization of graphene oxide thin films with controlled thickness on silicon-based substrates” **Poster Presentation**, Melbourne, Australia, 2017 (Abstract No. 144)
2. The World Conference on Carbon, “The use of p-Phenylenediamine to enhance the performance of graphene oxide membranes for water purification” **Poster Presentation**, Madrid, Spain, 2018, (Abstract No. 0620)
3. The World Conference on Carbon, “The fabrication of controlled thickness graphene oxide thin films by means of dip-assisted layer by layer assembly” **Oral Presentation**, Madrid, Spain, 2018, (Abstract No. 0649)
4. Postgraduate Research Conference, “The fabrication and enhancement of the water purification and stability of graphene-based membranes via crosslinking” **Oral Presentation**, Norwich, United Kingdom, 2018, (Abstract No. 007)
5. The World Conference on Carbon, “Enhanced covalent p-Phenylenediamine crosslinked graphene oxide membranes: towards superior contaminant removal from wastewaters and improved membrane reusability” **Oral Presentation**, Lexington, Kentucky, USA, 2019, (Abstract No. 150)
6. The World Conference on Carbon, “The impact of sonication on graphene oxide’s physicochemical properties and nanofiltration performance of

covalently crosslinked membranes” **Poster Presentation**, Lexington, Kentucky, USA, 2019, (Abstract No. 151)

TABLE OF CONTENTS

DECLARATION OF ORIGINALITY	iii
ABSTRACT	iv
ACKNOWLEDGEMENTS	vi
LIST OF PUBLICATIONS AND INTERNATIONAL CONFERENCE PRESENTATIONS	viii
PEER REVIEWED PUBLICATIONS	viii
INTERNATIONAL CONFERENCE PRESENTATIONS AND PROCEEDINGS	ix
TABLE OF CONTENTS	xi
LIST OF FIGURES	xvii
LIST OF TABLES	xxi
1.	1
INTRODUCTION	1
1.1 Background and Motivation	1
1.2 Research Aim and Objectives	6
1.3 Thesis Structure	9
2.	11
LITERATURE REVIEW – GRAPHENE, GRAPHENE OXIDE AND SEPARATION	
MEMBRANES	11
2.1 Graphene	11
2.1.2 Properties of graphene	13

2.1.3 Graphene fabrication methods	15
2.1.4 Main challenge in bringing graphene-based products to market	20
2.2 Graphene Oxide.....	21
2.2.1 Definition and structures	21
2.2.2 Properties of graphene oxide	24
2.2.3 Graphene Oxide fabrication methods	26
2.2.4 Graphene oxide's potential applications	30
2.3 Separation membranes.....	31
2.3.1 Background and historical overview	31
2.3.2 Graphene oxide as a nanofiltration/separation membrane material	34
2.3.4 Limitations of graphene oxide as a separation membrane material	35
2.3.3 Graphene oxide based membrane fabrication methods	36
2.3.5 Recent improvements in the use of graphene oxide as separation membrane material	40
2.4 Review Conclusions	44
3.	46
THE FABRICATION OF CONTROLLED THICKNESS CROSSLINKED GRAPHENE OXIDE THIN FILMS; SYSTEMATIC CONTROL OF SIGNIFICANT CHARACTERISTICS	
3.1 Introduction.....	46
3.2 Experimental Section.....	51
3.2.1 Materials	51
3.2.2 Study of interactions between GO and the crosslinkers.....	51

3.2.3 <i>Thin-film fabrication procedure</i>	53
3.2.4 <i>Post-film fabrication characterisations</i>	56
3.3 Results and Discussion	57
3.3.1 <i>Nature of interaction between GO and the crosslinkers</i>	57
3.3.2 <i>Film continuity analysis</i>	64
3.3.3 <i>Analysis of the hydrophilicity of the fabricated films</i>	66
3.3.4 <i>Film thickness and analysis</i>	69
3.4 Conclusions	72
4.	74
THE FABRICATION, CHARACTERISATION AND ENHANCEMENT OF GRAPHENE OXIDE NANOFILTRATION MEMBRANES FOR WATER PURIFICATION VIA LAYER BY LAYER CROSSLINKING	
	74
4.2 Experimental Section	80
4.2.1 <i>Materials</i>	80
4.2.2 <i>Membrane fabrication on PAN substrates</i>	80
4.2.5 <i>Membrane performance tests</i>	85
4.2.6 <i>Continuity of the fabricated membranes</i>	87
4.3 Results and Discussion	88
4.3.1 <i>Membrane continuity analysis</i>	88
4.3.2 <i>Analysis of membrane performance results</i>	93
4.3.3 <i>Membrane stability</i>	99

4.3.4 <i>Membrane separation mechanism, operational longevity and reusability</i>	102
4.3.5 <i>Further economic improvements: assembly on other substrates</i>	104
4.4 Conclusions	106
5.	107
THE IMPACT OF GRAPHENE OXIDE’S PHYSICOCHEMICAL CHARACTERISTICS ON THE FABRICATION AND PERFORMANCE OF CROSSLINKED NANOFILTRATION MEMBRANES	107
5.1 Introduction	107
5.2 Experimental section	109
5.2.1 <i>Materials</i>	109
5.2.2 <i>Preparation of different lateral sized GO suspensions</i>	109
5.2.3 <i>Sample characterizations</i>	110
5.2.4 <i>Membrane fabrication, characterisation and performance tests</i>	112
5.3 Results and Discussion	112
5.3.1 <i>Physicochemical characteristics of the GO samples.</i>	112
5.3.2 <i>Impact of GO’s physicochemical characteristics on membrane homogeneity, coverage and morphology</i>	118
5.3.4 <i>Membrane performance analysis</i>	120
5.4. Conclusions	122
6.	124

CONCENTRATION IMPACT ON GRAPHENE OXIDE MEMBRANE STABILITY AND	
PERFORMANCE: ENHANCING MATERIAL CONSERVATION	124
6.1 Introduction	124
6.2 Experimental section	126
<i>6.2.1 Materials and sample preparation</i>	<i>126</i>
<i>6.2.2 Membrane fabrication, characterisation and performance tests</i>	<i>127</i>
6.3 Results and Discussion.....	128
<i>6.3.1 Membrane morphology and thickness at changing concentrations</i>	<i>128</i>
<i>6.3.2 Concentration impact on membrane performance</i>	<i>132</i>
<i>6.3.3 Crosslinker concentration impact on membrane stability</i>	<i>135</i>
6.4 Conclusions	137
7.....	138
SUMMARY, CONCLUSIONS AND FUTURE WORK	138
7.1 General conclusions	138
7.2 Major findings	140
<i>7.2.1 Demonstration of successful quanta control of key thin-film/membrane</i> <i>characteristics via the dip-assisted layer by layer method</i>	<i>140</i>
<i>7.2.2 Enhanced membrane stability and improved nanofiltration performance</i> <i>.....</i>	<i>140</i>
<i>7.2.3 Optimisation of GO's physicochemical characteristics for enhanced</i> <i>membrane performance</i>	<i>141</i>
<i>7.2.4 Optimisation of GO and crosslinker preparatory concentrations</i>	<i>141</i>

7.3 Future work recommendations	142
<i>7.3.1 GO membrane modifications to improve permeation flux</i>	142
<i>7.3.2 Exploration of the crosslinked membranes' separation potential of other contaminants, heavy metals, divalent and monovalent salts</i>	142
<i>7.3.3 Use of other economically affordable sub nanometre sized crosslinkers</i>	143
<i>7.3.4 Further exploration of the membrane separation mechanisms and long-term stability</i>	143
REFERENCES	144
APPENDIX A; LIST OF ABBREVIATIONS	197
APPENDIX B; PERMISSIONS FOR THIRD PARTY COPYRIGHT WORKS	198
APPENDIX C: PUBLISHED PAPERS	199

LIST OF FIGURES

Figure 1. Crosslinkers to be used for the fabrication of GO-based thin films A) PPD, B) MLM and C) PEI.....	7
Figure 2. Pristine graphene structure	12
Figure 3. Left, Electronic dispersion in the graphene honeycomb lattice: Right; zoom in of the energy bands close to one of the Dirac points [61].....	14
Figure 4. Schematic of mechanical exfoliation fabrication method (scotch tape method illustration) [82].....	16
Figure 5. Unzipping of carbon nanotubes mechanism [85].....	17
Figure 6. Schematic showing the growth of multi-layer graphene sheets[106].....	19
Figure 7. Pyrolysis of sodium ethoxide (EtONa) to graphene schematic [108].....	20
Figure 8. Major GO models; A) the Hofmann model, B) the Ruess model, C) the Scholz-Boehm model, D) the Nakajima-Matsuo model E) the Dekany model, F) the Lerf-Klinowski model [112]	22
Figure 9. (E) as a function of oxygen coverage for both amorphous and ordered GO [125].....	25
Figure 10. Procedural chronological growth of GO using the Tang-Lau method [145].....	29
Figure 11. The tortuous path flow of water molecules across a GO membrane and additional GO separation mechanisms' illustrative schematic [169].....	35
Figure 12. Vacuum filtration membrane fabrication schematic [177].....	37
Figure 13. Illustrative fabrication schematic of the A) spin coating and B) the spray coating methods [183,189].....	38

Figure 14. Illustrative schematic showing the uncrosslinked GO membranes and those crosslinked by TMPyP [197].....	41
Figure 15. Change in the intactness of the GO membranes under different substrates signifying the enhancement stability and intactness by AAO [173].....	42
Figure 16. Schematic illustrating the use of the epoxy encapsulant to physically confine the GO nanosheets [50].....	43
Figure 17. Nadetech Innovations dip-coater (S/N: 522033).....	54
Figure 18. Schematic diagram of dip-assisted layer-by-layer fabrication technique	55
Figure 19. FTIR characterisation spectra for the GO-PPD and GO-MLM interactions after 1 minute and 5 minutes of reaction	59
Figure 20. The epoxy-ring opening reaction between: A) PPD and GO; and B) MLM and GO	60
Figure 21. FTIR characterisation spectra of GO, PEI and the GO-PEI interactions after 1 minute and 5 minutes of reaction	63
Figure 22. Photographs of the crosslinked thin films	65
Figure 23. SEM micrographs of the crosslinked thin films: A) GO-PPD 1'1; B) GO-PPD 1'20; C) GO-MLM 1'1; D) GO-MLM 1'20, E) GO-PEI 1'1; F) GO-PEI 1'20	66
Figure 24. Camera images of the contact angles formed by water droplets on the crosslinked thin films of PPD, MLM and PEI.....	68
Figure 25. Thickness measurements of the cross-linked thin films.....	70
Figure 26. PAN substrate mounted onto the stainless-steel metal plate before membrane fabrication.....	82

Figure 27. Schematic diagram showing fabrication of uncrosslinked membranes by dip-coating.....	83
Figure 28. Schematic diagram showing fabrication of crosslinked membranes by dip-assisted layer-by-layer assembly.....	84
Figure 29. The homemade nanofiltration cell unit in operation.....	85
Figure 30. MB absorbance: concentration calibration line.....	87
Figure 31. Photographic images of the fabricated uncrosslinked membranes on PAN substrates.....	89
Figure 32. SEM images of the respective fabricated uncrosslinked membranes on PAN substrates	90
Figure 33. Photographic images of the crosslinked membranes on PAN substrates	91
Figure 34. SEM images of the crosslinked membranes on PAN substrates.....	92
Figure 35. Photographic images of the MB permeate across each of the fabricated membranes.....	94
Figure 36. SEM images of the fabricated membranes post-nanofiltration.	100
Figure 37. Uncrosslinked and crosslinked membranes after pressure-assisted fabrication and drying	101
Figure 38 Images of the membranes fabricated on polycarbonate substrates.....	105
Figure 39 SEMs of membranes fabricated on PCB substrates.....	105
Figure 40. AFM images of the differently sonicated samples; A) GO-0' B) GO-30' C) GO-60' D) GO-120' and E) GO-180' and respective histograms depicting their lateral size distribution.	114
Figure 41. Absorbance coefficients of the prepared samples.....	115

Figure 42. *Photographic images of the fabricated membranes; A) plain PAN substrate, B) M-GO-0' C) M-GO-30', D) M-GO-60', E) M-GO-120' F) M-GO-180'*
 118

Figure 43. *SEM images of A) plain PAN substrate, B) M-GO-0' C) M-GO-30', D) M-GO-60', E) M-GO-120' and F) M-GO-180'* 119

Figure 44. *MB rejection results of the fabricated membranes with respective permeate solutions* 120

Figure 45. *Permeation flux of the fabricated membranes* 122

Figure 46. *Photographic images of the fabricated membranes at respective GO and crosslinker concentrations* 129

Figure 47. *SEM images of the fabricated membranes* 130

Figure 48. *SEM images of the membranes fabricated with 0.5 mg/ml of GO post nanofiltration* 136

LIST OF TABLES

Table 1. Filtration membranes and their respective sizes and a general comparative description of their separation mechanisms [160].....	32
Table 2. Nomenclature of the fabricated films at different immersion times and numbers of bi-layers	56
Table 3. Surface chemistry of GO and GO-PPD, GO-MLM reacted entities.	62
Table 4. XPS characterisations (GO-PEI).....	64
Table 5. Nomenclature of the fabricated membranes.....	84
Table 6. Results of membrane rejection tests.....	95
Table 7. Permeation fluxes of the fabricated membranes on PAN substrates.....	97
Table 8. Separation of dye from water by the 5-bi-layer crosslinked PPD membrane over prolonged hours of operation (Working pressure 1 bar, MB concentration 10 mg/l).....	102
Table 9. Relationship between increased feed concentration and membrane performance at short and long operation times (5-bi-layered crosslinked membrane).	103
Table 10. Surface chemistry of GO samples determined by XPS (at. %).....	116
Table 11. Zeta potential of the GO suspensions.....	117
Table 12. Thickness of the fabricated thin films at respective GO and PPD concentrations in nm.....	132
Table 13. Membrane performance (Rejection and permeation flux)	134

1.

INTRODUCTION

“I seem to have been only like a boy playing on the seashore, and diverting myself now and then finding a smoother pebble or a prettier shell than ordinary, whilst the great ocean of truth lay all undiscovered before me.”

SIR ISAAC NEWTON (1642 – 1727)

1.1 Background and Motivation

The eminent global water shortage intensified by an exponentially increasing global population and changing climate calls for the derivation of materials and processes to alleviate the impending impact [1–4]. Alarmingly, it is predicted that by 2050 global water scarcity could affect up to 5 billion people [5]. This highlights the urgent need for the implementation and improvement of current water purification, which involves the removal of particulates, undesirable chemicals, biological contaminants, suspended solids and gases as well as the removal of monovalent and divalent salts from water for consumptive means [6–8].

Several methods from physical processes such as distillation, sedimentation and filtration to chemical processes like flocculation and chlorination are currently being explored in these realms [9]. Notably, the chemical methods have low favourability owing to cost ineffectiveness due to large sludge generation and removal after purification [10]. Furthermore, potential damage to separation modules due to the introduction of chemical compounds is also a notable limitation that impedes their usage [11]. On the other hand, despite their relatively wide usage, physical methods

such as distillation's high energy consumption and increased operation costs limits the method's use [12].

Separation membranes on the contrary have a significant favourability over the other purification processes [13–15]. Environmental benignity and relative energy efficiency are among the key advantages of their use over other conventional methods in water purification [16]. Since their commercialization by Loeb and Sourirajan in the 1960s', several materials have been employed in the quest for efficient, affordable and highly stable membranes [17]. Both polymeric and inorganic membrane materials are being used at the moment owing to their abundance and large-scale production [18]. The most commonly used polymers are polyamides, cellulose acetate and poly (vinylidene fluoride) (PVDF) [16–19]. However, poor mechanical strength and susceptibility to fouling has resulted in fading of the use of polymeric membranes in favour of inorganic ceramic based membranes [23]. Ceramics' use in commercial membranes over the polymeric materials is heightened specifically by their high selectivity and stability in turbulent operation conditions [24]. Nonetheless, Joshi *et al* noted that limited permeability inhibits their use in large scale water purification plants [25]. Another inorganic membrane material currently in use is micro porous silica, but complexity in precise instillation of sub nanometre pore sizes for molecular filtration has been reported as a major limitation [25].

For instance, most recently at the Sorek Desalination plant in Rishon Lezion, Israel, Glass Reinforced Plastic (GRP) and polyamides are deployed as separation modules [26]. The major limitations reported for these materials modules were relatively low mechanical strength, in consequence the need to improve the overall performance of these plants cannot be understated. Similarly, the James W. Jardine Water Purification

Plant in Chicago currently employs ceramic modules whose limitations has been cited as limited permeability as aforementioned.

In the recent past decades, carbon-based materials with different dimensions have emerged as possible favourable next generation separation membrane materials. The first generation of these carbon-based groups are the 1-Dimensional single and multi-walled carbon nanotubes (CNTs) [8,27]. In addition to their mechanical strength, CNTs are advantageous in water purification, as they offer an ultrafast uni-directional transport channel of water molecules across fabricated membranes owing to the slip-flow phenomenon [28–30]. However, their poor dispersibility in water and most polar solvents, complexity in fabrication and hydrophobicity greatly limit their candidature as next generation separation membrane materials [31,32].

The successful isolation of graphene by Andre Geim and Konstantin Novoselov has ushered in a new generation of promising 2-Dimensional carbon-based separation material [33]. It is mechanically the strongest material ever tested, one atom thick with a high aspect ratio [33,34]. Its outstanding properties make it a very interesting precursor to most applicative devices including separation membranes [35–38].

Despite its outstanding properties and promising application capabilities, a great challenge in bringing graphene-based products to market has been the lack of an economically large-scale production method [39,40]. It is extremely challenging to fabricate continuous defect free graphene nanosheets for applicative industrial usage [41,42]. As such, graphene derivatives and related materials with large-scale production capabilities are considered as plausible alternatives.

Fortunately, graphene oxide (GO) is a reasonable substitute especially with regard to solution based separation membranes [25,43]. It can be fabricated in a facile manner

with an economically feasible large-scale production method [44]. GO is also chemically versatile, hydrophilic and atomically thin making it a favourable candidate as a next generation water purification membrane material [45]. In consequence, the aforementioned reasons are what mounted to its selection and usage in this doctoral research. The recentness in the use of GO as a separation membrane material alludes to the fact that the broader scope in terms of the membrane's operation mechanisms, limitations, influence of material characteristics on performance is yet to be established. The quest to understand this is among the driving motivations behind this doctoral research.

A major challenge in the use of GO in water purification has been established to be poor stability during operation. This stems from the widening of the membrane pore gap (interlayer spacing) during membrane performance, as a result of the accumulation of water molecules onto the membrane pores [46,47].

The alleviation of the GO pore-gap widening problem is thus of paramount importance to having efficient, stable and durable GO membranes. Several efforts have been undertaken to date to alleviate this problem. For instance, Huang *et al.* explored the use of reduced GO (r-GO) to diminish the oxygenated functional groups in GO membranes, hence limiting the entrapment of water molecules [48]. However, GO reduction results in loss of hydrophilicity and narrowing down of the interlayer spacing which lowers permeability hence the need for a higher operation pressure [49,50]. Abraham *et al.* used an epoxy encapsulate to physically confine the pore gap of GO membranes for water desalination [51]. The major limitation to the physical confinement method employed is that scale up for production of such membranes is a great challenge [51].

In this regard, the doctoral research analyses the use of different amino group containing crosslinkers to interconnect the GO nanosheets systematically to stabilise the membranes during nanofiltration via layer-by-layer crosslinking. A key advantage to the systematic layer-by-layer crosslinking is that it offers controlled interconnection of the GO nanosheets to enhance the overall stability of the membrane structure [52]. This in theory gives strong intactness to the membranes, hence enhancing their stability and performance during membrane operation [53]. This is also further likely to increase the operation longevity of the fabricated crosslinked membranes. The selected crosslinkers offer key advantages of affordability, facile preparation and storage together with the ease of fine-tuning of the GO membranes' pore gap.

Fabrication methods also have an impact on the degree of membrane crosslinking, hence determining the prime-end performance and stability of the membranes [54,55]. Conventionally, the commonly used membrane fabrication methods for GO based membranes are the phase inversion, vacuum filtration and spray coating methods [55–57]. Significant general drawbacks to these conventional fabrication methods can be deduced in the lack of quanta control of the significant membrane characteristics like thickness and requirement of complex equipment [57]. Higher material load usage, which decreases the economic viability of these methods, is also an observable limitation to the vacuum filtration and phase inversion methods. Hu and Mi further reported that the vacuum filtrated GO membranes are susceptible to disintegration in aqueous environments from the high hydrophilicity of the GO nanosheets [58]. After these considerations, the dip-assisted layer-by-layer fabrication method was opted for in this research from its ease of control of the membrane's key characteristics like thickness. Among the key characteristics are the membrane thickness, hydrophilicity and homogeneity. The method entails the interchangeable attachment of two or more

materials via either electrostatic, covalent or weak interactions [52]. It also comparatively uses low material load hence being economically efficient [59]. Furthermore, the dip-assisted layer-by-layer method offers controllable systematic crosslinking to fabricate stable superimposed GO membranes.

1.2 Research Aim and Objectives

Instability of the GO membranes during operation is an established limitation, which needs to be alleviated to bring forth GO based membranes as aforementioned. Moreover, characteristics of GO like nanosheet lateral size, surface chemistry, morphology and individuality also require further scrutiny in order to optimise GO nanofiltration membranes. All these modifications ought to be studied with respect to a specific membrane fabrication method, as there is a greater dependence between specific operating conditions during membrane fabrication and membrane performance.

The overall aim of the doctoral study was therefore **the controlled fabrication and optimisation of GO water purification membranes with enhanced stability, reusability and nanofiltration performance.**

The following key objectives were established to achieve the outlined aim:

- i) *To fabricate controlled thickness, GO thin films by means of dip-assisted layer-by-layer deposition.*

It was significant to demonstrate the feasibility of membrane fabrication prior. This bring about to understanding more in detail the impact of the operating conditions of the deposition method, specifically the immersion time and the number of assembly cycles, onto the fabricated membrane characteristics. As such, the initial aim of the

thesis was to fabricate respective p-phenylenediamine (PPD), 1,3,5-triazine-2,4,6-triamine (melamine) (MLM) and poly (ethyleneimine) (PEI) (Figure 1) layer-by-layer crosslinked GO films. This was done to show the plausibility of successful thin-film fabrication through relevant characterisations. Affordable glass slide substrates were used at this stage. The demonstrative fabrication of the thin films on glass slides was also in part carried out to establish a relation between the immersion time, number of assembly cycles and the significant crosslinked GO thin films characteristics like homogeneity, thickness, morphology and hydrophilicity.

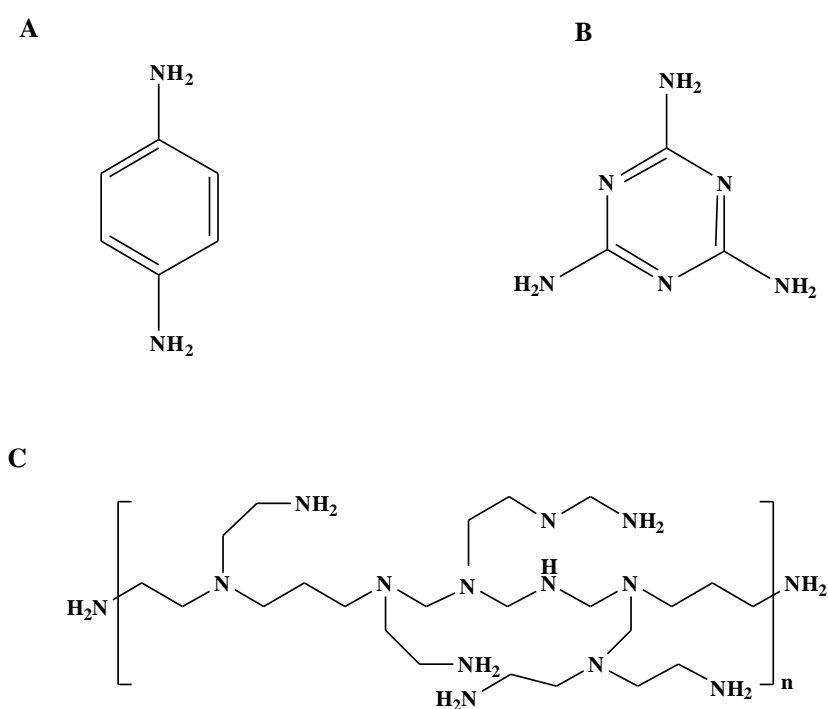


Figure 1. Crosslinkers to be used for the fabrication of GO-based thin films A) PPD, B) MLM and C) PEI

ii) **To evaluate the crosslinkers' enhancement of GO membrane water purification performance and stability.**

Following successful confirmation of the plausibility of GO crosslinked thin films via the dip-assisted layer-by-layer method, the thesis goes on to primarily evaluate the

impact of crosslinking in enhancing the water purification performance of GO membranes. Since different sized crosslinkers; PEI, MLM and PPD are employed in this study, a significant objective will be to look into the influence of each crosslinker onto the membrane nanofiltration performance. The crosslinkers hypothetically/theoretically improve the performance of the membranes through enhancing their stability through interlinking the nanosheets. A comparative analysis between the crosslinked layer-by-layer assembled membranes and uncrosslinked dip-coated GO membranes is to be undertaken to verify performance and stability enhancement.

Concurrently, performance dependence on the number of membrane layers and bi-layers is to be studied in this stage. Different porous substrates are to be used as well; 0.2 μm pore sized porous poly (acrylonitrile) (PAN) and polycarbonate (PCB) as support for the respective crosslinked GO membranes. Membrane separation performance is to be tested through the nanofiltration of an aqueous solution of methylene blue (MB) via a homemade poly (methyl methacrylate) nanofiltration cell. The conditions at which the membranes work, including maximum operation pressure, flux and rejection rate are therefore subject to the fabrication conditions i.e. number of bi-layers, crosslinker used and the immersion time.

iii) To investigate the impact of physicochemical characteristics of GO onto the nanofiltration performance of the crosslinked membranes.

Here an analysis of the impact of physicochemical properties like GO lateral size and surface chemistry onto overall membrane performance is to be studied. The relation between lateral size and the abundance of specific functional groups in GO is duly to be evaluated. These properties are normally altered during either fabrication or

preparatory ultrasonication of the GO suspensions. As such, the impact of different GO lateral size and chemical functionalities (functional group composition) on membrane performance are to be studied via different characterization means.

iv) Optimization of the impact of GO and crosslinker concentrations on membrane homogeneity and overall nanofiltration performance.

Impact of the concentration of both GO and crosslinker on the overall performance of the membranes is to be analysed under this objective. Concentration plays a significant role in the structural characteristics of fabricated membranes, such as membrane thickness, topographical roughness and homogeneity. This is also an attempt to further optimise membrane fabrication through determining the impact of GO and crosslinker concentrations on membrane performance. In consequence, instigating material conservation.

1.3 Thesis Structure

The thesis consists of 7 key chapters detailing in chronology the route towards the fabrication, enhancement and optimisation of GO membranes via crosslinking for water purification purposes. The motivation and background of the thesis together with an outline on the selection of GO as the principal membrane material in this regard are outlined in **Chapter 1**. The key objectives of the thesis are also sequentially outlined in this introductory chapter. Successively **Chapter 2** goes on to review previous works done elsewhere regarding the use and improvement of GO membranes in water purification and the limitations of these methods. Since graphene is the parent material to GO, the fabrication and properties of graphene are briefly discussed in the literature review chapter. This was to give a leeway to the discussion of the fabrication of GO and its properties and to give more detailed discussion on the equitability of

GO as a relevant graphene substitute. Background on separation membranes is also discussed in details in this chapter.

The subsequent chapters 3 to 6 outline the experimental work on the dip-assisted layer-by-layer crosslinked GO membranes together with their optimisations. First, the plausibility of the thin-films fabrication and control of their significant characteristics is detailed in **Chapter 3**. In **Chapter 4** the performance of the fabricated crosslinked membranes relative to uncrosslinked ones to confirm the impact of each of the crosslinkers in enhancing membrane performance and stability is analysed. Membrane operation mechanisms and reusability are also studied and demonstrated in this chapter. In the latter stages of the chapter the use of other substrates is also discussed in this chapter.

In **Chapter 5**, the impact of lateral size of GO nanosheets on their surface chemistry and colloidal suspension and subsequently on the membrane performance is explored. **Chapter 6** on the other hand looks into the impact of concentration of both the crosslinker and GO on the average performance of the fabricated layer-by-layer crosslinked membranes to enhance material conservation. In the end, the summary of the whole research is provided in **Chapter 7**, where the key findings and future works are also discussed.

2.

LITERATURE REVIEW – GRAPHENE, GRAPHENE OXIDE AND SEPARATION MEMBRANES

“It is of great advantage to the student of any subject to read the original memoirs on that subject, for science is always most completely assimilated when it is in the nascent state...”

JAMES CLARK MAXWELL, (1831 – 1879)

2.1 Graphene

2.1.1 Structure and historical overview

Graphene is a monolayer 2-dimensional carbon allotrope consisting of carbon atoms arranged in a hexagonal lattice of C-C bonds (Figure 2) [60]. The formation of different C-C bonds via orbital hybridization is well documented and in the case of graphene, the sp^2 hybridization occurs when one carbon atom is bonded to three others [61]. An s orbital is inter-joined to two p-orbitals forming a trigonal planar structure with a 0.142 nm σ bond between the carbon atoms [62]. The C-C-C angle is calculated to be 120° [63]. The strength and short length of the C-C bond heightens its high mechanical strength over other semi-conducting materials such as silicon [63]. The properties arising from the structure makes graphene a promising precursor material in the fabrication of various nanomaterials, from flexible nanoelectronics to polymer nanocomposites and even separation membranes [64].

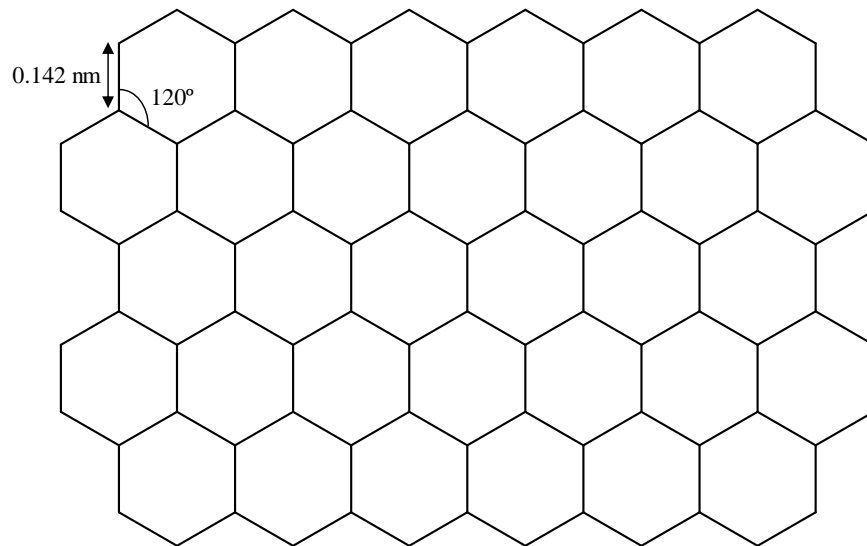


Figure 2. Pristine graphene structure

Sporadic theoretical studies of graphene can be traced back to 1859, when Benjamin Collins Brodie examined the lamellar structure of oxidised thermally reduced graphite oxide [65]. Further detailed theoretical postulations were carried out in 1947 by Phillip Russell Wallace through examining of the electrical properties of monolayers of 3D graphite [60]. Practically, observations of several layers of graphite by electronic microscopes have been reported as early as in 1962 by Hans-Peter-Boehm [66].

In 2004, Andre Geim and Konstantin Novoselov used the micromechanical exfoliation method; where *scotch tape* was used to repeatedly peel off layers of graphite until monolayers (graphene) were obtained (further details on the fabrication procedure in section 2.1.3) [67]. Stable 2-dimensional monocrystalline graphene films of high quality were produced from this technique [67]. It has since been proclaimed the wonder material of the 21st century as a result of its outstanding properties and scope of possible applications [68,69]. This has henceforth culminated in the *graphene gold rush*, where an exponential increase in research on graphene based products has been observed since [70].

2.1.2 Properties of graphene

2.1.2.1 Mechanical properties

The intrinsic mechanical strength of graphene has been reported by Hone *et al* via Atomic Force Microscopy (AFM) nano-identification, proving graphene to be the strongest material ever tested with a tensile strength of 42.1 N/m (130 GPa) [71]. Its Young's modulus of around 1 TPa makes graphene magnitudes stronger than most conventional materials [72]. Comparatively, strong regular materials like A36 structural steel and aramid (Kevlar) have a tensile strength of 0.4 GPa and 0.375 GPa respectively [73,74]. Despite being mechanically very strong, graphene is also very light. A square meter of the material only weighs 0.77 mg, which is a 1000 times lighter than a square meter of paper [75].

Furthermore, the C-C sp^2 bonds are able to rotate, this gives graphene excellent flexibility and elasticity [71]. Elastic stiffnesses of up to 690 N/m has been reported [71].

2.1.2.2 Electrical properties

Electrically, graphene is a zero-energy semiconductor [76]. This is due to the overlapping of the valence and conduction bands at the Dirac points (Figure 3). This offers unique charge transport characteristics, such as high ballistic transport and mobility of charge carriers at room temperature [77]. π electrons are present in the graphene plane and they are highly mobile, which gives graphene excellent electrical properties [77]. There is also a combination of electrons in the conduction band and holes in the valence band referred to as the electron-hole pair meeting at the Dirac points (Figure 3) [62]. These give an electron and hole conduction under the external electric field, which forms a microscopic current [62]. Charge carrier mobility in excess of 15000 $cm^2/V.s$ at room temperature has been recorded [70].

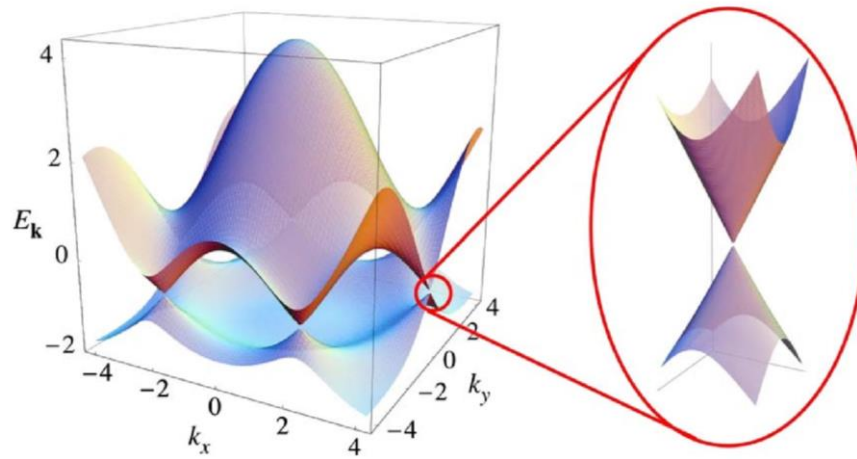


Figure 3. Left, Electronic dispersion in the graphene honeycomb lattice: Right; zoom in of the energy bands close to one of the Dirac points [62].

Electrons propagating through graphene sheets tend to lose their mass producing massless Dirac fermions (quasi particles), which also constitutes to the unique electronic properties of graphene [62]. This makes the electrons to hardly encounter any scattering, causing a high ballistic transport system at room temperature [62].

2.1.2.3 Optical properties

Optical properties of graphene are influenced by its high electron mobility. This makes graphene to have a relatively high opacity ($\pi\alpha = 2.3\%$ (red light)) for a monolayer material [78,79]. This optical absorption is attributed to the electron transition within and between the valence bands [80]. At increased number of layers of graphene, the opacity increases as more white light is absorbed by the same percentage. It has been experimentally proven that the visual transparency of graphene solely depends on the fine structure constant [79]. This is a fundamental physical constant detailing the interaction between electromagnetic waves and the charged atoms in a material [81].

2.1.3 Graphene fabrication methods

Since its isolation using the micromechanical exfoliation method [67], physical and chemical methods have so far been deployed to produce graphene sheets for research and commercial purposes. Present graphene synthesis methods entail both top-down and bottom-up approaches. In top-down approaches graphite is used as the precursor and separated to produce graphene sheets, while for bottom-up approaches self-assembly of carbon atoms to form graphene sheets is entailed [82].

2.1.3.1 Micromechanical exfoliation (Scotch tape) method

With graphite as the parent material, the micromechanical exfoliation procedure involves repetitive peeling of layers of graphite until single layers of graphene are obtained (Figure 4) [67]. The peeling, which is aided by scotch tape, overcomes weak forces interconnecting graphene layers in graphite [83]. This process is facilitated by a normal upward force and the shear force [83].

At present, mechanical exfoliation is the method giving the purest almost defect free graphene sheets in comparison to other production methods [84]. The extremely low yield of the method however, makes it impractical for large-scale production. As such it is mainly used for research and lab scale applications [82].

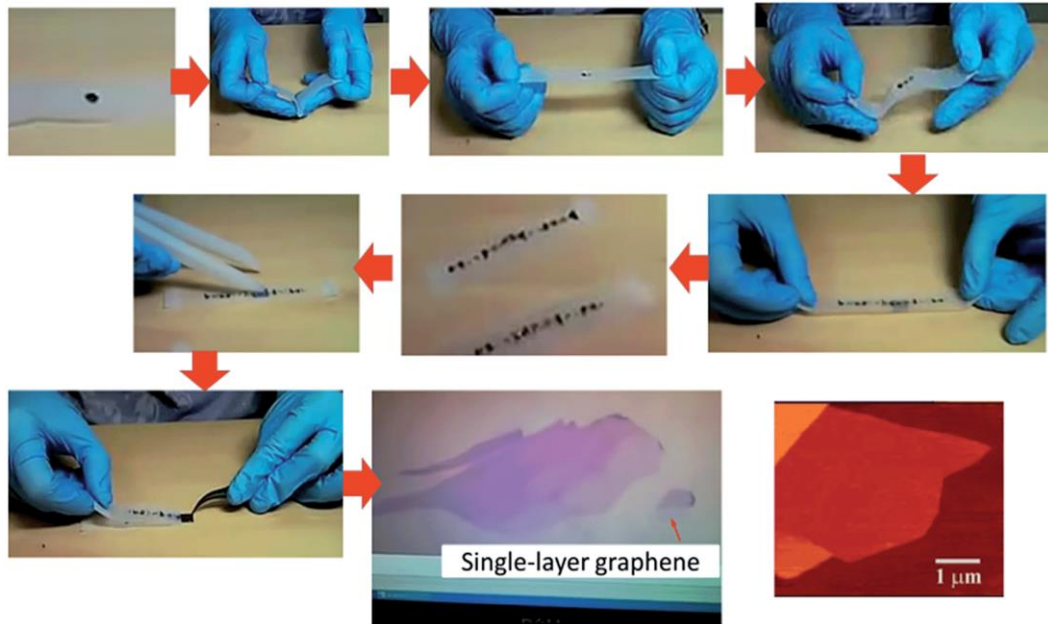


Figure 4. Schematic of mechanical exfoliation fabrication method (scotch tape method illustration) [83]

2.1.3.2 Unzipping of carbon nanotubes

Graphene nanoribbons can also be produced by unzipping carbon nanotubes. To fabricate graphene sheets, single walled (SWCNTs) and multi walled nanotubes (MWCNTs) are broken along the lines by various mechanisms [85]. One way of unzipping carbon nanosheets is through immersion of the nanotubes in sulphuric acid (H_2SO_4) and subsequently in potassium permanganate (KMnO_4) [86] (Figure 5). Other unzipping methods include etching of the nanotubes in plasma and sonication in organic solvents [87,88]. Though the lateral size of the produced graphene nanoribbons is relatively small and limited by the geometry of the nanotubes, the production of graphene nanoribbons in this manner has a potential for large scale production [86,89].

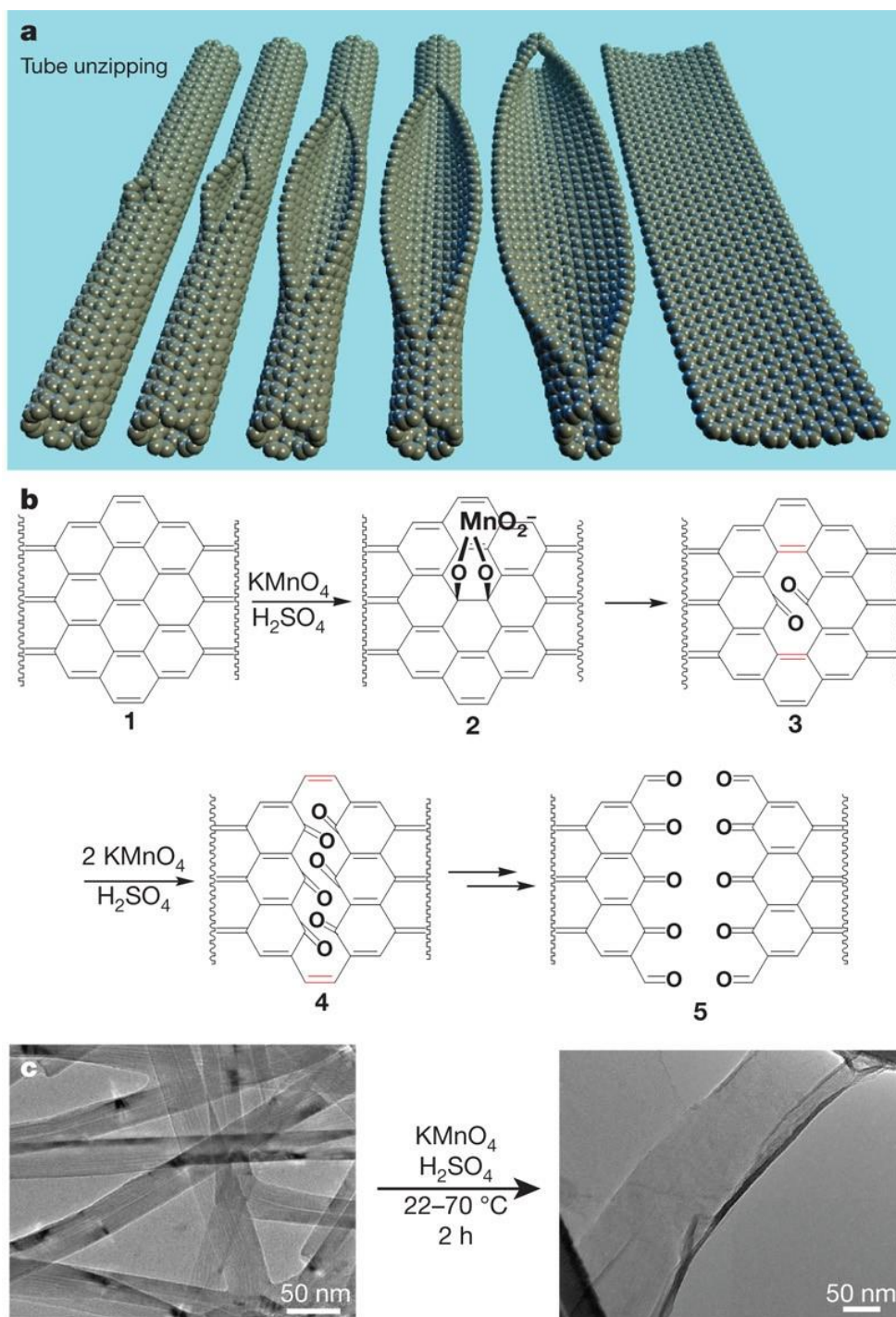


Figure 5. Unzipping of carbon nanotubes mechanism [86]

2.1.3.3 Chemical Vapour Deposition (CVD)

CVD is the art of depositing gaseous molecules onto substrates to assemble thin film structures [90]. The fabrication of graphene via CVD was pioneered by Somani *et al* using camphor (terpinoin, $\text{C}_{10}\text{H}_{16}\text{O}$) as the precursor material and nickel foil as the

holding substrate [91]. To produce graphene via CVD, gaseous precursor carbon molecules are obtained by heating (at ~1000°C) carbon-containing materials, most preferably hydrocarbons like methane in a reaction chamber [92]. The high temperature heating decomposes the hydrocarbons, leaving the carbon atoms to rearrange onto a substrate during a cooling phase in argon gas to form graphene sheets [93]. Transition metals like copper (Cu) and nickel (Ni) are the most regularly used assembly substrates [94,95].

Since high temperatures are entailed, to lower the temperatures during the pyrolysis and assembly stages, catalysts are usually used [96]. However, the introduction of catalysts result in increased impurities in the assembled graphene films, which is a notable limitation to the method [97].

Another drawback in the use of CVD as a fabrication method has been in the later stage of exfoliation of graphene films. This is because the graphene films ‘grow’ onto the substrate and removal and transfer without damage is highly unlikely [97]. Recent attempts to solve this problem has been in the use of Poly (methyl methacrylate) (PMMA) as an assembly substrate instead of the usual Cu and Ni [98]. The PMMA is then chemically etched leaving the graphene films intact [98].

2.1.3.4 Liquid phase exfoliation of graphite

To produce graphene via the liquid phase exfoliation, three stages are entailed i.e. dispersion of graphite flakes in a solvent, exfoliation and purification [99]. During the dispersion/suspension stage surfactants containing sulfonic groups are used to aid graphite suspension in solvents [100]. Significance is drawn to the solvent that is selected to suspend the graphite flakes during fabrication. This is because a good carrier solvent can minimise interfacial tension between graphite flakes thus

diminishing clustering of the graphene sheets [100].. The exfoliation stage entails ultrasonication, which is followed by centrifugation or sedimentation as purification stages to attain graphene sheets [101]. Graphene nanosheets of up to $1 \mu\text{m}^2$ have so far been reported [102,103].

2.1.3.5 Epitaxial growth on Silicon Carbide (SiC)

The epitaxial growth of graphene on silicon carbide is another widely recognised graphene production method. The method entails heating of SiC at high temperatures in excess of $1650 \text{ }^\circ\text{C}$ to sublimate the Si atoms [104]. This is because the vapour pressure of carbon is negligible in comparison to that of silicon. Therefore, at high temperatures the silicon atoms desorb leaving the carbon atoms to rearrange to form graphene thin films (Figure 6) [105]. Epitaxial growth falls into two categories; homo when the film and the substrates are of similar material composition and hetero when they are of different compositions [106].

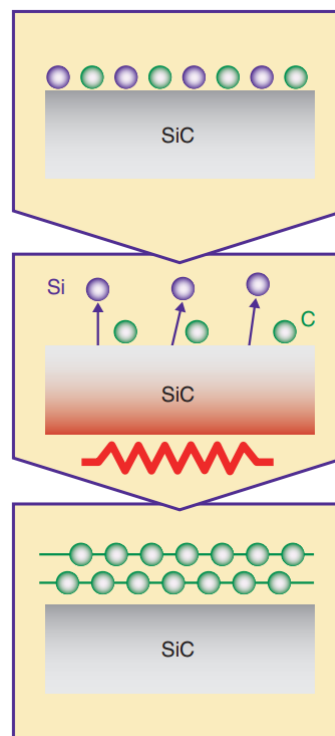


Figure 6. Schematic showing the growth of multi-layer graphene sheets[107].

2.1.3.6 Pyrolysis of sodium ethoxide

The pyrolysis of sodium ethoxide, which is also known as the solvothermal method, first involves thermal reaction of sodium and ethanol on a 1:1 ratio in a closed vessel to form sodium ethoxide [108]. This is followed by the pyrolysis of the produced sodium ethoxide in a nitrogen environment. In the process, carbon atoms rearrange in lattice formats to form graphene sheets. Sheets of up to 10 μm in lateral length have been reported in previous fabrications (Figure 7) [108]. The method offers low cost production, however, the quality of the graphene attained is relatively low due to the presence of up to 10% of ethanol and water impurities [108].

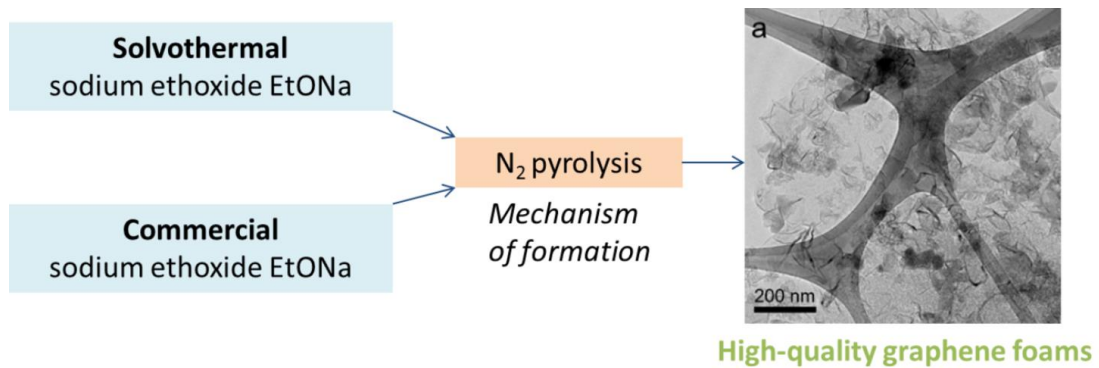


Figure 7. Pyrolysis of sodium ethoxide (EtONa) to graphene schematic [109].

Speyer *et al.* further explored the production of graphene under this method by introducing sodium ethoxide in an Inconel alloy crucible in an inert argon atmosphere [109]. The mixed entities were hereafter placed in a vertical tubular oven under a 500 mL min^{-1} nitrogen flow. After that the oven was heated to 850°C for 4 hours before cooling down while keeping the nitrogen flow constant [109]. This resulted in the formation of strands of high-quality graphene foam (Figure 7).

2.1.4 Main challenge in bringing graphene-based products to market

An overall limitation in bringing graphene-based product to market currently is the lack of production scalability of pure defect free graphene nanosheets at a competitive

price [110]. Currently, the method giving the purest defect free is the micromechanical exfoliation, which evidently cannot be scaled to mass production as aforementioned. However, progress is being made in bringing the cost of graphene down. For instance in the past 2 years a 30% reduction in graphene market price has been reported [39].

Alternatively, graphene's derivative graphene oxide (GO), is a reasonable substitute in various graphene related applications as it can be easily scaled up to mass production at relatively lower costs [110,111]. Moreover, in specific applications like water purification and desalination, GO has favourable physicochemical characteristics, such as hydrophilicity and unique water permeation pathway [45]. These ease water permeation and flow across the GO based membranes. In these regards, it is continually being explored as a precursor material for different next generation products as an alternative to graphene.

2.2 Graphene Oxide

2.2.1 Definition and structures

GO is a single layer of graphite oxide [112]. It is by definition a graphene sheet interrupted by various oxygenated functional groups. The prevalent oxygenated functionalities present being the epoxy, hydroxyl, carboxylic and carbonyl groups [113].

The chemical structure of GO in terms of the prevalence and position of certain functional groups is still under scrutiny and varying theoretical propositions exist [113]. The structural ambiguity stems from its non-stoichiometric nature [114]. Six major structural models have been proposed to date i.e. the Hofmann, Lerf-Klinowski, Ruess, Scholz-Boehm, Nakajima-Matsuo and Dekany models [113] (Figure 8).

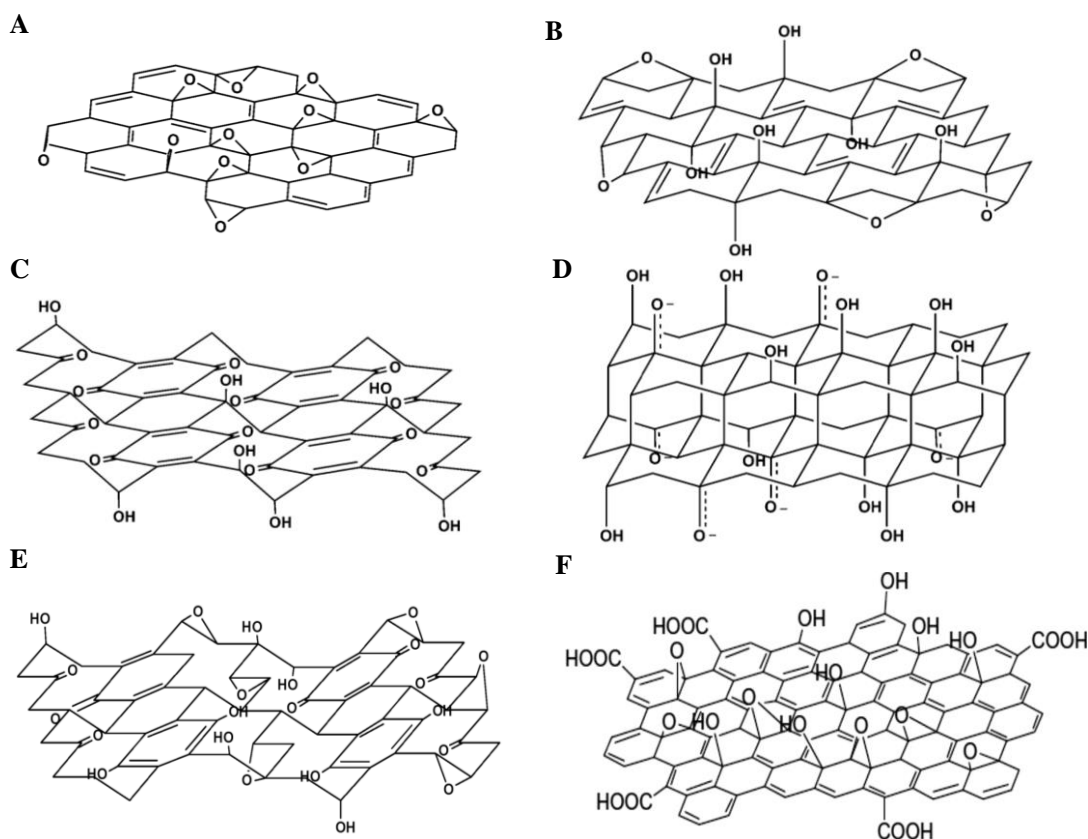


Figure 8. Major GO models; A) the Hofmann model, B) the Ruess model, C) the Scholz-Boehm model, D) the Nakajima-Matsuo model E) the Dekany model, F) the Lerf-Klinowski model [113]

The first theorised GO model was proposed by Hofmann and Holst. In this model, the predominant functional group presumed was the epoxy group in the sp^2 hybridised plane and edges of the graphene plane (Figure 8A) [115]. Basing on the Hofmann model, Ruess *et al.* proposed the introduction of hydroxyl groups together with a 1, 3 ether to the model, culminating in the Ruess GO model (Figure 8B) [112,116]. It consists of a sp^3 -hybridised system unlike the precursor model. The Ruess model further denotes that 25% of the cyclohexanes had epoxide groups at their 1, 3 positions, while the hydroxyls stood at the 4th position [116]. Later on, Scholz and Boehm proposed the incorporation of cyclohexane rings linked with quinoidal structure onto the Ruess structure to replace the epoxy and hydroxyl groups (Figure

8C) [66,117]. Another proposed model is the Nakajima-Matsuo model (Figure 8D), which contains a free lattice assembly that is similar to the poly (fluorocarbon) (CF₂) structure [118]. The proposition of these latter aforementioned lattice models were based on the chemical composition and XRD characterisations [119].

The Dekany model (Figure 8E) on the other hand is a combination of the Ruess and Scholz-Boehm models [119]. It is composed of two main characteristics; the trans linked cyclohexyl species consisting of tertiary alcohols together with the 1,3 ethers and a network of keto species to resemble the acidic nature of the material [120]. The model like the other ones do not incorporate the presence of any carboxylic groups, which makes it characteristically incomplete [112].

The most widely accepted model presently is the Lerf-Klinowski model, which rejects the lattice model in favour of a nonstoichiometric amorphous structure entailing epoxy, carbonyl, hydroxyl in the basal plane of the GO sheet and the carboxylic groups at the edges (Figure 8F) [121]. The functional groups' presence in this model are experimentally confirmed by both Nuclear Magnetic Resonance (NMR) and X-ray Photo-spectroscopy (XPS) together with Fourier transform infra-red (FTIR) characterisations [122].

Lerf and co-workers in proposing the structure of GO further demonstrated that carbon-carbon double bonds are either conjugated or aromatic. This was highlighted in conjunction with the fact that isolated carbon-carbon double bonds are likely to not exist in strong oxidising conditions during GO production [112].

In overall, ambiguity is still present regarding the chemical structure of GO nonetheless, propositions continue to emerge with the most recent nonstoichiometric based ones being the Tour and Ajayan models [123,124]. The Ajayan model is

structurally similar to the Lerf-Klinowski, however, relative ratios of functional groups are established at 115(hydroxyl and epoxide) :3(lactol O–C–O): 63(graphitic sp^2 carbon) :10(lactol + ester + acid carbonyl): 9(ketone carbonyl) [123]. The Tour model on the other hand propose a dynamic structure with definite functional groups alike in the Lerf-Klinowski model but their ratio constantly changing in the presence of aqueous solvents [124]. It was proposed to explain the high acidity of GO which is difficult to harmonise with the other proposed models. Using relevant characterisations from potentiometric titration, ^{13}C NMR, to thermogravimetric analysis, it was proven that GO does not contain a higher proportion of pre-existing acidic functional groups, they are produced as the nanosheets interact with water molecules in suspensions [124].

2.2.2 Properties of graphene oxide

2.2.2.1 Mechanical properties

GO's intrinsic mechanical strength and stiffness characterisations were pioneered by Ma *et al.* in 2007 [125]. Homogeneous cross sheet stress distribution of about 40 GPa and an intrinsic mechanical strength of 120 MPa was obtained [125]. In overall, E varies with the degree of coverage of the oxygenated functional groups. Values from 380 to 470 GPa for ordered GO and from 290 to 430 GPa for the amorphous GO have been reported (Figure 9) [126,127]. This proves that amorphousness, orderliness together with the oxidation degree play a significant role in the extent/magnitude of its mechanical strength and properties [126,127].

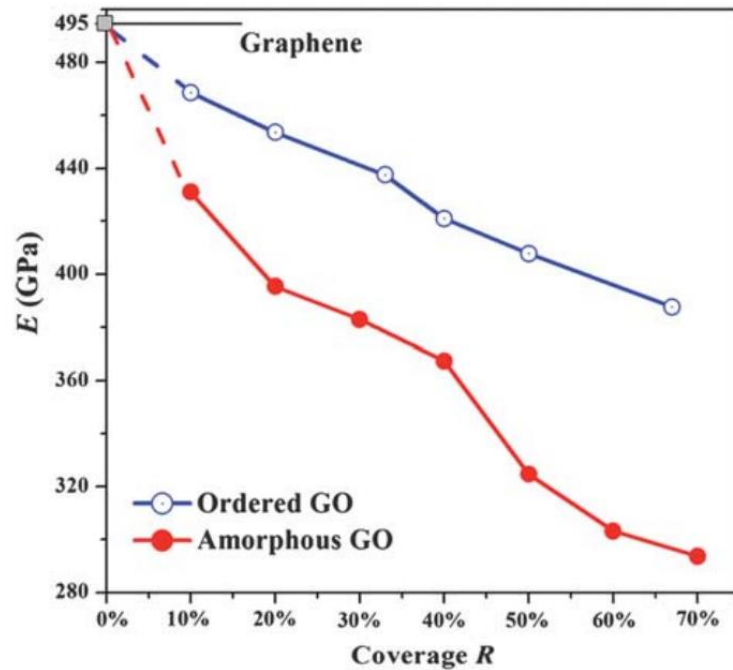


Figure 9. (E) as a function of oxygen coverage for both amorphous and ordered GO [126].

Mechanically GO is stronger than most conventional polymers like polyamide and poly (ethersulfone), hence its reported use in the enhancement of the mechanical properties of these polymers [128].

2.2.2.2 Electrical properties

The presence of various oxygenated functional groups in the material impedes the flow of charge carriers in GO, making it a non-conducting nanomaterial [129]. Nonetheless, electrical conductivity can be instigated through the removal of these oxygenated functional groups, either through chemical or thermal reduction to form reduced graphene oxide (r-GO). The threshold carbon to oxygen ratio for there to be an electrical conductivity after reduction has been noted to be 6 [130]. At this ratio, partial graphene structure is recovered making the reduced conjugate electrically conductive [130]. However, r-GO is still not as conductive as graphene owing to the presence of some oxygenated functional groups.

2.2.2.3 Hydrophilicity

From its possession of oxygenated functional groups, GO is inherently very hydrophilic [131]. However, the degree of hydrophilicity depends on the prevalence of the functional groups present. Water contact angles ranging from 30° to 60° have been reported validating this assertion [132]. Other determinants of the hydrophilicity of GO include the lateral size of the nanosheets and pH of the suspensions [133]. This is because these parameters determines the ionizability degree of the functional groups which affects the adsorption energy of the water molecules on GO surface and thus hydrophilicity [133].

2.2.3 Graphene Oxide fabrication methods

Various methods are currently being used to produce GO. Inherently, the quality of the GO differs owing to the different fabrication techniques and the precursor used [134]. Notably each fabrication approach has its own advantages and disadvantages, and modifications to improve method efficiency continue to be undertaken.

2.2.3.1 The Brodie Method

To fabricate GO via the Brodie method, graphite samples are first mixed with nitric acid (HNO₃) under continuous stirring at 0°C, usually in an ice bath to avoid agglomerations [65,135]. The quenching in the ice bath is followed by a slow addition of potassium chlorate (KClO₃) to the prepared mixture and stirred for about 18 hours at 0°C as well. KClO₃ is an oxidising agent and as such it incorporates the oxygenated functional groups onto the graphite inter planes. This enlarges the nanosheets inter-flake gap, which eases subsequent exfoliation. Special care has to be undertaken during the addition of KClO₃, as explosions are bound to occur due to the release of chlorine dioxide gas (ClO₂) [136]. Ionised water is added to the mixture after 18 hours of stirring. The mixture should be successively filtered under vacuum conditions until

a neutral pH in the filtrate is reached. The residue of the filtration process, which is graphite oxide powder, is then dried in vacuum at around 700°C and then sonicated in distilled water to obtain free flakes of GO [65,135].

2.2.3.2 *The Staudenmaier Method*

For the Staudenmaier method, graphite samples are first added to a mixture of concentrated H₂SO₄ and sodium nitrate HNO₃ [137]. This is done under cold conditions, usually in an ice bath. Successively, KClO₃ powder is added and the sample is left to quench for about 18 hours. The resultant solution is then washed in hydrochloric acid (HCl) to remove the formed sulphate ions followed by rinsing in distilled water until the pH of the sample is neutral. Here after it is dried overnight under vacuum conditions at 40°C [137]. The powder is then suspended in water and sonicated for a shorter period of about 30 minutes to exfoliate GO [138].

2.2.3.3 *Modified Hummers and Offerman's Method*

The modified Hummers method is a modification of the original Hummers' method which was initially employed to produce graphite oxide [139]. Graphite is first oxidised through the addition of H₂SO₄ in the presence of NaNO₃ at 0°C [140,141]. The oxidising agents enhance the formation of various oxygenated functional groups in the interlayer between the sheets in graphite. These weakens the van der Waals' forces connecting the graphene nanosheets in graphite and thus making exfoliation easier [139,142]. This is followed by adding potassium permanganate (KMnO₄) under constant stirring, which act as a catalyst to fasten the oxidation process under a 2-hour stirring. The mixture is then further stirred for a further 2-hour period at room temperature until a pasty brownish sample is observed. Hot water at around 96 °C is then added to further liquefy the sample [141]. Finally, to remove the excess of KMnO₄, hydrogen peroxide (H₂O₂) is slowly introduced to the mixture [143], which

is followed by centrifugation and rinsing in hydrochloric acid (HCl) to purify and collect the exfoliated GO via ultrasonication. The Modified Hummers' method is not only economical but also result in the production of highly oxygenated GO samples [144]. The fact that strong oxidising agents with high toxicity are entailed, is a limitation. The release of toxic gases such as nitrogen oxides (NO_x) is also a notable disadvantage [144]. Nonetheless, despite these limitations it is the widely employed method owing to its cost effectiveness and large-scale production.

Improvements to the Modified Hummers method in an attempt to produce a more environmentally friendly approach are continuing to be undertaken. For instance, Peng and co-workers substituted KMnO_4 and NaNO_3 with potassium ferrate (K_2FeO_4) to limit the production of toxic NO_x gases and the heavy metal pollutant Mn^{2+} waste that is generated by the original modified Hummers' method [145]. Their method entailed the reaction and stirring of a mixture of graphite, H_2SO_4 and the oxidising agent K_2FeO_4 at room temperature for an hour [145]. The purified precipitate of GO was then obtained by centrifuging the reacted mixture. However, iron (Fe) impurities in the resultant GO has been reported as a limitation to this modification [145].

2.2.3.4 Tang - Lau Method

Unlike the conventional top – down approaches starting with graphite, the Tang-Lau method is a newer bottom–up hydrothermal approach involving the use of glucose, sugar and fructose as reagents to grow GO nanosheets [146]. The basis of the method is the cyclic polymerisation of glucose by growing it on astatine (As) substrates. Glucose is dissolved in deionised water and then put under hydrothermal conditions, this result in the intermolecular dehydration of the glucose molecules, which causes the formation of planar GO nanosheets [146]. This physically grows the disentangled glucose bits to form GO [146].

The accumulated nanosheets are relatively hydrophobic, as such, they tend to float at the top of the dispersion. Dipping and lifting with As substrates is then undertaken followed by thorough rinsing prior to annealing at different temperatures (Figure 10).

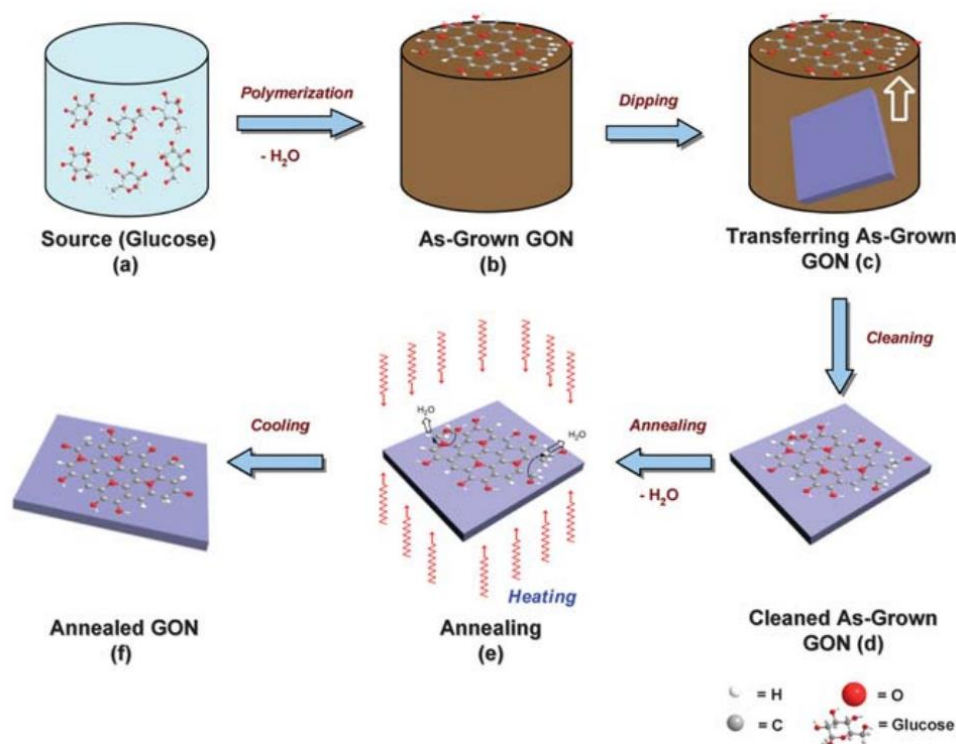


Figure 10. Procedural chronological growth of GO using the Tang-Lau method [146].

Most carbohydrates that have carbon: hydrogen: oxygen ratio of 1:2:1 can be used as raw materials (reagents) in this environmentally friendly fabrication process [146]. The merit to the method is that mass production of GO is easily attainable. It is however labour intensive as many synthesis stages are involved. Furthermore, lack of material purity is a further limitation to its implementation [146].

In most of the discussed preparatory methods, ultrasonication is undertaken and it is worth mentioning that apart from exfoliating the graphite oxide into GO nanosheets, the sonic waves also aid the suspension of GO into polar solvents. Other impacts like

onto the physicochemical characteristics of the nanosheets is further discussed in chapter 5.

2.2.3.5 The Tour Method

For the Tour method, KMnO_4 and graphite flakes are thoroughly mixed with H_2SO_4 and phosphoric acid (H_3PO_4) on a 9:1 ratio is added [140]. A thorough steering of the entities for about 12 hours at 50°C . follows this. The sample is then poured over deionised ice water followed by the addition of hydrogen peroxide (H_2O_2) and continuous stirring. This is filtered to remove the excess graphite to end with a solution of GO [140]. GO oxidation efficiency during fabrication is greatly increased in this regard [140]. Due to the omission of $\text{HNO}_3/\text{NaNO}_3$, the release of toxic NO_x gases is avoided, making it more environmentally friendly in comparison to the Modified Hummers method for instance [140].

2.2.4 Graphene oxide's potential applications

GO is a versatile material with promise in a wide range of applications from coating films, drug delivery materials to separation membranes as a result of its physicochemical characteristics [147].

For instance, its use in polymer nanocomposites as a nanofiller to enhance the mechanical and morphological properties of certain polymers is well reported [128,148,149]. The carboxyl, epoxides and hydroxyl functional groups help in facilitating the interaction between the GO nanofillers across the polymer matrix to enhance their properties [128]. Primary uses in nanoelectronics and related applications has also been reported [150], however in these applications it is usually reduced either thermally or chemically to recover electrical properties as aforementioned. Nonetheless, its use as a field effect transistors (FET) without

reduction has been noted [151]. Potential applications of GO in drug delivery systems in medicine have also been reported [152]. This stems out from the flexibility, two dimensionality and larger surface area of the material. Continual research in its use as a potential gas sensor precursor material owing to its 1-atom thick structure has been conveyed in the recent past-a-times [153]. For instance, its use in the detection of ethanol using optical fibre sensors is well noted [154].

Another emerging use of GO is as a water purification and desalination separation membrane material [45,155]. Its hydrophilicity and unique water pathways between its nanosheets offers ultrafast permeation and therefore makes GO a promising candidate in this area [45]. Henceforth, its potential as a separation membrane material, which is an area of interest in this doctoral research is discussed in detail in the latter sections of this chapter.

2.3 Separation membranes

2.3.1 Background and historical overview

Separation membranes date back to the 18th century from J. Abbe Nollet's initial investigations of the phenomenon of osmosis [156,157]. The first pressure based separations were carried out by Bechhold, who used paper and acetic acid collodion (nitrocellulose) to fabricate the first ultrafiltration membranes [158]. This paved a way to the major breakthrough by Loeb and Sourirajan, who fabricated the first controlled pore size membranes and asymmetric membranes [159].

The major mechanism of separation in operational conventional membranes is a physical filtration sieving (size exclusion) mechanism. Through size/molecular exclusion, different species are separated according to the relation between their size with respect to the membrane pore size [160]. With regard to size of their pores, the

separation membranes are classed from microfiltration, ultrafiltration, nanofiltration to reverse osmosis in accordance to the downward chronology of the membrane pore-size (Table 1) [161].

Another notable mechanism is the charge based Gibbs-Donnan effect, where separation is based on an electrostatic relation between charged solute and membrane charge [162,163]. However, this is mostly pronounced at the nanofiltration and reverse osmosis levels as that is where most of the particulates being separated, such as divalent and monovalent salts together with organic dyes, are charged [161].

Table 1. Filtration membranes and their respective sizes and a general comparative description of their separation mechanisms [161]

	Pore size (m)	Major separation mechanism	Entities separated	Limitations
Microfiltration	10^{-5} - 10^{-7}	Size exclusion (sieving)	Sand and clay particles. Green Algae and some bacteria	Limited separation range especially for smaller sized particles
Ultrafiltration	10^{-7} - 10^{-8}	Size exclusion	High MW Organic solids, bacteria and some viruses	Membrane susceptibility to fouling
Nanofiltration	10^{-8} - 10^{-10}	Size exclusion and the Donnan effect	Organic dyes, heavy metals and divalent salts	Relatively expensive and high membrane susceptibility to fouling
Reverse Osmosis	10^{-9} - 10^{-11}	Size exclusion and the Donnan effect	Organic dyes, heavy metals, divalent and	High operation costs High energy intensity

monovalent
salts

For GO based membranes, pore size is defined by the inter-flake gap between nanosheets. This is in the sub-nanometre range, and therefore the nanofiltration region is the area of interest in this study and for GO membranes.

Since their inception in 1980, the use of nanofiltration membranes has steadily increased [164], mainly because of their low energy consumptive nature and the wide scope of the species that can be separated. Furthermore, the properties of nanofiltration membranes, which overlap those of ultrafiltration and reverse osmosis, make them significantly versatile mounting to their reported wide usage and fabrication from a range of materials like polymers, ceramics and several metallic substrates [165,166].

The use of nanofiltration membranes has been widely noted in water desalination, purification and treatment [167]. Their use in the food industry for the treatment of whey effluents in dairy manufacturing has been reported [168]. Their use in these areas is strengthened by the fact that it is a non-destructive process that does not require any phase change [167].

As previously stated, separation basis of nanofiltration membranes is governed by sieve and electrostatic effects of the pores of the membranes (Table 2.1). The sieving separation happens when the molecular weight/hydrated diameter of the solutes being separated is larger than the pore sizes of the membranes or the maximum molecular weight cut-off (MWCO) [167]. However, in the case of charged solutes, separation can occur due to electrostatic repulsions, this is therefore governed by the charge relation between the particulates being separated and the membrane pores [169].

2.3.2 Graphene oxide as a nanofiltration/separation membrane material

The feasibility of GO as a water purification and desalination separation membrane material was first demonstrated in 2012 by Nair et al [45]. Unimpeded permeation of water through a micrometre thick GO membrane was observed in tandem with complete im-permeability to liquids, vapours, and gases including helium. The high-water permeability is attributed to both capillary driven force and low-friction flow of water between the GO nanosheets (*d*-spacing) [45].

The fast permeation of water molecules across the GO membranes is further advocated to the emergence of a high driving force (Δp) in the GO nanosheet channels with a driving capillary pressure of around 103 bar having been reported [45].

It is established that owing to the 2-dimensionality of the nanosheets, the permeation of water molecules across GO based membranes follows a tortuous route (Figure 11). Apart from the tortuous size exclusion-based separation mechanism, Donnan effect exclusion (electrostatic repulsions) also often occurs depending on the electrostatic nature of the species being separated (Figure 11) [170]. The incorporation of crosslinkers onto GO membranes aids these mechanisms in different ways, for instance in the case of size exclusion a constant pore size is maintained [53]. The chemistry and charge nature of the crosslinkers will also have an impact depending on the particulates being separated, repulsive or attractive separations can be observed.

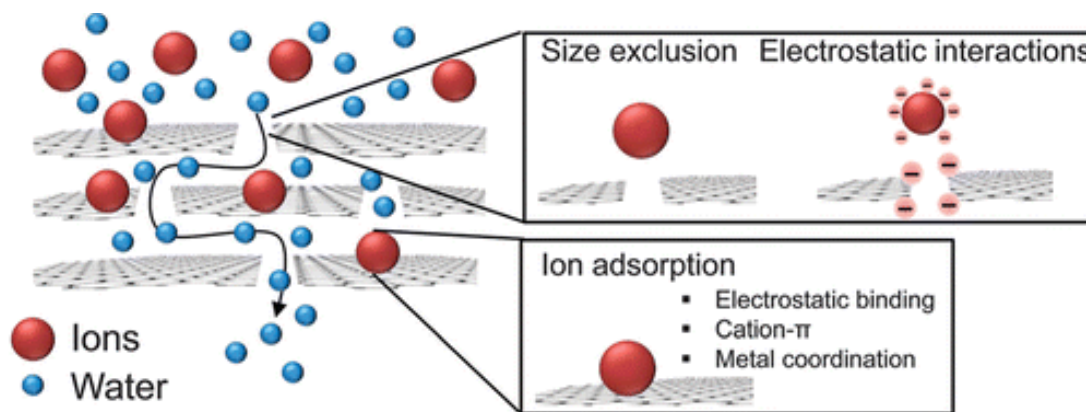


Figure 11. The tortuous path flow of water molecules across a GO membrane and additional GO separation mechanisms' illustrative schematic [170]

It is also significant to note that depending on the particulates, other separation mechanisms like $\pi - \pi$ and cation - π interactions can exist depending on the chemical structure of the solutes [171]. For instance, the $\pi - \pi$ interactions separation is especially applicable in organic dyes such as methylene blue, and methyl orange, which all in their chemical structure have an aromatic benzoic ring [171].

In spite of the plausibility of other separation mechanisms, the most significant feature of GO based membranes is the d -spacing as demonstrated in further experimentation by the Nair group. It was observed that when GO membranes are annealed at 250°C in a hydrogen-argon atmosphere, the d -spacing decreased from around 10Å to 4Å, causing a more than 100 times reduction in water permeation across the membranes [45,172].

2.3.4 Limitations of graphene oxide as a separation membrane material

The major challenge in the use of GO as a separation membrane for water purification has been outlined to be the swelling of the membrane during nanofiltration [173]. This causes the enlargement of the pore-gap as water molecules are entrapped by the hydrophilic oxygenated functional groups [46,47]. Furthermore, re-

dispersion/disentanglement of GO membranes in water during and post membrane operation has been noted as a major limitation [55,173]. Fine-tuning and fixing this inter-flake gap is thus of high significance in enhancing both aqueous stability and overtime performance of GO membranes [46,53].

2.3.3 Graphene oxide-based membrane fabrication methods

The fabrication techniques entailed impact membrane morphology and structural quality hence overall performance [55]. The existing various methods also have notable differences in terms of material usage and fabrication procedure. Respective established fabrication ways are hereby discussed;

2.3.3.1 Vacuum filtration

To fabricate the membranes via the vacuum filtration method, a GO suspension is filtrated over a substrate. Vacuum suction is used to instigate a pressure difference to assemble GO nanosheets onto the substrate as the solvent is filtrated across (Figure 12) [174,175]. To have membranes with good homogeneity, a well dispersed suspension is required [176]. The facile nature of this method validates its common use in fabricating GO based membranes [125].

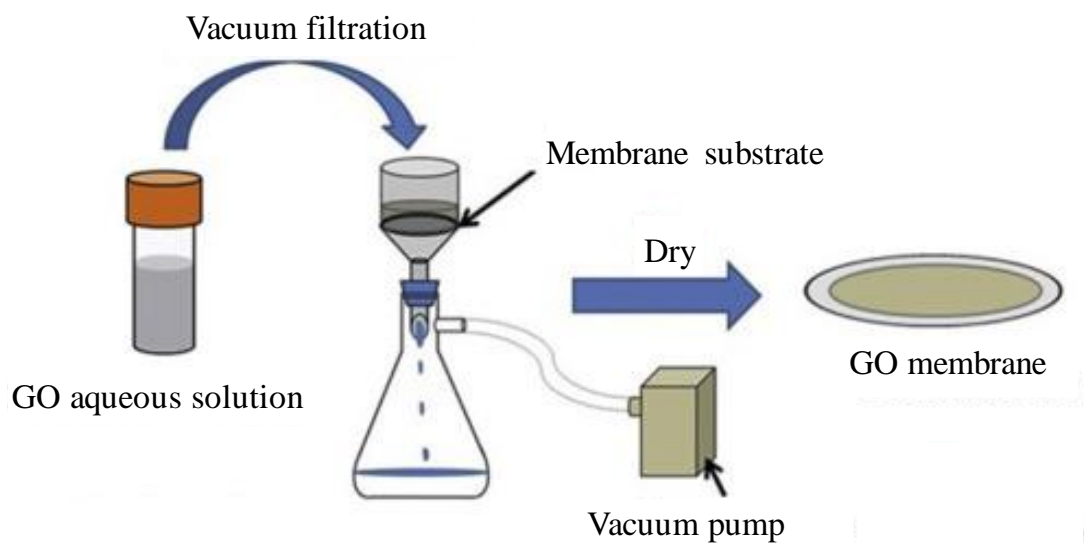


Figure 12. *Vacuum filtration membrane fabrication schematic* [177]

However, despite the method's wide use, fragility of the membranes when exfoliated from the substrate is a reported limitation [178]. Furthermore, difficulty in precise control of membrane homogeneity and thickness are major drawbacks to vacuum and pressure assisted filtration methods [179]. Mi *et al.* further highlighted that GO membranes fabricated in this way tends to disintegrate in aqueous environments during operation owing to the hydrophilicity of the GO nanosheets and poor membrane intactness [155].

2.3.3.2 Spin, Spray and Dip Coating

In the case of spin coating, the process commences with the introduction of a GO dispersion droplet followed by rotation of the substrate at high speeds to assemble the film/membranes via the centrifugation force (see schematic in Figure 13A) [180]. Membrane characteristics like thickness are controlled by varying the volume of the droplet introduced and the rotational speed [181,182].

Similarly, for spray coating the GO dispersion is spurted onto the substrate using a spray gun (Figure 13B) [183]. The thickness and physicochemical characteristics of membranes fabricated via this method are controlled by changing spray volume and the distance between the nozzle and the substrate [183,184].

Dip coating akin to its name entails repeated immersion of respective substrates in suspensions to fabricate GO based membranes [185]. Specifically, to assemble membranes on substrates, they are dipped in suspension material and a thin layer of the membrane self assembles during immersion and withdrawal stage [185]. Dipping time, immersion and withdrawal speeds together with the number of assembly cycles are key variables in controlling membrane thickness and physicochemical properties

via this method [186,187]. For instance, to fabricate membranes with higher thickness longer immersion times and more assembly cycles are entailed while the contrary for thinner membranes [188].

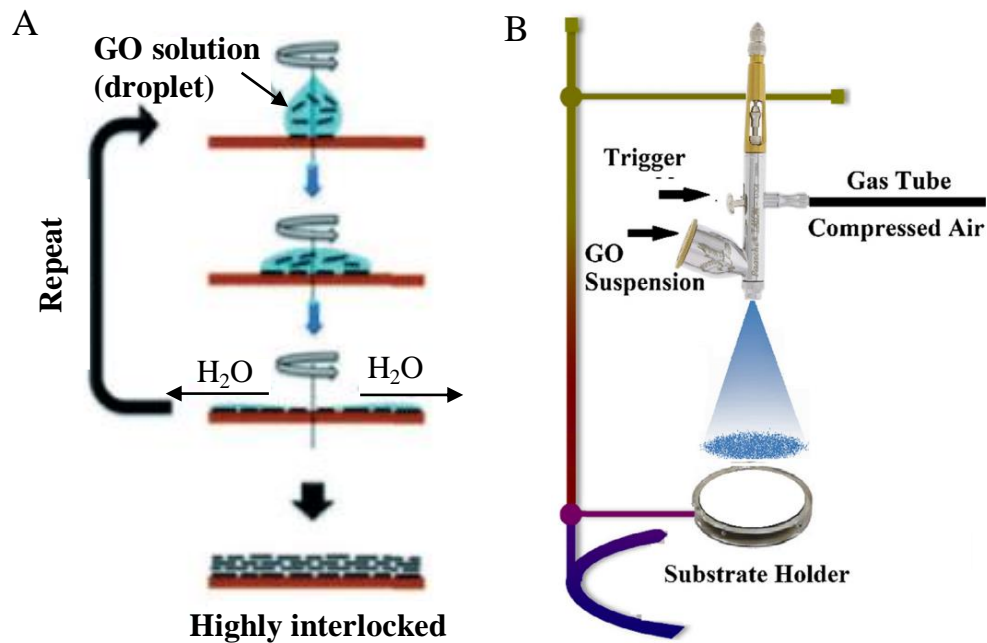


Figure 13. Illustrative fabrication schematic of the A) spin coating and B) the spray coating methods [183,189].

2.3.3.3 Layer by layer self-assembly

Developed in the 1960's by Iler [52], the layer by layer method is based on an interchangeable attachment of two or more materials either electrostatically, covalently or otherwise. Material interconnections via other chemical forces like the van der Waals forces, halogen and hydrogen bonding are also plausible [155,190].

In the case of electrostatic interactions, the negatively charged GO suspensions at lower pH values and room temperature and pressure in aqueous environments are usually interconnected alternatively with positively charged compounds and polymers

[52,191]. The GO nanosheets can be activated to have opposite charges for an electrostatic based assembly as it was the case when Shen *et al.* activated GO with acrylic acid (negatively charged) and acryl amine (positively charged) [192]. Similarly, Choi *et al.* also prepared aminated GO through the reaction of a GO dispersion and ethylenediamine (EDA) in the presence of a coupling agent the 1-(3-dimethylaminopropyl)-3-ethylcarbodiimide methiodide (EDC) to enhance amide formation in GO. The aminated GO, which is positively charged, was then used on a layer by layer basis with untreated negatively charged GO to fabricate electrostatically layer by layer assembled GO membranes [193].

In the case of covalent interactions, the oxygenated functional groups in GO chemically react with respective functional groups in the interconnecting agents forming covalent bonds at each interface. For instance, Hu *et al.* successfully interconnected GO nanosheets and 1, 3, 5-benzenetricarbonyl trichloride (TMC) via the carboxylate groups in GO and the carbonyl chloride in TMC to fabricate layer by layer assembled membranes [194].

The layer-by-layer assembly method is facilitated in several ways. These range from dip (immersion), spin, spray coating electromagnetic interactions assisted fabrications [195]. However, the commonly used offshoot is the dip-assisted layer-by-layer assembly.

A notable advantage of the dip assisted layer by layer assembly is that it is a very cost effective method with high material efficiency [194]. The method also offers ease of control of key membrane characteristics like thickness through altering fabrication conditions, especially the immersion time and the number of assembly cycles [196].

Given the interfacial interconnection of the materials via this method, crosslinked membranes with enhanced stability can be fabricated.

2.3.5 Recent improvements in the use of graphene oxide as a separation membrane material

As aforementioned, the major limitation to the use of GO as a separation membrane material is the widening of the membrane pore-gap during operation, in consequence, several attempts are being undertaken in order to enhance the stability of these membranes. For instance, Xu *et al.* incorporated cationic tetrakis(1-methylpyridinium-4-yl)porphyrin (TMPyP) onto vacuum filtrated GO based membranes to enhance their stability by holding the nanosheets together (Figure 14) [197]. Crosslinking GO membranes in this manner was facilitated by $\pi - \pi$ interactions between GO and TMPyP. Membrane performance in terms of the rejection of Na_2SO_4 solute increased from 58.0% to 86.7% with crosslinking owing to aqueous stability enhancement.

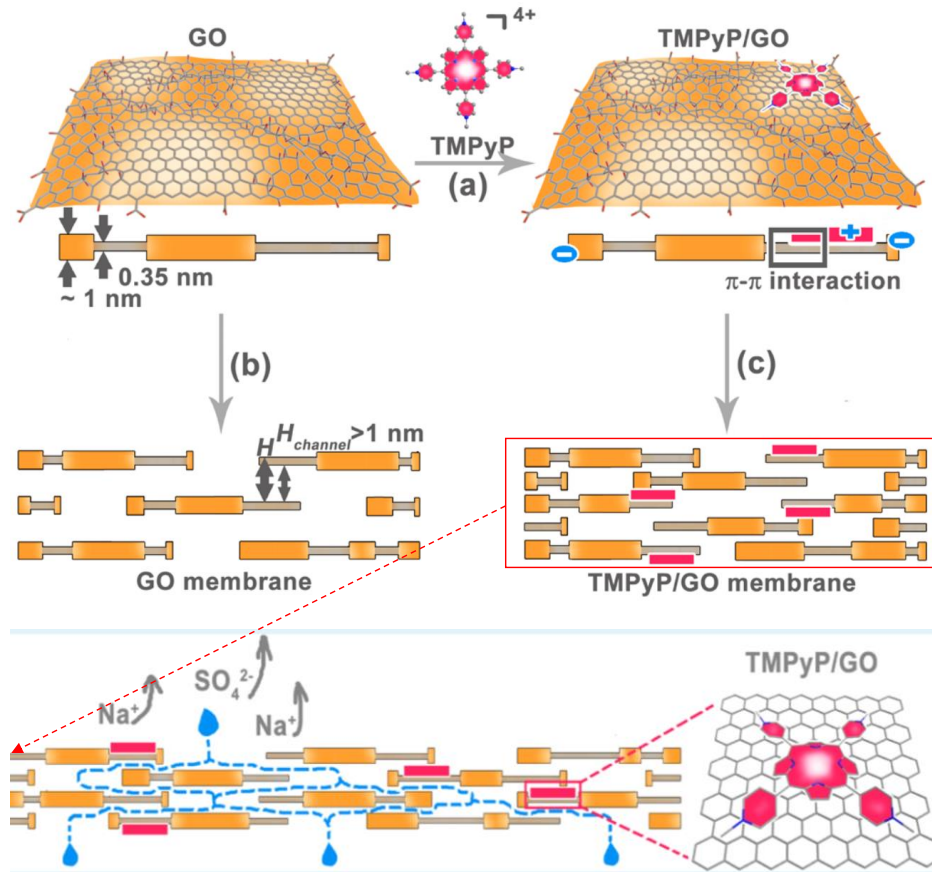


Figure 14. Illustrative schematic showing the uncrosslinked GO membranes and those crosslinked by TMPyP [197].

In other works, Cheng-Ning *et al.* enhanced GO membrane stability and intactness by using Anodised Aluminium Oxide (AAO) as substrates [198]. In this work, GO suspension was filtrated through porous AAO substrates to fabricate membranes with improved stability. The aluminium ions (Al^{3+}) enhanced the stability of the membranes through cationic electrostatic crosslinking [198]. The impact of the AAO substrates in improving GO membrane intactness was evident especially in comparison to other substrates like Teflon where overtime disintegration was observed (Figure 15).

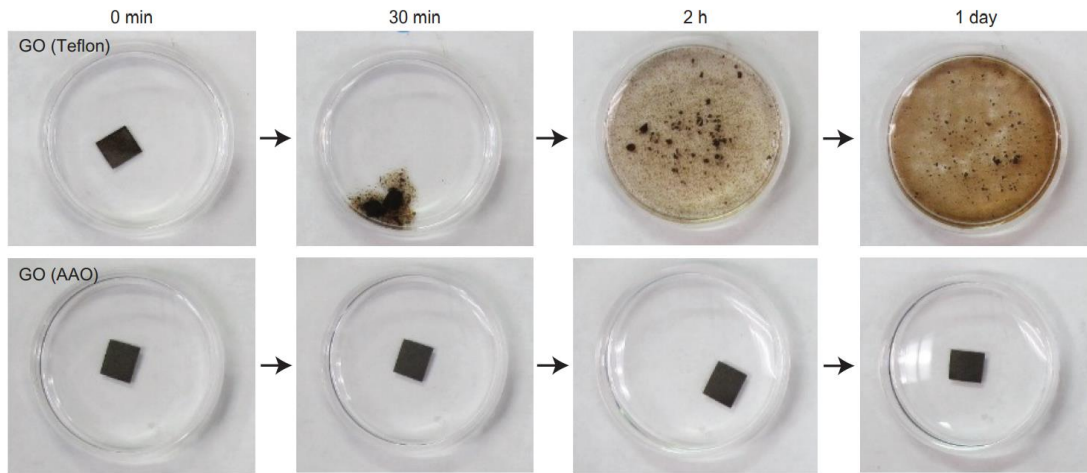


Figure 15. Change in the intactness of the GO membranes under different substrates signifying the enhancement stability and intactness by AAO [198]

Abraham *et al.* in a recent study used an epoxy encapsulant to physically confine the GO nanosheets, fine-tuning the pore-gap size for water purification and desalination applications (Figure 16) [51]. In this work, GO nanosheet with a sub-nanometer sized d-spacing was embedded in sty-cast epoxy to prevent the widening of the membrane pore-gap in aqueous environments. Notably, excellent NaCl rejections at about 97% was achieved [51]. Despite the promise of physical confinement as an improvement method, lack of upscaling of the method to mass production has been noted as a significant limitation to the implementation of the approach [51].

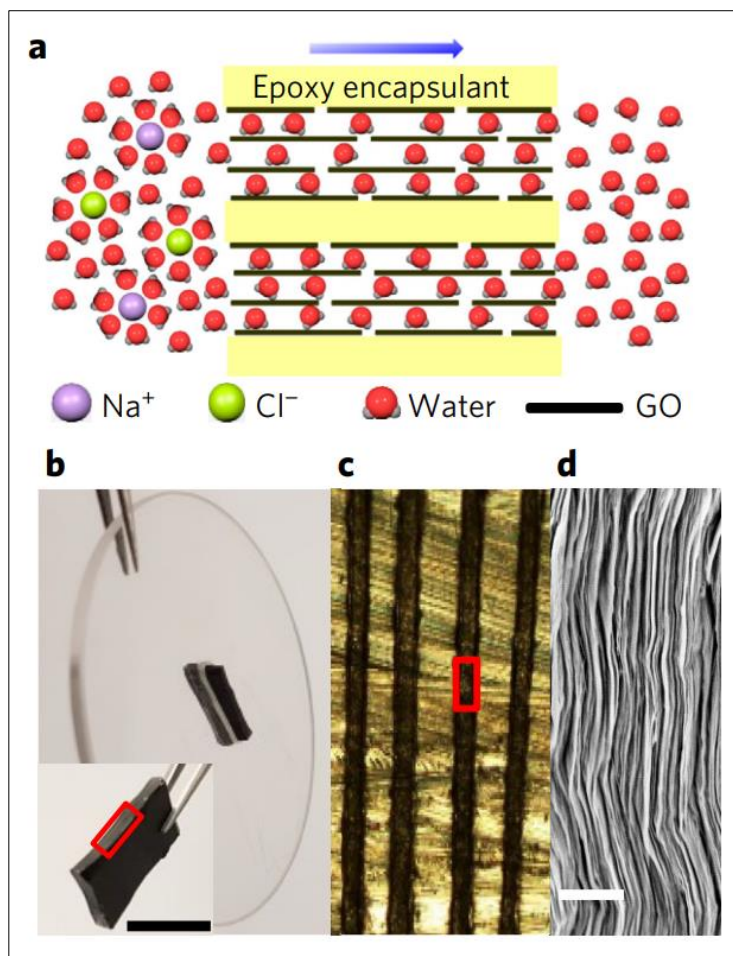


Figure 16. Schematic illustrating the use of the epoxy encapsulant to physically confine the GO nanosheets [51].

Elsewhere, sporadic attempts to limit the enlargement of the GO membrane pore gap during operation were in using chemically and thermally reduced GO [48,199]. Chemical reduction of GO is commonly done using hydrazine in an alkaline aqueous medium [48]. More environmentally friendly reducing agents such as vitamin C are now emerging as equitable substitute to the highly toxic hydrazine [200]. Thermal reduction on the other hand is done at temperatures in excess of 350°C [201]. Both thermal and chemical reduction of GO are done in lieu of the fact that the presence of oxygenated functional groups is responsible for pore-gap widening. Henceforth, their removal can alleviate this fundamental problem in GO membranes. Despite successful

improvement in membrane performance in the rejection of Na_2SO_4 , Gao *et al.* observed that the reduced nanosheets tends to aggregate overtime, their hydrophilicity and antifouling properties are also compromised [202]. Moreover, the removal of the oxygenated functional groups also narrows down the d-spacing in GO membranes [45]. This decreases the permeability across the membranes and therefore a high operating pressure will be required which is tantamount to higher operation costs [199].

Other attempts include the use of chemical compounds to interconnect the GO membranes via both covalent and electrostatic interactions. For instance, Hung *et al.* recently used diamines to fabricate crosslinked GO membranes with enhanced aqueous stability via the vacuum filtration method [53]. In another study, Nan *et al.* also incorporated polyethyleneimine polymers to fabricate electrostatically crosslinked GO membranes, which were evaluated for the removal of di-valent salts [191]. The successful demonstration of the use of the stated crosslinkers opens a pool of a variety of compounds that can be used and therefore an increasingly interesting way to economically fabricate improved GO membranes with good stability.

2.4 Review Conclusions

In summary, comparative analysis of the properties of graphene and GO highlights the superiority of graphene over GO, especially regarding mechanical and electrical properties.

However, in spite of it not being mechanically as strong as graphene, GO can be cost effectively produced. Most importantly, in nanofiltration GO based membranes offers a unique ultrafast water flow between the nanosheets. This flow is responsible for a higher permeation flux across the membrane without the need to instigate sub-

nanometre pore sizes for separation. Its high hydrophilicity is also another notable advantage in using GO. These key advantages of GO over graphene makes it an equitable alternative to graphene especially in water purification, hence its selection as the material to use in this doctoral thesis.

Regardless of its high plausibility as a next generation separation membrane material, there are still major challenges in using GO as a separation membrane, which include the widening of the membrane pore sizes in aqueous environments. Another limitation that requires improvement is poor membrane stability, which causes both membrane disentanglement during cross flow operation and the cracking infused by drying. This brings a problem of lack of membrane reusability, which ought to be instigated.

Several attempts are continuing to be carried out to improve the performance of GO membranes. The use of chemical species in crosslinking is one of the promising methods as it can be done in an economic way and there is also a variety of many compounds that can used. Different mechanisms of interactions from covalent and electrostatic are plausible. Systematic incorporation of the crosslinkers with an easily scalable fabrication technique that offers ease of operation and material efficiency is a necessity. Among the discussed methods, the dip-assisted layer by layer is one of the methods that offers this.

3.

THE FABRICATION OF CONTROLLED THICKNESS CROSSLINKED GRAPHENE OXIDE THIN FILMS; SYSTEMATIC CONTROL OF SIGNIFICANT CHARACTERISTICS

“I like the science spirit, the holding off, the being sure but not very sure, the willingness to surrender ideas when the evidence is against them: this is ultimately fine, it always keeps the way beyond open, always gives life, thought, affection, the whole man a chance to try over after a mistake, after a wrong guess.”

WALT WHITMAN (1819-1892)

1

3.1 Introduction

The performance efficiency of graphene oxide (GO) based films and coatings, including separation membranes, is governed by significant characteristics, such as thickness, morphology and hydrophilicity [203,204]. As such, having the ability to control these characteristics during product fabrication is of high importance. The

-
- Parts of this chapter have been peer-reviewed and published in the Progress in Organic Coatings Journal: **Kandjou V**, Hernaez M, Acevedo B, Melendi-Espina S, Interfacial crosslinked controlled thickness graphene oxide thin films by means of dip-assisted layer by layer assembly, *Progress in Organic Coatings Journal* 137 (2019) 105345, doi:10.1016/j.porgcoat.2019.105345
 - Parts of the work in this chapter were also presented at the World Conference on Carbon in Madrid, Spain, 2018: **Kandjou V**, Hernaez M, Mayes A.G, Acevedo B, Perez-Mas A. and Melendi-Espina S, “The fabrication of controlled thickness graphene oxide thin films by means of dip-assisted layer by layer assembly”, **Oral Presentation**, Abstract No. 0649
 - Parts of the work in this chapter were also presented at the World Conference on Carbon in Melbourne, Australia, 2017: Sanchez P, **Kandjou V**, Hernaez M, Zamarreño F, Arregui C.R, Mayes A.G, and Melendi-Espina S., “Graphene oxide film fabrication with controlled thickness on silicon-based substrates”, **Poster Presentation**, Abstract No 144.

overarching aim of the work explained in this thesis is to fabricate cost-effective GO nanofiltration membranes with enhanced performance for contaminants removal.

In this context, it is essential to develop, comprehensively study and optimise a method to fabricate thin-films with controlled characteristics, such as thickness and morphology. This would enable relevant fine-tuning modifications to enhance the performance of the products' intended applications. Importantly, successful thin-film fabrication and control of key characteristics enable their wide use in further different applications [154,205], hence the significance of this chapter beyond nanofiltration membrane fabrication. In this first part of the research, affordable glass-slides have been used as substrates for the deposition of the thin-films.

Different thin-film fabrication methods have been discussed in the literature [206]. The methods fall into two classes: chemical and physical deposition techniques [207]. With regard to the physical deposition techniques, thin films are fabricated through the conversion of materials from a condensed state to a vapour phase and then back to a thin-film condensed phase [208]. Examples of these physical deposition methods include sputtering and thermal evaporation [209,210]. Sputter deposition entails the ejection of a film fabrication material from a source of the film material to a substrate on which the thin film is assembled [211]. A self-sustaining plasma is generated from an electrically energised cathode. The gaseous atoms lose their electrons within the plasma to become positively charged [211]. They are then accelerated toward the target material from which they sputter the molecules or atoms that strike the substrate to form a thin film [211]. However, high kinetic energy of atoms during sputtering is known to cause damage to substrates and also nucleation of molecules resulting in poor film homogeneity [212].

In the evaporation technique, the source material is thermally evaporated in a vacuum to reassemble on the substrate, where it condenses to form a thin film [213]. A noted disadvantage of this method has been that gaseous contaminants are also activated in the plasma, and their incorporation in the film results in film contamination [214].

The chemical solution deposition techniques, on the other hand, are ex-situ methods where solutions are self-assembled onto substrates to form thin films [215]. The use of solution-based precursors makes these techniques relatively cost effective in comparison with the physical deposition techniques [216,217]. The most commonly used chemical deposition techniques include spray, spin, dip coating and layer-by-layer assembly [218].

To fabricate thin films via spin coating, material droplets are deposited onto a substrate, which is rotationally accelerated to a desired rate [180]. High rotational speed leads to film deposition due to the centrifugal force as the solvent is dispersed along the substrate [180,219]. Significant thin-film characteristics such as thickness are controlled by changing the rotational speed, surface tension and droplet viscosity [181,182]. In spray coating, suspensions of the thin-film fabrication material are sprayed onto the substrate using a spray gun [183]. The thickness of the thin films produced by this method is controlled by various parameters including the spray volume, solvent evaporation rate and the distance between the nozzle and the substrate [183,184]. Dip-coating, in contrast, entails assembly of thin films through immersion and withdrawal of substrates into and out of suspensions/coating media [185]. In this case, fundamental thin-film characteristics such as thickness are controlled through changing various parameters, such as the dipping time and number of assembly cycles [186,187].

Though the aforementioned chemical solution deposition techniques are readily used, specific drawbacks are notable for each method. For instance, in spin-coating, it is challenging to spin large substrates at sufficiently high rate to fine tune the film thickness [220]. Lack of efficient use of the material has been noted as the biggest disadvantage of the spin-coating deposition method [220]. With regard to spray coating, low thin-film homogeneity has been reported as a major downside [221].

Comparatively, the development of thin films via the layer-by-layer method has garnered considerable interest since initial development in the 1960s [52]. Layer-by-layer assembly entails the interchangeable attachment of two or more materials to the substrate to fabricate systematically intercalated structures [52,222]. Interchangeable film fabrication in this manner is aided by the combination of different processes, from immersion (dip-coating) to spray coating or spin coating, to assist in the layer-by-layer deposition [195]. Offshoots of various layer-by-layer techniques such as dip-assisted and spin-assisted layer-by-layer assemblies are well known [223].

Layer-by-layer assembly offers precise control over thicknesses at the nanometre level [195]. The availability of an extensive variety of materials and the ability to use different substrates are also significant advantages [195]. This means that thin films for various applications from optics, membranes and energy to biomedicine can be engineered easily through use of this method [196]. Furthermore, the physicochemical properties of the thin films can be altered easily with the layer-by-layer methods, which ultimately has an impact on the efficiency of their intended performance [196].

Though different techniques can be used for layer-by-layer assembly, the dip-assisted layer-by-layer fabrication method is favoured for uniformity, good alignment and ease of control of the thin-film thickness at low levels of material usage [59]. Simplicity of operation and ease of scale-up to mass production are further advantages of the method

[224]. The method further offers systematic interconnection of GO nanosheets to enhance structural stability and intactness, a significance in GO nanofiltration membranes [198].

These were primary reasons why, in the work described in this thesis, the dip-assisted layer-by-layer deposition was chosen over other thin-film/membrane fabrication methods. As an offshoot of the dip-coating method, key parameters in controlling thin-film thickness include the alteration of the immersion time, the immersion/withdrawal speed and the number of assembly cycles [225]. The nature and size of deposited materials used during fabrication also determine the step control of thickness and other characteristics, such as material hydrophilicity [195].

In this regard, different-sized crosslinkers that contained amine groups were selected to fabricate crosslinked thin films of controlled thicknesses. These crosslinkers were p-phenylenediamine (PPD), 1, 3, 5-Triazine-2, 4, 6-triamine (melamine) (MLM) and polyethyleneimine (PEI) as previously stated in the introduction (Figure 1). Due to the presence of the nucleophilic amine groups, the selected crosslinkers are in theory highly reactive [226]. Therefore, GO is likely to interact strongly with the crosslinkers due to the presence of oxygenated functionalities within it. However, the nature of the interactions between each of the crosslinkers and GO needed to be established. The compounds that contained small molecules (PPD and MLM) relative to those in PEI were selected in order to control the film thickness at smaller quanta than would be possible with branched PEI [227–229]. In order to produce a broad range of thin-film thicknesses, the relatively large-sized, branched polymer-based PEI was selected.

In summary, the work described in this chapter laid a foundation for the fabrication of crosslinked nanofiltration membranes through; firstly, determination of the interaction between GO and each of the crosslinkers; and, second, demonstration of the ease of

control of key membrane characteristics such as thickness, continuity coverage and hydrophilicity. The correlations between immersion times, number of bi-layers and the significant thin-film characteristics listed above were also demonstrated.

3.2 Experimental Section

3.2.1 Materials

GO powder (product code C889/GOB151/Pw) was commercially sourced from Graphenea Co. in Gipuzkoa, Spain. The selected crosslinkers were all purchased from Sigma-Aldrich, Haverhill, UK. PPD (99 % purity, product code: P6001) in granules form was ground in a pestle and mortar to aid its rate of dissolution during solution preparation; MLM powder (99% purity, product code: M2659) and 50% aqueous solution of PEI (product code: 03880) were used as purchased.

The crosslinked films were fabricated on glass-slide substrates (CAT.NO.7101, 1.0-1.2mm thick) obtained from Fisher Scientific (Loughborough, UK). A solution of 1M potassium hydroxide (KOH) was prepared from KOH powder (product code: P/5640/53) and used for substrate pre-treatment prior to thin-film fabrication. The powder was also purchased from Fisher Scientific (Loughborough, UK).

3.2.2 Study of interactions between GO and the crosslinkers

Prior to thin-film fabrication, it was significant to confirm the presence of notable functional groups in GO and the crosslinkers and to determine the predominant nature/mechanism of the interaction between them.

A 0.5 mg/ml aqueous GO suspension was prepared and 2.0 mg/ml PPD, MLM and PEI aqueous solutions were made. The anchor concentrations were selected based on literature results regarding the fabrication of layer-by-layer crosslinked membranes

[191,230]. Good solution solubility and suspension stability at these concentrations has been noted in literature with other solvents [231,232].

Following preparation of the GO suspension and crosslinker solutions, each crosslinker was reacted separately with GO at a 1:1 ratio for 1 minute and 5 minutes. These times were chosen as they were also the selected immersion times for the fabrication of the thin films via the dip assisted layer-by-layer technique later on. Further details on the deposition process are found in the following section 3.2.3.

To react GO with the crosslinkers for the designated times, a pH switch was used to control the reaction time through the addition of 99 % sulphuric acid (H_2SO_4) (product code: 07208, Sigma-Aldrich, UK). The reaction with H_2SO_4 resulted in the protonation of the reacting entities, which rendered them unreactive at addition [233,234]. Centrifugation of the reacted samples was then undertaken using a Bio-fuge Primo Heraeus centrifuge for 10 minutes at 6000 rpm with thorough rinsing. Rinsing was performed through a repetitive replacement of the supernatant with distilled water, shaking and re-centrifuging to remove the unreacted crosslinker and GO excess material.

The centrifuge residue samples were then collected for characterisation through Fourier Transform Infra-Red (FTIR) spectroscopy (ATR-FTIR PerkinElmer) and X-ray Photoelectron Spectroscopy (XPS) (Kratos Ultra-DLD XPS System (K-Alpha+)) to confirm the functional groups present and to verify GO-crosslinker interactions.

For the XPS characterisations, first a wide-scan spectrum in the binding energy range of 0–1000 eV was obtained to identify the functional groups present and their relative abundance in the prepared samples. A curve fitting of the carbon (C1s) spectra was then undertaken using a Gaussian- Lorentzian peak shape, after performing a Shirley

background correction. The major peaks for the C1s curve were seen for the C graphitic (binding energy (BE) = 284.3–284.4 eV), C-O epoxide/C-OH hydroxyl (BE = 285.6–285.7 eV), C=O carbonyl (BE = 286.9–287.0 eV), as well as the COOH carboxyl groups (BE = 288.9 eV). It is worth noting that at some binding energies, there is an overlap of oxygen and nitrogen functionalities, specifically between C(epoxy) and C=N, and between C=O and C-N [235,236]. Furthermore, there was a π - π^* shake-up signal (290.8 eV) that is typical for sp^2 -hybridised carbon [123].

3.2.3 Thin-film fabrication procedure

To fabricate the GO – crosslinked films, cleaned glass-slide substrates were first pre-treated by hydroxylation through immersion in 1M KOH for 30 minutes to accumulate a negative charge on the slides surface through the build-up of hydroxyl groups [237]. The slides were then thoroughly rinsed with deionised water to remove excess unattached KOH, and subsequently dried. The hydroxylated slides were then immersed in 2.0 mg/ml PEI, which is positively charged [191], for 5 minutes in order to instigate build-up of a positive charge on the glass slides electrostatically [191]. The PEI-treated glass slides were then rinsed in deionised water and dried before dip-assisted layer-by-layer assembly, which commenced with immersion in the negatively charged GO suspension.

Before commencing the fabrication, the 0.5 mg/ml suspension of the GO nanosheets was sonicated during 2 hours in an ultrasonic bath (Ultrawave Ltd, 50-60 Hz). Sonification enhances the suspension by application of acoustic energy to disrupt the formation of agglomerates [238].

A rotary dip-coater device (Nadotech Innovations, Spain) (ND-R 11/2, S/N: 522016) (Figure 17) was used to assemble the thin films. The coater was operated on an automated

interchangeable dipping basis between GO and the crosslinkers using the programmable ND-DC software to assemble all the thin films consistently.

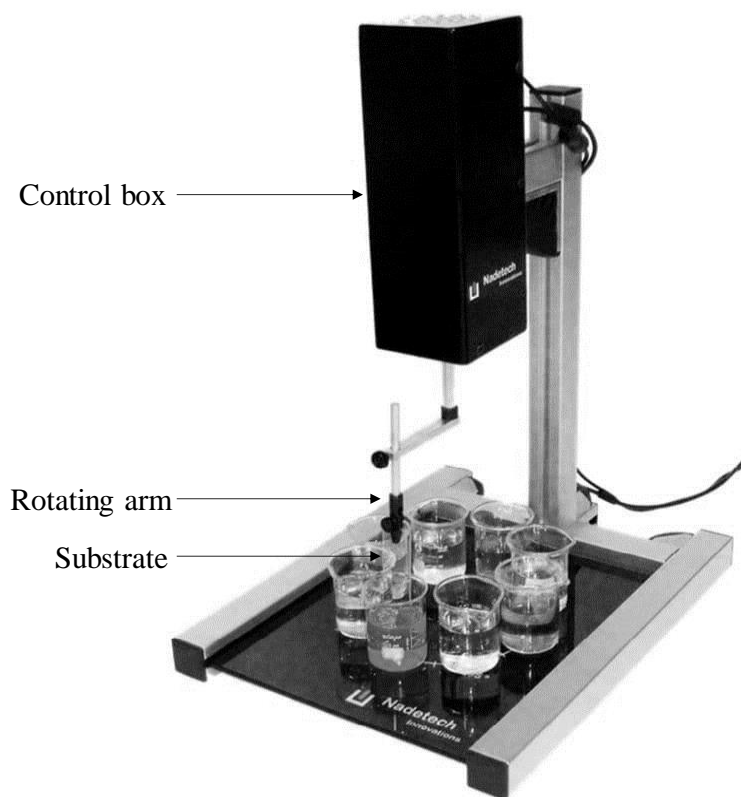


Figure 17. Nadetech Innovations dip-coater (S/N: 522033)

To perform the interchangeable immersion, the glass slides were rinsed in deionised water and dried prior to each immersion in either GO or the crosslinker (see schematic diagram of fabrication in Figure 18).

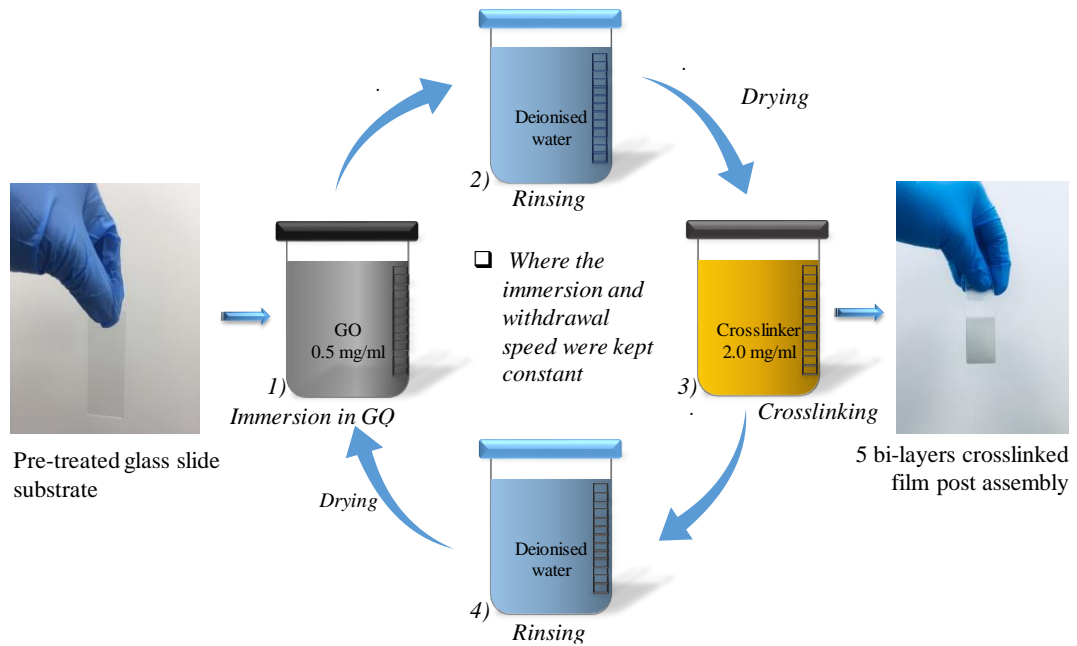


Figure 18. Schematic diagram of dip-assisted layer-by-layer fabrication technique

The films were fabricated in increasing numbers of assembly cycles (bi-layers) in order to determine the dependence of thickness on bi-layers. The cycles were set to produce 1, 5, 10 and 20 bi-layers, and at 1-minute and 5-minute immersion times. From previous experience, it was known that good material accumulation at each assembly stage was achieved at 2400 mm/min immersion and withdrawal speed [239,240]. The fabricated films were then labelled accordingly (see nomenclature in Table 2).

Table 2. *Nomenclature of the fabricated films at different immersion times and numbers of bi-layers*

Immersion time (mins)	Number of bi-layers			
	1	5	10	20
1	GO-X-1'1	GO-X-1'5	GO-X-1'10	GO-X-1'20
5	GO-X-5'1	GO-X-5'5	GO-X-5'10	GO-X-5'20

Where X is PPD, MLM or PEI

3.2.4 Post-film fabrication characterisations

A FEI NOVA NanoSEM450 Scanning Electron Microscope (SEM) was used to determine the coverage and continuity of the fabricated crosslinked thin films. The films on glass-slide substrates were cut into 1 cm² squares to fit in the characterisation chambers. The sputtering of a platinum coat using a high-resolution platinum sputter coater (CC7640 Quorum Technologies Gold Coater) enhanced the resolution of the images during characterisation.

The changes in thickness of the crosslinked thin films that corresponded with increased immersion times and numbers of assembly cycles were evaluated with the aid of a Bruker DektakXT Profiling System (Stylus Profiler). A razor cut was made in each of the thin films before scanning to determine an average thickness from 10 measurements. The standard deviation of each of the calculated averaged thicknesses was duly calculated and noted as error bars.

Similarly, the change in thin-film hydrophilicity with immersion time and the number of assembly cycles was determined by the measurement of water contact angles through introducing an approximately 3 ml pure water droplets. A DMK 31BF03 camera was used to record the contact images and the angles were processed by image

j software (1.50i/ Java 1.6.0) (Public Domain, BSD-2). The reliability of these characterisations was enhanced by taking an average of 10 measurements, which were made through the introduction of pure water droplets in different positions on the thin films and noting the standard deviation accordingly.

3.3 Results and Discussion

3.3.1 Nature of interaction between GO and the crosslinkers

The proof and nature of interaction between GO and each of the crosslinkers prior to thin-film fabrication is a significant step. This is because sufficient interaction between GO and the crosslinkers is a necessity for intra(horizontal) and inter(vertical) sheet crosslinking and hence thin-film assembly [241]. FTIR and XPS characterisation results that confirmed GO-crosslinker interactions are thus presented here.

First the presence of various oxygenated functional groups in GO is confirmed through XPS characterisations (Figure 19). For instance, the presence of hydroxyl (-OH) is verified by the observation of the absorption band at around 3340 cm^{-1} , while the presence of the ketone, carboxylic and/or ester groups (-C=O) is substantiated by the observed band at 1726 cm^{-1} (Figure 19) [140,242–245]. The peak at 1616 cm^{-1} corresponds to C=C stretching vibrations and the band at 1060 cm^{-1} can be assigned to C-O (epoxy) groups [227].

Regarding the molecular crosslinkers PPD and MLM, the most significant functional groups present in their spectra are related to amine groups. Three bands that occur between 3400 cm^{-1} and 3000 cm^{-1} in the spectra of these crosslinkers indicate the presence of primary amines [246–248] (Figure 19). In the case of MLM, however, similar bands at around 3460 cm^{-1} and 3580 cm^{-1} can be assigned to the -N-H symmetric and asymmetric stretching respectively [249]. Additionally, the spectra

bands observed at around 1630 cm^{-1} and 1516 cm^{-1} have been previously correlated with -N-H deforming vibrations [250,251]. Finally, the band at 1250 cm^{-1} identifies the occurrence of -C-N bonds in aromatic amines such as PPD [246,252], while in MLM, the band at 1418 cm^{-1} corresponds to its triazine ring [249]. The out-of-plane bending of the 1,3,5-s-triazine ring is presented by the absorption band that is observed at around 810 cm^{-1} (Figure 19) [253]. An -NH_2 deformation band in the MLM spectrum is also identifiable at 1653 cm^{-1} [253].

When looking at the reacted entities (GO-PPD and GO-MLM) spectra, it is observed that the characteristic triplet of primary amines in the $3400\text{-}3000\text{ cm}^{-1}$ region disappears after the 1-minute and 5-minute reaction times (Figure 19). A small but clear peak at 1510 cm^{-1} that can be assigned to the -N-H bend is observed in these spectra [248,251]. These findings suggest the existence of secondary amines [248], which consequently points to the occurrence of an epoxy ring opening reaction between GO-PPD and GO-MLM at both reaction times (see schematic in Figure 20).

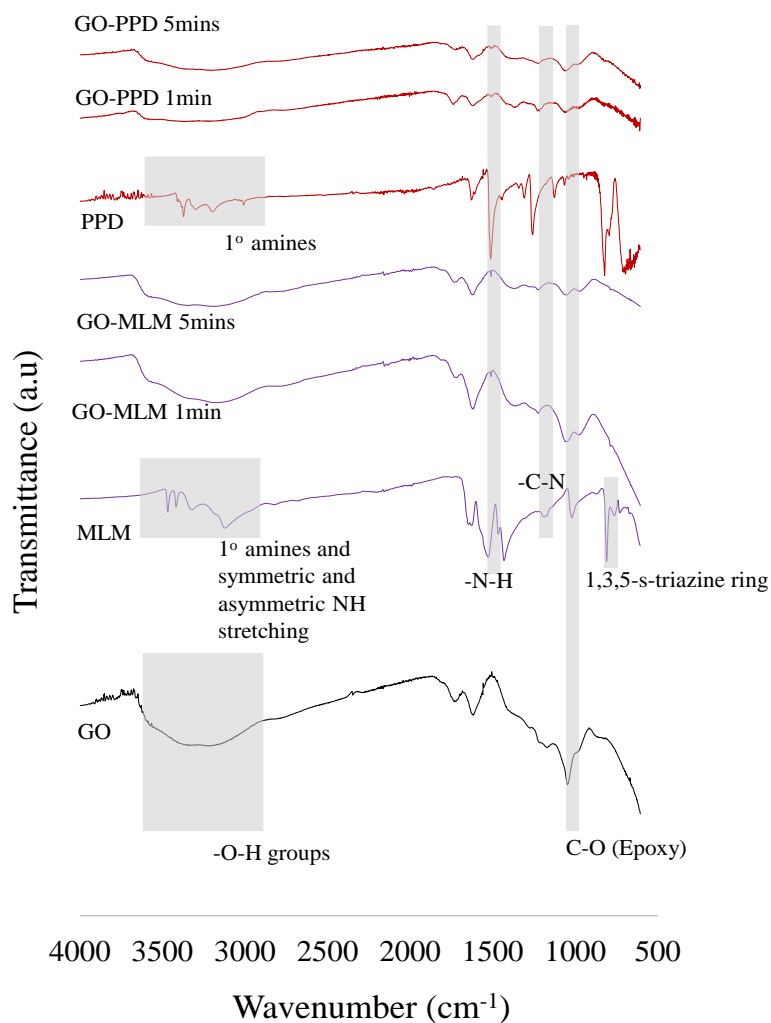


Figure 19. FTIR characterisation spectra for the GO-PPD and GO-MLM interactions after 1 minute and 5 minutes of reaction

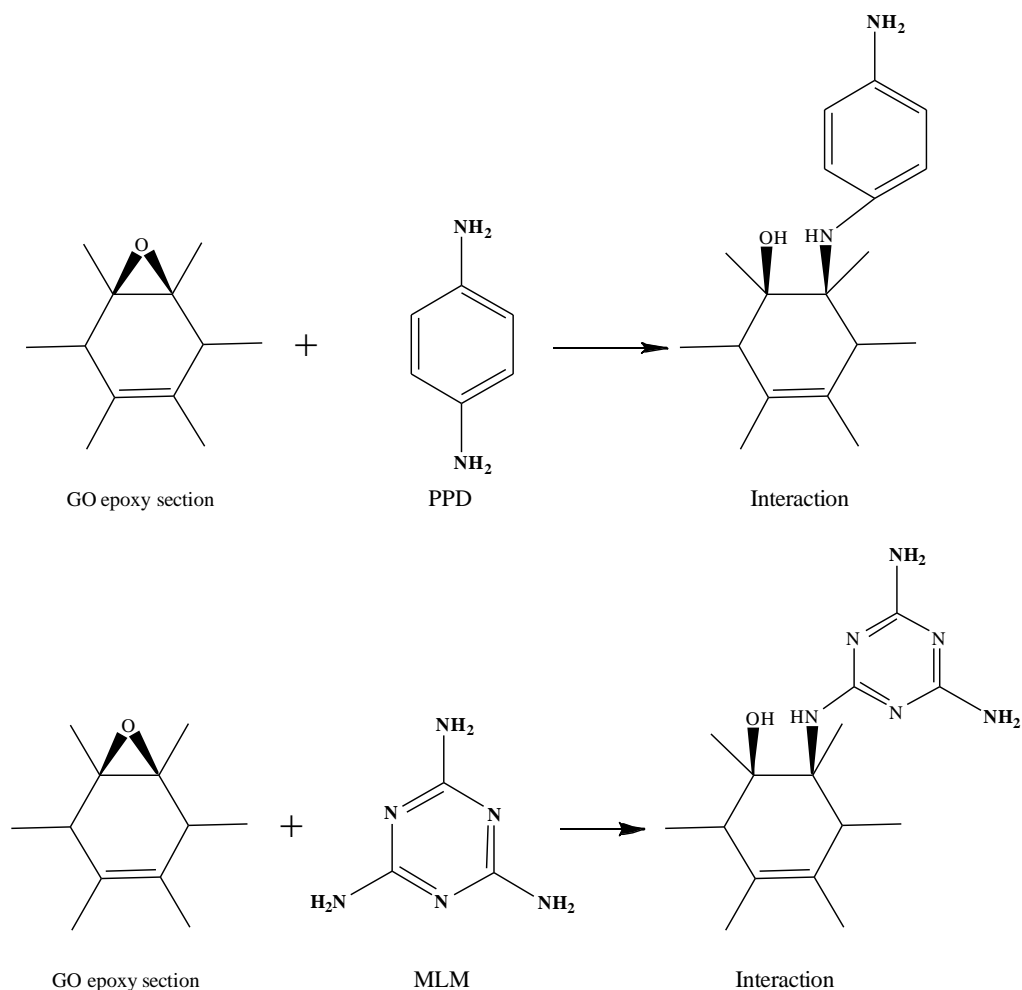


Figure 20. The epoxy-ring opening reaction between: A) PPD and GO; and B) MLM and GO

The indication that the epoxy ring opening reaction occurs in both MLM and PPD interactions with GO is further supported by the attenuation of the epoxy band at 1060 cm^{-1} [227]. This is in agreement with the XPS results shown in Table 3. These results show a reduction in the epoxide proportion of the GO-PPD reacted entities (37.1 % GO vs ~ 26.9 % and 25.7 % GO-PPD at increased reaction time) and to a lesser extent in the epoxide proportion of the GO-MLM reaction products (37.1 % GO vs ~34.5 % and 32.5 % for GO-MLM at increased reaction time) (Table 3). With regard to the GO-MLM interactions, overlapping of the C-O (epoxy) with the C=N functional groups present in MLM molecules (Figure 20) [235], clouds the diminishment of the

epoxy group in XPS characterisations. Additionally, the FTIR graphs for the reacted entities show the emergence of a –C-N band at $\sim 1220\text{ cm}^{-1}$ [246,252]. This band is also reflected in the XPS results, in which the C=O/C-N content increases from 1.2 % to 9.3 % and 15.7 % at the increased reaction time for GO-PPD interactions and to 13.0 % and 16.1 % for the GO-MLM interactions (Table 3).

The XPS characterisations also show a small introduction of nitrogen into the material that is absent in the GO starting material. The characterisations thus points to a predominant interaction between GO and the molecular crosslinkers being between the amines and epoxide groups over other functionalities like the carboxylates to form amides.

To explain the claimed lack of interaction of the carboxylates with amines, which is supported by the lack of significant reduction in composition of the COOH groups (Table 3), the reaction conditions ought to be considered. Formation of amides is heavily disfavoured under the aqueous reaction conditions used, especially in the absence of catalysts and coupling agents, since amide formation is a condensation reaction [254]. Normally acid-activation chemistry is required (e.g. starting materials in the form of acid chlorides, active esters or similar) to achieve such reactions [255]; even then there is a competitive reaction with water as an active nucleophile. Unlike the amide formation reaction, nucleophilic attack of epoxy groups to generate secondary amines readily occurs under mild aqueous conditions [256]. Indeed, such reactions are routinely used, for instance to couple proteins to epoxy-activated polymeric supports [257]. As a result, the confirmed epoxy-ring opening reaction is substantiated.

Table 3. Surface chemistry of GO and GO-PPD, GO-MLM reacted entities.

	GO	GO-PPD reacted 1 min	GO-PPD reacted 5 min	GO-MLM reacted 1 min	GO-MLM reacted 5min
C1s (%)	71.2	70.1	67.5	68.2	68.4
O1s (%)	27.4	27.6	29.9	31.0	30.9
S1s (%)	1.4	1.6	1.6	0.0	0.0
N1s (%)	---	0.7	1.0	0.8	0.7
Csp ² + Csp ³ (%)	58.5	57.8	51.9	47.6	48.9
C(epoxy)/C=N (%)	37.1	26.9	25.7	34.5	32.5
C=O/C-N (%)	1.2	9.3	15.7	13.0	16.1
COOH (%)	3.2	5.0	6.3	4.6	2.2
π - π * (%)	0.0	1.0	0.4	0.3	0.3

It is also worth noting that the presence of different functional groups may cause other non-covalent interactions such as van der Waals' forces and hydrogen bonds between the crosslinkers and GO [258]. These have been noted in reported studies of MLM and PPD [259,260]. Furthermore, GO's non-oxidised regions contain aromatic rings [261], and due to the presence of a benzoic ring and triazine in PPD and MLM, respectively, $\pi - \pi$ interactions are plausible [260,262].

On the other hand, the polymer PEI (Figure 1) contains many primary and secondary amine groups, as evidenced by the bands in the region between 3400 cm⁻¹ and 2900 cm⁻¹ and by the strong -N-H band at around 1640 cm⁻¹ (Figure 21) [248,250,263]. The band at 1460 cm⁻¹ corresponds to -CH₂ bending [248], and it can be detected in the reacted entities (Figure 21).

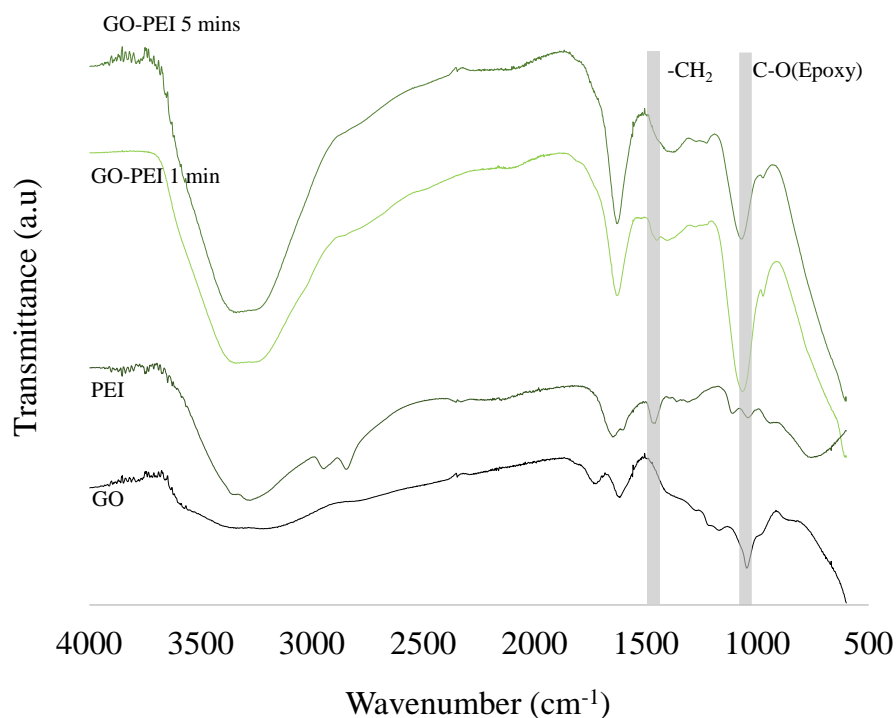


Figure 21. FTIR characterisation spectra of GO, PEI and the GO-PEI interactions after 1 minute and 5 minutes of reaction

The GO-PEI reacted samples show no disappearance of the band at 1060 cm^{-1} , which is ascribed to the epoxy group [227]. The FTIR characterisations therefore show no indication of the epoxy ring opening reaction in the interaction between GO and PEI (Figure 21). This result is further confirmed by the XPS characterisations (Table 4), which show minimal change in the percentage of epoxy groups even at the increased reaction time (37.1 % in the GO vs 35.7 % -35.4 % in the reacted entities).

However, at their recorded pH values (5.2 for GO and 8.3 for PEI) both compounds exhibit significant ionisation and opposing charges [191,263]. Ionisation of the -NH_2 groups in PEI to -NH_3^+ and of the -COOH to -COO^- will result in $\text{-NH}_3^+\text{OOC-}$ electrostatic interactions [264]. It can thus be rightly claimed that the predominant interaction between GO and PEI at the fabrication conditions entailed here is an electrostatic one.

Table 4. XPS characterisations (GO-PEI)

	GO	GO-PEI reacted 1 min	GO-PEI reacted 5 min
C1s (%)	71.2	67.5	61.8
O1s (%)	27.5	23.0	26.6
S1s (%)	1.3	2.6	3.1
N1s (%)	---	6.9	8.5
Csp ² + Csp ³ (%)	58.5	58.2	52.3
C(epoxy)/C=N (%)	37.1	35.7	35.4
C=O/C-N (%)	1.2	2.0	8.0
COOH (%)	3.2	4.1	4.1
π - π * (%)	0.0	0.0	0.2

3.3.2 Film continuity analysis

Successful assembly was evident through the observed uniformity across the thin films (Figure 22). The darkening of the glass slides at the increased immersion time of 5 minutes compared with 1 minute, and with the increasing number of bi-layers from 1 to 20, across all the crosslinked thin films can be attributed to increased material accumulation. Furthermore, good uniformity of film thickness at respective bi-layer numbers and immersion times is confirmed to an extent by the observed homogeneous change in surface colour.

Film continuity coverage and homogeneity is observed in further detail by means of SEM. This can be seen from the first bi-layer at 1-minute immersion time across all the crosslinked films (Figure 23). Some wrinkles can be observed on the surfaces; these are formed due to the folding of the GO nanosheets onto the substrates.

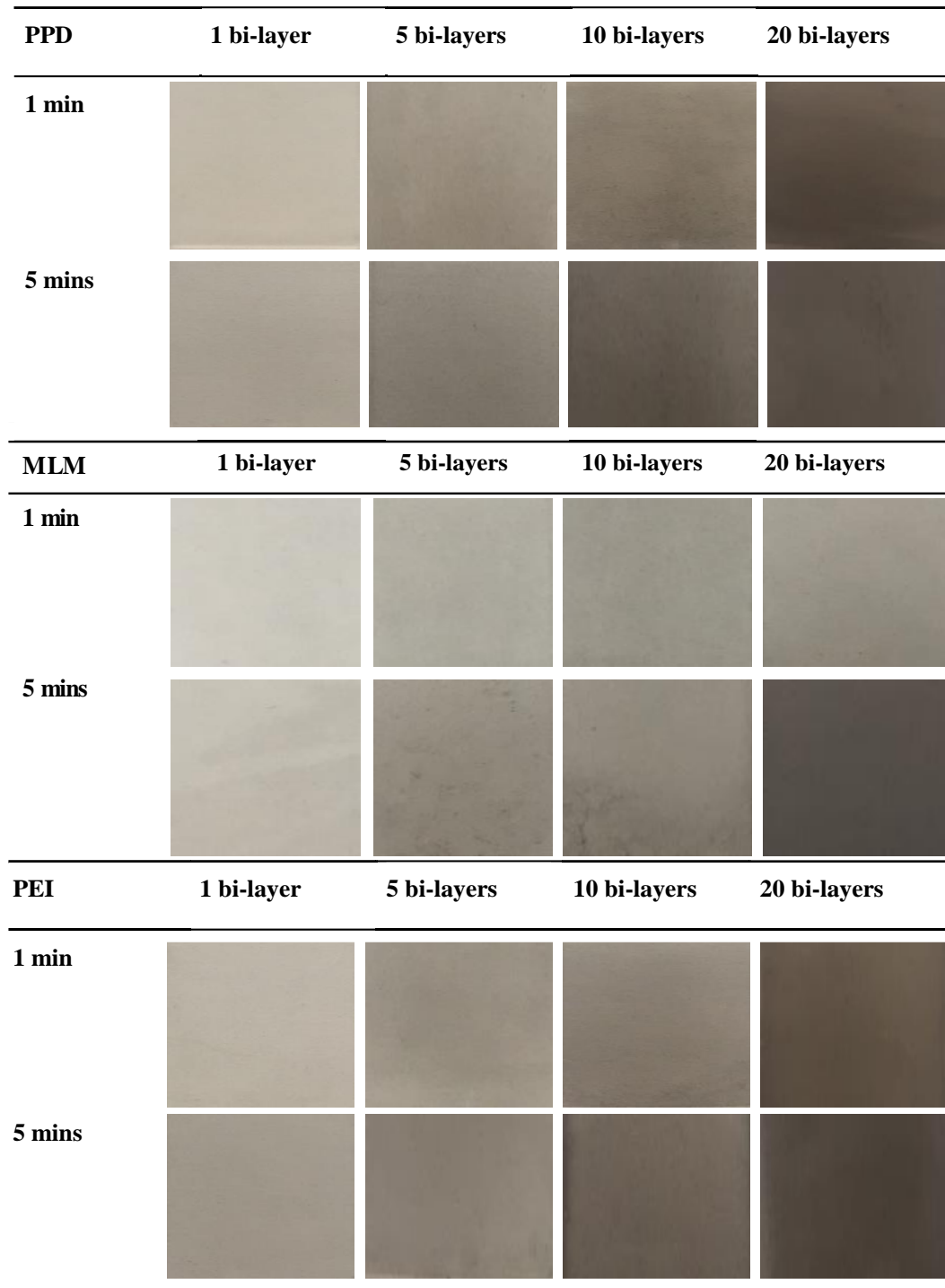


Figure 22. Photographs of the crosslinked thin films

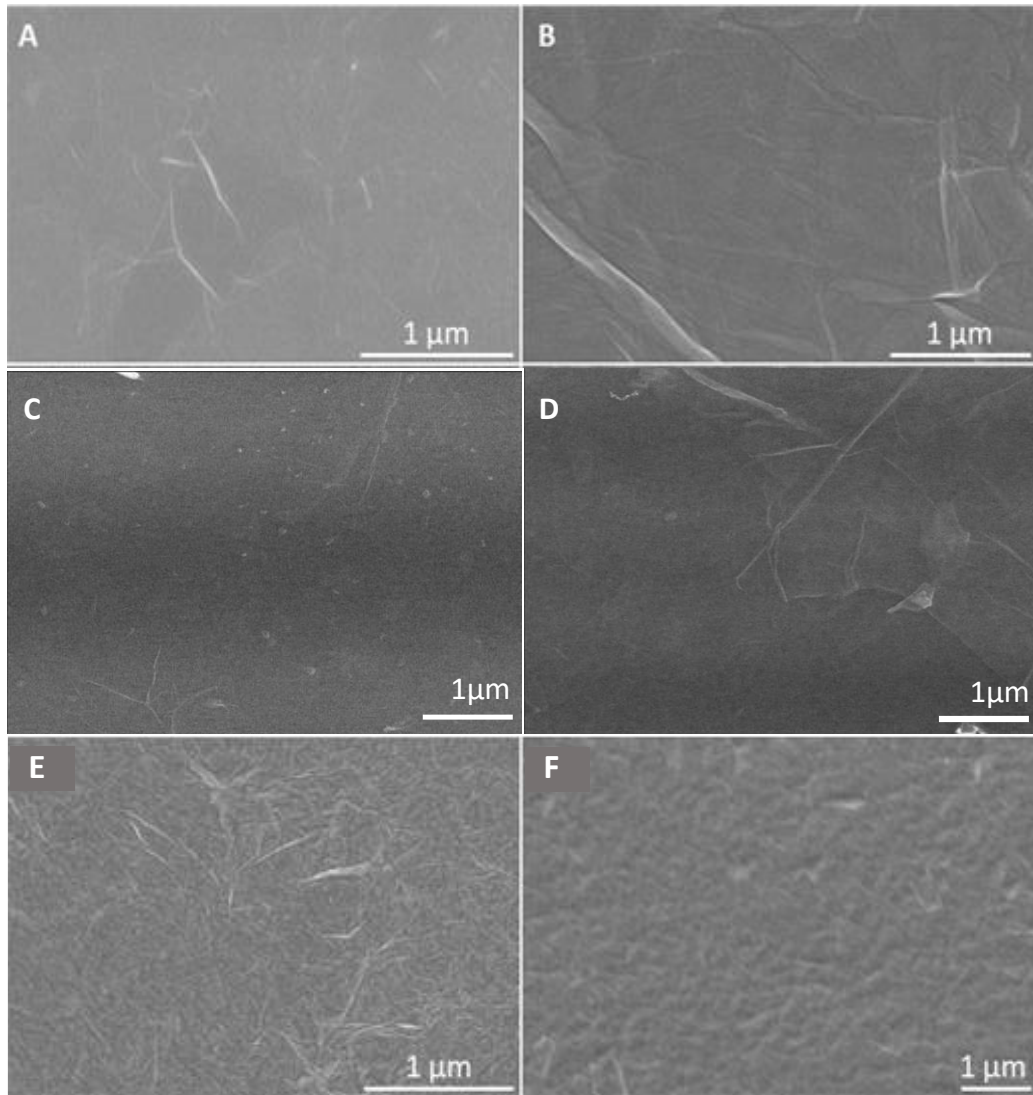


Figure 23. SEM micrographs of the crosslinked thin films: A) GO-PPD 1'1; B) GO-PPD 1'20; C) GO-MLM 1'1; D) GO-MLM 1'20, E) GO-PEI 1'1; F) GO-PEI 1'20

3.3.3 Analysis of the hydrophilicity of the fabricated films

Hydrophilicity is a significant characteristic of thin films. The significance of hydrophilicity mainly depends on the intended application of the thin films. Some applications require thin films of high hydrophilicity, while others demand low one. For example, for thin films that are used as surface coatings, low film hydrophilicity is required, while in water purification and desalination applications, high hydrophilicity (good membrane wettability) is key [191,265].

The magnitude of the water contact angle increases with increasing numbers of bi-layers and immersion time (Figure 24). A notable decrease in hydrophilicity is observed from the first bi-layer to the 10th for all film types, and then a gradual decrease is seen from the 10th bi-layer to the 20th. For instance, for the PPD crosslinked thin films under 1-minute immersion, the water contact angle rose from 45.3° to 62.8° and then gradually to 64.3° as the number of bi layers increased from 1 to 10 and subsequently to 20 (Figure 24). A similar trend was observed for the MLM and PEI crosslinked thin films.

The decrease in hydrophilicity at increased numbers of bi-layers and long immersion time is attributed to increasing accumulation of crosslinkers, which are hydrophobic relative to GO. The measurement estimates for the water contact angle of GO and individual crosslinkers are $31.4^\circ \pm 2.3^\circ$ for GO, $68.2^\circ \pm 6.8^\circ$ for PPD; $57.3^\circ \pm 4.3^\circ$ for PEI; and $54.3^\circ \pm 5.7^\circ$ for MLM. These values were gotten from depositing suspensions of just GO, PPD, MLM and PEI onto glass slides and letting them to dry to estimate their contact angles.

Larger contact angles were recorded for the PPD films in comparison with the MLM and PEI crosslinked films. The aromatic benzene ring in PPD has been noted in literature to enhance the hydrophobicity of the material monomer [53,266,267]. Furthermore, on-surface polymerisation of PPD during thin-film assembly can lead to higher hydrophobicity of the PPD crosslinked thin films. This is an established phenomenon that is used in the production of superhydrophobic GO-based thin films [268]. MLM, on the other hand, is reported to be an intrinsically hydrophilic material [269], which therefore produces a relatively less hydrophobic films. For the PEI crosslinked thin films, chemical reduction of GO by PEI monomers is likely to be a contributing factor to their reduced hydrophilicity as noted elsewhere [270]. A

plausible cause to the recorded higher hydrophobicity than PEI itself for the PEI film set at increased accumulation.

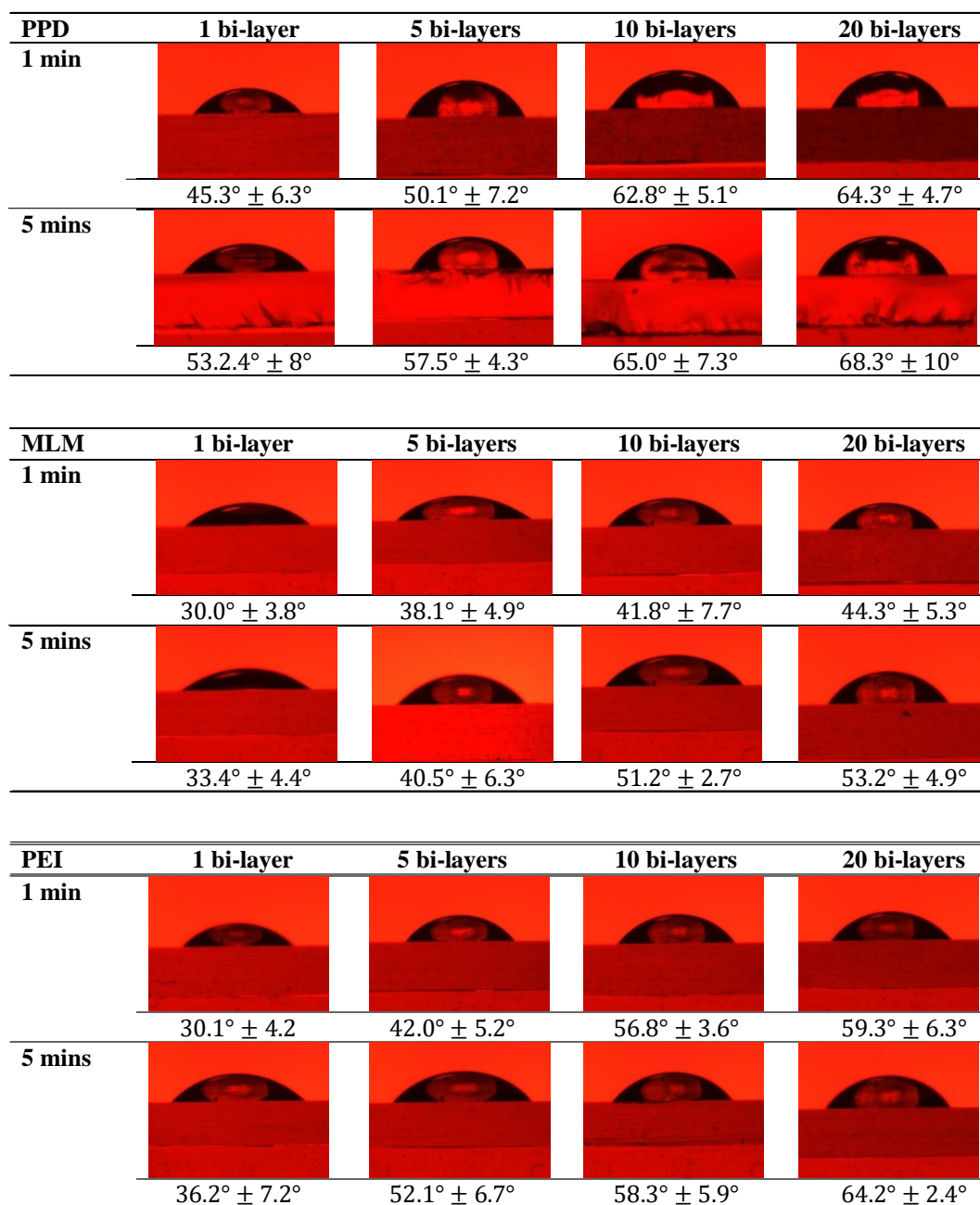


Figure 24. Camera images of the contact angles formed by water droplets on the crosslinked thin films of PPD, MLM and PEI.

3.3.4 Film thickness and analysis

The relationship between the change in film thickness as immersion times and the numbers of bi-layers increase is noted in Figure 25. A strong linear correlation between thin-film thickness and increasing numbers of bi-layers is observed across all the films.

It is important to highlight that, due to the thinness of the 1-bilayer films, especially of those deposited at 1-min immersion time, it was necessary to fabricate them on silicon wafers, as the roughness of the glass slides led to an inability to measure accurately the thickness.

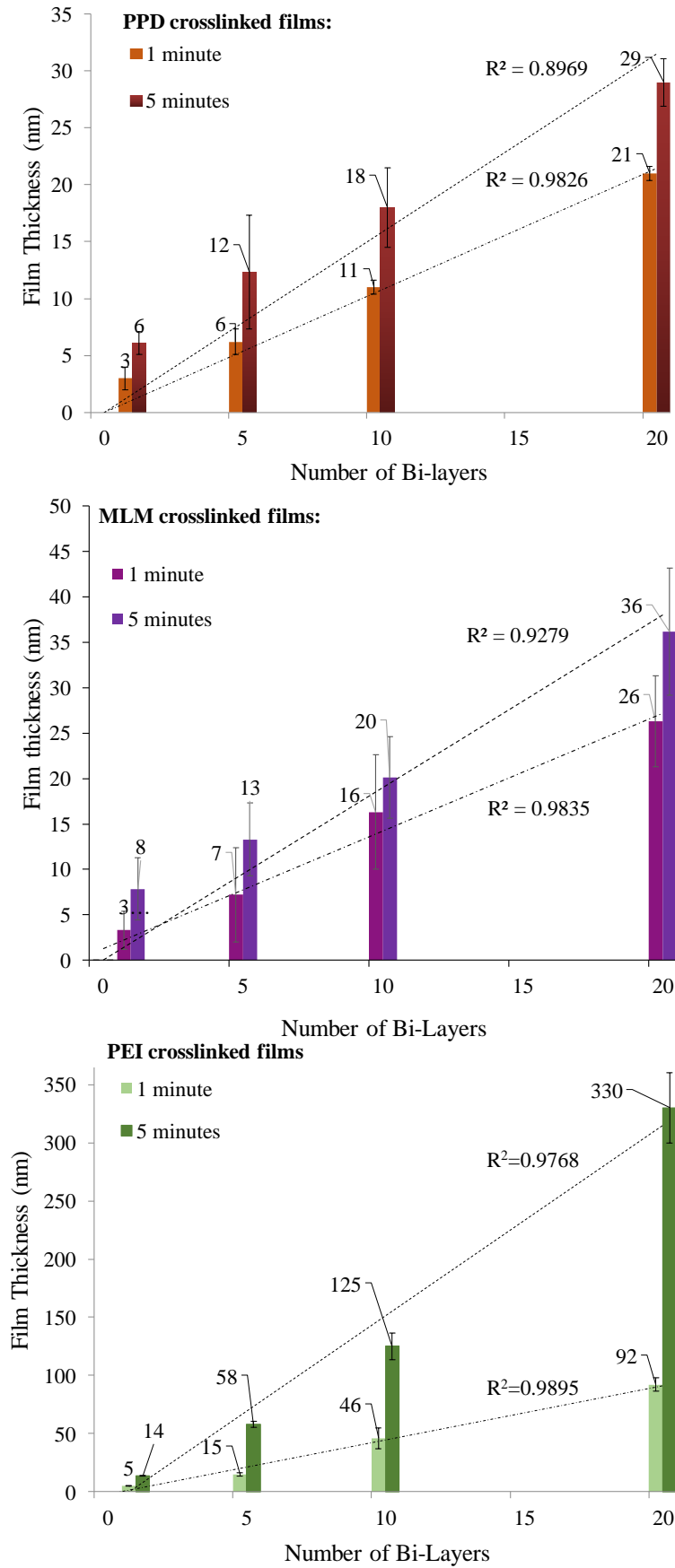


Figure 25. Thickness measurements of the cross-linked thin films

The general trend shows that thicker films are obtained with an increasing number of bi-layers and deposition times. This is due to the additional material accumulation as the immersion time and the number of bi-layers increases. Nevertheless, the thicknesses of the PEI-crosslinked films are much greater than those of the PPD and MLM thin films, as can be seen in Figure 25. For instance, the thickness of the PPD crosslinked film at 1-minute immersion rises from 3 nm to 21 nm as the number of bi-layers increases from 1 to 20 bi-layers, and from 6 nm to 29 nm at 5-minutes immersion time. For MLM, similarly, a 3 nm to 26 nm and an 8 nm to 36 nm increase at 1-min and 5-min immersion time, respectively, is observed. Given the similar molecular size of PPD and MLM (Figure 1) of about 0.5 nm due to the sizes of the aromatic and triazine rings [227,228], the thickness of the two crosslinked sets of films is of the same order. The recorded increase in thickness of these films is close to the theoretical expected increase of 1.5 nm per bi-layer from the ~0.5 nm benzene and triazine size and ~1.0 nm thickness of the GO nanosheets [227].

The thickness of the PEI crosslinked films increases from 5 nm to 92 nm (1 min dipping) and from 14 nm to 330 nm (5 min immersion time). PEI is a polymer, hence it contains a range of chain lengths, and consequently the expected step increase for these films cannot be predicted [229]. However, in all the sets a strong linear progression with the increasing number of bi-layers is observed.

The varying magnitude of increase in film thickness is mainly due to the differences in the sizes of the crosslinkers, as PPD and MLM are much smaller molecules than PEI, while PEI is a polymer with long branched chains and its use thus results in greater film thickness as the number of bi-layers increases.

Immersion time also has a significant impact on film thickness. In the case of PEI, increasing the immersion time from 1 minute to 5 minutes results in films 3 times

thicker and between 1.5 and 2 times for PPD and MLM-crosslinked films. The type of interlayer crosslinker and the deposition parameters (immersion time and number of bi-layers) are therefore key to the tuning and modifying the thickness of the thin films fabricated under the dip-assisted layer-by-layer method.

The overall importance of these results is the demonstration of the fabrication of GO crosslinked thin films and the ease with which specific thin-film characteristics, such as thickness and hydrophilicity, can be fine-tuned to specific industrial applications. The study verifies the significance of both inter- and intra-layer crosslinking in altering the significant properties of GO crosslinked thin films. In this regard the performance efficiency of the thin films can be easily enhanced for intended applications. Furthermore, successful fabrication of thin films on the glass-slide substrates highlights that various support substrates can be used depending on the intended applications of the films. This further opens the possibility of the use of other different-sized crosslinkers and polymers to adjust significant thin-film characteristics via dip-assisted layer-by-layer assembly.

3.4 Conclusions

Successful fabrication of GO crosslinked thin films was undertaken with the dip-assisted layer-by-layer assembly method. The magnitude of significant thin film characteristics, such as thickness, was also successfully controlled through the alteration of the fabrication operating conditions (immersion time and the number of assembly cycles). The control of these significant characteristics through the use of different-sized crosslinkers was also demonstrated. The work described in this chapter lays a significant foundation for the aim of the work undertaken for the thesis, which is to fabricate crosslinked GO membranes on microfiltration support substrates with

improved performance and stability for water purification. This further work is explained in subsequent chapters.

4.

THE FABRICATION, CHARACTERISATION AND ENHANCEMENT OF GRAPHENE OXIDE NANOFILTRATION MEMBRANES FOR WATER PURIFICATION VIA LAYER BY LAYER CROSSLINKING

“We can only see a short distance ahead, but we can see plenty there that needs to be done”

Alan Turing (1912-1954)

4.1 Introduction

The changing climate and the exponentially increasing global human population heightens the demand for clean water [4,271]. The diminishment of underground aquifers further amplifies the impending water shortage [272]. The 2018 edition of the World Water Development report outlined that by the year 2050 up 6 billion people

-
- Parts of this chapter have been peer reviewed and published in the Journal of Hazardous Materials: **Kandjou V**, Perez-Mas AM, Acevedo B, Hernaez M, Mayes AG, Melendi-Espina S, Enhanced covalent p-phenylenediamine-crosslinked graphene-oxide membranes: towards superior contaminant removal from wastewaters and improved membrane reusability, *Journal of Hazardous Materials* 380 (2019) 120840, doi.org/10.1016/j.jhazmat.2019.120840
 - Parts of the work in this chapter have also been presented at the World Conference on Carbon in Lexington, Kentucky, USA: **Kandjou V**, Hernaez. M, Acevedo. B, Mayes. A.G and Melendi-Espina S, “The enhancement of graphene-oxide membranes’ water purification performance and stability via covalent crosslinking with p-phenylenediamine”, 2019, **Oral Presentation**, Abstract No. 150.
 - Parts of the work in this chapter have also been presented at the World Conference on Carbon in Madrid, Spain: **Kandjou V**, Perez-Mas AM, Hernaez. M, Acevedo. B, Mayes. A.G and Melendi-Espina S, “The use of p-phenylenediamine to control graphene-oxide membrane pore-gap and stability for water purification” in 2018, **Poster Presentation**, Abstract No. 0620

will be affected by clean water scarcity [273]. To alleviate this predicted crisis, wastewater effluents can be purified, in consequence countering the water demand and mitigating environmental pollution [274]. The significance of water purification is also in ensuring the general health of the global population, especially in the developing world [275]. It is therefore imperative to find, derive and improve better next generation water purification means, and this is the arch-aim of the work done in this chapter.

As discussed in the introductory chapter, different water purification ways from distillation to separation membranes have been deployed depending on the nature and size of the particulates being separated [276,277]. Despite high product output, distillation is limited by high energy consumption [12]. Separation membranes, especially in the nanofiltration range, are increasingly being preferred over the other conventional methods owing to their environmental friendliness and energy efficiency [16]. Nanofiltration membranes further offers an advantage of having good rejection rates for a wide range of particulates at higher flux and lower energy consumption, especially in relation to reverse osmosis for similar species [278,279]. A variety of materials can also be used to fabricate nanofiltration membranes [280].

Conventional polymers like polyamide, polysulfone and poly(ethersulfone) are amongst the most used membrane materials due to their abundance and suitability, but poor corrosion resistivity and lack of durability are major limitations [281]. Susceptibility to fouling, which shortens their lifespan, has also been a notable disadvantage to most polymeric membrane materials [282]. Their modification for enhanced performance has also been noted to be laborious [280]. In lieu of these drawbacks, carbon-based materials like graphene and nanotubes have attracted much attention and are being considered as significant alternatives. This is due to their

notable properties, such as thermal tolerance, and chemical and mechanical stability [30,283–285]. Structurally, for graphene in particular, its 2-dimensionality and 1 – atom thickness makes it an ideal separation membrane material [284]. CNTs on the other hand, provide a unique 1-dimensional water flow [284], with high water flux of several orders higher than the predicted hydrodynamic flow having been reported [30]. Nonetheless, these carbon based materials are also bound by some limitations, for instance, for CNTs relative high cost, complexity in membrane fabrication (vertically alignment) and large-scale production challenges limits their use [31,32]. For graphene, as previously discussed, lack of large scale production scalability of defect free nanosheets is a notable limitation [39,40]. Moreover, graphene is impermeable and therefore to convert it to a nanofiltration membrane, cost intensive pore formation nucleation and ion bombardment processes are required [21, 22].

Fortunately, graphene oxide (GO) is emerging as an excellent substitute to the aforementioned carbon based materials owing to its large-scale production scalability, hydrophilicity and unique ultrafast water permeation pathways [45,288]. In spite of the promise of GO membranes as a next-generation water-purification membrane material, a notable limitation is the widening of the membrane pore-gap during nanofiltration, as discussed in Chapter 2 [46]. This is caused by the accumulation of water molecules in between GO nanosheets [46,47], which result in decreased performance overtime as the membrane pore gap widens. Poor membrane structural stability is also a restraint to the use of GO as a separation membrane material [289]. In this regard, specific modifications ought to be instigated to improve GO membrane performance.

Several attempts have so far been undertaken to enhance the performance of GO membranes, as detailed in the literature review. Some of these modifications include

the use of epoxy encapsulants to physically confine GO nanosheets to improve their structural stability and separation ability [51]. However, despite the method's promise in efficiency improvement, fabrication complexity and lack of production scalability are major limitations [51]. Another effort in improving GO membrane performance has been the chemical and/or thermal reduction of GO to remove the oxygenated functional groups that entrap water molecules, which compromises the separation degree of the membranes [48]. However, this approach culminates in diminished membrane hydrophilicity and increased susceptibility to fouling, which leads to the need for a higher operation pressure during use [290,291].

The use of chemical species (crosslinkers) to interconnect GO nanosheets is another economic potential approach to improve membrane performance. Crosslinking offers a variety of materials that can be used to link the GO nanosheets together to avoid swelling during nanofiltration [292]. The interconnection of the GO nanosheets is achieved either electrostatically, covalently or through non-covalent interactions depending on the structural properties of the crosslinkers, as discussed in detail in the literature review. As a way to improve GO nanofiltration separation capabilities, the work described in this chapter details the incorporation of the amine-containing crosslinkers; p-phenylenediamine (PPD), 1,3,5-Triazine-2,4,6-triamine (melamine) (MLM) and polyethyleneimine (PEI) onto the GO membranes. Due to the presence of the nucleophilic amine groups, the selected crosslinkers are in theory highly reactive [226]. GO is thus likely to interact strongly with the crosslinkers forming intercalated crosslinked membranes with improved nanofiltration performance. GO-crosslinker interconnections were successively proven in the chapter 3, where covalent interactions with the molecular sized crosslinkers (PPD and MLM) and electrostatic for the polymer-based PEI were confirmed.

The crosslinkers can be introduced onto GO membranes via different membrane fabrication methods from vacuum filtration and spin coating to spray coating [183,293,294]. However, there are notable limitations to the outlined methods, for instance, in the case of vacuum filtration, difficulty in controlling membrane thickness is a known limitation [179]. Drawbacks of the coating methods, as discussed in the literature review and previous chapter, include low efficiency of use of materials, difficulty in controlling significant membrane characteristics such as thickness, and poor membrane homogeneity [220,221].

An increasingly used method in the fabrication GO nanofiltration membranes is the layer-by-layer method. The dip-assisted layer by layer assembly in particular, offers ease of control of membrane thickness and other significant characteristics as proven in the previous chapter and elsewhere [295,296]. Another notable advantage of the method, hence its selection as the method to use in this chapter, is efficient use of material [59]. Furthermore, simplicity of operation and ease of scale-up to mass production are further advantages of the method [224]. It is also particularly suitable for fabricating large area membranes on irregularly shaped substrates especially relative to counterpart versions like the spray and spin-assisted layer by layer [190]. Through the dip-assisted layer-by-layer method, crosslinkers can be incorporated onto GO membranes via an interfacial interchangeable attachment resulting in an interconnection of the nanosheets. Henceforth, the method also offers potential improvement in membrane performance and stability. The arch-aim of this chapter is thus to assemble dip-assisted layer-by-layer crosslinked GO membranes for water purification.

Relatively thin membranes of nanometre thickness range can be fabricated via this method, as demonstrated in chapter 3. Support substrates are in consequence used so that the membranes can withstand the high pressures at which they are required to operate [55]. Various materials from polymer-based ones to inorganic anodic aluminium oxide (AAO) can be employed as base support [284]. The inorganic substrates are mechanically stronger, and some like AAO, helps in enhancing stability and intactness of GO membranes through their possession of Al^{3+} ions [198]. However, their limitation include high market price and brittleness [297]. As a result, the use of polymeric affordable substrates, such as polycarbonate (PCB) and poly (acrylonitrile) (PAN) has garnered attention [191,298]. PAN is a synthetic polymer with a negative charge, composed of an acrylonitrile and an aryl sulphonate [299]. Its electrostatic activity and chemical functionalities provide increased interactions with membrane assembly materials, hence its adoption as a support structure for various GO based separation membranes [300,301]. Furthermore, its ease of activation and excellent thermal stability prompted its use as a substrate for this work [302]. PCB, on the other hand, belongs to a family of thermoplastic polymers that contain a carbonate group [303,304]. Its selection is based on affordability, strength and toughness [305]. Consequently, relatively cheap microfiltration PAN and PCB substrates are used as support substrates for the assembly of GO membranes in this chapter.

In lieu of the fact that current conventional nanofiltration membranes are relatively expensive, have poor stability and short lifespans [306,307], this chapter details the fabrication of GO-based membranes on cheaper microfiltration support substrates to overcome these limitations. The enhancement of membrane performance is explored through a layer-by-layer incorporation of respective crosslinkers. To confirm the positive impact of the crosslinkers, uncrosslinked membranes are fabricated by dip-

coating in tandem. The impact of assembly immersion time and the number of bi-layers produced on the performance of the membranes is also studied.

4.2 Experimental Section

4.2.1 Materials

As in the previous chapter, GO powder purchased from Graphenea (product code: C28/GOB02/Pw, Spain) was used. Fibrous PAN microfiltration support substrates of 0.2 μm pore size and 47 mm diameter were purchased from Sterlitech Corporation (Washington, USA). The PCB support substrates of 0.2 μm pore size and 47 mm diameter were acquired from Whatman, UK.

The different sized amine group containing crosslinkers, which were used in the fabrication of thin films, PPD powder, (product code: P6001), MLM (product code: M2659) and PEI (product code 03880), were all commercially sourced from Sigma-Aldrich (Haverhill, UK).

As in the case of the glass slides in chapter 3, potassium hydroxide powder (KOH, product code: P/5640/53) was used to prepare 1M KOH for substrate activation and it was also purchased from Sigma-Aldrich, UK. A solution of methylene blue (MB), prepared from its powder version (MB, $\text{C}_{16}\text{H}_{18}\text{ClN}_3 \cdot 3\text{H}_2\text{O}$, >99% purity; product code: M9140) and procured from Sigma Aldrich (Haverhill, UK), was used to determine the performance of the crosslinked and uncrosslinked membranes.

4.2.2 Membrane fabrication on PAN substrates

4.2.2.1 Pre-treatment of PAN

There are several ways in which PAN substrates are modified to prepare them for GO membrane assembly. These include plasma-initiated graft polymerisation [301,308],

photo-induced grafting and, most commonly, hydrolysis [309–311]. Hydrolysis of PAN substrates in alkaline conditions is noted to be the most favourable and convenient activation method [312]. Consequently, for this research, the PAN substrates were first pre-treated via immersion in 1M KOH for 30 minutes at 70 °C. The hydroxylation edged the conversion of the nitriles ($-C\equiv N$) in PAN to carboxylic groups ($-COO^-$), thereby creating a negative charge on the substrates [191,313,314]. The substrates were then rinsed thoroughly with deionised water and dried prior to immersion in a positively charged 2.0 mg/ml PEI solution for 5 minutes. PEI conferred a positive charge onto the hydroxylated substrates electrostatically [191,314]. The positively charged substrates were rinsed in distilled water to remove excess of unattached PEI and then dried prior to membrane fabrication, which commenced with immersion in the negatively charged GO suspensions.

4.2.2.2 The fabrication of crosslinked and uncrosslinked GO membranes

The circular substrates were attached to home-made metal plates during the fabrication process (Figure 26). An automated rotary dip-coater (Nadetech Innovations, Navarra, Spain) was used to fabricate the membranes with pre-set immersion times and number of assembly cycles via the ND-R Rotary Coater Software.

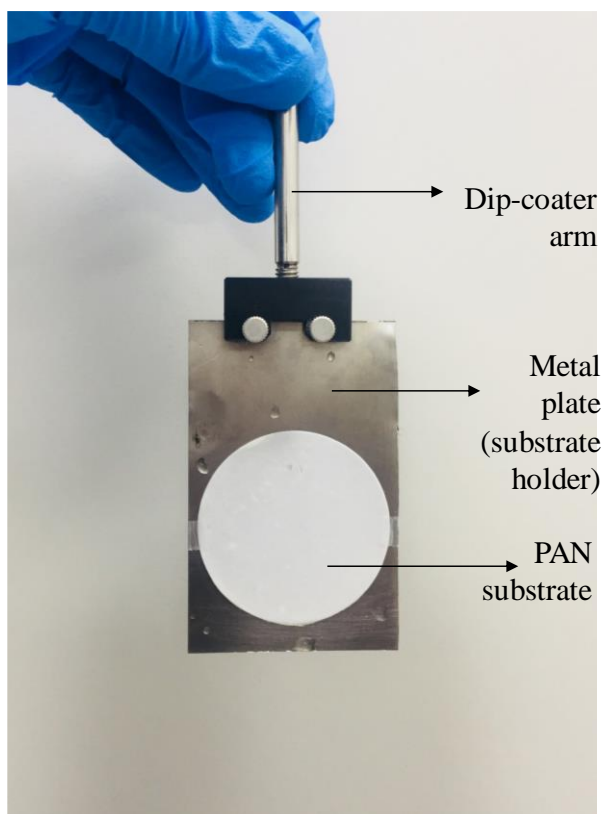


Figure 26. PAN substrate mounted onto the stainless-steel metal plate before membrane fabrication

A 0.5 mg/ml aqueous GO suspension was prepared and sonicated for two hours to improve individuality and aqueous suspension stability. Uncrosslinked GO membranes were fabricated via the dip-coating method. Following pre-treatment, the substrates were immersed in GO suspension with rinsing and drying between assembly cycles (see schematic diagram for fabrication in Figure 27). These were used as the control membranes to verify the impact of crosslinking on membrane performance.

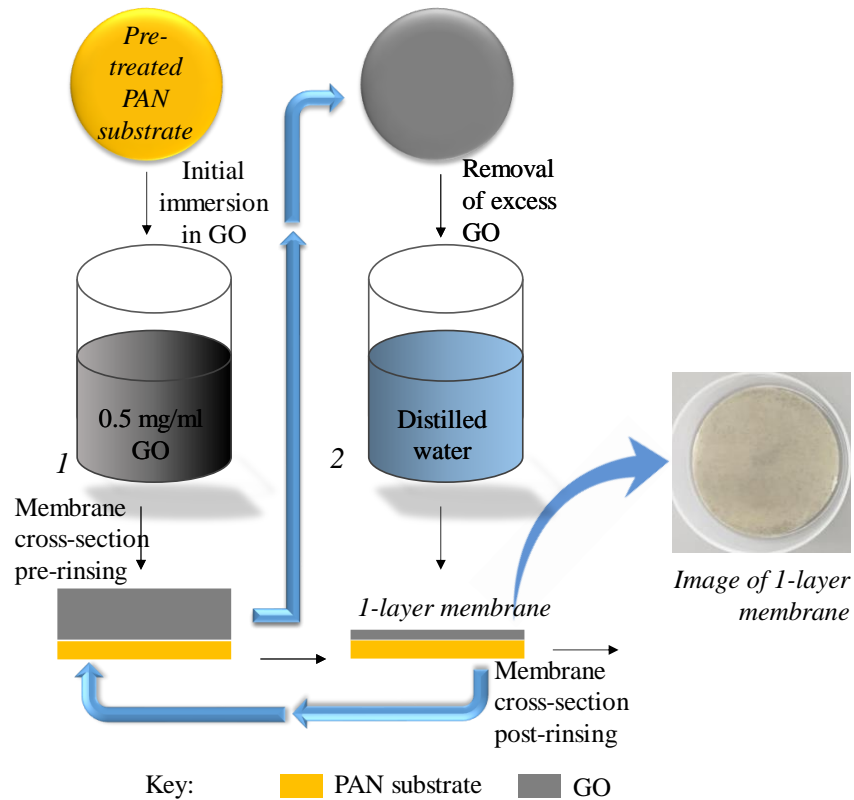


Figure 27. Schematic diagram showing fabrication of uncrosslinked membranes by dip-coating

The crosslinked membranes were fabricated following a procedure similar to that explained in the previous chapter for the fabrication of thin films. An alternating immersion between GO and the crosslinkers with rinsing and drying after each immersion in GO or crosslinker was carried out to remove extra unattached components (see schematic diagram shown in Figure 28).

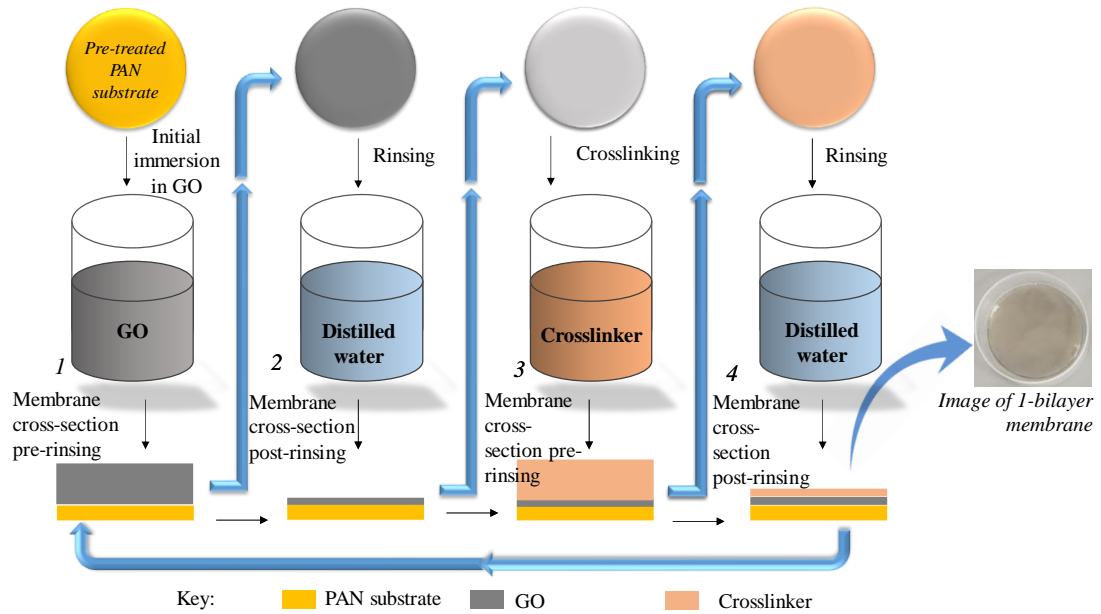


Figure 28. Schematic diagram showing fabrication of crosslinked membranes by dip-assisted layer-by-layer assembly

The membranes were fabricated in 1, 3 and 5 bi-layers at 1-minute and 5-minute immersion times. The number of bi-layers in this case was limited to a maximum of five as it was found that at higher number of assembly cycles, membrane tortuosity drastically increased, resulting in reduced permeation flux and membrane clogging. The fabricated membranes were accordingly labelled as in Table 5.

Table 5. Nomenclature of the fabricated membranes

Immersion time (mins)	Number of bi-layers		
	1	3	5
1	GO-X-1'1	GO-X-1'3	GO-X-1'5
5	GO-X-5'1	GO-X-5'3	GO-X-5'5

Where X is PPD, MLM or PEI

4.2.5 Membrane performance tests

4.2.5.1. Nanofiltration setup

To determine the nanofiltration performance of both crosslinked and uncrosslinked membranes, a dead-end filtration cell was constructed from poly (methyl methacrylate) (Figure 29). During nanofiltration performance tests, a porous sintered polyethylene disc with an effective area of 13.20 cm² supported the membranes. Neoprene gaskets were used to seal the filtration cell, as it was pressurised by inert nitrogen gas. An economic low pressure of 1 bar was used in order to determine membrane performance at reduced operational costs.

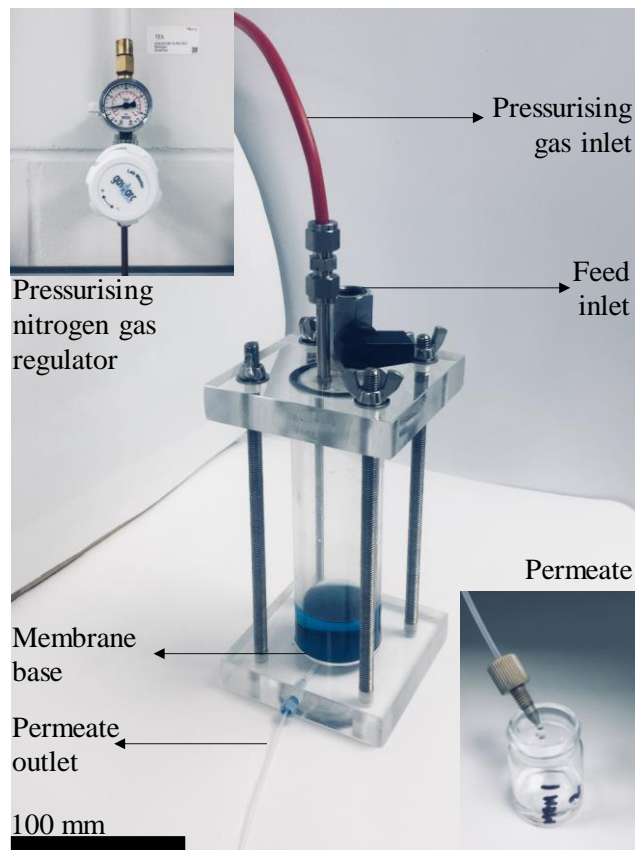


Figure 29. The homemade nanofiltration cell unit in operation

4.2.5.2. Membrane permeation flux and rejection

Performance of both crosslinked and uncrosslinked membranes was determined through the nanofiltration of 100 ml of 10 mg/l of an aqueous solution of MB through each of the fabricated membranes. Permeation flux (F) across all membranes was then duly determined from the total permeate volume collected (V) per unit time (t) and membrane effective/operation area (A) (area of the membrane in contact with the feed solution) (see Equation 1).

$$F = V/(A t) \quad \text{Eq (1)}$$

Rejection of the MB solution by the membrane was determined by UV-Vis (Hitachi U-3900 UV-Vis) characterisations of the permeate solutions relative to the feed solution at a wavelength of 664 nm (maximum absorbance of MB). This necessitated the construction of a calibration line in order to perform concentration-based MB rejection calculations. From three sets of concentration *vs* absorbance results, an average calibration line was established within the Lambert-Beer's law application linear range, given the low concentrations, as recorded elsewhere [315] (Figure 30).

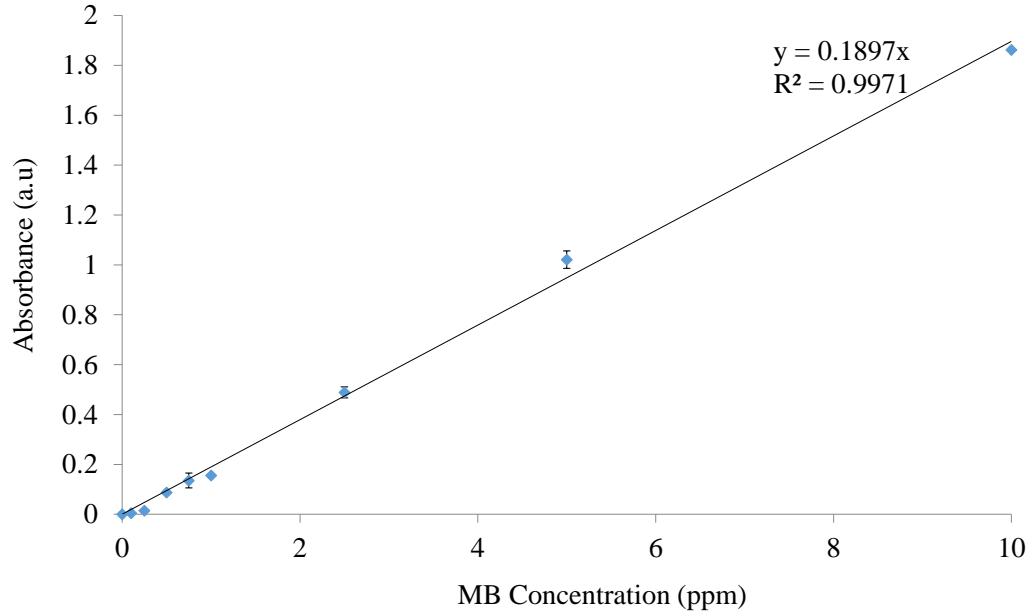


Figure 30. MB absorbance: concentration calibration line

The membrane percentage rejection [R (%)] was then calculated using Equation 2, in which C_p and C_f are the permeate (after 100 ml of permeation) and feed concentrations respectively. These values are interpolated from the constructed calibration-line equation.

$$R (\%) = \left(1 - \frac{C_p}{C_f}\right) \cdot 100 \quad \text{Eq (2)}$$

To enhance the reliability of the results, three membranes of the same type were fabricated and tested and subsequent standard deviations of the nanofiltration results were noted for both the average flux and rejection results.

4.2.6 Continuity of the fabricated membranes

Continuity and substrate coverage are essential to have a larger membrane operation area [316]. Morphology of the membranes (pre and post nanofiltration tests) was evaluated. For that it was firstly employed a JEOL JSM – 5900 Scanning Electron Microscope; following its technical breakdown, some characterisations were carried

out by means of a high-resolution FEI Nova NanoSEM450 that contained a Gatan cryo-system with detectors that used various methods from Energy Dispersive X-ray Spectroscopy (EDS) to Backscattered Electron Imaging (BSE). Both SEM equipment were operated at a low voltage of 1 kV in high-vacuum mode.

4.3 Results and Discussion

4.3.1 Membrane continuity analysis

The uncrosslinked dip-coated membranes at the respective immersion times and assembly cycles are displayed in Figure 31. From the darkening in membrane pigmentation, it can be observed that GO accumulation augment as the immersion time and number of assembly cycles increases. Detailed good membrane homogeneity and continuity coverage is proven via SEM characterisations (Figure 32). This is evident even at 1 layer for the membranes fabricated under 1-minute immersion time, which guaranteed good continuity at a high immersion time and number of layers. Assembly and coverage for these uncrosslinked membranes is aided by the intra-interactions between GO nanosheets through van der Waals' forces and hydrogen bonding [317].

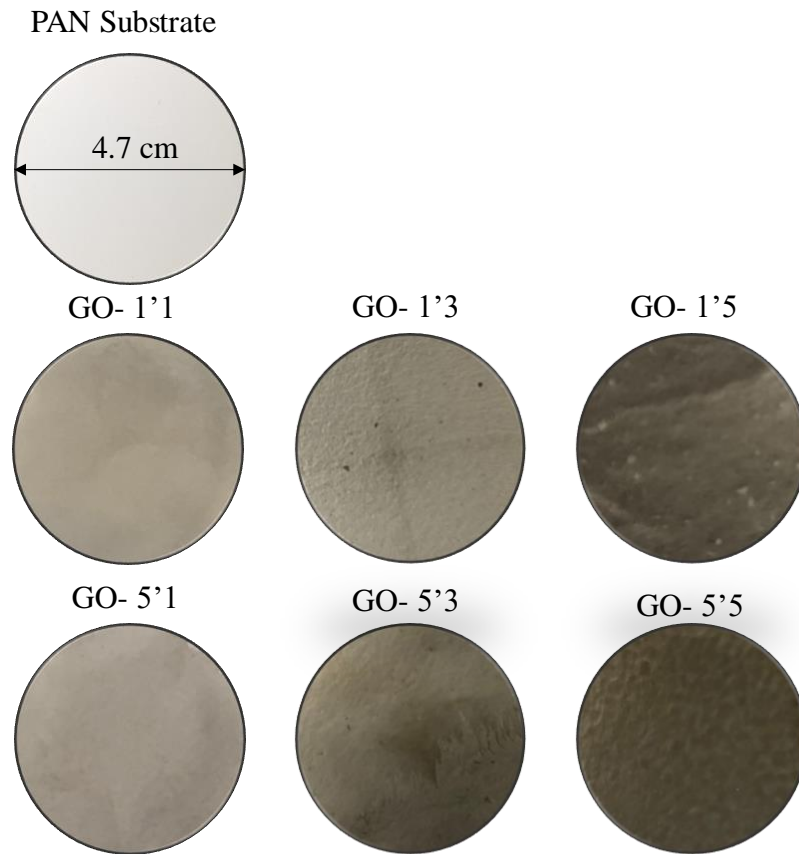


Figure 31. *Photographic images of the fabricated uncrosslinked membranes on PAN substrates*

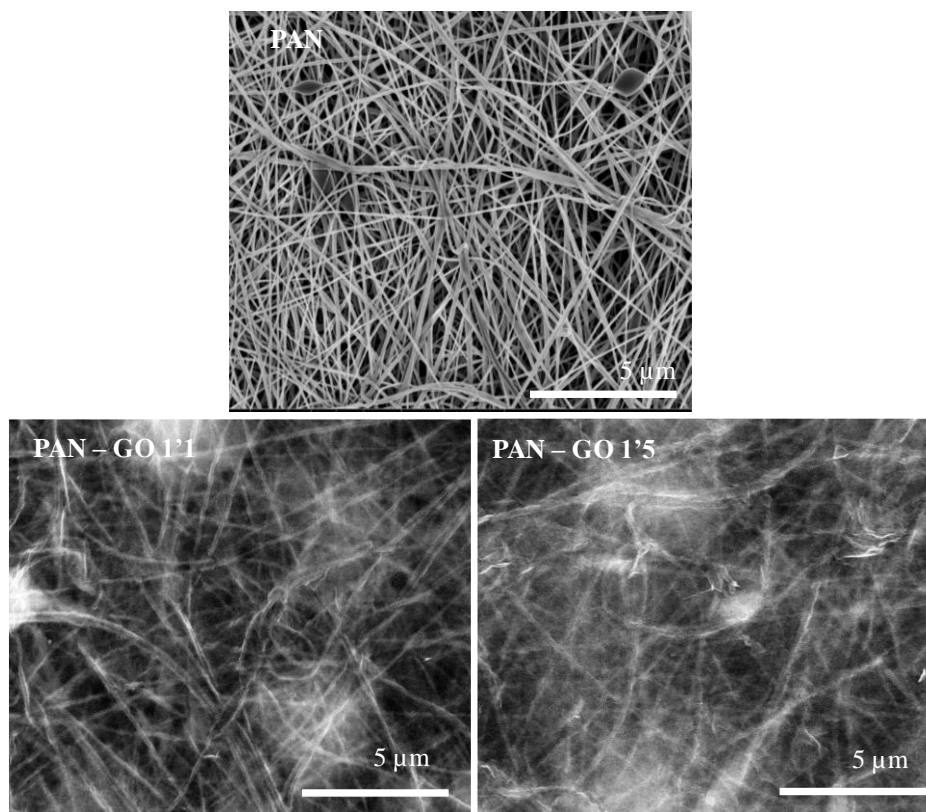


Figure 32. SEM images of the respective fabricated uncrosslinked membranes on PAN substrates

Correspondingly, the crosslinked membranes are displayed in Figure 33, and the SEM images at 1-minute immersion time at 1 and 5 bi-layers are shown in Figure 34. Good membrane homogeneity for all the crosslinked membranes at the respective assembly cycles is evident. Substrate coverage in this case is increased by horizontal intralayer and vertical interlayer nanosheet crosslinking/interactions, as reported in other related works [241,318], and in the previous chapter.



Figure 33. Photographic images of the crosslinked membranes on PAN substrates

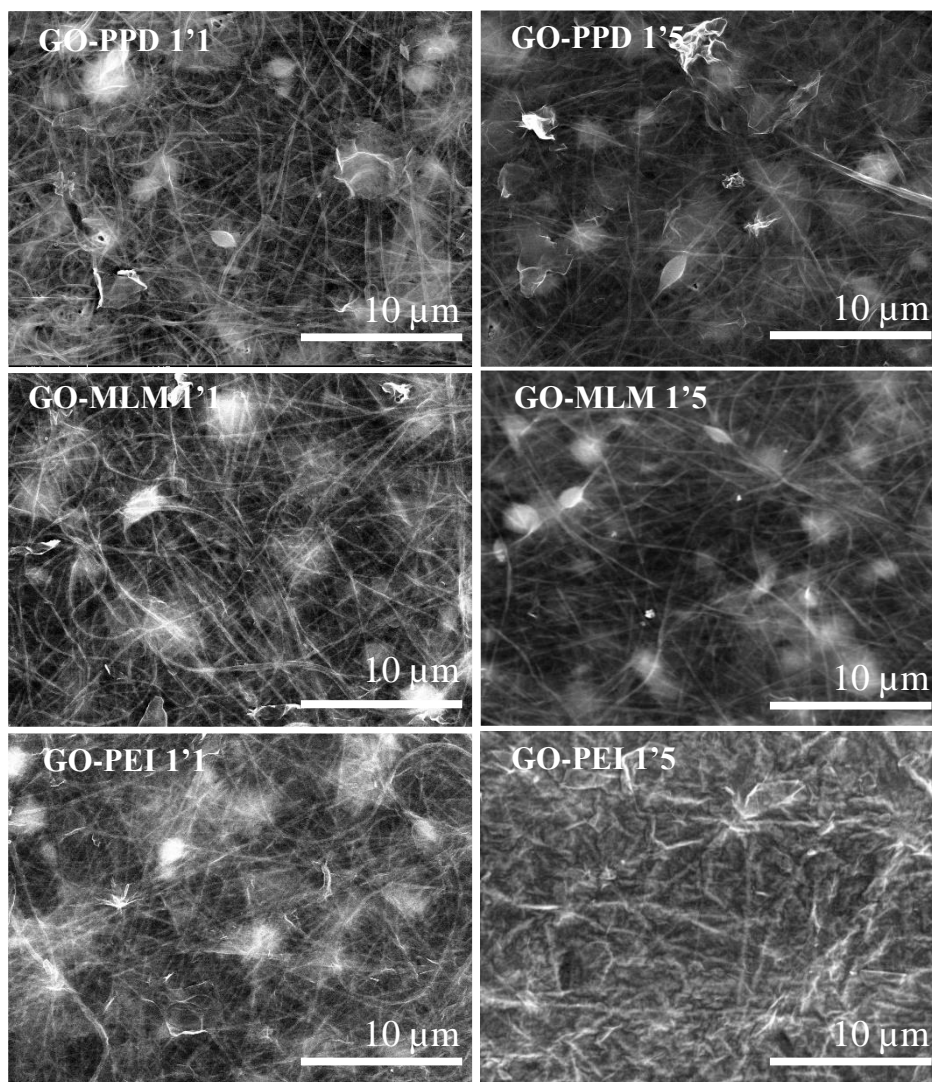


Figure 34. SEM images of the crosslinked membranes on PAN substrates

The SEM characterisations show that a greater accumulation of material is observed in the PEI- crosslinked membranes relative to the PPD and MLM (Figure 34). This claim is supported by the reduction in the protrusion of fibres of the PAN substrates. The observation is also in consonance with the high film thickness recorded for the PEI crosslinked films relative to the films of the molecular crosslinkers PPD and MLM in chapter 3. Specifically, the thickness of the PPD crosslinked film at 1-minute immersion rises from 3 nm to 6 nm as the number of bi-layers increased from 1 to 5 bi-layers, and from 6 nm to 12 nm at 5-minutes immersion time (Figure 25). For MLM, similarly, a 3 nm to 7 nm and an 8 nm to 13 nm increase at 1-min and 5-min immersion

time, respectively, has been noted (Figure 25). On the contrary, the thickness of the PEI crosslinked films increase from 5 nm to 15 nm (1 min dipping) and from 14 nm to 58 nm (5 min immersion time) (Figure 25), a relatively larger increase, which is in conjunction with the observed high material assembly here.

4.3.2 Analysis of membrane performance results

4.3.2.1 Rejection analysis

The enhancement of membrane performance by the crosslinkers is evident when comparing the separation of MB from water by retention of the dye between crosslinked and uncrosslinked membranes. MB removal in the case of uncrosslinked membrane is facilitated by -OH and -COOH groups electrostatically (attraction) together with $\pi - \pi$ interactions. The photographs of the permeates across each of the fabricated membranes is displayed in Figure 35 showing a diminishment in colour intensity at increasing MB rejection rate.

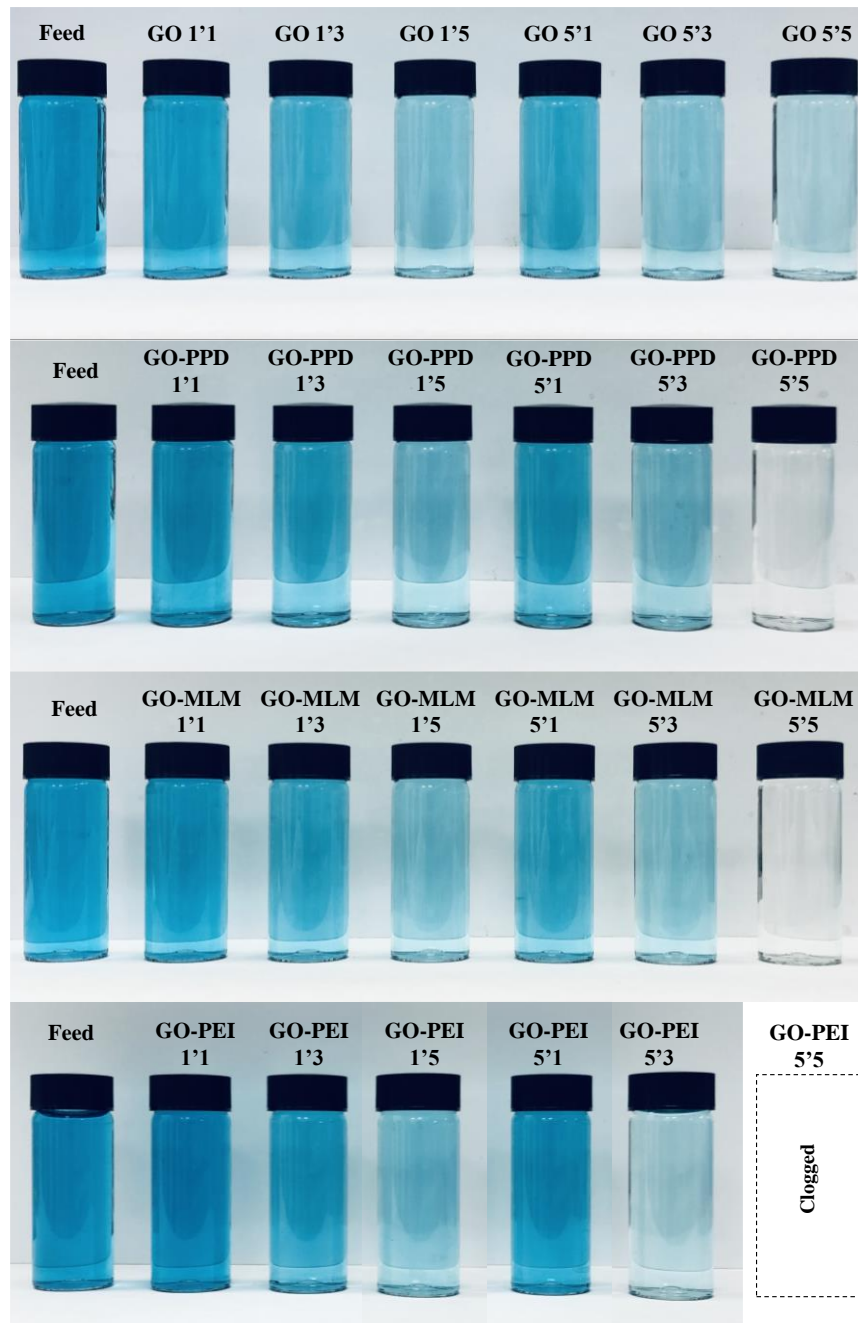


Figure 35. Photographic images of the MB permeate across each of the fabricated membranes

At similar fabrication conditions, all the crosslinked sets have a relatively higher performance than the uncrosslinked (Table 6). For instance, in the case of the PPD crosslinked membranes at 5-minute immersion time, the average MB rejection rate increases from 20.4 % to 99.8 % with the number of bi-layers from 1 to 5. Across the

same condition, the rejection rate for the MLM crosslinked membranes improves from 35.9 % to 99.7 %. For the PEI crosslinked membranes one other hand, a rejection rate of 34.2 % is recorded at the first bi-layer, however, increasing the bi-layers to 5 results in membrane clogging. Comparatively, the rejection rate increase for the uncrosslinked membranes is from 5.1 % to 87.4 % (Table 6), which is inferior to that observed for the crosslinked membranes. The lower average membrane performance for the uncrosslinked membranes can be attributed to the widening of pore gaps during operation, as previously noted elsewhere [46,47]. This finding validates the incorporation of crosslinkers to enhance GO membrane performance.

Table 6. Results of membrane rejection tests

Membrane	Average MB rejection (%)			
	Uncrosslinked	PPD crosslinked	MLM crosslinked	PEI crosslinked
GO-X-1'1	1.4 ± 0.1	10.7 ± 2.7	19.3 ± 3.1	14.6 ± 4.3
GO-X-1'3	20.6 ± 5.1	47.7 ± 8.2	54.7 ± 4.6	53.9 ± 5.5
GO-X-1'5	53.0 ± 4.1	62.3 ± 2.0	75.6 ± 3.1	68.5 ± 2.3
GO-X-5'1	5.6 ± 1.8	20.4 ± 6.9	35.9 ± 8.5	34.2 ± 7.9
GO-X-5'3	81.5 ± 0.1	86.0 ± 2.7	93.4 ± 1.8	90.6 ± 0.8
GO-X-5'5	87.4 ± 0.7	99.8 ± 0.2	99.7 ± 0.2	Clogged

MB rejection rate also improves with the number of bi-layers and immersion time for all the crosslinked and uncrosslinked membranes.

Improvement in performance of the covalently crosslinked membranes with regards the uncrosslinked, i.e. the PPD and MLM sets, gives indirect evidence that the crosslinkers hold the GO nanosheets together through covalent C-N bonds (as duly confirmed from FTIR and XPS characterisations in the previous chapter). This phenomenon was similarly observed elsewhere for differently fabricated amine-crosslinked membranes [53,319].

Similarly, for the PEI crosslinked membranes, enhancement of performance was evident. This is advocated to the PEI crosslinker electrostatically holding the GO nanosheets together, as confirmed from characterisations in chapter 3 and as also observed in related works elsewhere [191].

The MLM-crosslinked membranes showed improved MB separation performance compared with the PPD and PEI membranes. For instance, for GO-X-5'3, 93.4%, 86.0% and 90.6% average rejection rates are recorded for the MLM, PPD and PEI crosslinked membranes, respectively. A correlation between membrane relative hydrophilicity and performance is observable in this regard. The measurement estimates for the water contact angle of individual crosslinkers from the previous chapter are $68.2^\circ \pm 6.8^\circ$ for PPD; $57.3^\circ \pm 4.3^\circ$ for PEI; and $54.3^\circ \pm 5.7^\circ$ for MLM, with MLM being more hydrophilic. Although correlation does not mean causation, the significance of membrane hydrophilicity in enhancing membrane performance efficiency through increased wettability and antifouling improvement has been reported [320,321]. Hence, it is plausible that greater hydrophilicity has also an influence on performance improvement of the membranes.

MB rejection rate also improves with the number of bi-layers and immersion time for all the crosslinked and uncrosslinked membranes. In this case, higher material accumulation at longer immersion time and increased number of bi-layers leads to more adsorptive (physisorption) $\pi - \pi$ and electrostatic interactions between the membranes and MB, leading to improved rejection rates (Table 4.2) [322]. Additional to the covalent interactions, non-covalent conjugations such as dipole-dipole, hydrogen bonding and cation – π interactions between the amines groups and the non-oxidised regions in GO have been reported [53,260]. Furthermore, $\pi - \pi$ interactions

between GO and the aromatic ring in PPD and the triazine in MLM are also plausible [259,323]. These are likely to be contributing factors to the enhanced membrane stability in aqueous environments leading to improved performance for these membrane types.

4.3.2.2 Flux analysis

In line with the rejection results, permeation flux decreases as the number of assembly cycles and immersion times augment for both crosslinked and uncrosslinked membranes (Table 7). The lengthening of the tortuous path of the membranes at high material accumulation is a probable cause of the flux trend [324,325]. It is also noticeable that crosslinking results in a further decrease in flux. For instance, the 1-layer uncrosslinked GO membranes fabricated at 5-minute immersion times shows a flux of 18.7 l/m².h, and this decreases to 6.2 l/m².h, 7.4 l/m².h and 4.1 l/m².h for the PPD, MLM and PEI crosslinked membranes, respectively.

Table 7. Permeation fluxes of the fabricated membranes on PAN substrates

Membrane	Permeation flux (l/m ² h)			
	Uncrosslinked	PPD Crosslinked	MLM Crosslinked	PEI Crosslinked
GO-X-1'1	957.1 ± 62.9	859.6 ± 83.1	933.1 ± 56.3	826.9 ± 13.3
GO-X-1'3	221.5 ± 5.7	212.4 ± 4.4	115.2 ± 31.9	195.3 ± 3.4
GO-X-1'5	33.5 ± 4.1	23.2 ± 1.80	25.3 ± 1.9	12.2 ± 0.5
GO-X-5'1	18.7 ± 6.1	6.2 ± 0.54	7.4 ± 0.3	4.4 ± 0.5
GO-X- 5'3	6.0 ± 0.7	2.5 ± 0.87	5.2 ± 1.5	1.8 ± 0.3
GO-X-5'5	2.0 ± 0.7	1.8 ± 0.1	3.6 ± 0.1	Clogged

The decrease in flux with the number of assembly cycles for the crosslinked membranes is advocated to the increased intactness as the crosslinkers hold the nanosheets together. While for the uncrosslinked membranes, wetting result in enlarged membrane pore – gap and therefore a higher flux [46,53].

The PEI membrane clog at high immersion time and number of assembly cycles. This is due to higher tortuosity [326,327] relative to the other crosslinkers, as is confirmed by thickness measurements in the previous chapter (with a thickness of 58 nm at 5 minutes – 5 bilayers relative to only 12 nm and 13 nm for the PPD and MLM crosslinked thin-films, respectively).

Despite the relatively low fluxes recorded in this work at high number of bi-layers, the results obtained here show improvement in comparison to other studies, where a lower average flux at operational pressures 10 times higher than the one used in this study were observed. For instance, *Aba et al.* reported a flux rate in the range of 0.58 l/m².h to 0.60 l/m².h for the separation of organic dyes at an operational pressure of 10 bars [328]. In another work by Mi and Hu, a relatively low rejection rate of MB by layer by layer 1,3,5-benzenetricarbonyl trichloride crosslinked GO membranes between 43 and 66% has been obtained [329]. Thus, given the low operational pressure of 1 bar, the significance of the results described in this chapter are thus imperative.

A further importance of the work presented here is in the potential versatility of the membranes in the separation of molecular species other than MB. The molecular size of an individual (anhydrous) MB molecule is about 1.3 nm (13.84 Å) [330,331], being smaller than most textile dyes, such as remazol yellow and direct red 23 azo [330,332]. Although different separation mechanisms are used from dye to dye, based on selective permeation (molecular sieving) these fabricated membranes could separate other species. These are therefore significant results in water purification and gives an indication that the membranes can be refined further to separate even smaller entities, including divalent salts. The variety of the membranes, their ease of fabrication and

cost effectiveness are steps forward in the purification of contaminated waters and meeting the global water demand.

The performance of the membranes could be modelled with either molecular dynamic simulations or numerically basing on the tortuous permeation model, however, there are a variety of different factors that impact the performance of the membranes. These range from different interactions between the respective crosslinkers to pore gap, tortuosity, electrostatic repulsions between MB and PEI, stability/swelling, absence of $\pi - \pi$ interactions in the PEI and their presence in MLM and PPD. All these makes comparing the performance of the crosslinkers a challenge as the magnitude of each factor cannot be quantified with certainty for modelling without a higher number of assumptions.

4.3.3 Membrane stability

Post-operation membrane stability is a significant characteristic, as it governs the re-usability and longevity of the membranes. SEM characterisations were thus carried out after the nanofiltration experiments to study membrane stability (Figure 36).

It can be observed that micrometre-sized cracks appeared in the uncrosslinked membranes as they dry (Figure 36). This is promoted by the shrinkage of the GO nanosheets during drying [333]. No cracks are spotted on the crosslinked membranes. This finding demonstrates the influence of the crosslinkers on the intactness of the membranes, though holding the GO nanosheets together. This also further explains the observed lower MB rejection rate and higher flux for the uncrosslinked membranes relative to the crosslinked counterparts.

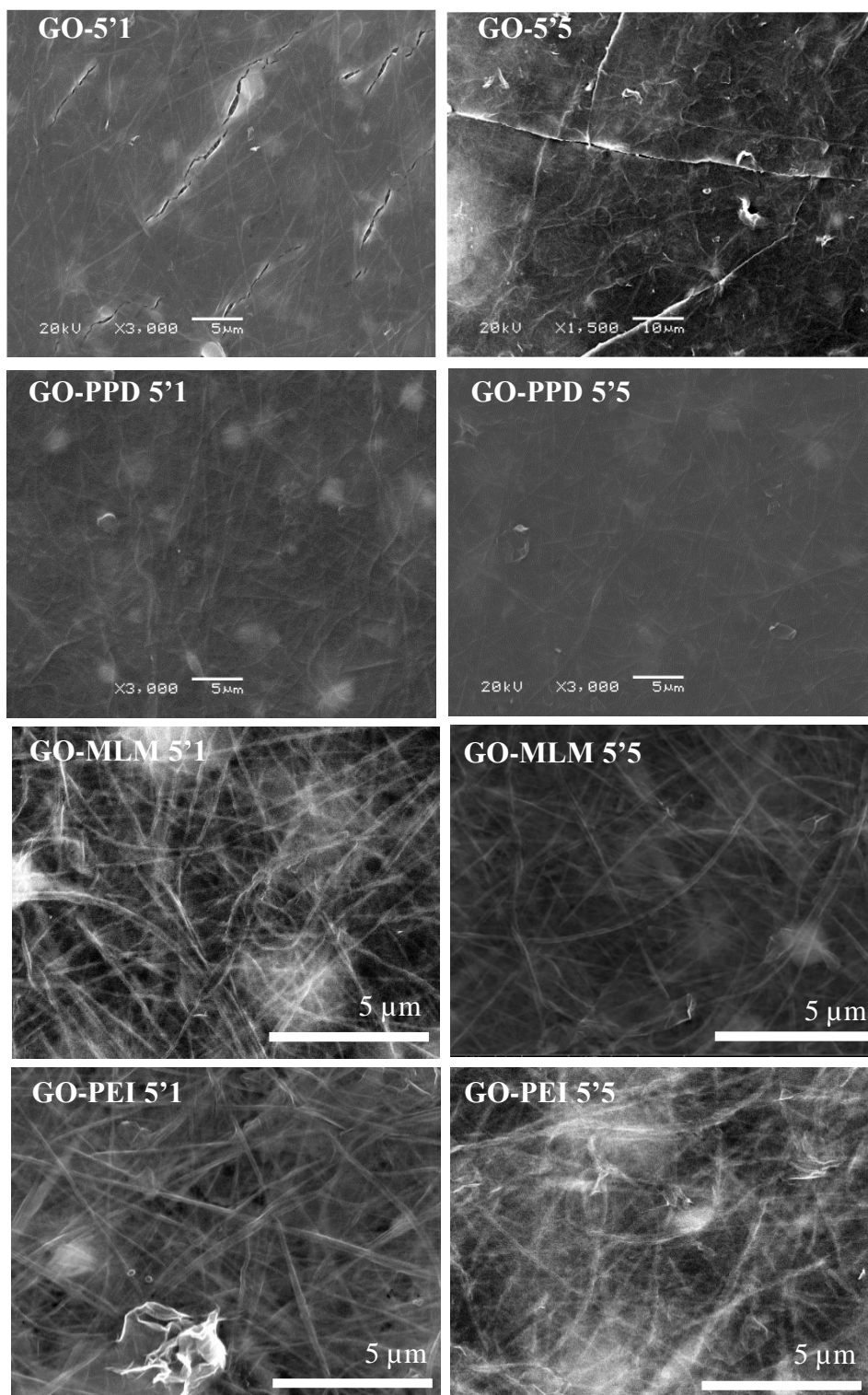


Figure 36. SEM images of the fabricated membranes post-nanofiltration.

To study membrane stability further, the respective crosslinked and uncrosslinked membranes were fabricated via a pressure-assisted filtration method in order to

increase the material load for observation. For the uncrosslinked membranes, a 15 ml solution of 0.5 mg/ml of GO was filtered through PAN substrates using the homemade nanofiltration cell (Figure 29) at a pressure of 3 bars. The crosslinked membranes, on the other hand, were fabricated by first reacting the GO and each of the crosslinker solutions and then filtering the reacted entities through the same device at the same pressure. The fabricated membranes were then dried for 24 hours to observe their stability over time in a dry environment (Figure 37).

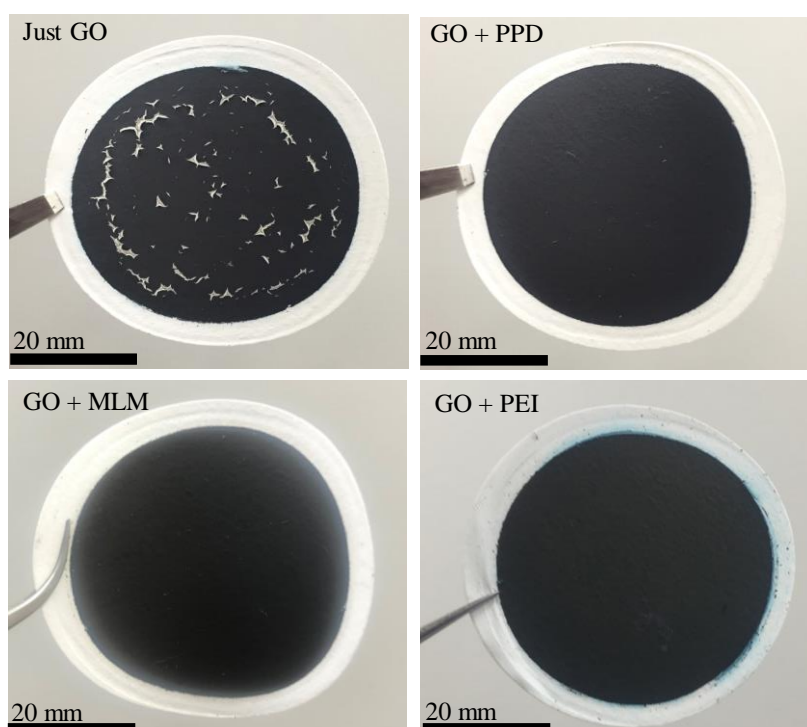


Figure 37. *Uncrosslinked and crosslinked membranes after pressure-assisted fabrication and drying*

It can be observed that uncrosslinked membranes tend to break and shrink after 24 hours of drying. This phenomenon is ascribed to the drying-related shrinkage [333]. The higher material load in this case results in evident, visible cracks (Figure 37). This finding validates the role of the crosslinker in improving the structural intactness and performance of the fabricated crosslinked membranes in this chapter.

4.3.4 Membrane separation mechanism, operational longevity and reusability

To understand the separation mechanism and operational longevity of the fabricated membranes, the over time performance by a sample of the crosslinked membranes (PPD crosslinked at 5 minutes and 5 bi-layers as a sample) was analysed. Continuous operation of the membrane for more than 120 hours at 1 bar shows no decrease in the membrane's selective separation abilities; however, the flux across the membrane considerably diminishes over time (Table 8). The maintenance of a constant rejection rate at an increased operation time leads to the conclusion that the predominant dye-separation mechanism in this instance was selective permeation (sieving) rather than selective binding [329,334–337].

Table 8. Separation of dye from water by the 5-bi-layer crosslinked PPD membrane (GO-PPD 5'5) over prolonged hours of operation (Working pressure 1 bar, MB concentration 10 mg/l)

Operation time (h)	MB rejection (%)	Permeation flux (l/m².h)
10	99.8	1.8
20	100.0	1.5
45	100.0	0.9
70	100.0	0.6
108	100.0	0.4
121	100.0	0.4

The separation was evaluated further by increasing the feed concentration from 10 mg/l to 125 mg/l and 250 mg/l. It is observed that the permeation flux at the high feed concentration decreases drastically as operation time increases (Table 9). This can be attributable to the increased initial adsorption of MB onto the GO membranes via electrostatic attractions between the negatively charged carboxylate groups in GO and the positively charged nitrogen containing groups in MB [335,338]. However, the

composition of carboxylate functional groups in GO is relatively low (6.3% for the GO-PPD 5 minutes reacted entity via XPS characterisations Table 3), in consequence, saturation of these sites would occur quite rapidly, even at low MB concentrations [335,338]. Importantly, the presence of aromatic rings in the GO, PPD and in MB (Figure 38) gives rise to $\pi - \pi$ interactions, which are likely to enhance the adsorption of MB onto the membranes in the initial operation stages of the permeation tests [171,339,340]. This narrows the permeation path significantly and thus results in decreased flux across the membrane and high MB rejection rates at prolonged membrane operation times.

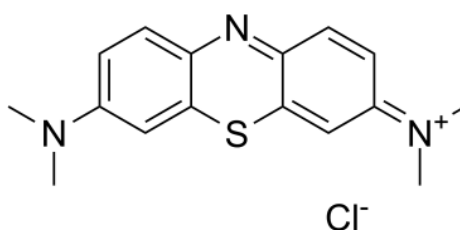


Figure 38. Structure of methylene blue (MB)

Table 9. Relationship between increased feed concentration and membrane performance at short and long operation times for GO-PPD 5'5.

Feed concentration (mg/l)	MB rejection (%) after		Permeation flux (l/m ² .h) after	
	3 hours	20 hours	3 hours	20 hours
10	99.8	100	1.8	1.5
125	98.3	100	0.8	0.4
250	96.7	98.1	0.2	0.1

The sample membranes are rendered reusable through rinsing after use in a 15% ethanol aqueous solution for 15 minutes. This results in the removal of attached MB and gives the membranes good operational efficiency post initial use. Nanofiltration

performance of the membranes post membrane rinsing is recovered almost to the initial measured flux of 1.8 l/m².h (Table 9) (Post-cleaning flux = 1.7 l/m².h average after 5 nanofiltration-cleaning cycles) and a rejection rate of 99.2% was achieved after rinsing. Given the more than 120 h operation longevity of the membranes per cycle before complete clogging and the excellent performance recovery, the use of the crosslinked membranes in nanofiltration is thus highly feasible. Stored in dry conditions at room temperature and pressure the membranes have been proven to have a shelf life of several months (observed for more than 8 months) without the use of any specific preservation methods. The lifetime of the membranes ought to be studied further in conjunction with specific operation conditions such as the operation pressure and fouling degree.

Overall, the modification of GO via crosslinking offers a myriad of opportunities for the use of these membranes in separation requirements. These findings show that GO membranes are potential alternatives to the current commercially available membranes such as polyamide, taking into account the low pressure used in this study.

4.3.5 Further economic improvements: assembly on other substrates

To further explore the use of other support substrates, sample membranes were assembled on polycarbonate (PCB) filters. Subject to their excellent mechanical strength, toughness, dimensional stability, flexibility and economic affordability [340,341], PCBs are good candidates to be used to support the thin crosslinked membranes.

From the previous results, excellent membrane performance in terms of rejection rate is achieved at a dipping time of 5 minutes and 5 bi-layers. Consequently, membranes at 5 minutes dipping time and 5 bi-layers for PPD were assembled on PCB substrates

to demonstrate their suitability. The membranes were fabricated following the same procedure as for those on PAN substrates. A similar pre-treatment procedure entailing the immersion of the membranes in H_2SO_4 and PEI respectively was entailed for the PCB substrates as well. The presence of a benzene ring in PCB [304] leads to attachment of the initial GO layer to the substrate electrostatically and through $\pi - \pi$ interactions [342].

The pictures and SEM images of the fabricated membranes are shown in Figures 39 and 40 respectively. Good membrane continuity of the respective membranes is evident, which signifies successful fabrication and assembly on the PCB substrates.

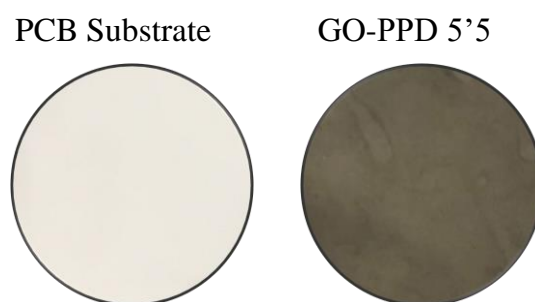


Figure 39 Images of the membranes fabricated on PCB substrates

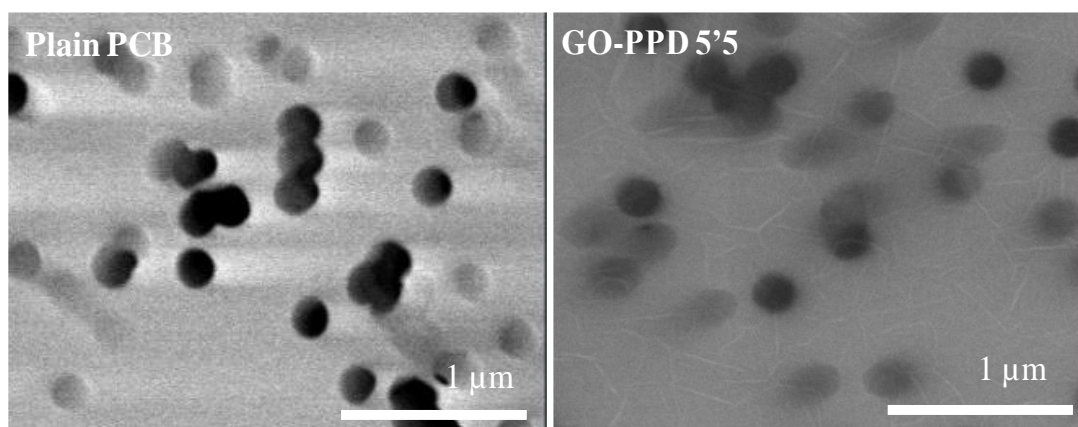


Figure 40 SEMs of membranes fabricated on PCB substrates

Excellent membrane performance in terms of rejection of 99.8% at a flux of 2.0 l/m².h was achieved for the PPD- membranes, this validates their use as potential substrates. Not only from the fact that PCBs are economically affordable, but also can be fabricated from easily recyclable polycarbonate waste discs, which enhances environmental conservation and sustainability [343]. Moreover, owing to their flexibility, varied shapes of crosslinked GO membranes can be assembled, for instance, tubular structures can easily be fabricated.

4.4 Conclusions

The role of crosslinkers on GO membrane performance has been verified following successful fabrication of crosslinked and uncrosslinked membranes. Crosslinking significance has been in turn manifested in enhanced stability and membrane intactness, which offer good membrane reusability and longevity. An improvement in membrane performance at higher immersion time and assembly cycles has been observed; excellent performance of ~100 % has been achieved for the PPD and MLM crosslinked membranes produced at 5-minute immersion time and with 5 bi-layers. Good membrane operation longevity at low operating pressure has been also demonstrated as continuous operation of sample membranes has been achieved over more than 120 hours with no reduction in dye rejection rate. Successful cycles of reusability demonstrated also validated the significance of crosslinking GO membranes. This work thus offers the potential use of these membranes with relevant modifications for the separation of other organic dyes, heavy metals and divalent salts.

5.

THE IMPACT OF GRAPHENE OXIDE'S PHYSICOCHEMICAL CHARACTERISTICS ON THE FABRICATION AND PERFORMANCE OF CROSSLINKED NANOFILTRATION MEMBRANES

“Man’s first glance at the universe discovers only variety, diversity, multiplicity of phenomena. Let that glance be illuminated by science, by the science which brings man closer to God, and simplicity and unity shine on all sides.”

LOUIS PASTEUR, (1822-1895)

5.1 Introduction

In the previous chapter, successful incorporation of crosslinkers onto graphene oxide (GO) membranes to enhance their performance was undertaken. However, little is understood about the impact of physicochemical characteristics of GO used as the starting material in both fabrication and performance of the crosslinked membranes.

The impact of GO's physicochemical characteristics on other GO based product efficiency has so far been reported. For instance, Kim *et al.* observed that for GO based

-
- ³Parts of this chapter are being peer reviewed for publication published in the Surfaces and Interfaces Journal : **Kandjou V**, Gonzalez Z, Acevedo B, Munuera JM, Paredes JI and Melendi-Espina S, The impact of graphene oxide's physicochemical characteristics on the performance of crosslinked nanofiltration membranes, *Surface and Coating Technology Journal* (2020) (Manuscript Under Review)
 - Parts of the work presented in the chapter have also been presented at the World Conference in Carbon in Lexington, Kentucky, USA, in 2019: **Kandjou V**, Acevedo B, Munuera JM, Paredes JI and Melendi-Espina S: The impact of sonication on graphene oxide's physicochemical properties and nanofiltration performance of covalently crosslinked membranes, **Poster Presentation**. Abstract No: 151.

nanocomposites, dispersing ability and mechanical strength, are strongly dependent on nanofiller lateral size [344]. Recently, the impact of lateral size on the performance of GO–polyamide membranes for forward osmosis applications has also been studied [345]. It was determined that at larger lateral sizes less homogeneous membranes emerged, which inhibited their performance [345]. There are theoretical simulations and experimental studies evaluating the impact of the synthesis conditions on the physicochemical and transport characteristics of GO laminates [346], as well as the influence of GO sheet lateral size on water permeance of GO pressure-assisted membranes [347]. However, there are no studies simultaneously investigating the effect of GO lateral size, its surface chemistry and colloidal stability on the subsequent crosslinked membranes' fabrication procedure and their nanofiltration performance. Therefore, it is important to study this to further understand, improve and optimise nanofiltration performance of the crosslinked membranes.

Lateral size and surface chemistry are inter-linked characteristics for GO when considering its non-stoichiometric Lerf–Klinowski structural model (Figure 8F) [121]. From the model, the position of specific oxygenated functional groups in GO is fixed to certain regions of the nanosheet plane [113]. Specifically, the epoxide and hydroxyl groups are situated at the basal plane, while the carboxylic groups are at the peripheries [113]. Considering the change in GO lateral size during production and preparation [125,348], it is significant to evaluate its impact on surface chemistry, suspension stability and subsequently on membrane nanofiltration performance.

In summation, this chapter entails the preparation of GO suspensions with different average lateral size and type/distribution of oxygen functional groups. The prepared suspensions were then used to fabricate cross-linked membranes to study in detail the

influence of GO physicochemical characteristics on membrane morphology and nanofiltration performance.

5.2 Experimental section

5.2.1 Materials

As in previous chapters, GO powder (product code: C889/GOB019/Pw2) was commercially sourced from Graphenea Co. (Spain). The crosslinker used in this study here was p-phenylenediamine (PPD, product code: P6001) from Sigma Aldrich. Polyethyleneimine (PEI, product code 03880) and potassium hydroxide powder (KOH), which were all used for substrate pre-treatment following the same procedure as in the previous chapters, as well as methylene blue (MB, $C_{16}H_{18}ClN_3S \cdot 3H_2O$, >99% purity; product code: M9140) for the preparation of solutions for nanofiltration tests, were all purchased from Sigma Aldrich (UK). Like in the previous chapter, the membranes were assembled on 0.2 μm pore sized, 47 mm diameter fibrous poly (acrylonitrile) (PAN) filter substrates purchased from Sterlitech Corporations in Washington DC, (USA).

5.2.2 Preparation of different lateral sized GO suspensions

To prepare the different lateral sized samples, an aqueous GO suspension in water at a concentration of 0.5 mg/ml was ultrasonicated at mild mechanical agitation, and used as the starting material (labelled GO-0'). Then, four aliquots of this parent sample were sonicated for different times (30, 60, 120 and 180 minutes) by means of a 280 W sonication power bath-type sonicator operated at a frequency of 55 Hz (Fisherbrand FB1505, Elmasonic S30H). The samples were labelled as GO-X', with X indicating the corresponding sonication time.

5.2.3 Sample characterizations

5.2.3.1 Atomic Force Microscopy (AFM)

The lateral size and the height of the different GO samples were measured using AFM imaging and profiling. This was done by depositing a drop (~50 μL) of a water suspension of each sample onto a highly oriented pyrolytic graphite (HOPG) substrate that was pre-heated at ~50-60 $^{\circ}\text{C}$. The GO sheets were imaged using a Nanoscope IIIa Multimode (Veeco Instruments) operating in tapping mode under ambient conditions, room temperature and pressure. Silicon cantilevers with a resonance frequency of 250-300 kHz and a ~40 N m^{-1} spring constant were used. The respective images for each of the sample were processed using Scanning Probe Image Processor (SPIP) software.

5.2.3.2 UV-Vis spectra measurements

Further confirmations of the alteration of the lateral size through ultrasonication means were proven by UV-Vis spectra measurements (Hitachi U-3900 UV-Vis). Respective calibration lines were constructed for each of the differently sonicated samples. This was done to calculate each sample's absorption coefficients (α_{GO}) based on the Lambert-Beer law (Eq.3) [349]. This coefficient is a lateral size dependent parameter.

$$A = \alpha_{\text{GO}} \cdot c \cdot l \quad \text{Eq. (3)}$$

Where A is the absorbance (a.u.), c (mg/ml), the concentration, and l (m) the optical path length, (length that the light passes through during UV-Vis measurements i.e. cuvette length (0.01 m)).

5.2.3.3 Surface chemistry characterisations via X-ray Photoelectron Spectroscopy measurements

The surface chemistry of the different GO samples was evaluated by X-ray Photoelectron Spectroscopy (XPS) measurements (Kratos Axis Ultra-DLD, K-Alpha⁺). Each suspension (GO-0' - GO-180') was centrifuged in a Bio-Fuge Primo Heraeus centrifuge (1000 rpm for 10 minutes) to collect the samples for the XPS characterisations.

The oxygenated functional groups present in the samples were estimated by first constructing a wide-scan spectrum in the binding energy range of 0–1000 eV. This was followed by a curve fitting for the C1s and O1s spectra using a Gaussian-Lorentzian peak shape, after performing a Shirley background correction. The major peaks for the C1s curve were the C graphitic (Binding energy, BE, = 284.3–284.4 eV), C-O epoxide/C-OH hydroxyl (BE = 285.6–285.7 eV), C=O carbonyl (BE = 286.9–287.0 eV), as well as the O-C=O carboxyl (B.E = 288.9 eV). However, it is important to note that overlap of oxygen functionalities, specifically between C(epoxy) and hydroxyls, was notable [235,236,350]. For the high-resolution O1s curve fittings, 5 major peaks similarly emerged, representing the (C=O) carbonyl, (C=O) carboxyl, (C-OH) hydroxyl, (C-O) epoxy and (C-O) carboxylic groups respectively [351].

5.2.3.4 Zeta (ζ) potential measurements

To determine GO suspension stability and dispersibility of the nanosheets at a changing lateral size, potential measurements, ζ , were undertaken using a Zetasizer Nano series (Nano ZS90, Malvern, UK) for a quantifiable relation. The pH of the suspension was measured at 5.2.

5.2.4 Membrane fabrication, characterisations and performance tests

As aforementioned, the parent aim of the work done in this chapter was to study the impact of the physicochemical characteristics of GO onto the fabrication and performance of the crosslinked GO membranes. PPD crosslinked membranes were then assembled. This was done under similar fabrication procedure described in the previous chapter. As previously, a rotary dip coater (ND-R 11/2, S/N: 522016) was used to alternatively immerse the pre-treated PAN substrates in the corresponding GO suspensions and PPD solution. In this study, the membranes were fabricated under 1-minute immersion time and 5 bi-layers were assembled. The fabricated crosslinked membranes were accordingly labelled as M-GO-X' (with X being the sonication duration of the GO suspension used as starting material).

Membrane morphology was then analysed by means of a JEOL JSM – 5900 LV Scanning Electron Microscope (SEM). Similarly, nanofiltration performance was evaluated by permeating a 10 mg/l aqueous solution of methylene blue (MB) through each of the fabricated membranes under 1 bar. Three membranes of each GO sample type were fabricated and tested to have good results reliability. The average of the three measured rejections and fluxes were taken, noting down the standard deviation in error bars.

5.3 Results and Discussions

5.3.1 Physicochemical characteristics of the GO samples.

5.3.1.1 GO average lateral size with sonication

The average lateral size of the GO nanosheets significantly diminishes with an increase in sonication time (Figure 41). The decrease is more pronounced after the

first 60 minutes, leading to a reduction of the average lateral size from 3.9 to 1.7 μm . Longer sonication duration (up to 180 minutes) is not as effective in reducing the GO lateral size, hence its plateauing from 1.7 to 1.3 μm is observed. These results are in qualitative agreement with previous works elsewhere, where an exponential decay in GO nanosheet size with sonication time has been reported [352,353].

Besides having larger sheets, GO-0' and GO-30' also show a wider size distribution, containing sheets with lateral dimensions above 4 μm , which are not present in samples sonicated for longer periods (Figure 41) [354].

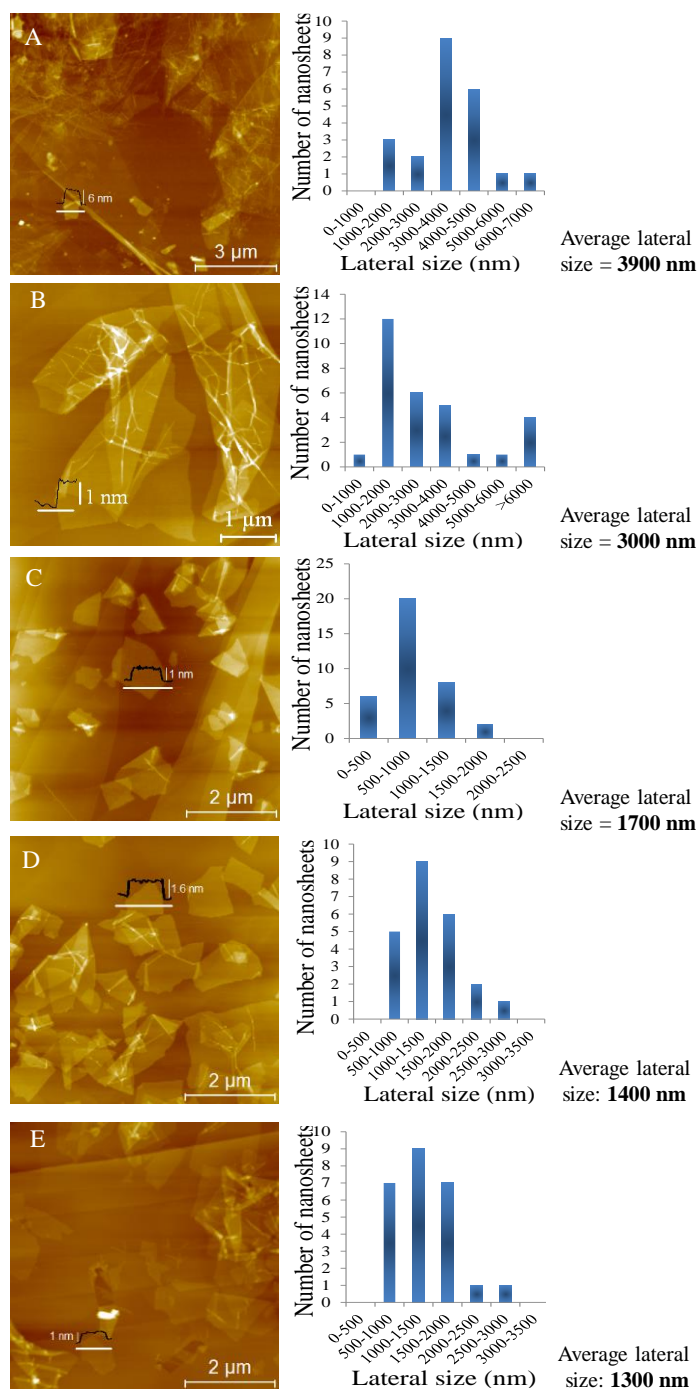


Figure 41. AFM images of the differently sonicated samples; A) GO-0' B) GO-30' C) GO-60' D) GO-120' and E) GO-180' and respective histograms depicting their lateral size distribution.

To further confirm the alteration of lateral size with sonication, UV-Vis absorption spectroscopy characterisations have been carried out. Though a cumulative

combination of factors (such as the number of layers and surface chemistry) also affect UV-Vis related absorbance, GO lateral-size has been noted to be a key factor [355]. The absorbance coefficient (α) of each suspension has been calculated from the absorbance values at a 660 nm wavelength, because at this wavelength there is minimal interference on absorbance from GO's chemical functionalities, and hence absorbance is predominantly a function of the lateral size [356].

This relationship between suspension lateral size and light absorption has been detailed elsewhere, where an increase in absorption as the lateral size decreases has been reported [355]. This is in agreement with the results here, where an inverse relation between the absorption coefficient and lateral size is observed (Figure 42). The optical absorbance in the visible region is enhanced with sonication time, as evidenced by an increase in the absorption coefficient from 670 to 830 $\text{ml mg}^{-1} \text{m}^{-1}$.

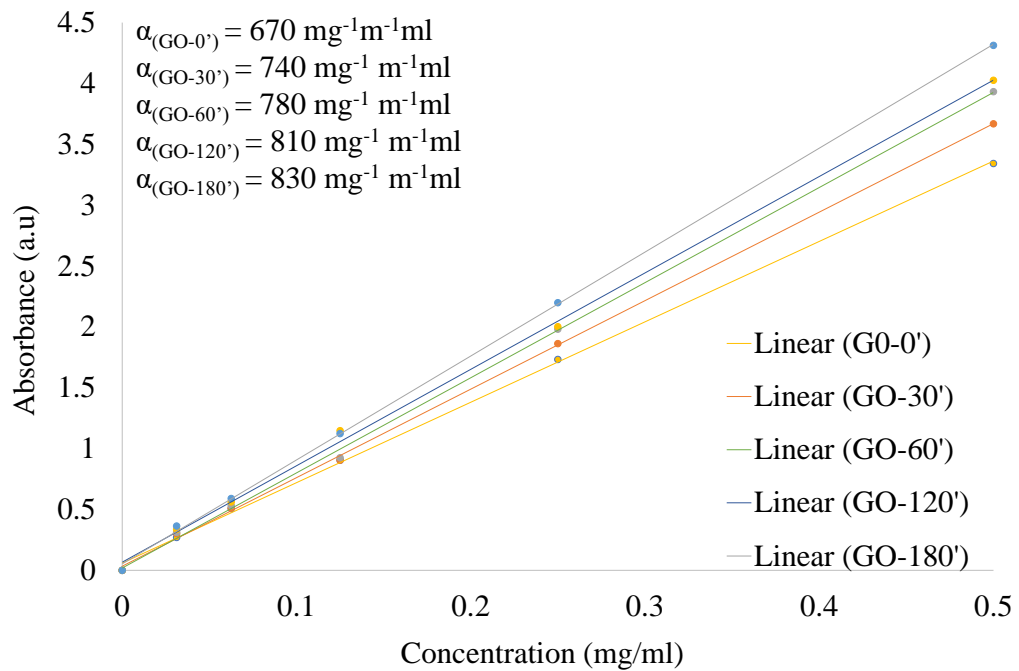


Figure 42. Absorption coefficients of the prepared samples.

5.3.1.2 Average lateral size – surface chemistry relation and impact on suspension stability

The decrease in GO lateral size is accompanied by noticeable changes in surface chemistry, mainly in terms of type and quantity of oxygen functional groups (Table 10).

Table 10. Surface chemistry of GO samples determined by XPS (at. %)

	GO-0'	GO-30'	GO-60'	GO-120'	GO-180'
C 1s curve (%)					
C1s	71.2	67.9	67.6	68.8	68.1
O1s	27.4	31.3	31.4	31.5	31.2
C/O	2.6	2.3	2.2	2.2	2.2
Csp ² +Csp ³	58.0	42.5	44.0	43.4	45.4
C-O Hydroxyl/Epoxy	36.6	50.1	44.7	42.6	39.2
C=O Carbonyl	1.2	1.7	5.8	7.7	9.0
COOH Carboxyl	4.2	4.7	4.5	5.0	5.4
$\pi^*-\pi^*$	0.0	1.0	1.0	1.3	1.0
O 1s curve (%)					
C=O Carbonyl	8.8	10.0	10.8	12.2	14.4
C=O Carboxyl	3.2	5.3	6.5	7.6	9.4
C-O Hydroxyl	54.4	49.7	47.9	45.5	40.3
C-O Epoxy	30.4	29.7	28.3	27.1	26.5
C-O Carboxyl	3.2	5.3	6.5	7.6	9.4

A notable drop in abundance of the overlapping basal plane GO functional groups (hydroxyls and epoxy groups) is observed at a decreasing lateral size (Table 10).

There is still ambiguity in processes that lead to the fragmentation of GO nanosheets from ultrasonication at atomistic level, however Li *et al.* proposed that cooperatively aligned epoxy groups initiates fragmentation of GO nanosheets with prolonged ultrasonication [357]. As such, the abundance of the epoxide decreases with lessening in nanosheet lateral size during fragmentation.

For the peripheral carbonyl and carboxylic groups on the other hand, an upsurge in their abundance at a decreasing lateral size is notable (Table 10). This is explicable from the fact that, as the nanosheets fragment, the cumulative peripheral area rises culminating in an increase in the abundance of these oxygenated functionalities.

The rise in the prevalence of the oxygenated groups located at the sheet edges correlates with an improvement in suspension stability [358,359], which is reflected on the measured zeta potential of the samples (Table 11). Zeta potential is equivalent to the degree of electrostatic repulsions between adjacent nanoparticles/nanosheets and therefore it is an important parameter to quantify both dispersibility and stability of colloidal samples [359,360]. The zeta potential increases (in absolute value) from -18.1 to -34.8 mV, as the GO lateral size decreases (Table 11). GO-0' and GO-30' are categorized as incipiently unstable, with their absolute value below ± 30 mV, meaning they tend to flocculate and agglomerate (which was indeed the case for GO-0' and GO-30' after standing undisturbed for several days). At decreased lateral size, GO-60', GO-120' and GO-180', with electrostatic repulsion above ± 30 mV (absolute value), are inherently stable and therefore their nanosheets are well suspended [361,362].

Table 11. Zeta potential of the GO suspensions

Sample	ζ (mV)
GO-0'	-18.1
GO-30'	-25.0
GO-60'	-32.5
GO-120'	-34.0
GO-180'	-34.8

5.3.2 Impact of graphene oxide's physicochemical characteristics on membrane homogeneity, coverage and morphology

As aforementioned, GO samples obtained at different sonication times have been used for the fabrication of a variety of PPD crosslinked membranes. An increase in the degree of GO accumulation can be observed when comparing the darker pigmentation of the membranes from M-GO-0' to M-GO-180' (Figure 43). This can be due to an improved interaction between GO and PPD during layer-by-layer assembly, which is promoted by the enhanced stability of the samples with time of sonication, as confirmed by the zeta potential measurements.

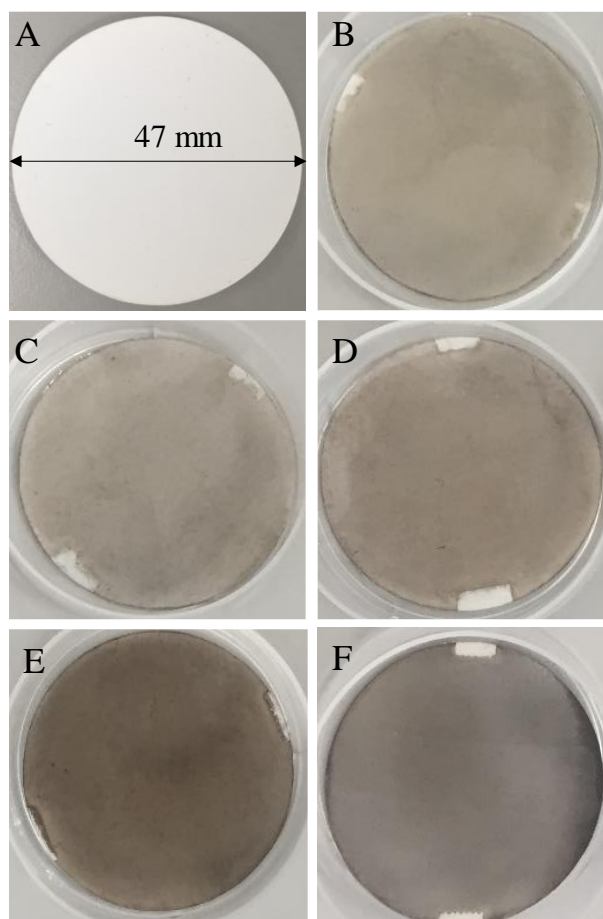


Figure 43. Photographic images of the fabricated membranes; A) plain PAN substrate, B) M-GO-0' C) M-GO-30', D) M-GO-60', E) M-GO-120' F) M-GO-180'

Furthermore, from SEM characterisations, M-GO-0' exhibits evident discontinuity in covering the substrate, as notches of PAN fibres are clearly visible (Figure 44B). This is inherently due the lack of appropriate suspension stability of the GO sheets in sample GO-0', according to its low zeta potential (-18.1 mV, Table 11). On the other hand, membranes from M-GO-30' to M-GO-180' show a homogeneous coverage of the substrate with highly reduced presence of visible PAN fibres (Figures 44 C-F), which is in agreement with their improved physicochemical characteristics.

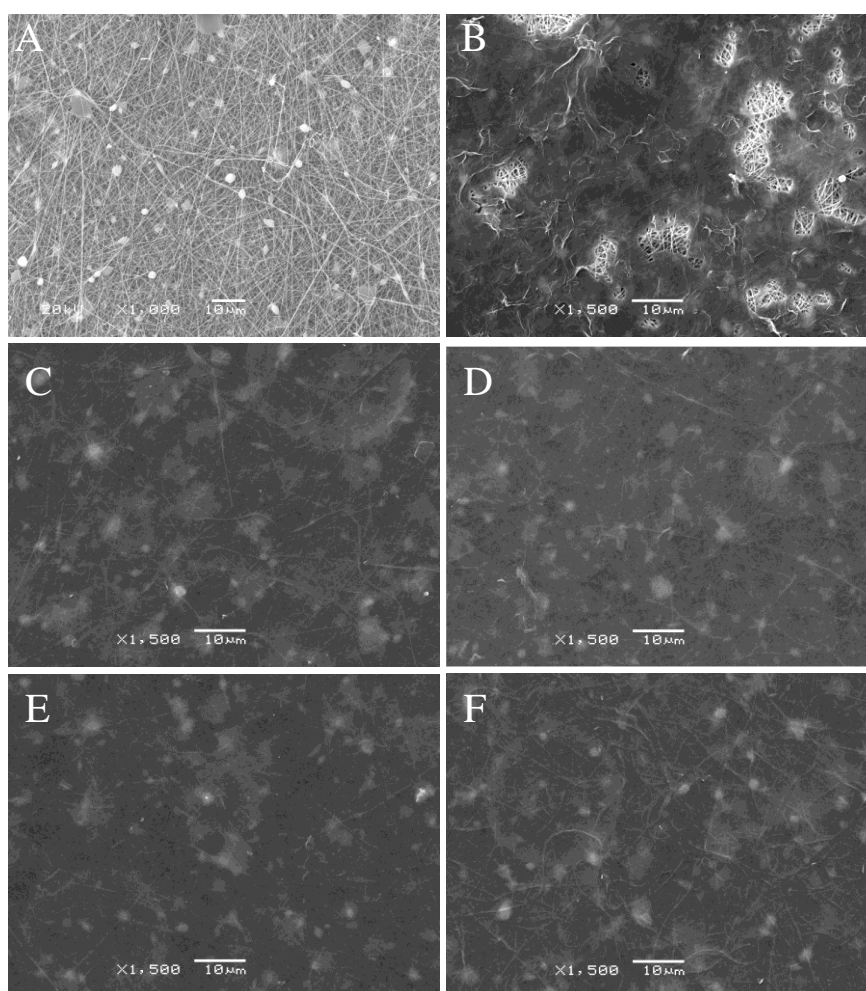


Figure 44. SEM images of A) plain PAN substrate, B) M-GO-0' C) M-GO-30', D) M-GO-60', E) M-GO-120' and F) M-GO-180'

5.3.4 Membrane performance analysis

5.3.4.1 Membrane rejection

Analysis of the performance results show that membrane rejection rate significantly improves as the GO lateral size decreases. The average rejection rises from 59.8% to 93.9% for M-GO-0' and M-GO-30', respectively (Figure 45). Plateauing in performance post M-GO-60' with an average increased rejection of $97.8\% \pm 0.6\%$ is observed (Figure 44). These results are in correlation with zeta potential suspension stability measurements and SEM characterisations, thus corroborating the influence of lateral size on membrane homogeneity and continuity coverage on their performance. The good colloidal stability of GO-60', GO-120' and GO-180' (i.e. the higher amount of individual GO sheets in these suspensions) is mainly due to their optimum lateral size and the type/distribution of oxygen functional groups (e.g., increased fraction of edges with ionisable oxygen groups). This offers enhanced suspension stability and suitable conditions for a more effective crosslinking with PPD as afore-discussed in the previous section.

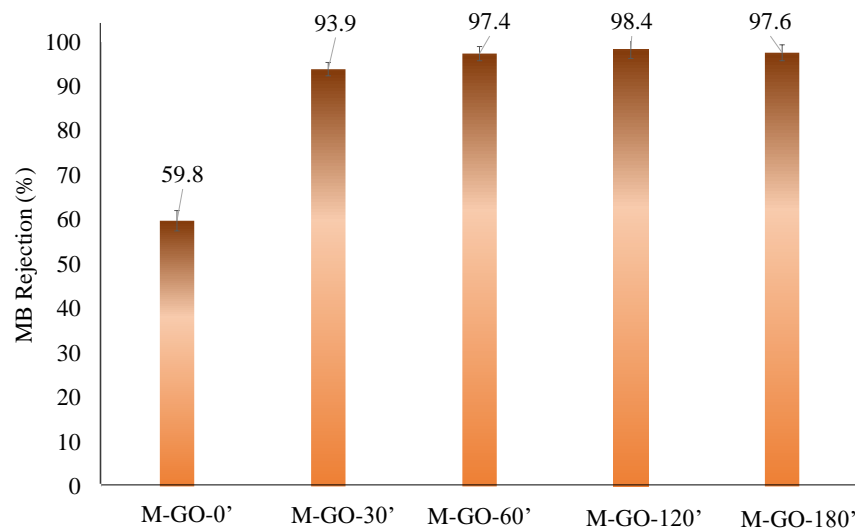


Figure 45. MB rejection results of the fabricated membranes with respective permeate solutions

5.3.4.2 Permeation flux across the membranes

The flux expectedly counters the rejection results, as the higher the flux, the lower the rejection. For M-GO-0', a very high flux of 890.7 l/m².h has been recorded (Figure 46). This is advocated to the lack of uniform coverage of this membrane (Figure 44 B). The large notches in the areas of no coverage are a contributing factor to the observed high flux and low rejection. This validates the significance of continuity and homogeneity as significant properties in membrane separation performance [363]. The impact of membrane homogeneity, or its lack of, is therefore apparent in membrane rejection, flux and other significant membrane characteristics as observed. Fluxes in the 3.6 – 5.5 l/m².h range have been subsequently recorded for the M-GO-60' to M-GO-180' membranes, owing to excellent membrane homogeneity and intactness.

Although M-GO-30' shows an appropriate morphology (Figure 44 C), its rejection of MB is less efficient and the flow across this membrane is higher than that for M-GO-60', M-GO-120' and M-GO-180'. The somewhat inferior colloidal stability of the parent sample GO-30', which presents a zeta potential below the ± 30 mV threshold established for a stable suspension (Table 11) is a likely contributing factor to the recorded lower rejection. At better dispersibility, more GO nanosheets are exposed for better crosslinking with PPD via an epoxy ring opening reaction [53] during membrane fabrication, which likely enhance membrane stability and performance.

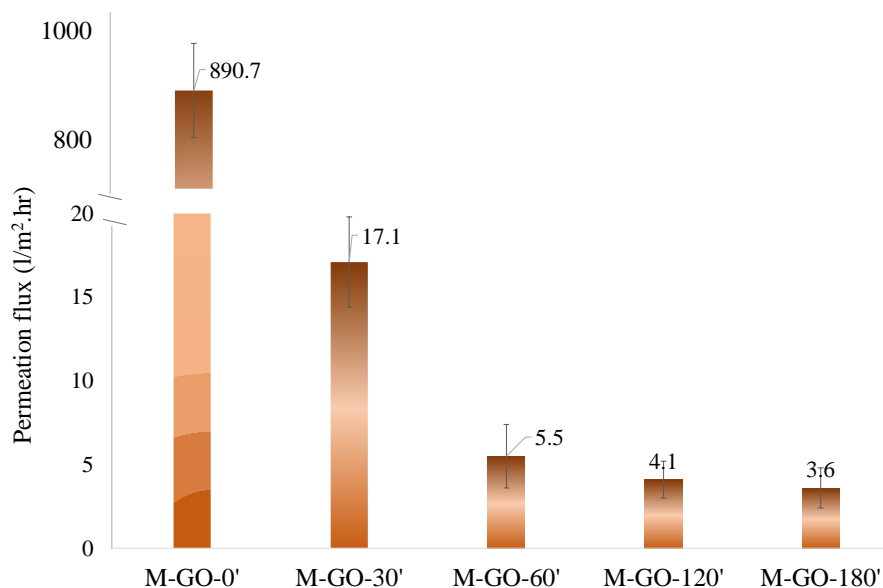


Figure 46. Permeation flux of the fabricated membranes

In summation, the lifetime of these membranes can thus be extended through fabrication using smaller more stable nanosheets as they give more stable suspensions resulting in good membrane continuity.

5.4. Conclusions

The chapter documents the relation between the physicochemical characteristics of GO and how their alteration affects membrane fabrication and performance. The GO sonication time appears to be a key parameter, determining important characteristics of the resulting sheets, such as average lateral size, type/amount of oxygenated functional groups and colloidal stability. The relation between GO lateral size and surface chemistry has been established. Specifically, hydroxyl and epoxy groups, located in the basal plane, decrease with the GO lateral size while carbonyl and carboxylic groups are promoted. The different physicochemical characteristics influence not only on the stability and individuality of the GO sheets, but also on the effectiveness of crosslinking, and consequently on the nanofiltration performance of

the resultant membranes. Up to a $97.8\% \pm 0.6\%$ of MB separation has been achieved at decreasing lateral size relative to only 59.8% for M-GO-0'.

Therefore, the starting GO material is significant in determining actual performance of GO crosslinked membranes. Relevant optimisations are thus always a necessity to conserve operational costs.

6.

⁴CONCENTRATION IMPACT ON CROSSLINKED GRAPHENE OXIDE MEMBRANES' STABILITY AND PERFORMANCE: ENHANCING MATERIAL CONSERVATION

“...aiming at simplicity and lucidity is a moral duty of all intellectuals: lack of clarity is a sin, and pretentiousness is a crime.”

SIR KARL RAIMUND POPPER, (1902-1994)

6.1 Introduction

The influence of physicochemical characteristics of graphene oxide (GO), specifically the average lateral size, colloidal stability and surface chemistry on membrane fabrication and performance were duly carried out in the previous chapter. This chapter in tandem explores material conservation through studying and evaluating the impact of GO and crosslinker concentrations on membrane morphology, stability and overall nanofiltration performance. This is essential in enhancing performance efficiency together with reducing production and operation costs for nanofiltration membranes [364]. A systematic way to optimise GO suspension and crosslinker solution concentrations used in membrane fabrication is through establishing how it

-
- Parts of the work in this chapter is due to be submitted for publication in the Separation and Purification Technology Journal, 2020: **Kandjou V**, Casal M.D, Melendi-Espina S, Optimising the fabrication concentration of layer by layer crosslinked graphene oxide membranes: enhancing membrane material conservation, *Separation and Purification Technology Journal* (2020)

impacts the rejection rate and permeation flux. Fundamentally, in the case of the crosslinker, it is also essential to study the degree to which it affects the mechanical strength of the fabricated membranes. The chapter therefore primarily details how concentration influences fundamental membrane characteristics like homogeneity, relative thickness and nanofiltration performance.

Intermittent studies on the impact of concentration on differently fabricated GO based membrane performance continue to be undertaken. For instance, Bala *et al.* studied the effect of varying GO concentration on both membrane fouling susceptibility and permeation flux for ultrafiltration membranes [365]. In the study, pure water flux increased with GO concentration as a result of improved membrane surface hydrophilicity and changes in morphology [365]. Further related works by Zhao *et al.* also established a proportional relation between GO concentration and nanofiltration performance of nanocomposites membranes [366]. In layered nanofiltration GO membranes however, a decrease in permeation flux at higher GO loading due to increased thickness and tortuosity has so far been established [204,284,367].

The afore-discussed impacts of concentration on performance and morphologies were studied on GO membranes fabricated by the vacuum filtration and pressure assisted methods. As the degree of impact of concentration is likely to vary from one fabrication method to another, it is important to study this for the dip-assisted layer by layer fabricated membranes. In consequence, respective crosslinked membranes with varying GO and p-phenylenediamine (PPD) (as the sample crosslinker) concentrations were fabricated and their nanofiltration performance duly evaluated. Relevant characterisations from thickness measurements to pre and post nanofiltration membrane SEM characterisations were undertaken to determine homogeneity, surface intactness and stability.

6.2 Experimental section

6.2.1 Materials and sample preparation

As in the previous chapters, the GO powder (product code C889/GOB019/Pw2) used was commercially sourced from Graphenea Co., Spain. Similarly, the membranes were assembled on microfiltration polyacrylonitrile (PAN) substrates from Sterlitech Corporation (Washington, DC, USA). To estimate the relative thickness of the membranes at changing concentrations, glass slides (CAT.NO.7101, 1.0-1.2mm thick) from Fisher Scientific (Loughborough, UK) were used to assemble alike crosslinked thin films for these characterisations. At lower GO concentration of 0.125 mg/ml, the thin films were assembled on silicon wafers as the roughness of the glass slides limited the accuracy of the measurements.

The crosslinker, PPD (product code P6001), the polyethyleneimine (PEI, product code 03880) and potassium hydroxide powder (KOH) used to pre-treat the membranes, as well as the methylene blue (MB, C₁₆H₁₈ClN₃.3H₂O, >99% purity; product code M9140) to evaluate nanofiltration performance, were all purchased from Sigma Aldrich, UK.

In the previous chapters, excellent membrane performance was achieved with a GO concentration of 0.5 mg/ml and a PPD concentration of 2.0 mg/ml. Therefore, in an attempt to enhance material conservation and optimise the required amount of crosslinker, it was decided to study the impact of concentrations lower than these anchor concentrations. Consequently, respective aqueous suspensions of 0.125, 0.25 and 0.5 mg/ml concentrations for GO and 0.1, 0.2, 0.3, 0.5, 1.0, 2.0 mg/ml for PPD were prepared.

Similarly, the respective GO samples were sonicated for 2 hours in a bath type sonicator with 280W sonication power at a 55Hz frequency (Fisherbrand FB1505, Elmasonic S30H) to enhance nanosheet colloidal dispersion.

6.2.2 Membrane fabrication, characterisations and performance tests

The membranes were fabricated like in chapter 4 and 5 with the aid of a rotary dip-coater (ND-R 11/2, S/N: 522016). 5 bi-layered crosslinked membranes assembled under 1-minute immersion time membranes at different GO and PPD concentrations were successfully fabricated. A labelling notation of GO_xPPD_y , where x and y are the concentrations of GO suspensions and PPD solutions was used. Results reliability was enhanced through fabricating and testing three membranes of each type at the respective concentrations.

The relative change in membrane thickness was estimated through fabricating alike thin films on glass slides and then using a Bruker DektakXT Profiling System (Stylus Profiler). Thickness reliability was enhanced by taking an average of 10 measurements noting down the standard deviations.

Membrane surface homogeneity and structural quality before and after use was examined by a high-resolution FEI Nova NanoSEM450 containing a Gatan cryo-system with various detectors from Energy Dispersive X-ray Spectroscopy (EDS) to Backscattered Electron Imaging (BSE). The SEM was operated in a low voltage of 1 kV in high vacuum mode. The pre and post nanofiltration surface characterisations were carried to examine the stability and overtime intactness of the respective membranes.

Membrane nanofiltration performance was evaluated using a low economic 1 bar pressure in a dead-ended filtration process as in the previous chapters. 100 ml of 10

mg/l of MB was passed through each of the fabricated membranes to calculate their rejection and permeation flux. An average rejection and flux of the three membranes of each type was obtained and the standard deviation was respectively recorded.

6.3 Results and Discussion

6.3.1 Membrane morphology and thickness at changing concentrations

Photographic images of the fabricated membranes at respective GO and crosslinker concentrations are displayed in Figure 47. A homogeneous intensification in membrane pigmentation at an increasing GO concentration is observable and further confirmed by means of FESEM (Figure 48). Excellent membrane continuity and structural quality for the fabricated membranes is evident at the respective concentrations.

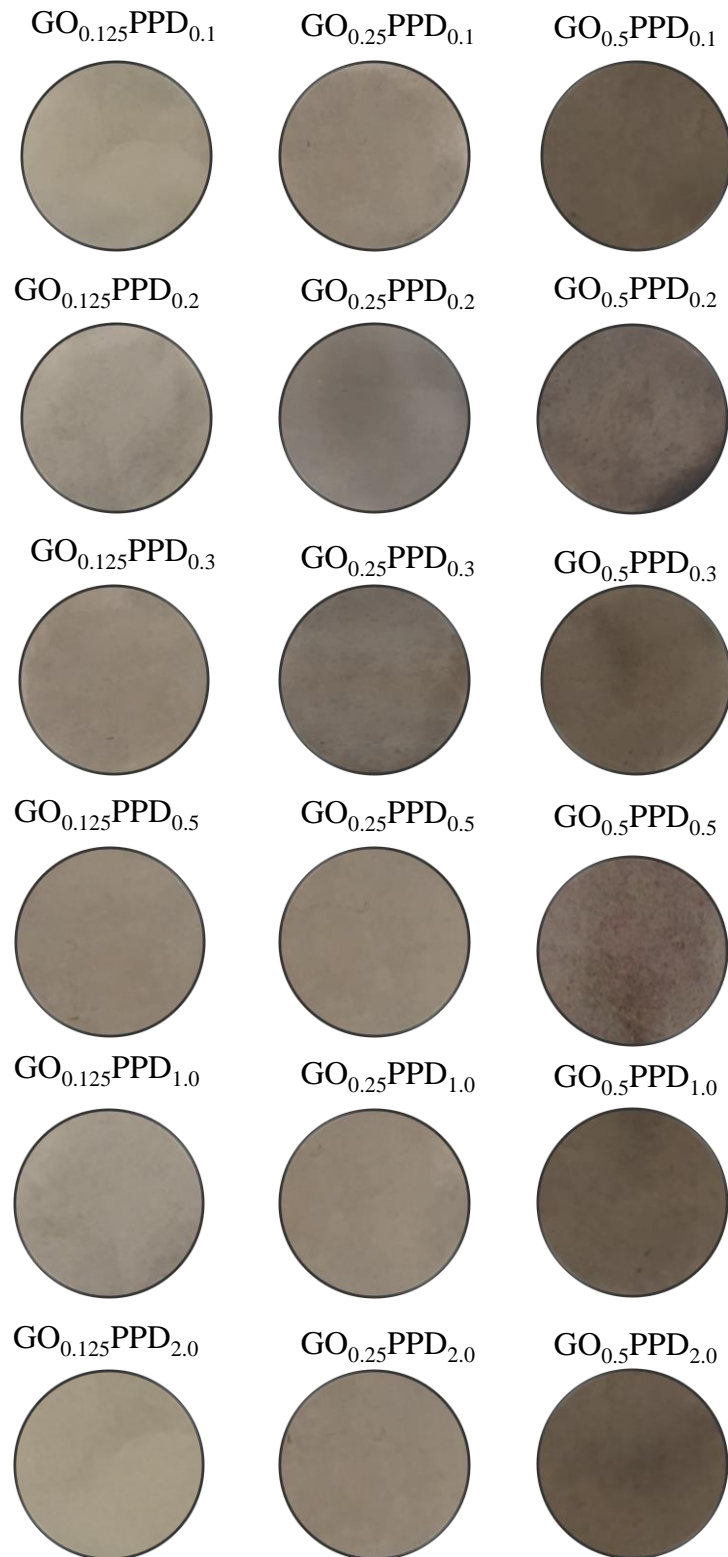


Figure 47. Photographic images of the fabricated membranes at respective GO and crosslinker concentrations

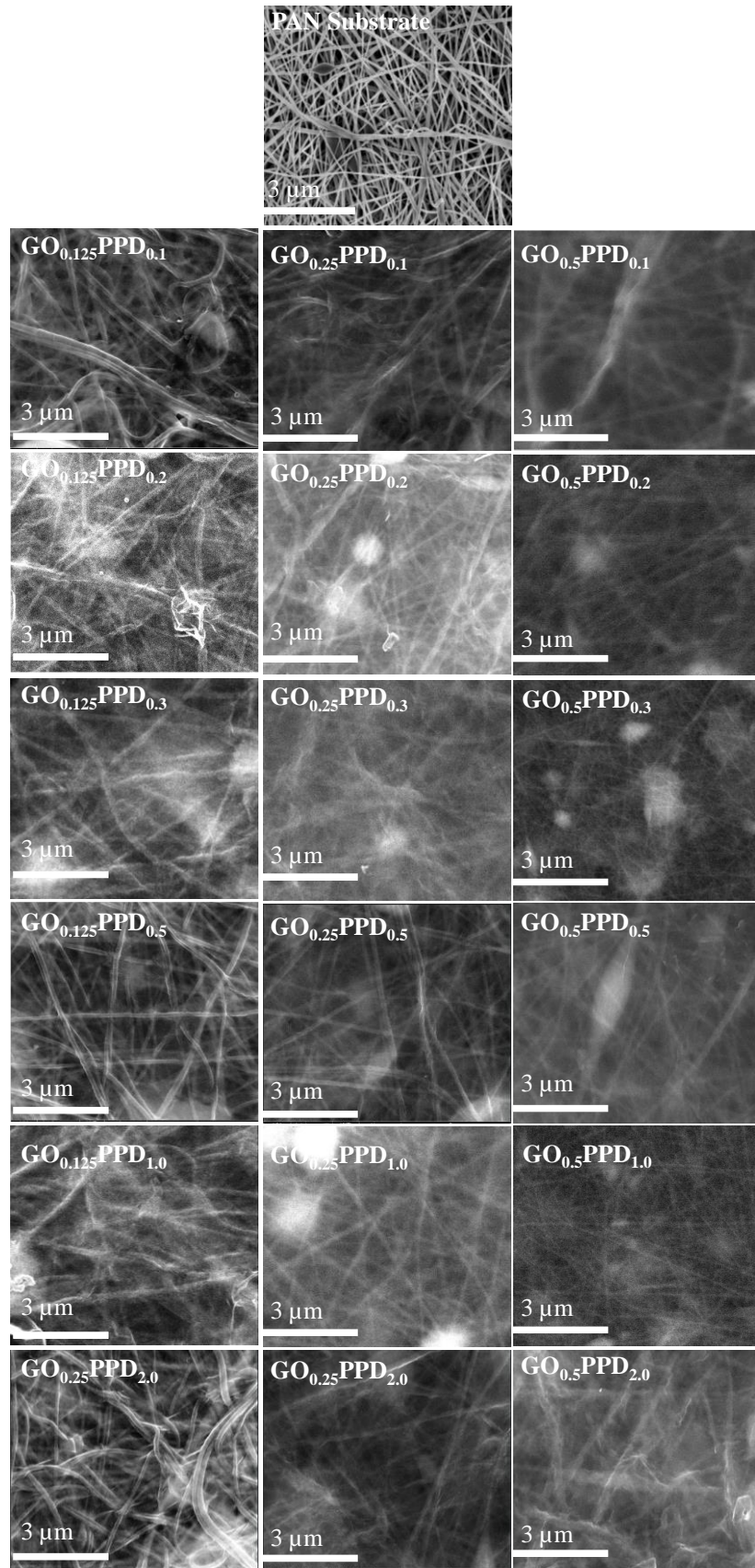


Figure 48. SEM images of the fabricated membranes

It is observable that nanosheets accumulation onto the PAN substrates heightened with GO concentration. This is evidenced by the lessening visibility of the protrusion of the fibres of the PAN filters, these were pronounced for $GO_{0.125}PPD_y$ membranes relative to $GO_{0.25}PPD_y$ and $GO_{0.5}PPD_y$ (Figure 48). A similar fit of increased GO accumulation onto the substrates at changing suspension concentrations has been observed elsewhere [368], where it was advocated to clustering and agglomeration of the GO nanosheets.

Akin to the photographic images, the change in concentration of the crosslinker have less observable change on membrane morphology. It seems that continuity coverage is predominantly dependent on the large surface area material GO, in comparison to the molecular PPD [113,121].

With regard to the membrane thickness, it primarily depends on the concentration range of GO (Table 12). For instance, at a crosslinker concentration of 2.0 mg/ml, 2.2 nm thin films are obtained with a GO suspension of 0.125 mg/ml, this increases to 6.2 nm if the concentration of GO is raised to 0.5 mg/ml. Similar trend has been observed elsewhere where a GO concentration-thickness proportional relation has been reported [265,369]. This is inherently tied to the higher *intra*-interaction between GO nanosheets via dipole – dipole, van der Waal's forces, hydrogen bonding and $\pi - \pi$ stacking [317], which is likely to increase with GO concentration .

On the other hand, keeping GO concentration constant while increasing that of PPD from 0.1 mg/ml to 2.0 mg/ml result in a minimal change in thickness of up to 1.6 nm (Table 12).

Table 12. Thickness of the fabricated thin films at respective GO and PPD concentrations in nm

Membrane	Relative thickness (nm)
GO _{0.125} PPD _{0.1}	1.1 ± 1.4
GO _{0.125} PPD _{0.2}	1.6 ± 1.6
GO _{0.125} PPD _{0.3}	1.4 ± 1.3
GO _{0.125} PPD _{0.5}	1.9 ± 1.2
GO _{0.125} PPD _{1.0}	2.1 ± 1.4
GO _{0.125} PPD _{2.0}	2.2 ± 0.8
GO _{0.25} PPD _{0.1}	3.7 ± 1.1
GO _{0.25} PPD _{0.2}	3.6 ± 0.7
GO _{0.25} PPD _{0.3}	3.4 ± 0.5
GO _{0.25} PPD _{0.5}	3.9 ± 0.6
GO _{0.25} PPD _{1.0}	4.0 ± 0.6
GO _{0.25} PPD _{2.0}	4.2 ± 0.4
GO _{0.5} PPD _{0.1}	4.6 ± 0.8
GO _{0.5} PPD _{0.2}	5.2 ± 0.6
GO _{0.5} PPD _{0.3}	5.7 ± 0.8
GO _{0.5} PPD _{0.5}	6.1 ± 0.4
GO _{0.5} PPD _{1.0}	5.9 ± 0.3
GO _{0.5} PPD _{2.0}	6.2 ± 0.4

6.3.2 Concentration impact on membrane performance

The performance results show that membrane rejection rate rises notably with concentrations of both GO and the crosslinker (Table 13). Two main reasons are proposed for the observed trend; the first one being lengthening of membrane tortuosity with GO accumulation. The claim of tortuosity increase with concentration is backed by the thickness characterisations, where a proportional relation between concentration and thickness can be observed (Table 12).

The separation mechanism of this membranes is based on selective permeation and adsorption via MB–GO/PPD–MB $\pi - \pi$ interactions [322,370], as described in detail in chapter 4. Therefore, at higher concentrations the membranes achieve a better rejection rate due to the increased sieving potential [371,372]. Moreover, greater GO concentration also comes with an increase in membrane hydrophilicity [365]. This is

a considerable factor for the improved performance, as it provides high wettability and reduced anti-fouling, as demonstrated elsewhere for both GO and polymer based nanofiltration membranes [320,321,365]. Excellent rejection rate is achieved at a GO concentration of 0.5 mg/ml with at least ~95% rejection rate being recorded.

Secondly, the positive impact of the concentration of PPD in MB rejection rate is also notable (Table 13), which may be due to the higher crosslinking degree achieved on the membranes. As the crosslinker concentration increases, the quantity of interconnected GO nanosheets is likely to be more. This results in reduced membrane swelling and therefore enhanced performance [53]. This assertion has been reported elsewhere, where a diminishment in GO membrane swelling degree by a factor of 75 due to covalent interactions was noted [266]. Stabilisation from other non-covalent interactions like cationic – π has also been noted in literature [373], which are also plausible here as a result of the protonation of the amines [53]. These studies are in agreement with the observed improvement in performance as the crosslinker concentration increases.

Table 13. Membrane performance (Rejection and permeation flux)

	Rejection (%)	Flux (l/m².h)
GO _{0.125} PPD _{0.1}	74.6 ± 2.1	29.5 ± 3.5
GO _{0.125} PPD _{0.2}	75.3 ± 3.3	28.3 ± 3.2
GO _{0.125} PPD _{0.3}	74.6 ± 3.7	26.2 ± 2.8
GO _{0.125} PPD _{0.5}	75.4 ± 2.3	25.2 ± 2.3
GO _{0.125} PPD _{1.0}	76.9 ± 3.3	25.2 ± 1.7
GO _{0.125} PPD _{2.0}	77.7 ± 1.9	24.7 ± 2.1
GO _{0.25} PPD _{0.1}	87.7 ± 2.4	18.5 ± 1.9
GO _{0.25} PPD _{0.2}	90.2 ± 2.7	18.2 ± 1.1
GO _{0.25} PPD _{0.3}	91.2 ± 2.1	17.2 ± 1.6
GO _{0.25} PPD _{0.5}	91.7 ± 1.3	16.2 ± 1.3
GO _{0.25} PPD _{1.0}	91.3 ± 1.1	16.5 ± 1.8
GO _{0.25} PPD _{2.0}	91.4 ± 0.7	15.7 ± 0.9
GO _{0.5} PPD _{0.1}	94.4 ± 1.0	9.3 ± 1.6
GO _{0.5} PPD _{0.2}	94.2 ± 0.6	8.1 ± 0.8
GO _{0.5} PPD _{0.3}	95.0 ± 0.8	6.0 ± 1.1
GO _{0.5} PPD _{0.5}	97.7 ± 0.4	4.6 ± 0.9
GO _{0.5} PPD _{1.0}	98.0 ± 0.3	4.4 ± 0.5
GO _{0.5} PPD _{2.0}	98.3 ± 0.4	3.9 ± 1.4

With respect to the permeation flux, an increase in GO and crosslinker concentrations has a reciprocal impact onto the flux magnitude. This is similarly advocated to both lengthening membrane tortuosity, due to GO concentration increase and enhanced intactness from crosslinking, which results in the maintenance of a smaller pore gap as swelling is alleviated [53,324]. Moreover, material concentration is proportional to membrane thickness (Table 12), and this is inversely proportional to the flux as described by the Hagen-Poiseuille law [374].

However, the maintenance of constant performance efficiency post a GO: PPD 1:1 approximate concentration ratio is observable. For instance, for GO_{0.25}PPD_y membranes, little change in rejection rate from 91.2 to 91.4% as the crosslinker increases from 0.3 to 2.0 mg/ml is recorded. A similar fit is observed for the GO_{0.5}PPD_y membranes where a rejection rate changes slightly from 97.7 to 98.3% as the crosslinker concentration increases from 0.5 mg/ml to 2.0 mg/ml.

6.3.3 Crosslinker concentration impact on membrane stability

The role of the diamine crosslinkers in influencing GO membrane stability and pore gap intactness is documented in related works [363,375,376]. From the previous results (Table 13), excellent membrane performance was achieved for the GO_{0.5}PPD_y membranes relative to the other membrane sets at lower GO concentration. Consequently, post nanofiltration SEM characterisations of these membranes is hereby reported to verify the extent of membrane integrity maintenance at varying crosslinker concentration.

At lower crosslinker concentration of 0.1 to 0.3 mg/ml, micro-cracking and defects of the membranes post nanofiltration can be observed (Figure 49). This is advocated to a lesser degree of crosslinking at low PPD concentration. PPD enhances the stability of the GO membranes covalently and non-covalently through $\pi - \pi$ interactions, hydrogen bonding and van der Waal's forces [188,363]. At lower concentrations, there are likely to be fewer molecules to hold the nanosheets together hence the observed dry infused cracking, as it was previously noticed for the uncrosslinked (zero crosslinker concentration) membranes in chapter 4. At higher PPD loading on the contrary more GO-PPD C-N covalent interactions occur (as described in chapter 3), which result in more nanosheets being held together, thus improved structural intactness and the alleviation of cracking (Figure 48). From the results it can be observed that a 1:1 crosslinker; GO concentration is enough for enhancing both the performance and suspension stability.

I

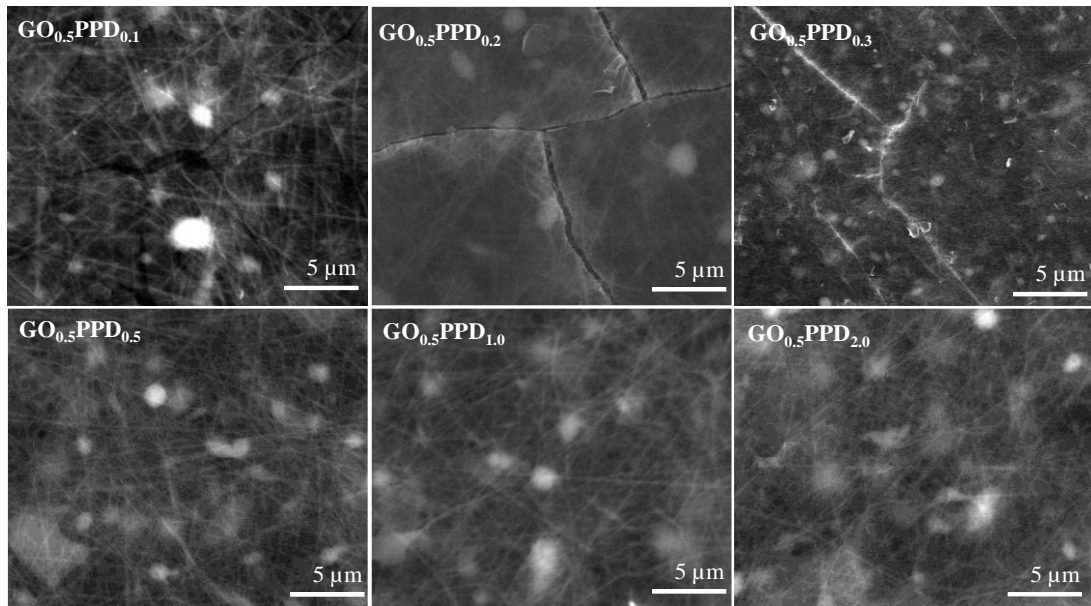


Figure 49. SEM images of the membranes fabricated with 0.5 mg/ml of GO post nanofiltration

In a related study by Jia *et al*, the impact of concentration of a diamine crosslinker, ethylenediamine (EDA), in improving membrane intactness and mechanical strength was similarly eminent [319]. At higher EDA concentration, the elastic modulus of the membranes augmented due to more C-N bonding [319]. It is therefore apparent that a similar enhancement is plausible with increasing the concentration of PPD in this case. The improvement in nanofiltration performance with crosslinker concentration can therefore be advocated to better membrane intactness and stability instigated by the crosslinker. Conclusively, basing on the performance results and the stability maintenance post nanofiltration, a GO and crosslinker concentration of 1:1 ratio at 0.5 mg/ml is commendable. This constitutes a 75% reduction in crosslinker load in comparison to the initial work in the previous chapters while achieving excellent performance and enhancing stability.

6.4 Conclusions

The chapter detailed the relation between membrane performance and the concentration of the suspensions of GO and crosslinker as a way of enhancing material conservation. Nanofiltration notably increases with GO concentration with the highest rejection rate being achieved at 0.5 mg/ml for these membranes. The work presented also gives intuition in the significance of crosslinking degree as this is evidenced by an augmentation in rejection rate at increasing crosslinker concentration. Crosslinking significance is also manifested through improved membrane stability and intactness. Post nanofiltration at higher crosslinker concentration membrane intactness is maintained while the cracking was imminent for lower crosslinker concentrations. The work in this chapter is thus of significance in the optimisation of crosslinked GO membranes and also in reducing membrane fabrication costs through enhanced material conservation. Up to 75% reduction in material usage for the crosslinker relative to the previous chapters has in turn been demonstrated.

7.

SUMMARY, CONCLUSIONS AND FUTURE WORK

“Progress is made by trial and failure; the failures are generally a hundred times more numerous than the successes; yet they are usually left unchronicled.”

SIR WILLIAM RAMSAY, (1852-1916)

7.1 General conclusions

The thesis primarily focused on the enhancement of graphene oxide (GO) membrane's stability and nanofiltration performance through the use of different sized amine group containing compounds. Sub-nanometre sized molecular covalent based; p-phenylenediamine (PPD) and 1,3,5-triazine – 2,4,6 triamine (melamine) (MLM) and electrostatic based polyethyleneimine (PEI) were the selected crosslinkers. The membrane fabrication method entailed was the dip-assisted layer by layer method. It was selected for its systematic interconnection of the crosslinkers and GO, ease of scale up to mass production and control of key membrane characteristics. First, crosslinked thin films on cheap glass slide substrates were successfully fabricated. Ease of control of film thickness was demonstrated as a strong linear correlation coefficient (R^2) of above 0.85 between the number of bi-layers and film thickness for all set of crosslinkers was notable.

Crosslinked membranes showed significant improvement in membrane performance and stability. Up to 100% rejection of MB was achieved for the crosslinked membranes at 5 minutes immersion time and 5 bi-layers. To optimise the impact of

the physicochemical characteristics of GO onto membrane performance different crosslinked GO lateral sized membranes were fabricated. First, a correlation between GO lateral size, chemical functionalities and suspension stability was established. Further membrane optimisations were done to enhance material conservation and membrane operation efficiency. The degree of crosslinking in enhancing membrane performance was also determined in this stage and conclusively a 1:1 GO; crosslinker ratio is recommendable. These optimisations were mainly for economic conservation of both material and sonication energy entailed in the fabrication of crosslinked GO membranes.

At the low 1 bar pressure used in the study, the results are promising, which means further particulates and solutes can be separated. Similarly, the successful fabrication of crosslinked membranes points to the fact that other different economically affordable crosslinkers can be incorporated for the customisation of the separation of other entities.

7.2 Major findings

The significant findings entailed in the thesis are here summarised;

7.2.1 Demonstration of successful quanta control of key thin-film/membrane characteristics via the dip-assisted layer by layer method

In Chapter 3, the control of the thin-film characteristics; thickness, hydrophilicity was accurately controlled by changing the immersion time and the number of bi-layers. As a result, required film characteristics can easily be extrapolated/interpolated for relevant applications. This gave a scope for the fabrication of systematically crosslinked membranes with different sized crosslinkers, where the significant features can easily be controlled. These differences in size and type of the crosslinkers also gives a wide range of thickness giving the fabricated thin films more versatility in various applications.

7.2.2 Enhanced membrane stability and improved nanofiltration performance

Through a comparative analysis of the uncrosslinked and crosslinked membranes, it was evident that the introduction of crosslinkers came with both the enhancement of membrane stability and nanofiltration performance. All the crosslinked membranes at similar immersion time and number of bi-layers showed enhanced performance of more than 15% improvement in membrane performance. An increase in membrane performance (MB rejection) of up to 100% at higher immersion time and the number of bi-layers was also established. The improvement is attributed to the holding of the GO nanosheets together by the crosslinkers. This kept the nanosheets intact, hence preventing them from shrinking and cracking during storage unlike for the uncrosslinked membranes. Similarly, performance improvement with the number of bi-layers was evident. This was concluded to be due to increased material

accumulation leading to increased membrane tortuosity resulting in better performance.

Additionally, the use of relatively cheaper polycarbonate supporting substrates was in the end demonstrated and successfully achieved, this further decreases the overall costs of the process.

7.2.3 Optimisation of GO's physicochemical characteristics for enhanced membrane performance

The interrelation between GO lateral size and chemistry is a major factor in having good suspension stability. It is thus a significant factor in resultant membrane quality and performance. Chapter 5 analysed optimisation of GO lateral size that gives enhanced membrane performance from improved suspension stability at decreasing lateral size and increasing carboxylate groups. This was significant because during GO suspension preparation, sonication is carried out and it is established that it results in GO nanosheet fragmentation. In this case a sonication duration of 120 minutes gave an average nanosheet size of 1.3 μm and improved overtime GO dispersion and individuality as confirmed through ζ – potential measurements. Enhanced stability was crucial for improved membrane topographical intactness through heightened GO crosslinker interactions via different mechanism.

7.2.4 Optimisation of GO and crosslinker preparatory concentrations

Establishing and understanding the impact of the concentrations of GO and crosslinker on overall membrane performance was achieved. Specifically, the impact of GO concentration was manifested in increasing membrane tortuosity resulting in improved performance. This was achieved at increasing concentration while for the crosslinker increasing crosslinking degree culminated in improved membrane performance. A 1:1

concentration ratio GO-PPD at increased concentration of 0.5 mg/ml was demonstrated to be the optimum concentration ratio for the sample membranes based on performance primarily.

7.3 Future work recommendations

7.3.1 GO membrane modifications to improve permeation flux

The crosslinked GO membranes showed excellent sieving characteristics at higher immersion time and bi-layers. However, a low water permeation flux under the pressure-driven process was experienced. This is due to both the low pressure entailed and also the long water transport path from the heightened membrane tortuosity. In this regard, more work can be done to improve the membrane performance by reducing the transport path length. For instance, systematic ways to generate microstructural defects in an attempt to reduce the tortuous path. Sub-nanometre pores can be instigated onto the nanosheets through either plasma etching or nucleation like for graphene membranes. A plausible improvement in permeation flux is also through operating the membranes at a higher operation pressure.

7.3.2 Exploration of the crosslinked membranes' separation potential of other contaminants, heavy metals, divalent and monovalent salts

With evident promise of the fabricated crosslinked membranes in water purification, the versatility of the membranes in other contaminants can be explored further. These include testing performance in the separation of heavy metals, divalent and monovalent salts. Relevant modification can be instigated. Since it has been observed that membrane separation degree increases with an increase in the number of bi-layers, as such, the optimum number of bi-layers and immersion time for each of the contaminants ought to be established.

7.3.3 Use of other economically affordable sub nanometre sized crosslinkers

The dip-assisted layer-by-layer method has been demonstrated as an affordable facile technique with ease of control of key membrane characteristics. Other sub-nanometre sized crosslinkers like ethylenediamine (EDA) and can be explored to fine tune the membrane pore gap and enhance membrane stability covalently. The use of smaller sized crosslinkers will narrow the membrane pore-gap and as such a variety of smaller sized particulates can in turn be separated. Furthermore, coupling agents like 1, 1'-Carbonyldiimidazole (CDI) can be employed to inter-connect the GO nanosheets together and further enhance membrane stability. This also activates other oxygenated functional groups in GO to enhance the interaction between GO and the crosslinkers.

7.3.4 Further exploration of the membrane separation mechanisms and long-term stability

Despite the efforts in understanding the permeation of water molecules across GO and related hybrid membranes, the fast transport permeation theory ought to be understood in further details. As such, a more accurate transport mechanism ought to be hypothesised. This could be achieved by a combination of both molecular dynamics simulations coupled with verifying experimentations to understand the operation mechanisms and thus optimising the performances further.

REFERENCES

- [1] M. Kummu, J.H.A. Guillaume, H. De Moel, S. Eisner, M. Flörke, M. Porkka, The world ' s road to water scarcity : shortage and stress in the 20th century and pathways towards sustainability, *Nat. Publ. Gr.* (2016) 1–16.
doi:10.1038/srep38495.
- [2] S.J. Mcgrane, Impacts of urbanisation on hydrological and water quality dynamics , and urban water management : a review water management : a review, *Hydrol. Sci. J.* 61 (2016) 2295–2311.
doi:10.1080/02626667.2015.1128084.
- [3] V. Srinivasan, E.F. Lambin, S.M. Gorelick, B.H. Thompson, S. Rozelle, The nature and causes of the global water crisis : Syndromes from a meta-analysis of coupled human-water studies, 48 (2012) 1–16.
doi:10.1029/2011WR011087.
- [4] R.I. McDonald, P. Green, D. Balk, B.M. Fekete, C. Revenga, M. Todd, M. Montgomery, Urban growth, climate change, and freshwater availability, *Proc. Natl. Acad. Sci. U. S. A.* 108 (2011) 6312–6317.
doi:10.1073/pnas.1011615108.
- [5] W. World Health Organization, Meeting the MDG drinking water and sanitation, the urban and rural challenge of the decade, Geneva, 2007.
http://www.who.int/water_sanitation_health/monitoring/jmpfinal.pdf.
- [6] K. Balke, Y. Zhu, Natural water purification and water management by artificial groundwater recharge, *J. Zhejiang Univ. Sci. B.* 9 (2008) 221–226.
doi:10.1631/jzus.B0710635.

- [7] M. Shatat, S.B. Riffat, Water desalination technologies utilizing conventional and renewable energy sources, *Int. J. Low-Carbon Technol.* 9 (2014) 1–19. doi:10.1093/ijlct/cts025.
- [8] M. Elimelech, W.A. Phillip, The Future of Seawater Desalination: Energy, Technology and the Environment, *Science* (80-.). 333 (2011) 712–718. doi:10.1126/science.1200488.
- [9] A. Grumezescu, *Water Purification (Nanotechnology in the Agri-Food Industry)*, 2nd ed., Academic Press, London, 2017. <https://www.abebooks.com/9780128043004/Water-Purification-Nanotechnology-Agri-Food-Industry-0128043008/plp>.
- [10] S. Bolisetty, M. Peydayesh, R. Mezzenga, Sustainable technologies for water purification from heavy metals: review and analysis, *Chem. Soc. Rev.* 48 (2019) 463–487. doi:10.1039/c8cs00493e.
- [11] M. Al-Abri, B. Al-Ghafri, T. Bora, S. Dobretsov, J. Dutta, S. Castelletto, L. Rosa, A. Boretti, Chlorination disadvantages and alternative routes for biofouling control in reverse osmosis desalination, *NPJ Clean Water.* 2 (2019) 1–16. doi:10.1038/s41545-018-0024-8.
- [12] S. Sharma, A. Bhattacharya, Drinking water contamination and treatment techniques, *Appl. Water Sci.* 7 (2017) 1043–1067. doi:10.1007/s13201-016-0455-7.
- [13] P. Bernardo, G. Clarizia, 30 Years of Membrane Technology for Gas Separation, *Chem. Eng. Trans.* 32 (2013) 1999–2004.
- [14] S. Heinrich, *Membranes and Membrane Separation Processes*, 1st ed., Wiley-

- VCH, 2005. doi:10.1002/14356007.a16_187.pub2.
- [15] S. LOEB, S. SRINIVASA, Sea Water Demineralization by Means of an Osmotic Membrane, in: 2nd ed., American Chemical Society, Calif, 1963: pp. 117–132. doi:10.1021/ba-1963-0038.ch009.
- [16] Z. Wang, A. Wu, Recent Advances in Nanoporous Membranes for Water Purification, *Nanomaterials*. 9 (2018). doi:10.3390/nano8020065.
- [17] E.. Mason, From pig bladders and cracked jars to polysulfones: An historical perspective on membrane transport, *J. Memb. Sci.* 20 (1991) 125–145. doi:10.1016/S0376-7388(00)81529-X.
- [18] W.. Koros, M.. Hellums, Gas separation membrane material selection criteria: Differences for weakly and strongly interacting feed components, *Fluid Phase Equilib.* 53 (1989) 339–354. doi:10.1016/0378-3812(89)80102-5.
- [19] Y. Yampolskii, Polymeric Gas Separation Membranes, *Macromolecules*. 45 (2012) 3298–3311. doi:10.1021/ma300213b.
- [20] L.M. Robeson, Polymer membranes for gas separation, *Curr. Opin. Solid State Mater. Sci.* 4 (2000) 549–552. doi:10.1016/S1359-0286(00)00014-0.
- [21] G.M. Geise, H. Lee, D.J. Miller, B.D. Freeman, J.E. Mcgrath, D.R. Paul, H. Lee, D.J. Miller, Water Purification by Membranes : The Role of Polymer Science, *J. Polym. Sci. Part B Polym. Phys.* 48 (2010) 1685–1718. doi:10.1002/POLB.
- [22] H. Ma, C. Burger, B.S. Hsiao, B. Chu, Highly Permeable Polymer Membranes Containing Directed Channels for Water Purification, *ACS Macroletters*. 1 (2012) 723–726. doi:10.1021/mz300163h.

- [23] C.A.. Siskens, Chapter 13 Applications of ceramic membranes in liquid filtration, *Membr. Sci. Technol.* 4 (1996) 619–639. doi:10.1016/S0927-5193(96)80016-7.
- [24] J.. Kilner, *Encyclopedia of Separation Science*, Academic Press, 2000.
<https://www.sciencedirect.com/science/article/pii/B012226770205571X>.
- [25] R.K. Joshi, S. Alwarappan, M. Yoshimura, V. Sahajwalla, Y. Nishina, Graphene oxide: The new membrane material, *Appl. Mater. Today.* 1 (2015) 1–12. doi:10.1016/j.apmt.2015.06.002.
- [26] H. Water, Sorek Desalination Plant, (2015).
<https://www.hutchisonwater.com/projects/sorek/> (accessed September 5, 2020).
- [27] R. Das, M.E. Ali, S.B.A. Hamid, S. Ramakrishna, Z.Z. Chowdhury, Carbon nanotube membranes for water purification: A bright future in water desalination, *Desalination.* 336 (2014) 97–109.
doi:10.1016/j.desal.2013.12.026.
- [28] A. Kalra, S. Garde, G. Hummer, Osmotic water transport through carbon nanotube membranes, *Proc. Natl. Acad. Sci. U. S. A.* 100 (2003) 10175–10180. doi:10.1073/pnas.1633354100.
- [29] J.K. Holt, H.G. Park, Y. Wang, M. Stadermann, A.B. Artyukhin, C.P. Grigoropoulos, A. Noy, O. Bakajin, Fast Mass Transport Through Sub – 2- Nanometer Carbon Nanotubes, *Science* (80-.). 312 (2006) 1034–1038.
doi:10.1126/science.1126298.
- [30] M. Majumder, N. Chopra, B.J. Hinds, Mass transport through carbon

- nanotube membranes in three different regimes: Ionic diffusion and gas and liquid flow, *ACS Nano*. 5 (2011) 3867–3877. doi:10.1021/nn200222g.
- [31] M. Yu, H.H. Funke, J.L. Falconer, R.D. Noble, High Density, Vertically-Aligned Carbon Nanotube Membranes, *Nano Lett.* 9 (2009) 225–229. doi:10.1021/nl802816h.
- [32] S. Kim, J.R. Jinschek, H. Chen, D.S. Sholl, E. Marand, Scalable fabrication of carbon nanotube/polymer nanocomposite membranes for high flux gas transport, *Nano Lett.* 7 (2007) 2806–2811. doi:10.1021/nl071414u.
- [33] A.K.G. K. S. Novoselov, D.J. S. V. Morozov, A.A.F. Y. Zhang, S. V. Dubonos, I. V. Grigorieva, Electric Field Effect in Atomically Thin Carbon Films, *Science* (80-.). 306 (2004) 666–669. doi:10.1126/science.1102896.
- [34] P. Avouris, C. Dimitrakopoulos, Graphene: Synthesis and applications, *Mater. Today*. 15 (2012) 86–97. doi:10.1016/S1369-7021(12)70044-5.
- [35] N. Song, X. Gao, Z. Ma, X. Wang, Y. Wei, C. Gao, A review of graphene-based separation membrane : Materials, characteristics, preparation and applications, *Desalination*. 437 (2018) 59–72. doi:10.1016/j.desal.2018.02.024.
- [36] P. Liu, T. Yan, J. Zhang, L. Shi, D. Zhang, Separation and recovery of heavy metal ions and salt ions from wastewater by 3D graphene-based asymmetric electrodes via capacitive deionization, *J. Mater. Chem. A*. 5 (2017) 14748–14757. doi:10.1039/c7ta03515b.
- [37] R.P. Pandey, G. Shukla, M. Manohar, V.K. Shahi, Graphene oxide based nanohybrid proton exchange membranes for fuel cell applications : An

- overview, *Adv. Colloid Interface Sci.* 240 (2017) 15–30.
doi:10.1016/j.cis.2016.12.003.
- [38] R.I. Jafri, N. Rajalakshmi, S. Ramaprabhu, Nitrogen doped graphene nanoplatelets as catalyst support for oxygen reduction reaction in proton exchange membrane fuel cell, *J. Mater. Chem.* 20 (2010) 7114–7117.
doi:10.1039/c0jm00467g.
- [39] A. Zurutuza, C. Marinelli, Challenges and opportunities in graphene commercialization, *Nat. Nanotechnol.* 9 (2014) 730–734.
doi:10.1038/nnano.2014.225.
- [40] L. Dong, J. Yang, M. Chhowalla, K.P. Loh, Synthesis and reduction of large sized graphene oxide sheets, *Chem. Soc. Rev.* 46 (2017) 7306–7316.
doi:10.1039/c7cs00485k.
- [41] S.P. Surwade, S.N. Smirnov, I. V. Vlassiuk, R.R. Unocic, G.M. Veith, S. Dai, S.M. Mahurin, Water desalination using nanoporous single-layer graphene, *Nat. Nanotechnol.* 10 (2015) 459–464. doi:10.1038/nnano.2015.37.
- [42] J.R. Werber, C. Osugi, M. Elimeneck, Materials for next-generation desalination and water purification membranes, *Nat. Mater.* 1 (2016).
doi:10.1038/natrevmats.2016.18.
- [43] R.K. Joshi, P. Carbone, F.C. Wang, V.G. Kravets, Y. Su, I. Grigorieva, H. Wu, A.K. Geim, R.R. Nair, Precise and Ultrafast Molecular Sieving Through Graphene Oxide Membranes, *Science* (80-.). 343 (2014) 752–755.
doi:10.1126/science.1245711.
- [44] W.S. Hummers, R.E. Offeman, Preparation of Graphitic Oxide, *J. Am. Chem.*

- Soc. 80 (1958) 1339. doi:10.1021/ja01539a017.
- [45] R.. Nair, H.. Wu, A. V. Jayaram, V. Grigorieva, A.. Geim, Unimpeded Permeation of Water Through Helium-Leak–Tight Graphene-Based Membranes, *Science* (80-.). 335 (2012) 442–445. doi:10.1126/science.1211694.
- [46] S. Zheng, Q. Tu, J.J. Urban, S. Li, B. Mi, Swelling of Graphene Oxide Membranes in Aqueous Solution: Characterization of Interlayer Spacing and Insight into Water Transport Mechanisms, *ACS Nano*. 11 (2017) 6440–6450. doi:10.1021/acsnano.7b02999.
- [47] Y. Mo, X. Zhao, Y. xiao Shen, Cation-dependent structural instability of graphene oxide membranes and its effect on membrane separation performance, *Desalination*. 399 (2016) 40–46. doi:10.1016/j.desal.2016.08.012.
- [48] L. Huang, J. Chen, T. Gao, M. Zhang, Y. Li, L. Dai, L. Qu, G. Shi, Reduced Graphene Oxide Membranes for Ultrafast Organic Solvent Nanofiltration, *Adv. Mater*. 28 (2016) 8669–8674. doi:10.1002/adma.201601606.
- [49] S. Abdolhosseinzadeh, H. Asgharzadeh, H.S. Kim, Fast and fully-scalable synthesis of reduced graphene oxide, *Sci. Rep.* 5 (2015) 1–7. doi:10.1038/srep10160.
- [50] M. Omidvar, M. Soltanieh, S.M. Mousavi, E. Saljoughi, A. Moarefian, H. Saffaran, Preparation of hydrophilic nanofiltration membranes for removal of pharmaceuticals from water, *J. Environ. Heal. Sci. Eng.* 13 (2015) 1–9. doi:10.1186/s40201-015-0201-3.

- [51] J. Abraham, K.S. Vasu, C.D. Williams, K. Gopinadhan, Y. Su, C.T. Cherian, J. Dix, E. Prestat, S.J. Haigh, I. V. Grigorieva, P. Carbone, A.K. Geim, R.R. Nair, Tunable sieving of ions using graphene oxide membranes, *Nat. Nanotechnol.* 12 (2017) 546–550. doi:10.1038/nnano.2017.21.
- [52] R. Iler, Multilayers of colloidal particles, *J. Colloid Interface Sci.* 21 (1965) 569. doi:10.1016/0095-8522(66)90018-3.
- [53] W.S. Hung, C.H. Tsou, M. De Guzman, Q.F. An, Y.L. Liu, Y.M. Zhang, C.C. Hu, K.R. Lee, J.Y. Lai, Cross-linking with diamine monomers to prepare composite graphene oxide-framework membranes with varying d-spacing, *Chem. Mater.* 26 (2014) 2983–2990. doi:10.1021/cm5007873.
- [54] B.S. Lalia, V. Kochkodan, R. Hashaikeh, N. Hilal, A review on membrane fabrication: Structure, properties and performance relationship, *Desalination.* 326 (2013) 77–95. doi:10.1016/j.desal.2013.06.016.
- [55] J. Ma, D. Ping, X. Dong, Recent developments of graphene oxide-based membranes: A review, *Membranes (Basel).* 7 (2017). doi:10.3390/membranes7030052.
- [56] B. Tang, L. Zhang, R. Li, J. Wu, M.N. Hedhili, P. Wang, Are vacuum-filtrated reduced graphene oxide membranes symmetric?, *Nanoscale.* 8 (2016) 1108–1116. doi:10.1039/c5nr06797a.
- [57] J. Lyu, X. Wen, U. Kumar, Y. You, V. Chen, R. Joshi, Separation and purification using GO and r-GO membranes, *RSC Adv.* 2 (2018) 23130–23151. doi:10.1039/c8ra03156h.
- [58] M. Hu, B.X. Mi, Layer-by-layer assembly of graphene oxide membranes via

- electrostatic interaction, *J. Memb. Sci.* 469 (2014) 80–87.
doi:10.1016/j.memsci.2014.06.036.
- [59] G. Decher, Fuzzy Nanoassemblies: Towards Layered Polymeric Multicomposites, *Science* (80-.). 277 (1997) 1232. doi:10.1126/science.277.5330.1232.
- [60] P.. Wallace, The band theory of graphite, *Phys. Rev.* 71 (1947) 622–634.
doi:10.1103/PhysRev.71.622.
- [61] L. Pauling, *The Nature of the Chemical Bond*, Cornell University Press, Ithaca, New York, 1960.
- [62] A.H.C. Neto, F. Guinea, N.M.. Peres, K.. Novoselov, A.. Geim, The electronic properties of graphene, *Rev. Mod. Phys.* 81 (2009).
doi:10.1103/RevModPhys.81.109.
- [63] A.Z. Alzahrani, Structural and electronic properties of graphene upon molecular adsorption: DFT Comparative Analysis, in: J. Gong (Ed.), *Graphene Simul.*, InTech, Rijeka, 2011: pp. 22–38.
- [64] M. Coros, F. Pogacean, L. Magerusan, C. Socaci, S. Pruneanu, A brief overview on synthesis and applications of graphene and graphene-based nanomaterials, *Front. Mater. Sci.* 13 (2019) 23–32. doi:10.1007/s11706-019-0452-5.
- [65] B.C. Brodie, On the atomic weight of graphite, *Phylosophical Trans. R. Soc. London.* 149 (1859) 249–259. doi:1859RSPT.149.249B.
- [66] H.. Boehm, A. Clauss, G.. Fischer, U. Hofmann, Das Adsorptionsverhalten sehr dünner Kohlenstoff-Folien, *Zeitschrift Für Anorg. Und Allg. Chemie.*

- 316 (1962) 119–127. doi:10.1002/zaac.19623160303.
- [67] K.. Novoselov, A.. Geim, S.. Morozov, D. Jiang, Y. Zhang, S.. Dubonos, I.. Grigorieva, A.. Firsov, Electric Field Effect in Atomically Thin Carbon Films, *Science* (80-.). 306 (2004) 666–670.
- [68] A. Dietl, Graphene: the wonder material of the 21st century, *News Eur. Parliam.* (2015). doi:20150603STO62104.
- [69] D.S.. Abergel, V. Apalkov, J. Berachevich, K. Ziegler, C. Tapash, Properties of graphene: a theoretical perspective, *Adv. Phys.* 59 (2010) 261–482. doi:10.1080/00018732.2010.487978.
- [70] A.. Geim, K.. Novoselov, The rise of graphene, *Nat. Mater.* 3 (2007) 183–191. doi:10.1038/nmat1849.
- [71] C. Lee, X. Wei, J.W. Kysar, J. Hone, Measurement of the Elastic Properties and Intrinsic Strength of Monolayer Graphene, *Science* (80-.). 321 (2008) 385–388. doi:10.1126/science.1157996.
- [72] I.. Ovid’ko, Mechanical properties of graphene, *Rev. Adv. Mater. Sci.* 34 (2013) 1–11.
- [73] A.I. of S.C. Construction, *Steel Construction Manual*, in: *Steel Constr. Man.*, 8th Editio, 1986.
- [74] J. Quintanilla, Microstructure and properties of random heterogeneous materials : a review of theoretical results, *Polym. Eng. Sci.* 39 (1990) 559–585. doi:10.1002/pen.11446.
- [75] S. Bharech, R. Kumar, A review on the properties and applications of Graphene, *J. Mater. Sci. Mech. Eng.* 2 (2025) 70–73.

- [76] D.R. Cooper, B. D'Anjou, N. Ghattamaneni, B. Harack, M. Hilke, A. Horth, N. Majlis, M. Massicotte, L. Vandsburger, E. Whiteway, V. Yu, *Experimental Review of Graphene*, *ISRN Condens. Matter Phys.* 2011 (2012) 1–56.
doi:10.5402/2012/501686.
- [77] J. Wang, F. Ma, W. Liang, M. Sun, *Electrical properties and applications of graphene , hexagonal boron nitride (h-BN), and graphene / h-BN heterostructures*, *Mater. Today Phys.* 2 (2017) 6–34.
doi:10.1016/j.mtphys.2017.07.001.
- [78] A.B. Kuzmenko, E. Van Heumen, F. Carbone, D. Van Der Marel, *Universal optical conductance of graphite*, *Phys. Rev. Lett.* 100 (2008) 2–5.
doi:10.1103/PhysRevLett.100.117401.
- [79] R.R. Nair, P. Blake, A.N. Grigorenko, K.S. Novoselov, T.J. Booth, T. Stauber, N.M.R. Peres, A.K. Geim, *Fine structure constant defines visual transparency of graphene*, *Science* (80-.). 320 (2008) 1308.
doi:10.1126/science.1156965.
- [80] B. Rolf, *Optical Properties of Graphene*, World Scientific Publishing Co, London, 2016.
- [81] T. Kinoshita, *Reports on Progress in Physics Related content*, *Rep. Prog. Phys.* 59 (1996) 1665–1735. doi:10.1088/0034-4885/77/5/056502.
- [82] S. Alam, B. Nizam, U. Maksudul, *Synthesis of graphene*, *Int. Nano Lett.* 6 (2016) 65–83. doi:10.1007/s40089-015-0176-1.
- [83] M. Yi, Z. Shen, *A review on mechanical exfoliation for the scalable production of graphene*, *J. Mater. Chem. A.* 3 (2015) 11700–11715.

doi:10.1039/c5ta00252d.

- [84] F.. Kusmartsev, W.. Wu, M.. Pierpoint, K.. Yung, *Application of Graphene Within Optoelectronic Devices and Transistors*, 1st ed., Springer Publishing, Singapore, 2014.
- [85] S. Iijima, Helical microtubules of graphitic carbon, *Nature*. 354 (1991) 412–414. doi:10.1038/354056a0.
- [86] D. V. Kosynkin, A.L. Higginbotham, A. Sinitskii, J.R. Lomeda, A. Dimiev, B.K. Price, J.M. Tour, Longitudinal unzipping of carbon nanotubes to form graphene nanoribbons, *Nature*. 458 (2009) 872–876.
doi:10.1038/nature07872.
- [87] L. Jiao, L. Zhang, X. Wang, G. Diankov, H. Dai, Narrow graphene nanoribbons from carbon nanotubes, *Nature*. 458 (2009) 877–880.
doi:10.1038/nature07919.
- [88] L. Jiao, X. Wang, G. Diankov, H. Wang, H. Dai, Facile synthesis of high-quality graphene nanoribbons, *Nature*. 5 (2010) 321–325.
doi:10.1038/nnano.2010.54.
- [89] Y.S. Li, J.L. Liao, S.Y. Wang, W.H. Chiang, Intercalation-assisted longitudinal unzipping of carbon nanotubes for green and scalable synthesis of graphene nanoribbons, *Sci. Rep.* 6 (2016) 1–12. doi:10.1038/srep22755.
- [90] A. Kempster, *The Principles and Applications of Chemical Vapour Deposition*, *Int. J. Surf. Eng. Coatings*. 70 (1992) 68–75.
doi:10.1080/00202967.1992.11870945.
- [91] P.R. Somani, S.P. Somani, M. Umeno, Planer nano-graphenes from camphor

- by CVD, *Chem. Phys. Lett.* 430 (2006) 56–59.
doi:10.1016/j.cplett.2006.06.081.
- [92] Y. Zhang, L. Zhang, C. Zhou, Review of chemical vapor deposition of graphene and related applications, *Acc. Chem. Res.* 46 (2013) 2329–2339.
doi:10.1021/ar300203n.
- [93] Z.Y. Juang, C.Y. Wu, A.Y. Lu, C.Y. Su, K.C. Leou, F.R. Chen, C.H. Tsai, Graphene synthesis by chemical vapor deposition and transfer by a roll-to-roll process, *Carbon N. Y.* 48 (2010) 3169–3174.
doi:10.1016/j.carbon.2010.05.001.
- [94] X. Li, W. Cai, J. An, S. Kim, J. Nah, D. Yang, R. Piner, A. Velamakanni, I. Jung, E. Tutuc, S.K. Banerjee, L. Colombo, R.S. Ruoff, Large-area synthesis of high-quality and uniform graphene films on copper foils, *Science* (80-.). 324 (2009) 1312–1314. doi:10.1126/science.1171245.
- [95] A. Reina, X. Jia, J. Ho, D. Nezich, H. Son, V. Bulovic, M. Dresselhaus, K. Jing, Large Area, Few-Layer Graphene Films on Arbitrary Substrates by Chemical Vapor Deposition, *Nanochemistry.* 9 (2008) 30–35.
doi:10.1021/nl801827v.
- [96] J. De la Fuente, Properties of graphene, *Graphenea.* (2016).
<https://www.graphenea.com/pages/graphene-properties#.XZJM7kZKhnl>
(accessed September 30, 2019).
- [97] G. Kalita, M. Tanemura, Fundamentals of Chemical Vapor Deposited Graphene and Emerging Applications, in: *Graphene Mater. - Adv. Appl.*, InTech, 2012: p. 13. doi:10.1016/j.colsurfa.2011.12.014.

- [98] W. Choi, M.A. Shehzad, S. Park, Y. Seo, Influence of removing PMMA residues on surface of CVD graphene using a contact-mode atomic force microscope, *RSC Adv.* 7 (2017) 6943–6949. doi:10.1039/c6ra27436f.
- [99] M. Lotya, Y. Hernandez, P.J. King, R.J. Smith, V. Nicolosi, L.S. Karlsson, F.M. Blighe, Z. Wang, I. De, Suakanda McGovern, G.S. Duesberg, J.N. Coleman, Liquid Phase Production of Graphene by Exfoliation of Graphite in Surfactant/Water Solutions, *J. Am. Chem. Soc.* 131 (2009) 3611–3620. doi:10.1021/ja807449u.
- [100] M. Monajjemi, Liquid-phase exfoliation (LPE) of graphite towards graphene: An ab initio study, *J. Mol. Liq.* 230 (2017) 461–472. doi:10.1016/j.molliq.2017.01.044.
- [101] M. Hernaez, C.R. Zamarreño, S. Melendi-Espina, L.R. Bird, A.G. Mayes, F.J. Arregui, Optical fibre sensors using graphene-based materials: A review, *Sensors (Switzerland)*. 17 (2017) 1–24. doi:10.3390/s17010155.
- [102] Y. Hernandez, V. Nicolosi, M. Lotya, F.M. Blighe, Z. Sun, S. De, I. McGovern, M. Holland, Brendan Byrne, Y.K. Gun'Ko, J.J. Boland, P. Niraj, S. Duesberg, Georg Krishnamurthy, R. Goodhue, J. Hutchison, J.N. Scardaci, Vittorio Ferrari, Andrea C. Coleman, High-yield production of graphene by liquid-phase exfoliation of graphite, *Nat. Nanotechnol.* 3 (2008) 563–568. doi:nano.2008.215.
- [103] T. Felice, T. Hasan, W. Wu, Z. Sun, A. Lombardo, T.S. Kulmala, G.-W. Hsieh, S. Jung, F. Bonaccorso, P.J. Paul, D. Chu, A.C. Ferrari, Inkjet-Printed Graphene Electronics, *ACS Nano*. 6 (2012) 2992–3006. doi:10.1021/nn2044609.

- [104] K. V Emtsev, A. Bostwick, K. Horn, J. Jobst, G.L. Kellogg, L. Ley, J.L. McChesney, T. Ohta, S.A. Reshanov, J. Rohrl, E. Rotenberg, A.K. Schmid, D. Waldmann, H.B. Weber, T. Seyller, Towards wafer-size graphene layers by atmospheric pressure graphitization of silicon carbide, *Nat. Mater.* 8 (2009) 203–207. doi:10.1038/nmat2382.
- [105] H. Huang, S. Chen, A.T. Wee, W. Chen, Epitaxial growth of graphene on silicon carbide (SiC), in: *Graphene Prop. Prep. Characterisation Devices*, Woodhead Publishing, 2014: pp. 3–26.
- [106] H. Kageshima, H. Hibino, M. Nagase, H. Yamaguchi, Theoretical study of epitaxial graphene growth on SiC(0001) surfaces, *Appl. Phys. Express.* 2 (2009) 1–4. doi:10.1143/APEX.2.065502.
- [107] H. Hibino, H. Kageshima, M. Nagase, Growth of graphene layers on silicon carbide, *Spec. Featur. Front. Mater. Res.* 8 (2010) 199–202. doi:10.4028/www.scientific.net/MSF.615-617.199.
- [108] M. Choucair, P. Thordarson, J. Stride, Gram-scale production of graphene based on solvothermal synthesis and sonication, *Nat. Nanotechnol.* (2009) 30–33. doi:10.1038/nnano.2008.365.
- [109] L. Speyer, S. Fontana, S. Cahen, C. Hérold, Simple production of high-quality graphene foams by pyrolysis of sodium ethoxide, *Mater. Chem. Phys.* 219 (2018) 57–66. doi:10.1016/j.matchemphys.2018.08.020.
- [110] I. Levchenko, K.K. Ostrikov, J. Zheng, X. Li, M. Keidar, K.B.K. Teo, Scalable graphene production: Perspectives and challenges of plasma applications, *Nanoscale.* 8 (2016) 10511–10527. doi:10.1039/c5nr06537b.

- [111] H. Yu, B. Zhang, C. Bulin, R. Li, R. Xing, High-efficient Synthesis of Graphene Oxide Based on Improved Hummers Method, *Sci. Rep.* 6 (2016) 1–7. doi:10.1038/srep36143.
- [112] D.R. Dreyer, A.D. Todd, C.W. Bielawski, Harnessing the chemistry of graphene oxide, *Chem. Soc. Rev.* 43 (2014) 5288–5301. doi:10.1039/c4cs00060a.
- [113] D.R. Dreyer, S. Park, C.W. Bielawski, R.S. Ruoff, The chemistry of graphene oxide, *R. Soc. Chem.* 39 (2010) 228–240. doi:10.1039/b917103g.
- [114] S. Mao, H. Pu, J. Chen, Graphene oxide and its reduction: Modeling and experimental progress, *RSC Adv.* 2 (2012) 2643–2662. doi:10.1039/c2ra00663d.
- [115] U. Hofmann, R. Holst, Über die säurenatur und die methylierung von graphitoxyd, *Berichte Der Dtsch. Chem. Gesellschaft.* 72 (1939) 754–771.
- [116] G. Ruess, Über das graphitoxhydroxyd (graphitoxyd), *Monatshefte Für Chemie.* 76 (1946) 381–417.
- [117] W. Scholz, H.P. Boehm, Untersuchungen am graphitoxid. VI. Betrachtungen zur struktur des graphitoxids, *Zeitschrift Für Anorg. Und Allg. Chemie.* 369 (1969) 327–340.
- [118] T. Nakajima, Y. Matsuo, Formation process and structure of graphite oxide, *Carbon N. Y.* 32 (1994) 469–475. doi:10.1016/0008-6223(94)90168-6.
- [119] L.H. Sen, M.A.M. Nainar, S. Begum, Model, synthesis and applications of graphene oxide: a review, *Nanomater. Energy.* 3 (2014) 61–65. doi:10.1680/nme.13.00031.

- [120] T. Szabó, O. Berkesi, P. Forgó, K. Josepovits, Y. Sanakis, D. Petridis, I. Dékány, Evolution of Surface Functional Groups in a Series of Progressively Oxidized Graphite Oxides Evolution of Surface Functional Groups in a Series of Progressively Oxidized Graphite Oxides, *Chem. Mater.* 18 (2006) 2740–2749. doi:10.1021/cm060258.
- [121] A. Lerf, H. He, M. Forster, J. Klinowski, Structure of Graphite Oxide Revisited¹, *J. Phys. Chem. B.* 102 (1998) 4477–4482. doi:10.1021/jp9731821.
- [122] H. He, T. Riedl, A. Lerf, J. Klinowski, Solid-State NMR Studies of the Structure of Graphite Oxide, *J. Phys. Chem.* 100 (1996) 19954–19958. <http://dx.doi.org/10.1021/jp961563t>.
- [123] W. Gao, L.B. Alemany, C. Lijie, P.M. Ajayan, New insights into the structure and reduction of graphite oxide, *Nat. Chem.* 1 (2009) 403–408. doi:10.1038/nchem.281.
- [124] A.M. Dimiev, L.B. Alemany, J.M. Tour, Graphene oxide. Origin of acidity, its instability in water, and a new dynamic structural model, *ACS Nano.* 7 (2012) 576–588. doi:10.1021/nn3047378.
- [125] J. Ma, D. Ping, X. Dong, Y. Han, Z.Z. Xu, C. Gao, D.A. Dikin, S. Stankovich, E.J. Zimney, R.D. Piner, G.H.B. Dommett, G. Evmenenko, S.T. Nguyen, R.S. Ruoff, K. Ranganathan, S. Jeyapaul, D.C. Sharma, C. Tsou, Q. An, S. Lo, M. De Guzman, W. Hung, F. Resources, C.J. Vo, P. Green, Y. Wada, L.P.H. Van Beek, M.F.P. Bierkens, N. Wei, X. Peng, Z.Z. Xu, Preparation and characterization of graphene oxide paper, *Nature.* 23 (2007) 457–460. doi:10.3390/membranes7030052.
- [126] L. Liu, J. Zhang, J. Zhao, L. Feng, Mechanical properties of graphene oxides,

- Nanoscale. 4 (2012) 5910–5916. doi:10.1039/c2nr31164j.
- [127] Q. Zheng, Y. Geng, S. Wang, Z. Li, J.K. Kim, Effects of functional groups on the mechanical and wrinkling properties of graphene sheets, *Carbon N. Y.* 48 (2010) 4315–4322. doi:10.1016/j.carbon.2010.07.044.
- [128] L. Zhang, S. Tu, H. Wang, Q. Du, Preparation of polymer/graphene oxide nanocomposites by a two-step strategy composed of in situ polymerization and melt processing, *Compos. Sci. Technol.* 154 (2018) 1–7. doi:10.1016/j.compscitech.2017.10.030.
- [129] S.H. Kang, T.H. Fang, Z.H. Hong, Electrical and mechanical properties of graphene oxide on flexible substrate, *J. Phys. Chem. Solids.* 74 (2013) 1783–1793. doi:10.1016/j.jpics.2013.07.009.
- [130] C. Punckt, F. Muckel, S. Wolff, I.A. Aksay, C.A. Chavarin, G. Bacher, W. Mertin, The effect of degree of reduction on the electrical properties of functionalized graphene sheets, *Appl. Phys. Lett.* 102 (2013). doi:10.1063/1.4775582.
- [131] M. Shams, L.M. Guiney, L. Huang, M. Ramesh, X. Yang, M.C. Hersam, I. Chowdhury, Influence of functional groups on the degradation of graphene oxide nanomaterials, *Environ. Sci. Nano.* 6 (2019) 2203–2214. doi:10.1039/c9en00355j.
- [132] K. Xu, J. Zhang, X. Hao, C. Zhang, N. Wei, C. Zhang, Wetting properties of defective graphene oxide: A molecular simulation study, *Molecules.* 23 (2018) 1–8. doi:10.3390/molecules23061439.
- [133] X. Hu, Y. Yu, W. Hou, J. Zhou, L. Song, Effects of particle size and pH value

- on the hydrophilicity of graphene oxide, *Appl. Surf. Sci.* 273 (2013) 118–121.
doi:10.1016/j.apsusc.2013.01.201.
- [134] P. Feicht, R. Siegel, H. Thurn, J.W. Neubauer, M. Seuss, T. Szabó, A. V. Talyzin, C.E. Halbig, S. Eigler, D.A. Kunz, A. Fery, G. Papastavrou, J. Senker, J. Breu, Systematic evaluation of different types of graphene oxide in respect to variations in their in-plane modulus, *Carbon N. Y.* 114 (2017) 700–705. doi:10.1016/j.carbon.2016.12.065.
- [135] C. Botas, P. Álvarez, P. Blanco, M. Granda, C. Blanco, R. Santamaria, L.J. Romasanta, R. Verdejo, M.A. Lopez-Manchado, R. Menéndez, Graphene materials with different structures prepared from the same graphite by the Hummers and Brodie methods, *Carbon N. Y.* 65 (2013) 156–164.
doi:10.1016/j.carbon.2013.08.009.
- [136] P. Feicht, J. Biskupek, T.E. Gorelik, J. Renner, C.E. Halbig, M. Maranska, F. Puchtler, U. Kaiser, S. Eigler, Brodie's or Hummers' Method: Oxidation Conditions Determine the Structure of Graphene Oxide, *Chem. - A Eur. J.* (2019) 8955–8959. doi:10.1002/chem.201901499.
- [137] L. Staudenmaier, Verfahren zur Darstellung der Graphitsäure, *Berichte Der Dtsch. Chem. Gesellschaft.* 246 (1898) 1481. doi:10.1002/cber.18980310237.
- [138] H.L. Poh, F. Šaněk, A. Ambrosi, G. Zhao, Z. Sofer, M. Pumera, Graphenes prepared by Staudenmaier, Hofmann and Hummers methods with consequent thermal exfoliation exhibit very different electrochemical properties, *Nanoscale.* 4 (2012) 3515–3522. doi:10.1039/c2nr30490b.
- [139] W.S. Hummers, R.E. Offeman, Preparation of Graphitic Oxide, *J. Am. Chem. Soc.* 80 (1958) 1339. doi:10.1021/ja01539a017.

- [140] D.C. Marcano, D. V Kosynkin, J.M. Berlin, A. Sinitskii, Z. Sun, A. Slesarev, L.B. Alemany, W. Lu, J.M. Tour, Improved Synthesis of Graphene Oxide, *ACS Nano*. 4 (2010). doi:10.1021/nn1006368.
- [141] N. K, V. Ramana G, S. D, V. V, Synthesis of Graphene Oxide by Modified Hummers Method and Hydrothermal Synthesis of Graphene-NiO Nano Composite for Supercapacitor Application, *J. Mater. Sci. Eng.* 05 (2016). doi:10.4172/2169-0022.1000284.
- [142] M. Hirata, T. Gotou, S. Horiuchi, M. Fujiwara, M. Ohba, Thin-film particles of graphite oxide 1: High-yield synthesis and flexibility of the particles, *Carbon N. Y.* 42 (2004) 2929–2937. doi:10.1016/j.carbon.2004.07.003.
- [143] N.I. Zaaba, K.L. Foo, U. Hashim, S.J. Tan, W.W. Liu, C.H. Voon, Synthesis of Graphene Oxide using Modified Hummers Method: Solvent Influence, *Procedia Eng.* 184 (2017) 469–477. doi:10.1016/j.proeng.2017.04.118.
- [144] M.D.P. Lavin-Lopez, A. Romero, J. Garrido, L. Sanchez-Silva, J.L. Valverde, Influence of different improved hummers method modifications on the characteristics of graphite oxide in order to make a more easily scalable method, *Ind. Eng. Chem. Res.* 55 (2016) 12836–12847. doi:10.1021/acs.iecr.6b03533.
- [145] L. Peng, Z. Xu, Z. Liu, Y. Wei, H. Sun, Z. Li, X. Zhao, C. Gao, An iron-based green approach to 1-h production of single-layer graphene oxide, *Nat. Commun.* 6 (2015) 1–9. doi:10.1038/ncomms6716.
- [146] L. Tang, X. Li, R. Ji, K.S. Teng, G. Tai, J. Ye, C. Wei, S.P. Lau, Bottom-up synthesis of large-scale graphene oxide nanosheets, *J. Mater. Chem.* 22 (2012) 5676–5683. doi:10.1039/c2jm15944a.

- [147] S. Ray, Applications of Graphene and Graphene-Oxide based Nanomaterials, 1st ed., Elsevier, Johannesburg, 2015. doi:10.1016/C2014-0-02615-9.
- [148] D. Liu, Q. Bian, Y. Li, Y. Wang, A. Xiang, H. Tian, Effect of oxidation degrees of graphene oxide on the structure and properties of poly (vinyl alcohol) composite films, *Compos. Sci. Technol.* 129 (2016) 146–152. doi:10.1016/j.compscitech.2016.04.004.
- [149] H. Ha, J. Park, S. Ando, C. Bin Kim, K. Nagai, B.D. Freeman, C.J. Ellison, Gas permeation and selectivity of poly(dimethylsiloxane)/graphene oxide composite elastomer membranes, *J. Memb. Sci.* 518 (2016) 131–140. doi:10.1016/j.memsci.2016.06.028.
- [150] X. Dong, W. Huang, P. Chen, In Situ Synthesis of Reduced Graphene Oxide and Gold Nanocomposites for Nanoelectronics and Biosensing, *Nanoscale Res. Lett.* 6 (2011) 1–6. doi:10.1007/s11671-010-9806-8.
- [151] M. Jin, H.K. Jeong, W.J. Yu, D.J. Bae, B.R. Kang, Y.H. Lee, Graphene oxide thin film field effect transistors without reduction, *J. Phys. D: Appl. Phys.* 42 (2009). doi:10.1088/0022-3727/42/13/135109.
- [152] S. Mohamadi, M. Hamidi, Chapter 3 - The new nanocarriers based on graphene and graphene oxide for drug delivery applications, in: *Nanostructures Drug Deliv.*, Elsevier, Karaj, 2017: pp. 107–147. doi:10.1016/B978-0-323-46143-6.00003-8.
- [153] A. Lipatov, A. Varezhnikov, P. Wilson, V. Sysoev, A. Kolmakov, A. Sinitskii, Highly selective gas sensor arrays based on thermally reduced graphene oxide, *Nanoscale.* 5 (2013) 5426–5434. doi:10.1039/c3nr00747b.

- [154] M. Hernaez, A.G. Mayes, S. Melendi-Espina, Graphene Oxide in Lossy Mode Resonance-Based Optical Fiber Sensors for Ethanol Detection, *Sensors*. 18 (2018). doi:10.3390/s18010058.
- [155] B. Mi, Graphene Oxide Membranes for Ionic and Molecular Sieving, *Science* (80-.). 343 (2014) 740–742. doi:10.1126/science.1250247.
- [156] A. Nollet, *Lecons de Physique Experimentale, hez les Frères Guérin, Paris*, 1748.
- [157] J. Glater, Early history of reverse osmosis membrane development, *Desalination*. 117 (1998) 297–309. doi:10.1016/S0011-9164(98)00122-2.
- [158] H. Bechhold, Kolloidstudien mit der Filtrationsmethode, *Z. Phys. Chem.* 60 (1907).
- [159] S. Loeb, S. Sourirajan, Saline Water Conversion–II, in: *Adv. Chem. Ser.* Number 28, American Chemical Society, Washington, DC, 1963: pp. 117–132. doi:10.1021/ba-1963-0038.ch009.
- [160] G.K. Ackers, Molecular Exclusion and Restricted Diffusion Processes in Molecular-Sieve Chromatography, *Biochemistry*. 3 (1964) 723–730. doi:10.1021/bi00893a021.
- [161] L. Letterman, *Water Quality and Treatment*, 5th ed., McGraw-Hill, Inc, Toronto, 1999.
- [162] P. Schirg, F. Widmer, Characterisation of nanofiltration membranes for the separation of aqueous dye-salt solutions, *Desalination*. 89 (1992) 89–107. doi:10.1016/0011-9164(92)80154-2.
- [163] F.G. Donnan, Theory of membrane equilibria and membrane potentials in the

- presence of non-dialysing electrolytes. A contribution to physical-chemical physiology, *J. Memb. Sci.* 100 (1995) 45–55. doi:10.1016/0376-7388(94)00297-C.
- [164] D.L. Oatley-Radcliffe, M. Walters, T.J. Ainscough, P.M. Williams, A.W. Mohammad, N. Hilal, Nanofiltration membranes and processes: A review of research trends over the past decade, *J. Water Process Eng.* 19 (2017) 164–171. doi:10.1016/j.jwpe.2017.07.026.
- [165] A.W. Mohammad, Y.H. Teow, W.L. Ang, Y.T. Chung, D.L. Oatley-Radcliffe, N. Hilal, Nanofiltration membranes review: Recent advances and future prospects, *Desalination.* 356 (2015) 226–254. doi:10.1016/j.desal.2014.10.043.
- [166] R. Weber, H. Chmiel, V. Mavrov, Characteristics and application of new ceramic nanofiltration membranes, *Desalination.* 157 (2003) 113–125. doi:10.1016/S0011-9164(03)00390-4.
- [167] X.L. Wang, W.J. Shang, D.X. Wang, L. Wu, C.H. Tu, Characterization and applications of nanofiltration membranes: State of the art, *Desalination.* 236 (2009) 316–326. doi:10.1016/j.desal.2007.10.082.
- [168] H.S. Alkhatim, M.I. Alcaina, E. Soriano, M.I. Iborra, J. Lora, J. Arnal, Treatment of whey effluents from dairy industries by nanofiltration membranes, *Desalination.* 119 (1998) 177–183. doi:10.1016/S0011-9164(98)00142-8.
- [169] J. Schaep, C. Vandecasteele, W.A. Mohammad, R.W. Bowen, Analysis of the Salt Retention of Nanofiltration Membranes Using the Donnan–Steric Partitioning Pore Model, *Sep. Sci. Technol.* 34 (1999).

doi:<https://doi.org/10.1081/SS-100100819>.

- [170] F. Perreault, A.F. De Faria, M. Elimenech, Environmental applications of graphene-based nanomaterials, *Chem. Soc. Rev.* (2015). doi:10.1039/C5CS00021A.
- [171] S. Yang, S. Chen, Y. Chang, A. Cao, Y. Liu, H. Wang, Removal of methylene blue from aqueous solution by graphene oxide, *J. Colloid Interface Sci.* 359 (2011) 24–29. doi:10.1016/j.jcis.2011.02.064.
- [172] M.J. McAllister, J.L. Li, D.H. Adamson, H.C. Schniepp, A.A. Abdala, J. Liu, M. Herrera-Alonso, D.L. Milius, R. Car, R.K. Prud'homme, I.A. Aksay, Single sheet functionalized graphene by oxidation and thermal expansion of graphite, *Chem. Mater.* 19 (2007) 4396–4404. doi:10.1021/cm0630800.
- [173] C.N. Yeh, K. Raidongia, J. Shao, Q.H. Yang, J. Huang, On the origin of the stability of graphene oxide membranes in water, *Nat. Chem.* 7 (2015) 166–170. doi:10.1038/nchem.2145.
- [174] D. LI, M.B. Müller, S. Gilje, R.B. Kaner, G.G. Wallace, Processable aqueous dispersions of graphene nanosheets, *Nat. Nanotechnol.* 3 (2008) 101–105. doi:10.1038/nnano.2007.451.
- [175] D.A. Dikin, S. Stankovich, E.J. Zimney, R.D. Piner, G.H.B. Dommett, G. Evmenenko, S.T. Nguyen, R.S. Ruoff, Preparation and characterization of graphene oxide paper, *Nature.* 448 (2007) 457–460. doi:10.1038/nature06016.
- [176] C. Cheng, D. Li, Solvated graphenes: An emerging class of functional soft materials, *Adv. Mater.* 25 (2013) 13–30. doi:10.1002/adma.201203567.
- [177] E. Yang, C.M. Kim, J. ho Song, H. Ki, M.H. Ham, I.S. Kim, Enhanced

- desalination performance of forward osmosis membranes based on reduced graphene oxide laminates coated with hydrophilic polydopamine, *Carbon N. Y.* 117 (2017) 293–300. doi:10.1016/j.carbon.2017.03.005.
- [178] J. Lyu, X. Wen, U. Kumar, Y. You, V. Chen, R.K. Joshi, Separation and purification using GO and r-GO membranes, *RSC Adv.* 8 (2018) 23130–23151. doi:10.1039/C8RA03156H.
- [179] A. Ali, M. Aamir, K.H. Thebo, J. Akhtar, Laminar Graphene Oxide Membranes Towards Selective Ionic and Molecular Separations: Challenges and Progress, *Chem. Rec.* (2019) 344–354. doi:10.1002/tcr.201900024.
- [180] D. Hall, P. Underhill, J.M. Torkelson, Spin coating of thin and ultrathin polymer films, *Polym. Eng. Sci.* 38 (1998) 2039–2045. doi:10.1002/pen.10373.
- [181] M.D. Tyona, A theoretical study on spin coating technique, *Adv. Mater. Res.* 2 (2013) 195–208. doi:10.12989/amr.2013.2.4.195.
- [182] N.-T. Nguyen, *Micromixers Fundamentals, Design and Fabrication* A volume in *Micro and Nano Technologies*, 2nd editio, Elsevier, 2012. doi:https://doi.org/10.1016/C2011-0-69734-0.
- [183] A.F.M. Ibrahim, Y.S. Lin, Synthesis of graphene oxide membranes on polyester substrate by spray coating for gas separation, *Chem. Eng. Sci.* 190 (2018) 312–319. doi:10.1016/j.ces.2018.06.031.
- [184] H. Shi, C. Wang, Z. Sun, Y. Zhou, K. Jin, G. Yang, Transparent conductive reduced graphene oxide thin films produced by spray coating, *Sci. China Physics, Mech. Astron.* 58 (2015) 1–5. doi:10.1007/s11433-014-5614-y.

- [185] J. Puetz, M.A. Aegerter, *Dip Coating Technique.*, Springer, Boston, MA, Boston, 2004. doi:10.1007/978-0-387-88953-5_3.
- [186] D. Energy, M. Elimelech, W.A. Phillip, R. Das, M.E. Ali, S.B.A. Hamid, S. Ramakrishna, Z.Z. Chowdhury, J. Ma, D. Ping, X. Dong, A. Geim, K. Novoselov, P. Bernardo, G. Clarizia, N. Song, X. Gao, Z. Ma, X. Wang, Y. Wei, C. Gao, B. Tang, L. Zhang, R. Li, J. Wu, M.N. Hedhili, P. Wang, A. Mcrobie, B. Eckhardt, E. Ott, J.K. Holt, H.G. Park, Y. Wang, M. Stadermann, A.B. Artyukhin, C.P. Grigoropoulos, A. Noy, O. Bakajin, R.P. Pandey, G. Shukla, M. Manohar, V.K. Shahi, H. Ma, C. Burger, B.S. Hsiao, B. Chu, S.J. Mcgrane, K. Balke, Y. Zhu, R.I. Jafri, N. Rajalakshmi, S. Ramaprabhu, L.M. Robeson, Y. Yampolskii, Z. Wang, A. Wu, J. Lyu, X. Wen, P. Liu, T. Yan, J. Zhang, L. Shi, D. Zhang, V. Srinivasan, E.F. Lambin, S.M. Gorelick, B.H. Thompson, S. Rozelle, R.I. Mcdonald, P. Green, D. Balk, B.M. Fekete, C. Revenga, M. Todd, M. Shatat, S.B. Riffat, G.M. Geise, H. Lee, D.J. Miller, B.D. Freeman, J.E. Mcgrath, D.R. Paul, H. Lee, D.J. Miller, Carbon nanotube membranes for water purification: A bright future in water desalination, *Desalination*. 336 (2017) 97–109. doi:10.1016/j.desal.2013.12.026.
- [187] D.F. Lii, J.L. Huang, L.J. Tsui, S.M. Lee, Formation of BN films on carbon fibers by dip-coating, *Surf. Coatings Technol.* 150 (2002) 269–276. doi:10.1016/S0257-8972(01)01539-0.
- [188] V. Kandjou, M. Hernaez, B. Acevedo, S. Melendi-espina, Interfacial crosslinked controlled thickness graphene oxide thin- fi lms through dip-assisted layer-by-layer assembly means, *Prog. Org. Coatings*. 137 (2019). doi:10.1016/j.porgcoat.2019.105345.

- [189] H.W. Kim, H.W. Yoon, S. Yoon, B.M. Yoo, B.K. Ahn, Y.H. Cho, H.J. Shin, H. Yang, U. Paik, S. Kwon, Selective Gas Transport Through Few-Layered Graphene and Graphene Oxide, *Science* (80-.). 342 (2013) 91–95.
doi:10.1126/science.1236098.
- [190] Y. Li, X. Wang, J. Sun, Layer-by-layer assembly for rapid fabrication of thick polymeric films, *Chem. Soc. Rev.* 41 (2012) 5998–6009.
doi:10.1039/c2cs35107b.
- [191] Q. Nan, P. Li, B. Cao, Fabrication of positively charged nanofiltration membrane via the layer-by-layer assembly of graphene oxide and polyethylenimine for desalination, *Appl. Surf. Sci.* 387 (2016) 521–528.
doi:10.1016/j.apsusc.2016.06.150.
- [192] J. Shen, Y. Hu, C. Li, C. Qin, M. Shi, M. Ye, Layer-by-layer self-assembly of graphene nanoplatelets, *Langmuir.* 25 (2009) 6122–6128.
doi:10.1021/la900126g.
- [193] W. Choi, J. Choi, J. Bang, J.H. Lee, Layer-by-layer assembly of graphene oxide nanosheets on polyamide membranes for durable reverse-osmosis applications, *ACS Appl. Mater. Interfaces.* 5 (2013) 12510–12519.
doi:10.1021/am403790s.
- [194] M. Hu, B. Mi, Layer-by-layer assembly of graphene oxide membranes via electrostatic interaction, *J. Memb. Sci.* 469 (2014) 80–87.
doi:10.1016/j.memsci.2014.06.036.
- [195] J.J. Richardson, M. Björnmalm, F. Caruso, Technology-driven layer-by-layer assembly of nanofilms, *Science* (80-.). 348 (2015).
doi:10.1126/science.aaa2491.

- [196] J.J. Richardson, J. Cui, M. Björnmalm, J.A. Braunger, H. Ejima, F. Caruso, Innovation in Layer-by-Layer Assembly, *Chem. Rev.* 116 (2016) 14828–14867. doi:10.1021/acs.chemrev.6b00627.
- [197] X.L. Xu, F.W. Lin, Y. Du, X. Zhang, J. Wu, Z.K. Xu, Graphene Oxide Nanofiltration Membranes Stabilized by Cationic Porphyrin for High Salt Rejection, *ACS Appl. Mater. Interfaces.* 8 (2016) 12588–12593. doi:10.1021/acsami.6b03693.
- [198] C.N. Yeh, K. Raidongia, J. Shao, Q.H. Yang, J. Huang, On the origin of the stability of graphene oxide membranes in water, *Nat. Chem.* 7 (2015) 166–170. doi:10.1038/nchem.2145.
- [199] Y. Li, W. Zhao, M. Weyland, S. Yuan, Y. Xia, H. Liu, M. Jian, J. Yang, C.D. Easton, C. Selomulya, X. Zhang, Thermally reduced nanoporous graphene oxide membrane for desalination, *Environ. Sci. Technol.* 53 (2019) 8314–8323. doi:10.1021/acs.est.9b01914.
- [200] M.J. Fernández-Merino, L. Guardia, J.I. Paredes, S. Villar-Rodil, P. Solís-Fernández, A. Martínez-Alonso, J.M.D. Tascón, Vitamin C is an ideal substitute for hydrazine in the reduction of graphene oxide suspensions, *J. Phys. Chem. C.* 114 (2010) 6426–6432. doi:10.1021/jp100603h.
- [201] I. Sengupta, S. Chakraborty, M. Talukdar, S. Pal, Thermal reduction of graphene oxide: How temperature influences purity, *J. Mater. Res.* 33 (2018) 4113–4122. doi:10.1557/jmr.2018.338.
- [202] W. Gao, L.B. Alemany, L.J. Ci, P.M. Ajayan, New insights into the structure and reduction of graphite oxide, *Nat. Chem.* 1 (2009) 403–408. doi:10.1038/nchem.281.

- [203] C. Sun, Y. Wang, Q. Su, The impacts of graphene concentration and thickness on the photocatalytic performance of Bi₂TiO₅/graphene composite thin films, *Mater. Res. Express*. 4 (2017). doi:10.1088/2053-1591/aa7f53.
- [204] M. Na, W. Zhao, X. Zhang, Kinetic study of water transport in layered graphene oxide membranes, *Environ. Pollut. Bioavailab.* 31 (2019) 174–181. doi:10.1080/26395940.2019.1604163.
- [205] H.Y. Jeong, J.Y. Kim, J.W. Kim, J.O. Hwang, J.E. Kim, J.Y. Lee, T.H. Yoon, B.J. Cho, S.O. Kim, R.S. Ruoff, S.Y. Choi, Graphene oxide thin films for flexible nonvolatile memory applications, *Nano Lett.* 10 (2010) 4381–4386. doi:10.1021/nl101902k.
- [206] O.O. Abegunde, E.T. Akinlabi, O.P. Oladijo, S. Akinlabi, A.U. Ude, Overview of thin film deposition techniques, *AIMS Mater. Sci.* 6 (2019) 174–199. doi:10.3934/MATERSCI.2019.2.174.
- [207] I. Shishkovsky, P. Lebedev, *Nanocoatings and Ultra-Thin Films Technologies and Applications*, in: *Woodhead Publishing Series in Metals and Surface Engineering*, 2011: pp. 57–77. doi:10.1533/9780857094902.1.57.
- [208] A. Jilani, M. Shaaban Abdel-wahab, A. Hosny Hammad, *Advance Deposition Techniques for Thin Film and Coating*, in: *Mod. Technol. Creat. Thin-Film Syst. Coatings*, 2005. doi:10.5772/65702.
- [209] P.M. Martin, *Handbook of Deposition Technologies for Films and Coatings*. Science, applications and technology, 3rd ed., Elsevier, 2010.
- [210] H. Nanto, T. Minami, S. Takata, Photoluminescence in sputtered ZnO thin films, *Phys. Status Solidi*. 65 (1981) K131–K134.

doi:10.1002/pssa.2210650252.

- [211] J.E. Mahan, *Physical Vapor Deposition of Thin Films*, Wiley-VCH, 2000.
- [212] D.A. Jameel, *Thin Film Deposition Processes*, *Int. J. Mod. Phys. Appl.* 1 (2015) 193–199. doi:10.1557/S0883769400063879.
- [213] R. Luttge, *Microfabrication for Industrial Applications*, Elsevier, 2011.
- [214] D.M. Mattox, *Physical vapor deposition (PVD) processes*, *Met. Finish.* 100 (2002) 394–408. doi:10.1016/S0026-0576(02)82043-8.
- [215] J.E. Crowell, *Chemical methods of thin film deposition: Chemical vapor deposition, atomic layer deposition, and related technologies*, *J. Vac. Sci. Technol. A.* 21 (2003). doi:10.1116/1.1600451.
- [216] M. Faustini, G.L. Drisco, C. Boissiere, D. Grosso, *Liquid deposition approaches to self-assembled periodic nanomasks*, *Sripta Mater.* 74 (2013) 13–18. <https://doi.org/10.1016/j.scriptamat.2013.07.029>.
- [217] K.. Habig, *Chemical vapor deposition and physical vapor deposition coatings: Properties, tribological behavior, and applications*, *J. Vac. Sci. Technol. A.* 4 (1986). doi:10.1116/1.573687.
- [218] A. Ulman, *An Introduction to Ultrathin Organic Films: From Langmuir–Blodgett to Self-Assembly*, Academic Press Inc., San Diego, 1991.
- [219] A.G. Emslie, F.T. Bonner, L.G. Peck, *Flow of a Viscous Liquid on a Rotating Disk*, *J. Appl. Phys.* 29 (1958). doi:10.1063/1.1723300.
- [220] N. Sahu, B. Parija, S. Panigrahi, *Fundamental understanding and modeling of spin coating process: A review*, *Indian J. Phys.* 83 (2009) 493–502.

doi:10.1007/s12648-009-0009-z.

- [221] U. Bielecka, P. Lutsyk, K. Janus, J. Sworakowski, W. Bartkowiak, Effect of solution aging on morphology and electrical characteristics of regioregular P3HT FETs fabricated by spin coating and spray coating, *Org. Electron.* 12 (2011) 1768–1776. doi:10.1016/j.orgel.2011.06.027.
- [222] G. Decher, J.-D. Hong, Buildup of ultrathin multilayer films by a self-assembly process, 1 consecutive adsorption of anionic and cationic bipolar amphiphiles on charged surfaces, *Makromol. Chemie. Macromol. Symp.* 46 (1991) 321–327. doi:10.1002/masy.19910460145.
- [223] J. Hong, S.W. Kang, Carbon Decorative Coatings by Dip-, Spin-, and Spray-Assisted Layer-by-Layer Assembly Deposition, *J. Nanosci. Nanotechnol.* 11 (2011) 7771–7776. doi:10.1166/jnn.2011.4737.
- [224] X. Zhang, H. Chen, H. Zhang, Layer-by-layer assembly: from conventional to unconventional methods, *Chem. Commun.* (2007) 1395–1405. doi:10.1039/B615590A.
- [225] X. Tang, X. Yan, Dip-coating for fibrous materials: mechanism, methods and applications, *J. Sol-Gel Sci. Technol.* 81 (2017) 378–404. doi:10.1007/s10971-016-4197-7.
- [226] J. March, *Advanced Organic Chemistry: Reactions, Mechanisms, and Structure*, 4th ed., Wiley, New York, NY, 1992.
- [227] X. Liu, N. Wen, X. Wang, Y. Zheng, Layer-by-Layer Self-Assembled Graphene Multilayer Films via Covalent Bonds for Supercapacitor Electrodes, *Nanomater. Nanotechnol.* 5 (2015) 14. doi:10.5772/60596.

- [228] G.F. Jin, H.S. Ban, H. Nakamura, J.D. Lee, O-carboranylalkoxy-1,3,5-triazine derivatives: Synthesis, characterization, X-ray structural studies, and biological activity, *Molecules*. 23 (2018) 1–13. doi:10.3390/molecules23092194.
- [229] C.N. Lungu, M. V. Diudea, M. V. Putz, I.P. Grudziński, Linear and branched PEIs (Polyethylenimines) and their property space, *Int. J. Mol. Sci.* 17 (2016). doi:10.3390/ijms17040555.
- [230] S. Kim, O. Park, J.H. Lee, B. Ku, Layer-by-layer assembled graphene oxide films and barrier properties of thermally reduced graphene oxide membranes, *Carbon Lett.* 14 (2013) 247–250. doi:10.5714/CL.2013.14.4.247.
- [231] W. Yu, H. Xie, X. Wang, X. Wang, Highly Efficient Method for Preparing Homogeneous and Stable Colloids Containing Graphene Oxide, *Nanoscale Res. Lett.* 6 (2011) 1–7. doi:10.1007/s11671-010-9779-7.
- [232] X. Liang, J. Zhang, T.T. Liu, L. Li, Illegally additives determination by thin layer chromatography, *MATEC Web Conf.* 63 (2016) 1–4. doi:10.1051/mateconf/20166301021.
- [233] M.I. Verkhovsky, A. Jasaitis, M.L. Verkhovskaya, J.E. Morgan, M. Wikström, Proton translocation by cytochrome c oxidase., *Nature*. 400 (1999) 480–483. doi:10.1038/22813.
- [234] M. Frasconi, R. Tel-vered, J. Elbaz, I. Willner, Electrochemically-Stimulated pH Changes : A Route to Control Chemical Reactivity, *J. Am. Chem. Soc.* 132 (2010) 1–3. doi:10.1021/ja9094796.
- [235] A.P. Dementjev, A. de Graaf, M.C.. van de Sanden, A.. Maslakov, K.I

- Naumkin, A.. Serov, X-Ray photoelectron spectroscopy reference data for identification of the C₃ N₄ phase in carbon-nitrogen films., *Diam. Relat. Mater.* 9 (2000) 1904–1907. doi:10.1016/S0925-9635(00)00345-9.
- [236] S. Bhattacharyya, J. Hong, G. Turban, Determination of the structure of amorphous nitrogenated carbon films by combined Raman and x-ray photoemission spectroscopy, *J. Appl. Phys.* 83 (1998) 3917. doi:10.1063/1.367312.
- [237] S.D. Chandradoss, A.C. Haagsma, Y.K. Lee, J.-H. Hwang, J.-M. Nam, C. Joo, Surface Passivation for Single-molecule Protein Studies, *J. Vis. Exp.* (2014) 1–8. doi:10.3791/50549.
- [238] S. Pradhan, J. Hedberg, E. Blomberg, S. Wold, I. Odnevall Wallinder, Effect of sonication on particle dispersion, administered dose and metal release of non-functionalized, non-inert metal nanoparticles, *J. Nanoparticle Res.* 18 (2016) 1–14. doi:10.1007/s11051-016-3597-5.
- [239] P. Sanchez, V. Kandjou, M. Hernaez, F.. Zamarreño, C.R Arregui, A.. Mayes, S. Melendi-Espina, Graphene oxide film fabrication with controlled thickness on silicon-based substrates, in: *World Conf. Carbon, 2017*: p. 302.
- [240] V. Kandjou, M. Hernaez, B.M. Acevedo, A.M. Perez-Mas, S. Melendi-Espina, The fabrication of controlled thickness graphene oxide films by means of dip-assisted layer by layer assembly, in: *World Conf. Carbon, Madrid, 2018*: p. Paper 0649.
- [241] Z. Jia, Y. Wang, Covalently crosslinked graphene oxide membranes by esterification reactions for ions separation, *J. Mater. Chem. A.* 3 (2015) 4405–4412. doi:10.1039/c4ta06193d.

- [242] M. Aleksandrzak, P. Adamski, W. Kukulka, B. Zielinska, E. Mijowska, Effect of graphene thickness on photocatalytic activity of TiO₂ - graphene nanocomposites, *Appl. Surf. Sci.* 331 (2015) 193–199. doi:10.1016/j.apsusc.2015.01.070.
- [243] G. Wang, B. Wang, J. Park, J. Yang, X. Shen, J. Yao, Synthesis of enhanced hydrophilic and hydrophobic graphene oxide nanosheets by a solvothermal method, *Carbon N. Y.* 7 (2008) 6–10. doi:10.1016/j.carbon.2008.09.002.
- [244] C. Hontoria-Lucas, A.. Lopez-Peinado, de D. Lopez-Gonzalez, M.. Cervantes-Rojas, R.. Martin-Aranda, Study of oxygen containing groups in a series of graphite oxides: Physical and Chemical Characterization, *Carbon N. Y.* 95 (1995). doi:10.1016/0008-6223(95)00120-3.
- [245] J.I. Paredes, S. Villar-Rodil, A. Martyinez-Alonso, J.M.D. Tascon, Graphene Oxide Dispersions in Organic Solvents, *Langmuir.* (2008) 10560–10564. doi:10.1021/la801744a.
- [246] X. Li, M. Huang, Y. Yang, Synthesis and Characterization of Poly(aniline-co-xylylidine)s, *Polym. J.* 42 (2001). doi:10.1295/polymj.32.348.
- [247] R.H. Sestrem, D.C. Ferreira, R. Landers, M.L.A. Temperini, M. Gustavo, Structure of chemically prepared poly- (para -phenylenediamine) investigated by spectroscopic techniques, *Polymer (Guildf).* 50 (2009) 6043–6048. doi:10.1016/j.polymer.2009.10.028.
- [248] N.P.G. Roeges, Guide to the complete interpretation of infrared spectra of organic structures, John Wiley and Sons Ltd. Baffins Lane, Chichester, West Sussex, 1994.

- [249] N.E. Mircescu, M. Oltean, V. Chis, N. Leopold, FTIR, FT-Raman, SERS and DFT study on melamine, *Vib. Spectrosc.* 62 (2012) 165–171.
doi:10.1016/j.vibspec.2012.04.008.
- [250] R.A. Heacock, L. Marion, The infrared spectra of secondary amines and their salts, *Can. J. Chem.* 34 (2011) 1782–1795. doi:10.1139/v56-231.
- [251] A.P. Cleaves, E.K. Plyler, The Infra-Red Absorption Spectrum of Methylamine Vapor, *J. Chem. Phys.* 7 (1939) 563–569.
doi:10.1063/1.1750491.
- [252] R.M. Silverstein, F.X. Webster, D.J. Kiemle, Identification of organic compounds (Spectrometric Identification of Organic Compounds. 4th ed), 4th ed., Wiley, New York, 1981.
- [253] S. Jawaid, F.N. Talpur, H.I. Afridi, S.M. Nizamani, A.A. Khaskheli, S. Naz, Quick determination of melamine in infant powder and liquid milk by Fourier transform infrared spectroscopy, *Anal. Methods.* (2014).
doi:10.1039/C4AY00558A.
- [254] H. Charville, D.A. Jackson, G. Hodges, A. Whiting, M.R. Wilson, The uncatalyzed direct amide formation reaction - Mechanism studies and the key role of carboxylic acid h-bonding, *European J. Org. Chem.* (2011) 5981–5990.
doi:10.1002/ejoc.201100714.
- [255] R.M. De Figueiredo, J.S. Suppo, J.M. Campagne, Nonclassical Routes for Amide Bond Formation, *Chem. Rev.* 116 (2016) 12029–12122.
doi:10.1021/acs.chemrev.6b00237.
- [256] N. Azizi, M.R. Saidi, Highly chemoselective addition of amines to epoxides

- in water, *Org. Lett.* 7 (2005) 3649–3651. doi:10.1021/ol051220q.
- [257] C. Mateo, V. Grazu, J.M. Palomo, F. Lopez-Gallego, R. Fernandez-Lafuente, J.M. Guisan, Immobilization of enzymes on heterofunctional epoxy supports, *Nat. Protoc.* 2 (2007) 1022–1033. doi:10.1038/nprot.2007.133.
- [258] W. Gao, *Graphene Oxide: Reduction Recipes, Spectroscopy, and Applications*, Springer, Cham, 2015. doi:10.1007/978-3-319-15500-5.
- [259] H.L. Ma, H. Bin Zhang, Q.H. Hu, W.J. Li, Z.G. Jiang, Z.Z. Yu, A. Dasari, Functionalization and reduction of graphene oxide with p-phenylene diamine for electrically conductive and thermally stable polystyrene composites, *ACS Appl. Mater. Interfaces.* 4 (2012) 1948–1953. doi:10.1021/am201654b.
- [260] J. Xia, Y. Zhu, Z. He, F. Wang, H. Wu, Superstrong Noncovalent Interface between Melamine and Graphene Oxide, *ACS Appl. Mater. Interfaces.* 11 (2019) 17068–17078. doi:10.1021/acsami.9b02971.
- [261] J. Li, X. Zeng, T. Ren, E. van der Heide, The Preparation of Graphene Oxide and Its Derivatives and Their Application in Bio-Tribological Systems, *Lubricants.* 2 (2014) 137–161. doi:10.3390/lubricants2030137.
- [262] S. Dai, Z. Xu, M. Zhu, Y. Qian, C. Wang, Detection of p-phenylenediamine based on a glassy carbon electrode modified with nitrogen doped graphene, *Int. J. Electrochem. Sci.* 10 (2015) 7063–7072. doi:10(9):7063-7072.
- [263] L. Zhao, H. Zhang, N. Hoon, D. Hui, J. Hee, Q. Li, H. Sun, P. Li, Preparation of graphene oxide /polyethyleneimine layer-by-layer assembled film for enhanced hydrogen barrier property, *Compos. Part B Eng.* 92 (2016) 252–258. doi:10.1016/j.compositesb.2016.02.037.

- [264] D. Pakulski, S. Witomska, A. Aliprandi, V. Patroniak, A. Ciesielski, Graphene oxide-branched polyethyleneimine foams for efficient removal of toxic cations from water, *J. Mater. Chem. A.* (2018) 9384–9390. doi:10.1039/c8ta01622d.
- [265] T. Lee, S.H. Min, M. Gu, Y.K. Jung, W. Lee, J.U. Lee, D.G. Seong, B.S. Kim, Layer-by-Layer Assembly for Graphene-Based Multilayer Nanocomposites: Synthesis and Applications, *Chem. Mater.* 27 (2015) 3785–3796. doi:10.1021/acs.chemmater.5b00491.
- [266] Z. Jia, W. Shi, Tailoring permeation channels of graphene oxide membranes for precise ion separation, *Carbon N. Y.* 101 (2016) 290–295. doi:10.1016/j.carbon.2016.02.016.
- [267] G. Graziano, Hydrophobicity of benzene, *Biophys. Chem.* 82 (1999) 69–79. doi:https://doi.org/10.1016/S0301-4622(99)00105-2.
- [268] Y. Wang, Y. Yu, X. Hu, A. Feng, F. Jiang, L. Song, p-Phenylenediamine strengthened graphene oxide for the fabrication of superhydrophobic surface, *Mater. Des.* 127 (2017) 22–29. doi:10.1016/j.matdes.2017.04.033.
- [269] C.R. Crick, I.P. Parkin, Aerosol assisted deposition of melamine-formaldehyde resin: Hydrophobic thin films from a hydrophilic material, *Thin Solid Films.* 519 (2011) 2181–2186. doi:10.1016/j.tsf.2010.10.062.
- [270] H. Liu, K. Tapas, N.H. Kim, B.-C. Kud, J.H. Lee, In situ synthesis of the reduced graphene oxide–polyethyleneimine composite and its gas barrier properties, *J. Mater. Chem. A.* 1 (2013) 3739–3746. doi:10.1039/C3TA01228J.

- [271] P.H. Gleick, *Water in Crisis: A Guide to the World's Freshwater Resource*, Oxford University Press, 1993.
- [272] T. Shah, R. Molden, David Sakthivadivel, D. Seckler, *Global Groundwater Situation: Opportunities and Challenges*, *Econ. Polit. Wkly.* 26 (2001) 4142–4150. <https://www.jstor.org/stable/4411304>.
- [273] A. Boretti, L. Rosa, *Reassessing the projections of the World Water Development Report*, *Npj Clean Water.* 2 (2019). doi:10.1038/s41545-019-0039-9.
- [274] O.B. Akpor, D.A. OTohinoyi, *Pollutants in Wastewater Effluents: Impacts and Remediation Processes*, *Int. J. Environ. Res. Earth Sci.* 27 (2014) 249–253. doi:10.1007/s10162-014-0441-4.
- [275] T. Juneja, A. Chaudhary, *Assessment of water quality and its effects on the health of residents of Jhunjhunu district , Rajasthan : A cross sectional study*, *J. Public Heal. Epidemiol.* 5 (2013) 186–191. doi:10.5897/JPHE12.096.
- [276] S. Babel, T.A. Kurniawan, *Low-cost adsorbents for heavy metals uptake from contaminated water: A review*, *J. Hazard. Mater.* 97 (2003) 219–243. doi:10.1016/S0304-3894(02)00263-7.
- [277] F. Fu, Q. Wang, *Removal of heavy metal ions from wastewaters: A review*, *J. Environ. Manage.* 92 (2011) 407–418. doi:10.1016/j.jenvman.2010.11.011.
- [278] R. Rautenbach, A. Groschl, *Separation potential of nanofiltration membranes*, *Desalination.* 77 (1990) 73–84. doi:[https://doi.org/10.1016/0011-9164\(90\)85021-2](https://doi.org/10.1016/0011-9164(90)85021-2).
- [279] J. Wang, C. Zhao, T. Wang, Z. Wu, X. Li, J. Li, *Graphene oxide*

- polypiperazine-amide nanofiltration membrane for improving flux and anti-fouling in water purification, *RSC Adv.* 6 (2016) 82174–82185.
doi:10.1039/c6ra17284a.
- [280] Z. Yang, Y. Zhou, Z. Feng, X. Rui, T. Zhang, Z. Zhang, A review on reverse osmosis and nanofiltration membranes for water purification, *Polymers (Basel)*. 11 (2019) 1–22. doi:10.3390/polym11081252.
- [281] R.J. Petersen, Composite reverse osmosis and nanofiltration membranes, *J. Memb. Sci.* 83 (1993) 81–150. doi:10.1016/0376-7388(93)80014-O.
- [282] A.J. Schäfer, A.G. Fane, T.D. Waite, Fouling effects on rejection in the membrane filtration of natural waters, *Desalination*. 131 (2000) 215–224. doi:10.1016/S0011-9164(00)90020-1.
- [283] S.P. Surwade, S.N. Smirnov, I. V. Vlassiuk, R.R. Unocic, G.M. Veith, S. Dai, S.M. Mahurin, Water desalination using nanoporous single-layer graphene, *Nat. Nanotechnol.* 10 (2015) 459–464. doi:10.1038/nnano.2015.37.
- [284] Y. Han, Z. Xu, C. Gao, Ultrathin graphene nanofiltration membrane for water purification, *Adv. Funct. Mater.* 23 (2013) 3693–3700. doi:10.1002/adfm.201202601.
- [285] L.F. Dumée, K. Sears, J. Schütz, N. Finn, C. Huynh, S. Hawkins, M. Duke, S. Gray, Characterization and evaluation of carbon nanotube Bucky-Paper membranes for direct contact membrane distillation, *J. Memb. Sci.* 351 (2010) 36–43. doi:10.1016/j.memsci.2010.01.025.
- [286] C.J. Russo, J.A. Golovchenko, Atom-by-atom nucleation and growth of graphene nanopores, *Proc. Natl. Acad. Sci.* 109 (2012) 5953–5957.

- doi:10.1073/pnas.1119827109.
- [287] S.C. O'Hern, B. Michael S. H., I. Juan-Carlos, Y. Song, K. Jing, L. Tahar, A. Muataz, K. Rohit, Selective Ionic Transport through Tunable Subnanometer Pores in Single-Layer Graphene Membranes, *Nano Lett.* 3 (2014) 1234–1241. doi:10.1021/nl404118f.
- [288] T. Tene, G.T. Usca, M. Guevara, R. Molina, F. Veltri, M. Arias, L.S. Caputi, C.V. Gomez, Toward large-scale production of oxidized graphene, *Nanomaterials.* 10 (2020) 1–11. doi:10.3390/nano10020279.
- [289] A. Ghaffar, L. Zhang, X. Zhu, ChenBaoliang, Scalable graphene oxide membranes with tunable water channels and stability for ion rejection, *Environ. Sci. Nano.* 6 (2019) 904–915. doi:10.1039/C8EN01273C.
- [290] J. Wang, X. Gao, H. Yu, Q. Wang, Z. Ma, Z. Li, Y. Zhang, C. Gao, Accessing of graphene oxide (GO) nanofiltration membranes for microbial and fouling resistance, *Sep. Purif. Technol.* 215 (2019) 91–101. doi:10.1016/j.seppur.2019.01.018.
- [291] S. Liu, T.H. Zeng, M. Hofmann, E. Burcombe, J. Wei, R. Jiang, J. Kong, Y. Chen, Antibacterial activity of graphite, graphite oxide, graphene oxide, and reduced graphene oxide: Membrane and oxidative stress, *ACS Nano.* 5 (2011) 6971–6980. doi:10.1021/nn202451x.
- [292] R. Yi, R. Yang, R. Yu, J. Lan, J. Chen, Z. Wang, L. Chen, M. Wu, Ultrahigh permeance of a chemical cross-linked graphene oxide nanofiltration membrane enhanced by cation- π interaction, *RSC Adv.* 9 (2019) 40397–40403. doi:10.1039/c9ra07109a.

- [293] C. Xu, A. Cui, Y. Xu, X. Fu, Graphene oxide-TiO₂ composite filtration membranes and their potential application for water purification, *Carbon N. Y.* 62 (2013) 465–471. doi:10.1016/j.carbon.2013.06.035.
- [294] C. Chi, X. Wang, Y. Peng, Y. Qian, Z. Hu, J. Dong, D. Zhao, Facile Preparation of Graphene Oxide Membranes for Gas Separation, *Chem. Mater.* 28 (2016) 2921–2927. doi:10.1021/acs.chemmater.5b04475.
- [295] S. Qi, C.. Tang, *Cross-Linked Layer-by-Layer Membranes*, Springer Berlin Heidelberg, 2016. doi:10.1007/978-3-662-44324-8.
- [296] C. Qiu, S. Qi, C.Y. Tang, Synthesis of high flux forward osmosis membranes by chemically crosslinked layer-by-layer polyelectrolytes, *J. Memb. Sci.* 381 (2011) 74–80. doi:10.1016/j.memsci.2011.07.013.
- [297] G.E.J. Poinern, N. Ali, D. Fawcett, Progress in nano-engineered anodic aluminum oxide membrane development, *Materials (Basel)*. 4 (2010) 487–526. doi:10.3390/ma4030487.
- [298] C.M. Chen, Q. Zhang, X.C. Zhao, B. Zhang, Q.Q. Kong, M.G. Yang, Q.H. Yang, M.Z. Wang, Y.G. Yang, R. Schlögl, D.S. Su, Hierarchically aminated graphene honeycombs for electrochemical capacitive energy storage, *J. Mater. Chem.* 22 (2012) 14076–14084. doi:10.1039/c2jm31426f.
- [299] K. Sada, K. Kokado, Y. Furukawa, Polyacrylonitrile (PAN)., *Encycl. Polym. Nanomater.* (2015). doi:10.1007/978-3-642-29648-2.
- [300] J. Wang, Z. Yue, J.S. Ince, J. Economy, Preparation of nanofiltration membranes from polyacrylonitrile ultrafiltration membranes, *J. Memb. Sci.* 286 (2006) 333–341. doi:https://doi.org/10.1016/j.memsci.2006.10.022.

- [301] Z. Zhao, J. Li, D. Zhang, C.-X. Chen, Nanofiltration membrane prepared from polyacrylonitrile ultrafiltration membrane by low-temperature plasma: I. Graft of acrylic acid in gas, *J. Memb. Sci.* 232 (2004) 1–8.
doi:10.1016/j.memsci.2003.11.009.
- [302] Z.G. Wang, L.S. Wan, Z.K. Xu, Surface engineerings of polyacrylonitrile-based asymmetric membranes towards biomedical applications: An overview, *J. Memb. Sci.* 304 (2007) 8–23. doi:10.1016/j.memsci.2007.05.012.
- [303] H.. Pham, S. Munjal, C.. Bosnyak, Polycarbonates,” in *Handbook of Thermoplastics*, New York, NY, 1997.
- [304] H. Schnell, *Chemistry and Physics of Polycarbonates*, Wiley Interscience, New York, NY, 1964.
- [305] O. Hauenstein, M.M. Rahman, M. Elsayed, R. Krause-Rehberg, S. Agarwal, V. Abetz, A. Greiner, Biobased Polycarbonate as a Gas Separation Membrane and “Breathing Glass” for Energy Saving Applications, *Adv. Mater. Technol.* 2 (2017). doi:10.1002/admt.201700026.
- [306] B. Van der Bruggen, M. Mänttärä, M. Nyström, Drawbacks of applying nanofiltration and how to avoid them: A review, *Sep. Purif. Technol.* 63 (2008) 251–263. doi:10.1016/j.seppur.2008.05.010.
- [307] W. Wang, X. Fenjuan, J. Wanqin, X. Nanping, Solvent Resistant Nanofiltration Membranes, *Prog. Chem.* 19 (2007) 1592–1597.
doi:10.1002/9781118522318.emst120.
- [308] Z. Zhao, J. Li, D. Wang, C.-X. Chen, Nanofiltration membrane prepared from polyacrylonitrile ultrafiltration membrane by low-temperature plasma: 4.

- grafting of N-vinylpyrrolidone in aqueous solution, *Desalination*. 184 (2005) 37–44. doi:<https://doi.org/10.1016/j.desal.2005.04.036>.
- [309] G. Zhang, H. Yan, S. Ji, Z. Liu, Self-assembly of polyelectrolyte multilayer pervaporation membranes by a dynamic layer-by-layer technique on a hydrolyzed polyacrylonitrile ultrafiltration membrane, *J. Memb. Sci.* 292 (2007) 1–8. doi:[10.1016/j.memsci.2006.11.023](https://doi.org/10.1016/j.memsci.2006.11.023).
- [310] G. Zhang, X. Gao, S. Ji, Z. Liu, Electric field-enhanced assembly of polyelectrolyte composite membranes, *J. Memb. Sci.* 307 (2008) 151–155. doi:[10.1016/j.memsci.2007.09.030](https://doi.org/10.1016/j.memsci.2007.09.030).
- [311] X.P. Wang, N. Li, W.Z. Wang, Pervaporation properties of novel alginate composite membranes for dehydration of organic solvents, *J. Memb. Sci.* 193 (2001) 85–95. doi:[10.1016/S0376-7388\(01\)00498-7](https://doi.org/10.1016/S0376-7388(01)00498-7).
- [312] G. Zhang, H. Meng, S. Ji, Hydrolysis differences of polyacrylonitrile support membrane and its influences on polyacrylonitrile-based membrane performance, *Desalination*. 242 (2009) 313–324. doi:[10.1016/j.desal.2008.05.010](https://doi.org/10.1016/j.desal.2008.05.010).
- [313] O. Sanli, Homogeneous hydrolysis of polyacrylonitrile by potassium hydroxide, *Eur. Polym. J.* 26 (1990) 9–13. doi:[10.1016/0014-3057\(90\)90089-M](https://doi.org/10.1016/0014-3057(90)90089-M).
- [314] M. Jassal, S. Bhowmick, S. Sengupta, P.K. Patra, D.I. Walker, Hydrolyzed Poly(acrylonitrile) Electrospun Ion-Exchange Fibers, *Environ. Eng. Sci.* 31 (2014) 288–299. doi:[10.1089/ees.2013.0436](https://doi.org/10.1089/ees.2013.0436).
- [315] E. Sogbochi, C.K. Balogoun, C. Pascal, A. Dossa, D. Codjo, K. Sohounhloue,

- Evaluation of Adsorption Capacity of Methylene Blue in Aqueous Medium by Two Adsorbents : The Raw Hull of *Lophira lanceolata* and Its Activated Carbon, *Am. J. Phys. Chem.* 6 (2017) 76–87.
doi:10.11648/j.ajpc.20170605.11.
- [316] Y. Wei, Y. Zhang, X. Gao, Z. Ma, X. Wang, C. Gao, Multilayered Graphene Oxide Membrane for Water Treatment: A Review, *Carbon N. Y.* 139 (2018) 964–981. doi:10.1016/j.carbon.2018.07.040.
- [317] V. Georgakilas, J.N. Tiwari, K.C. Kemp, A.B. Perman, Jason A. Bourlinos, K.S. Kim, R. Zboril, Noncovalent Functionalization of Graphene and Graphene Oxide for Energy Materials, Biosensing, Catalytic, and Biomedical Applications, *Chem. Rev.* 116 (2016) 5464–5519.
doi:10.1021/acs.chemrev.5b00620.
- [318] Y. Wei, Y. Zhang, X. Gao, Z. Ma, X. Wang, C. Gao, Multilayered graphene oxide membranes for water treatment: A review, *Carbon N. Y.* 139 (2018) 964–982. doi:10.1016/j.carbon.2018.07.040.
- [319] Z. Jia, Y. Wang, W. Shi, J. Wang, Diamines cross-linked graphene oxide free-standing membranes for ion dialysis separation, *J. Memb. Sci.* 520 (2016) 139–144. doi:10.1016/j.memsci.2016.07.042.
- [320] H. Karkhanechi, R. Takagi, H. Matsuyama, Biofouling resistance of reverse osmosis membrane modified with polydopamine, *Desalination.* 336 (2014) 87–96. doi:10.1016/j.desal.2013.12.033.
- [321] J.H. Li, X.S. Shao, Q. Zhou, M.Z. Li, Q.Q. Zhang, The double effects of silver nanoparticles on the PVDF membrane: Surface hydrophilicity and antifouling performance, *Appl. Surf. Sci.* 265 (2013) 663–670.

- doi:10.1016/j.apsusc.2012.11.072.
- [322] W. Zhang, C. Zhou, W. Zhou, A. Lei, Q. Zhang, Q. Wan, B. Zou, Fast and considerable adsorption of methylene blue dye onto graphene oxide, *Bull. Environ. Contam. Toxicol.* 87 (2011) 86–90. doi:10.1007/s00128-011-0304-1.
- [323] G.F. Wang, H. Qin, X. Gao, Y. Cao, W. Wang, F.C. Wang, H.A. Wu, H.P. Cong, S.H. Yu, Graphene Thin Films by Noncovalent-Interaction-Driven Assembly of Graphene Monolayers for Flexible Supercapacitors, *Chem.* 4 (2018) 896–910. doi:10.1016/j.chempr.2018.01.008.
- [324] R.K. Bharadwaj, Modeling the barrier properties of polymer-layered silicate nanocomposites, *Macromolecules.* 34 (2001) 9189–9192.
doi:10.1021/ma010780b.
- [325] J.Y. Chong, B. Wang, C. Mattevi, K. Li, Dynamic microstructure of graphene oxide membranes and the permeation flux, *J. Memb. Sci.* 549 (2018) 385–392. doi:10.1016/j.memsci.2017.12.018.
- [326] A.A. Sapolidis, F.K. Katsaros, N.K. Kanellopoulos, PVA / Montmorillonite Nanocomposites: Development and Properties, *Nanocomposites Polym. with Anal. Methods.* (2011). doi:10.5772/18217.
- [327] Y. Kojima, A. Usuki, O. Kawasumi, Masaya Okada, Akane Kurauchi, Toshio Kamigaito, Synthesis of nylon 6–clay hybrid by montmorillonite intercalated with ϵ -caprolactam, *Polym. Chem.* 31 (1993) 983–986.
doi:10.1002/pola.1993.080310418.
- [328] D.A. Aba Nor Farah, J.Y. Chong, B. Wang, C. Mattevi, K. Li, Graphene Oxide Membranes on ceramic hollow fibers - Microstructural stability and

- nanofiltration performance, *J. Memb. Sci.* 484 (2015) 87–94.
doi:10.1016/j.memsci.2015.03.001.
- [329] M. Hu, B. Mi, Enabling graphene oxide nanosheets as water separation membranes, *Environ. Sci. Technol.* 47 (2013) 3715–3723.
doi:10.1021/es400571g.
- [330] J. de S. Macedo, N.B. da Costa Júnior, L.E. Almeida, E.F. da S. Vieira, A.R. Cestari, I. de F. Gimenez, N.L. Villarreal Carreño, L.S. Barreto, Kinetic and calorimetric study of the adsorption of dyes on mesoporous activated carbon prepared from coconut coir dust, *J. Colloid Interface Sci.* 298 (2006) 515–522.
doi:10.1016/j.jcis.2006.01.021.
- [331] M. Oz, D.E. Lorke, M. Hasan, G.A. Petroianu, Cellular and Molecular Actions of Methylene Blue in the Nervous System, *Med Res Rev.* 31 (2012) 93–117. doi:10.1002/med.20177.Cellular.
- [332] M.J.S. Dewar, E.G. Zoebisch, E.F. Healy, J.J.P. Stewart, Development and use of quantum mechanical molecular models. 76. AM1: a new general purpose quantum mechanical molecular model, *J. Am. Chem. Soc.* 107 (1985) 3902–3909. doi:10.1021/ja00299a024.
- [333] W.P. Lee, A.F. Routh, Why Do Drying Films Crack?, *Langmuir.* 20 (2004) 9885–9888. doi:10.1021/la049020v.
- [334] D. Qiuju, S. Jiankun, L. Yanhui, Y. Xiaoxia, W. Xiaohui, W. Zonghua, X. Linhua, Highly enhanced adsorption of congo red onto graphene oxide/chitosan fibers by wet-chemical etching off silica nanoparticles, *Chem. Eng. J.* 245 (2014) 99–106. doi:10.1016/j.cej.2014.02.006.

- [335] L. Chen, Y. Li, S. Hu, J. Sun, Q. Du, X. Yang, Q. Ji, Z. Wang, D. Wang, Y. Xia, Removal of methylene blue from water by cellulose/graphene oxide fibres, *J. Exp. Nanosci.* 11 (2016) 1156–1170. doi:10.1080/17458080.2016.1198499.
- [336] Q. Ling, Z. Xuehua, Y. Wenrong, W. Yufei, S. George P, L. Dan, Controllable corrugation of chemically converted graphene sheets in water and potential application for nanofiltration, *Chem. Commun.* 47 (2011) 5810–5812. doi:10.1039/C1CC10720H.
- [337] K. Viktor, W. Wilfried, U. Mathias, Molecularly imprinted composite membranes for selective binding of desmetryn from aqueous solutions, *Desalination.* 149 (2002) 323–326. doi:10.1016/S0011-9164(02)00802-0.
- [338] W. Peng, H. Li, Y. Liu, S. Song, Adsorption of methylene blue on graphene oxide prepared from amorphous graphite : Effects of pH and foreign ions, *J. Mol. Liq.* 221 (2016) 82–87. doi:10.1016/j.molliq.2016.05.074.
- [339] L. Ai, C. Zhang, Z. Chen, Removal of methylene blue from aqueous solution by a solvothermal-synthesized graphene / magnetite composite, *J. Hazard. Mater.* 192 (2011) 1515–1524. doi:10.1016/j.jhazmat.2011.06.068.
- [340] M. Yuan, S. Tong, S. Zhao, C.Q. Jia, Adsorption of polycyclic aromatic hydrocarbons from water using petroleum coke-derived porous carbon, *J. Hazard. Mater.* 181 (2010) 1115–1120. doi:10.1016/j.jhazmat.2010.05.130.
- [341] T. Adachi, S.S. Latthe, S.W. Gosavi, N. Roy, N. Suzuki, H. Ikari, K. Kato, K. ichi Katsumata, K. Nakata, M. Furudate, T. Inoue, T. Kondo, M. Yuasa, A. Fujishima, C. Terashima, Photocatalytic, superhydrophilic, self-cleaning TiO₂ coating on cheap, light-weight, flexible polycarbonate substrates, *Appl.*

- Surf. Sci. 458 (2018) 917–923. doi:10.1016/j.apsusc.2018.07.172.
- [342] B. Shen, W. Zhai, M. Tao, D. Lu, W. Zheng, Enhanced interfacial interaction between polycarbonate and thermally reduced graphene induced by melt blending, *Compos. Sci. Technol.* 86 (2013) 109–116. doi:10.1016/j.compscitech.2013.07.007.
- [343] C.H. Lin, H.Y. Lin, W.Z. Liao, S.A. Dai, Novel chemical recycling of polycarbonate (PC) waste into bis-hydroxyalkyl ethers of bisphenol A for use as PU raw materials, *Green Chem.* 9 (2007) 38–43. doi:10.1039/b609638g.
- [344] J. Kim, S.W. Kim, H. Yun, B.J. Kim, Impact of size control of graphene oxide nanosheets for enhancing electrical and mechanical properties of carbon nanotube-polymer composites, *RSC Adv.* 7 (2017) 30221–30228. doi:10.1039/c7ra04015f.
- [345] N. Akther, Z. Yuan, Y. Chen, S. Lim, S. Phuntsho, N. Ghaffour, H. Matsuyama, H. Shon, Influence of graphene oxide lateral size on the properties and performances of forward osmosis membrane, *Desalination*. 484 (2020) 114421. doi:10.1016/j.desal.2020.114421.
- [346] A. Paneri, S. Moghaddam, Impact of synthesis conditions on physicochemical and transport characteristics of graphene oxide laminates, *Carbon N. Y.* 86 (2015) 245–255. doi:10.1016/j.carbon.2015.01.024.
- [347] V. Saraswat, R.M. Jacobberger, J.S. Ostrander, C.L. Hummell, A.J. Way, J. Wang, M.T. Zanni, M.S. Arnold, Invariance of water permeance through size-differentiated graphene oxide laminates, *ACS Nano*. 12 (2018) 7855–7865. doi:10.1021/acsnano.8b02015.

- [348] S. Ye, J. Feng, The effect of sonication treatment of graphene oxide on the mechanical properties of the assembled films, *RSC Adv.* 6 (2016) 39681–39687. doi:10.1039/c6ra03996k.
- [349] M. Lotya, P.J. King, U. Khan, S. De, J.N. Coleman, High-concentration, surfactant-stabilized graphene dispersions, *ACS Nano.* 4 (2010) 3155–3162. doi:10.1021/nn1005304.
- [350] S. Bhattacharyya, C. Cardinaud, G. Turban, Spectroscopic determination of the structure of amorphous nitrogenated carbon films, *J. Appl. Phys.* 83 (1998) 4491.
- [351] Y.C.G. Kwan, G.M. Ng, C.H.A. Huan, Identification of functional groups and determination of carboxyl formation temperature in graphene oxide using the XPS O 1s spectrum, *Thin Solid Films.* 590 (2015) 40–48. doi:10.1016/j.tsf.2015.07.051.
- [352] S. Kumar, A. Garg, A. Chowdhuri, Sonication effect on graphene oxide (GO) membranes for water purification applications, *Mater. Res. Express.* 6 (2019). doi:10.1088/2053-1591/ab1ffd.
- [353] A.F. Rodrigues, L. Newman, N. Lozano, S.P. Mukherjee, B. Fadeel, C. Bussy, K. Kostarelos, A blueprint for the synthesis and characterisation of thin graphene oxide with controlled lateral dimensions for biomedicine, *2D Mater.* 5 (2018). doi:10.1088/2053-1583/aac05c.
- [354] P. Solís-Fernández, J.I. Paredes, S. Villar-Rodil, A. Martínez-Alonso, J.M.D. Tascón, Determining the thickness of chemically modified graphenes by scanning probe microscopy, *Carbon N. Y.* 48 (2010) 2657–2660. doi:10.1016/j.carbon.2010.03.033.

- [355] M. Hashemi, B. Muralidharan, M. Omid, J. Mohammadi, Y. Sefidbakht, E.S. Kima, H.D.C. Smyth, M. Shalbaf, T.E. Milner, Effect of size and chemical composition of graphene oxide nanoparticles on optical absorption cross-section, *J. Biomed. Opt.* 23 (2018) 1. doi:10.1117/1.jbo.23.8.085007.
- [356] S. Pandit, M. De, Empirical Correlation and Validation of Lateral Size-Dependent Absorption Coefficient of Graphene Oxides, *ChemistrySelect.* 2 (2017) 10004–10009. doi:10.1002/slct.201701893.
- [357] J.-L. Li, K.K. Kudin, M.J. McAllister, R.K. Prud'homme, I.A. Aksay, R. Car, Oxygen-Driven Unzipping of Graphitic Materials, *Infect. Immun.* 96 (2006) 432–434. doi:10.1103/PhysRevLett.96.176101.
- [358] D.W. Johnson, B. S.Coleman, K. Dobson, A manufacturing perspective on graphene dispersions, *Curr. Opin. Colloid Interface Sci.* 20 (2015) 367–382. doi:10.1016/j.cocis.2015.11.004.
- [359] R.J. Hunter, *Zeta Potential in Colloid Science*, 1st ed., Oxford University Press, New York, 1988.
- [360] J. Taha-Tijerina, D. Venkataramani, C.P. Aichele, C.S. Tiwary, J.E. Smay, A. Mathkar, P. Chang, P.M. Ajayan, Quantification of the particle size and stability of graphene oxide in a variety of solvents, *Part. Part. Syst. Charact.* 32 (2015) 334–339. doi:10.1002/ppsc.201400099.
- [361] R. Hunter, “Electro kinetics and zeta potential” in *Foundations of Colloid Science*, 2nd ed., Oxford University Press, New York, NY, 2001.
- [362] S. Kashyap, S. Mishra, S.K. Behera, Aqueous Colloidal Stability of Graphene Oxide and Chemically Converted Graphene, *J. Nanoparticles.* 2014 (2014) 1–

6. doi:10.1155/2014/640281.
- [363] V. Kandjou, A.M. Perez-mas, B. Acevedo, M. Hernaez, A.G. Mayes, S. Melendi-espina, Enhanced covalent p-phenylenediamine crosslinked graphene oxide membranes : Towards superior contaminant removal from wastewaters and improved membrane reusability, *J. Hazard. Mater.* 380 (2019) 120840. doi:10.1016/j.jhazmat.2019.120840.
- [364] P.L. Mores, A.M. Arias, N.J. Scenna, J.A. Caballero, S.F. Mussati, M.C. Mussati, Membrane-based processes: Optimization of hydrogen separation by minimization of power, membrane area, and cost, *Processes.* 6 (2018). doi:10.3390/pr6110221.
- [365] S. Bala, D. Nithya, M. Doraisamy, Exploring the effects of graphene oxide concentration on properties and antifouling performance of PEES / GO ultrafiltration membranes, *High Perform. Polym.* 30 (2018) 375–383. doi:10.1177/0954008317698547.
- [366] C. Zhao, X. Xu, J. Chen, F. Yang, Effect of graphene oxide concentration on the morphologies and antifouling properties of PVDF ultrafiltration membranes, *J. Environ. Chem. Eng.* 1 (2013) 349–354. doi:10.1016/j.jece.2013.05.014.
- [367] H. Huang, Z. Song, N. Wei, L. Shi, Y. Mao, Y. Ying, L. Sun, Z. Xu, X. Peng, Ultrafast viscous water flow through nanostrand-channelled graphene oxide membranes, *Nat. Commun.* 4 (2013). doi:10.1038/ncomms3979.
- [368] E.A. Chiticaru, L. Pilan, C.M. Damian, E. Vasile, J.S. Burns, M. Ionita, Influence of graphene oxide concentration when fabricating an electrochemical biosensor for DNA detection, *Biosensors.* 9 (2019) 1–18.

doi:10.3390/bios9040113.

- [369] K. Huang, G. Liu, Y. Lou, Z. Dong, J. Shen, W. Jin, A graphene oxide membrane with highly selective molecular separation of aqueous organic solution, *Angew. Chemie - Int. Ed.* 53 (2014) 6929–6932.
doi:10.1002/anie.201401061.
- [370] B. Zhang, Y. Li, T. Wu, D. Sun, W. Chen, X. Zhou, Magnetic iron oxide/graphene oxide nanocomposites: Formation and interaction mechanism for efficient removal of methylene blue and p-tert-butylphenol from aqueous solution, *Mater. Chem. Phys.* 205 (2018) 240–252.
doi:10.1016/j.matchemphys.2017.11.015.
- [371] N.S. Kaya, A. Yadav, M. Wehrhold, L. Zuccaro, K. Balasubramanian, Binding Kinetics of Methylene Blue on Monolayer Graphene Investigated by Multiparameter Surface Plasmon Resonance, *ACS Omega.* 3 (2018) 7133–7140. doi:10.1021/acsomega.8b00689.
- [372] C.R. Minitha, M. Lalitha, Y.L. Jeyachandran, L. Senthilkumar, R.T. Rajendra Kumar, Adsorption behaviour of reduced graphene oxide towards cationic and anionic dyes: Co-action of electrostatic and $\pi - \pi$ interactions, *Mater. Chem. Phys.* 194 (2017) 243–252. doi:10.1016/j.matchemphys.2017.03.048.
- [373] P. Sun, F. Zheng, M. Zhu, Z. Song, K. Wang, M. Zhong, D. Wu, R.B. Little, Z. Xu, H. Zhu, Selective trans-membrane transport of alkali and alkaline earth cations through graphene oxide membranes based on cation- π interactions, *ACS Nano.* 8 (2014) 850–859. doi:10.1021/nn4055682.
- [374] P. Sheath, M. Majumder, Flux accentuation and improved rejection in graphene-based filtration membranes produced by capillary-force-assisted

self-assembly, *Philos. Trans. R. Soc. A Math. Phys. Eng. Sci.* 374 (2016).

doi:10.1098/rsta.2015.0028.

- [375] S. Rajesh, A.B. Bose, Development of Graphene Oxide Framework Membranes via the “from” and “to” Cross-Linking Approach for Ion-Selective Separations, *ACS Appl. Mater. Interfaces*. 11 (2019) 27706–27716. doi:10.1021/acsami.9b05465.

- [376] W.-S. Hung, Y.-H. Chiao, A. Sengupta, Y.-W. Lin, S.R. Wickramasinghe, C.C. Hu, H.-A. Tsai, K.R. Lee, J.Y. Lai, Tuning the interlayer spacing of forward osmosis membranes based on ultrathin graphene oxide to achieve desired performance, *Carbon N. Y.* 142 (2019) 337–345. doi:10.1016/j.carbon.2018.10.058.

APPENDIX A; LIST OF ABBREVIATIONS

GO – Graphene Oxide

PVDF – Poly (vinylidene fluoride)

CNTs – Carbon nanotubes

r-GO – Reduced Graphene Oxide

PPD – P-Phenylenedimine

MLM – Melamine (1, 3, 5 – Triazine – 2, 4, 6 – triazine)

PEI – Polyethyleneimine

PAN – Poly (acrylonitrile)

PCB – Polycarbonate

SWCNTs – Single Walled Carbon Nanotubes

MWCNTs – Multi Walled Carbon Nanotubes

KMnO₄ – Potassium permanganate

H₂SO₄ – Sulphuric acid

CVD – Chemical Vapour Deposition

SiC – Silicon Carbide

PMMA – Poly (methylmethacrylate)

EtONa – Sodium ethoxide

XPS – Xray Photospectroscopy

NMR – Nuclear Magnetic Resonance

FTIR – Fourier Transform Infra-Red

HNO₃ – Nitric acid

KClO₃ - Potassium chlorate

KOH – Potassium hydroxide

ClO₂ - Chlorine dioxide

H₃PO₄ – Phosphoric acid

EDA – Ethylenediamine

TMPyP – Tetrakis (1-methyl-pyridinium-4-yl) porphyrin

AAO – Anodised Aluminium Oxide

APPENDIX B; PERMISSIONS FOR THIRD PARTY COPYRIGHT WORKS

Page No.	Work type	Source	Copyright holder and year	Permission request date	Permission license status
14	Figure	Reference 61	APS Physics, 2009	25/05/2020	Granted
16	Figure	Reference 82	Royal Society of Chemistry, 2015	25/05/2020	Granted
17	Figure	Reference 85	Springer Nature, 2009	25/05/2020	Granted
19	Figure	Reference 106	Scientific.Net, 2009	25/05/2020	Pending
20	Figure	Reference 108	Elsevier, 2018	25/05/2020	Pending
25	Figure	Reference 125	Royal Society of Chemistry, 2012	25/05/2020	Granted
29	Figure	Reference 145	Royal Society of Chemistry, 2012	25/05/2020	Granted
34	Figure	Reference 169	Royal Society of Chemistry, 2015	25/05/2020	Granted
36	Figure	Reference 177	Elsevier, 2017	25/05/2020	Pending
38	Figure	Reference 183	Elsevier, 2018	25/05/2020	Pending
38	Figure	Reference 189	Science AAAS, 2013		Granted
40	Figure	Reference 197	ACS Publications	25/05/2020	Pending
41	Figure	Reference 173	Nature Publishing Group, 2015	25/05/2020	Pending
42	Figure	Reference 50	Nature Publishing Group, 2017	25/05/2020	Pending

APPENDIX C: PUBLISHED PAPERS

Progress in Organic Coatings 137 (2019) 105345



Interfacial crosslinked controlled thickness graphene oxide thin-films through dip-assisted layer-by-layer assembly means

Vepika Kandjou, Miguel Hernaez, Beatriz Acevedo, Sonia Melendi-Espina^{*}

Engineering, Faculty of Science, University of East Anglia (UEA), Norwich, England, UK

ARTICLE INFO

Keywords:
Graphene oxide
Layer-by-layer
Crosslinking
Thin film
Thickness

ABSTRACT

The augmentation of research in graphene based thin films has been of great interest to various current industrial stakeholders. This is mainly due to the wide scope of films applications, ranging from nanoelectronics to separation membranes. Therefore, establishing a relation between graphene based thin film key characteristics and the fabrication operating conditions is of high significance. This study entails the successful fabrication of controlled-thickness crosslinked graphene oxide (GO) thin films on inexpensive silicon-based glass slide substrates. The method of film fabrication used is the dip-assisted layer-by-layer assembly, which has an added advantage of step-control of this film thickness, good film uniformity and continuity. The thickness was primarily tuned through the use different sized crosslinkers; a covalent based sub-nanometer sized p-phenylene-diamine and an electrostatic based polyethyleneimine on an interchangeable assembly with GO. Pvc film fabrication, Fourier Transform Infra-Red and X-Ray Photoelectron Spectroscopy characterizations were carried out to determine the nature of interactions between GO and the crosslinkers. Post film fabrication, scanning electron microscopy, water contact angle measurements and profilometry analysis were undertaken for film continuity, hydrophilicity and thickness measurements respectively. A strong linear trend between film thickness of the differently crosslinked films and the number of bi-layers was established.

1. Introduction

Thin films are of high importance in various applications, these varies from nanoelectronic optical instruments and sensors [1,2] to large scale operations like separation membranes and solar cells [3,4]. The effectiveness, durability and ease of operation of thin films in these various applications are dependent on their thickness, topographical roughness, continuity and homogeneity among other key characteristics [5]. Consequently, controlling the magnitude of these key characteristics is essential in thin film fabrication and operation [6].

From polymers to ceramics different materials have been employed in the fabrication of thin films for different purposes [7]. The recently discovered graphene is a great candidate material for usage as a thin film precursor because of its 2-dimensionality, mechanical strength and electrical properties [7,8]. However, despite its outstanding properties and promise in various applications, the use of graphene as a thin film precursor is limited by the material's lack of production scalability without compromising its structure, morphology and properties [9]. Low solubility of graphene in polar solvents is also a limitation to its usage as it cannot be easily dispersed in polar solvents to dispersions for the fabrication of thin films via solution requiring processes [10–13].

Owing to its ease of fabrication and large scale production scalability, graphene oxide (GO) has caught the attention of many researchers as a reasonable graphene alternative in the fabrication of thin films for various applications [14–20]. The most notable GO production method is the Modified Hummers method, which uses affordable graphite as a precursor raw material [21]. Although its mechanical and electrical properties are not as outstanding as those of graphene, in some applications like sensors and separation membranes the properties of GO are sufficient. This makes it a notable graphene substitute pertaining to these applications [22–27]. Another key advantage of GO is its containment of oxygenated functional groups; the epoxy, hydroxyl and carboxylic groups, which make the material chemically active [28,29]. This means that it can be crosslinked with different molecules and thus improving the continuity of the GO based films via both vertical and horizontal crosslinking [30]. Crosslinking further introduces the ability to control the thickness, roughness and to enhance the stability of the fabricated films [14,15,31].

Elsewhere different attempts to control film thickness and other key characteristics have been employed using various thin film fabrication techniques. For instance Shi-Hongfei et al. used spray coating to control film thickness via different spray volumes [32]. Green and Hersam on

^{*} Corresponding author.

E-mail address: s.melendi-espina@uea.ac.uk (S. Melendi-Espina).

<https://doi.org/10.1016/j.porgcoat.2019.105345>

Received 7 July 2019; Received in revised form 12 September 2019; Accepted 17 September 2019

0300-9440/ © 2019 Elsevier B.V. All rights reserved.

the other hand used solution phase production of graphene films and the thickness was controlled by density differentiation [33]. In this study the dip-assisted layer by layer assembly technique was entailed to ease the control and modification of key thin-film characteristics on a step by step basis.

The aforementioned methods are relatively costly in comparison to the dip-assisted layer-by-layer assembly [34]. The basis of this fabrication method is an interchangeable attachment of two or more materials on a layer-by-layer basis. The attachment can either be predominantly covalent based or electrostatic based depending on the nature and chemistry of the materials being assembled [14,15]. The layer-by-layer technique gives frameworks of controlled thickness through the use of different sized crosslinkers and operating conditions [35]. Specifically, dip-assisted layer-by-layer assembly offers cost effectiveness and ease of scale up to mass production as important advantages. The key operating conditions in dip assisted layer-by-layer assembly are the immersion time, number of assembly cycles together with the immersion and withdrawal speeds [36].

Consequently, this study intended to demonstrate the fabrication of controlled thickness crosslinked GO films on affordable silicon-based glass slides to demonstrate the effectiveness of the dip assisted layer-by-layer assembly in controlled thin film thickness production. As such, two types of crosslinkers, a sub-nanometer sized covalent based *p*-phenylenediamine (PPD) and an electrostatic based polyethyleneimine (PEI) were used with GO. In specificity, this work aimed at evaluating the correlation between immersion times (1 and 5 min), number of bi-layers (1, 5, 10 and 20) significant thin film characteristics like; film thickness, continuity and hydrophilicity.

2. Experimental section

2.1. Materials

GO powder (product code C889/GOB019/Pw2) was purchased from Graphenea Co, Spain. The crosslinkers; PPD powder (99% product code: P6001) and 50% aqueous solution of PEI (product code: 03880) were both purchased from Sigma, Aldrich, UK. The films were fabricated on silicon-based substrates (CAT.NO.7101, 1.0-1.2 mm thick) purchased from Fisher Scientific, UK. 1M of potassium hydroxide (KOH) prepared from KOH powder (product code: P/5640/53) used for substrate pre-treatment was purchased from Fisher Scientific, UK as well.

2.2. Study of interaction between GO and crosslinkers

Prior to thin-film fabrication it was significant to determine the plausibility of GO - crosslinker interaction. The key to this was to firstly verify the presence of notable functional groups in GO and the crosslinkers and secondly to determine predominant interaction nature between GO and each of the crosslinkers.

Following preparation of the 0.5 mg/ml aqueous GO dispersion and 2.0 mg/ml of PPD and PEI aqueous solutions, each crosslinker was separately reacted with GO (1:1 ratio,) for 1 and 5 min. The reaction time was controlled by a pH switch after the designated reaction times through the addition of 99% sulphuric acid (Product code: 07208, Sigma Aldrich, UK), which resulted in the protonation of the reacting entities, hence rendering them unreactive [37,38]. The reacted samples were then centrifuged using a Bio-fuge Primo Heraeus centrifuge for 10 min at 6000 rpm with thorough rinsing through a repetitive replacement of the supernatant with distilled water to remove the unreacted crosslinker and GO excess material.

The four centrifuge residue samples were then collected for Fourier Transform Infra-Red (ATR-FTIR PerkinElmer) and X-Ray Photoelectron Spectroscopy (Kratos Ultra-DLD XPS System (K-Alpha+)) characterizations to verify GO-crosslinker interactions. For XPS characterizations wide-scan spectra in the binding energy range of approximately

0-1000 eV were obtained to identify the elements present on the surfaces of the GO and the reacted entities. Additionally, high resolution spectra were obtained. Five peaks emerged when the C1s peak was curve fitted, corresponding to C graphitic (Binding energy, BE_c = 284.3-284.4 eV), C-O epoxide/CO-H (BE = 285.6-285.7 eV), C=O carbonyl (BE = 286.9-287.0), the band at 288.9 attributed to COOH carboxyl groups as well as the π - π^* shake-up signal (290.8 eV) typical for sp^2 -hybridized carbon. It is worth it to mention that at these binding energies there is an overlap of oxygen and nitrogen functionalities, specifically between C(epoxy) and C=N and among CO and CN= [39-41].

2.3. Thin film fabrication procedure

To fabricate the GO - crosslinked films, the glass slide substrates were pre-treated, first by hydroxylation through immersion in 1 M KOH for 30 min to instigate a negative charge onto the slides through the formation of hydroxyls [42]. This was followed by thorough rinsing with deionized water and drying. The hydroxylated slides were subsequently immersed in a positively charged 2.0 mg/ml aqueous PEI for 5 min in order to instigate a positive charge on the glass slides [43]. The positively charged glass slides were then rinsed in deionized water and then dried before dip-assisted layer-by-layer assembly, which commenced with immersion in the negatively GO dispersion (Fig. 1).

A rotary dip-coater device (Nadetch Innovations, Spain) (ND-R 11/2, S/N: 522016) was used to fabricate the films on an automated interchangeable dipping basis between GO and the crosslinkers (Fig. 1). This process was done with rinsing of the glass slides in deionized water and drying prior to each immersion in either GO or the crosslinker. The dispersion of the GO nanosheets was enhanced by a 2-h pre-fabrication sonication in a bath type sonicator (Ultrawave limited, Hz - (50-60)). The films were fabricated under different dip-coating conditions i.e. 1, 5, 10 and 20 bi-layers and 1- and 5-minutes immersion times (see nomenclature in Table 1). Based on previous experience [15,22], other dip-assisted layer by layer operating conditions like the immersion and withdrawal speeds were kept constant at 2400 mm/min.

2.4. Post film fabrication characterizations

The fabricated film surface coverage and homogeneity were characterised by means of a scanning electron microscope (SEM). The water contact angle measurements were subsequently recorded with a DMC 31BF03 camera and the angles were processed by image j software (1.50i/ Java 1.6.0) (Public Domain, RSD-2). To enhance the reliability of the results, an average of 10 contact angle measurements was taken. Pure water drops were introduced to the films in different positions from two different fabrication sets of the same film type. The thickness of the films on the other hand was evaluated by a Bruker DektakXT Profiling System (Stylus Profiler), Bruker's Vision64 software was then used to analyse the film thickness. Similarly, the reliability of the thickness results was enhanced by taking an average of 10 thickness measurements and noting the standard deviations of each recorded thickness in error bars.

3. Results and discussion

3.1. Nature of interaction between GO and the crosslinkers

Primarily, the nature of interaction between GO and the crosslinkers was determined and confirmed. This was significant as it is a precursor to intra(horizontal) and inter(vertical) sheet crosslinking during film fabrication [30].

The FTIR characterizations confirm the presence of oxygen containing functionalities in GO. For instance, the O-H presence was verified by the absorption band at around 3340 cm^{-1} , while the band at 1726 cm^{-1} is attributed to the CO= stretching of ketone, carboxylic

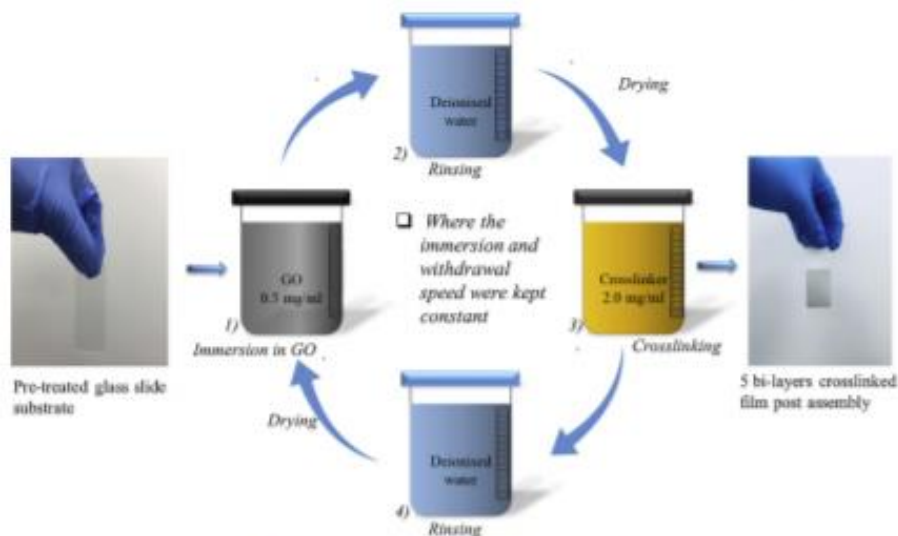


Fig. 1. Dip-assisted layer by layer fabrication technique schematic.

Table 1
Nomenclature of the fabricated films at different immersion times and bi-layers.

Immersion time (min)	Number of bi-layers			
	1	5	10	20
1	GO-X-1'1	GO-X-1'5	GO-X-1'10	GO-X-1'20
5	GO-X-5'1	GO-X-5'5	GO-X-5'10	GO-X-5'20

Key: X = PEI or PPD.

and/or ester groups (Fig. 2). Furthermore, the peak at 1616 cm^{-1} corresponds to $\text{C}=\text{C}$ stretching vibrations and the band at 1060 cm^{-1} can be assigned to C–O (epoxy) groups [44–48].

The most significant functional groups present in the PPD spectrum are related to amine groups. Three bands between $3400\text{--}3000\text{ cm}^{-1}$ indicate the presence of primary amines [45–47]. Additionally, the

spectral bands at 1630 cm^{-1} and 1516 cm^{-1} have been correlated with --NH-- deforming vibrations [52,53]. Finally, the band at 1250 cm^{-1} identifies the occurrence of $\text{C}=\text{N--}$ bonds in aromatic amines [49,54] and the --NH-- wagging vibrations are distinguished by the sharp peak at 832 cm^{-1} [51].

The GO-PPD reacted entities illustrate that the characteristic triplet of primary amines in the $3400\text{--}3000\text{ cm}^{-1}$ region disappears at 1 and 5 min reaction times (Fig. 2) and there is a small but very clear peak at 1510 cm^{-1} assigned to NH-- bend [51,53]. These two facts suggest the existence of secondary amines [51], which consequently points to an epoxy ring opening reaction between GO and PPD at both reaction times [36] (Fig. 3).

The indication of the epoxy ring opening is further supported by the attenuation of the epoxy band at 1060 cm^{-1} (Fig. 2), which is in agreement with the XPS results shown in Table 2, where a reduction in the epoxide proportion of the GO-PPD reacted entities (37% GO vs 26%

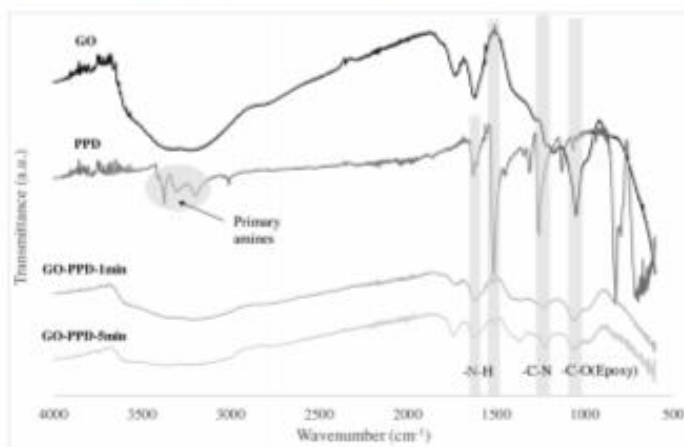


Fig. 2. FTIR characterization spectra for the GO-PPD interactions after 1 and 5 min of reaction and the GO and PPD spectra.

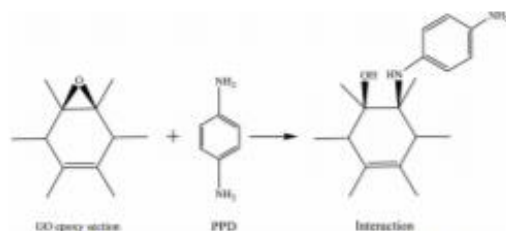


Fig. 3. The epoxy ring opening reaction between PPD and GO.

Table 2
Surface chemistry of GO and GO-crosslinker reacted entities.

	GO	GO-PPD reacted 1 min	GO-PPD reacted 5 min	GO-PEI reacted 1 min	GO-PEI reacted 5 min
C1s (at.%)	71.2	70.1	67.5	67.5	61.9
O1s (at.%)	27.4	27.6	29.9	23.0	26.6
Si1s (at.%)	1.4	1.6	1.6	2.6	3.0
N1s (at.%)	—	0.7	1.0	6.9	8.5
Cap ⁺ + Cap ⁰ (%)	58.5	57.8	51.9	56.2	52.3
C(epoxy)/C-OH/C=N (%)	37.1	26.9	25.7	35.7	35.4
C = O/C-N (%)	1.3	9.3	15.7	2.0	8.0
COOH (%)	3.2	5.0	6.3	4.1	4.1
n-n ⁺ (%)	0.0	1.0	0.4	0.0	0.2

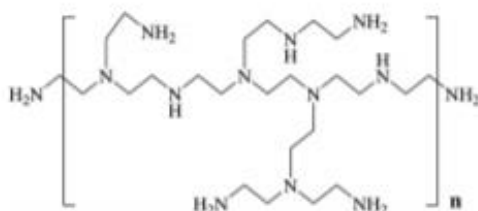


Fig. 4. PEI monomer (branched ethyleneimine).

GO-PPD) is evident. Additionally, the reacted entities show the formation of a -CN band at 1220 cm^{-1} [49,54], which is also reflected in the XPS results, where the C=O/CN- content increases from

1.2% up to 15.7% at 5 min reaction time.

Given the presence of different functional groups it is also most likely that other minor interactions like van der Waals forces and hydrogen bonding are occurring [29]. Structurally, GO, in some areas where the oxygenated functional groups are not present, contains aromatic lattices and since PPD contains a benzene ring another possible interaction between GO and PPD is via the $\pi-\pi$ interactions [55,56].

On the other hand, PEI (Fig. 4) contains a large amount of primary and secondary amine groups as well, which are evident in the region between 3400 cm^{-1} and 2900 cm^{-1} and by the strong NH- band at around 1640 cm^{-1} (Fig. 5) [47,48,53]. The band at 1460 cm^{-1} corresponds to the C-H_2 bending [51] and it can be also detected in the reacted entities (Fig. 5).

In the GO-PEI reacted samples there is no disappearance of the band at 1060 cm^{-1} , hence no indication of the epoxy ring opening reaction (see Fig. 5). This is in accordance with the XPS results (Table 2) that show a constant percentage of epoxy groups regardless the reaction time (37.1% in the GO vs 35.7%–35.4% in the reacted entities). Moreover, pH of GO suspension and PEI solution were 5.2 and 8.3 respectively, at these pH values both compounds have significant ionization and opposite charges [43,57], which supports the claim that their interaction is predominantly an electrostatic based one.

3.2. Film continuity analysis

Very good uniformity and homogeneity across the thin films can be observed in the pictures shown in Fig. 6. The darkening of the glass slides indicates that coating and material assembly increase with the number of bi-layers and the immersion time in both sets. Uniform thickness of the coatings is to an extent confirmed by the homogeneous change in surface colour after all the different number of coating cycles.

As it can be seen in further detail in Fig. 7, excellent continuity coverage is achieved from the very first layer. Some wrinkles can be observed on the surface due to the folding of the GO nanosheets (Fig. 7).

3.3. Thin film hydrophilicity

Hydrophilicity is among the significant thin film characteristics. High film hydrophilicity can be of sentimental value or a limitation depending on the intended application of the fabricated films. For instance in surface coating lower film hydrophilicity is required while in water purification and desalination higher hydrophilicity is preferred

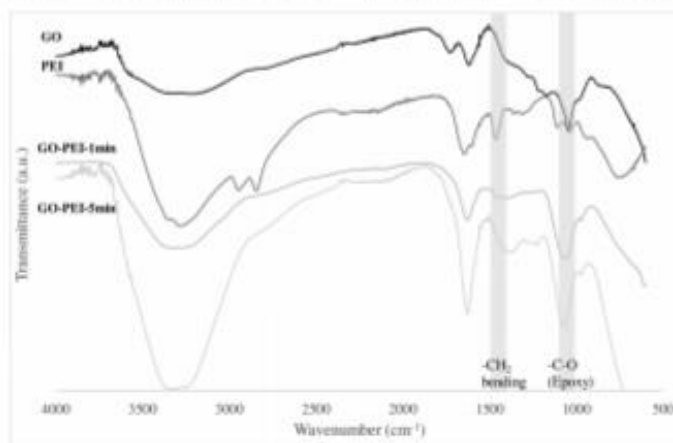


Fig. 5. FTIR characterization spectra for the GO-PEI interactions after 1 and 5 min of reaction and the GO and PEI spectra.

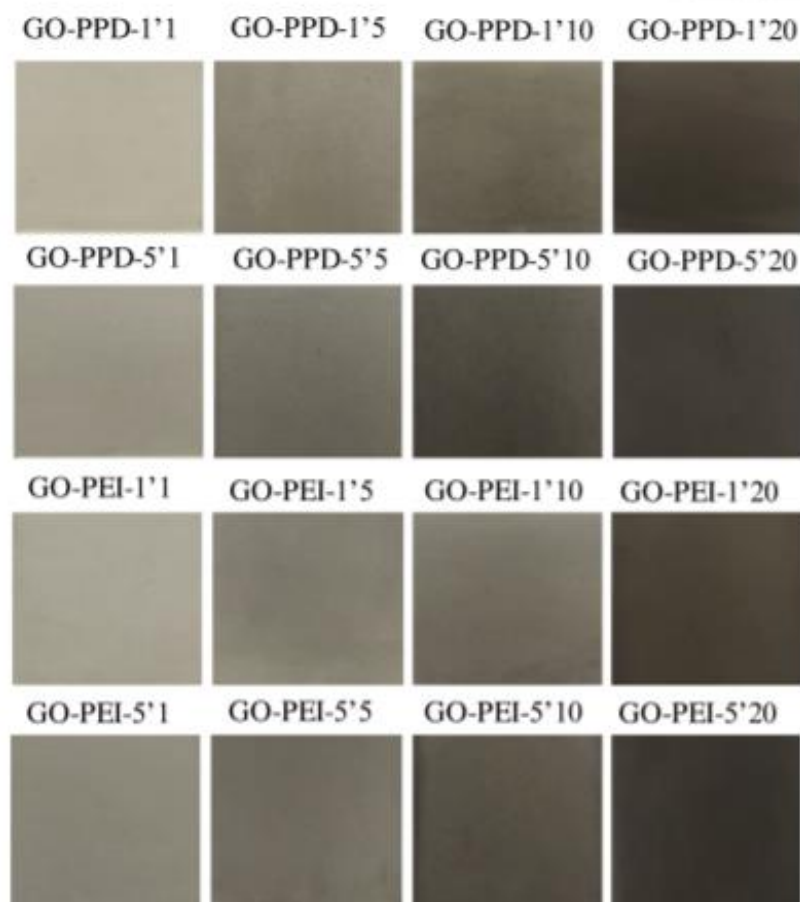


Fig. 6. Camera pictures of the crosslinked thin films.

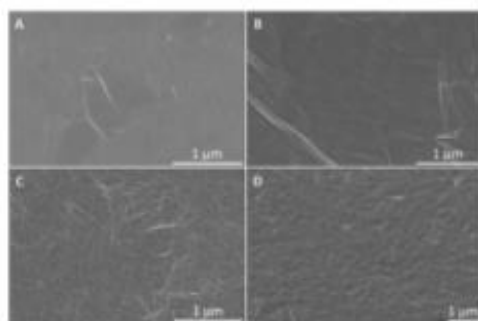


Fig. 7. SEM images of the crosslinked thin films. A) GO-PPD 1'1; B) GO-PPD 1'20; C) GO-PEI 1'1; D) GO-PEI 1'20.

[43,58]. Film hydrophilicity was evaluated by measurements of the water contact angles of the fabricated films (Fig. 8). As aforementioned, 10 measurements in different positions from two differently fabricated

films under the same operating conditions were undertaken and the average contact angle and standard deviations were noted.

The general hydrophilicity trend shows that the water contact angle increases as the number of bi-layers increases. A notable decrease in hydrophilicity is observed from the first bi-layer to the 10th for both crosslinkers and eventually a gradual decrease from the 10th bi-layer to the 20th is observed at both immersion times for both crosslinkers (Fig. 8).

The more hydrophobic nature of the crosslinkers in comparison to GO is the likely cause for the observed decrease in hydrophilicity of the fabricated films as the number of bi-layers and immersion time increases, owing to increased crosslinker accumulation fabrication.

Larger contact angles were recorded for the PPD crosslinked films in comparison to the PEI crosslinked films, which is due to the hydrophobic aromatic ring structure of the PPD monomer [59]. This is in agreement with the recorded magnitudes for the individual compounds ($68.2^\circ \pm 6.8^\circ$ for PPD; $57.3^\circ \pm 4.3^\circ$ for pure PEI) and therefore proving the influence of the characteristics of the crosslinkers onto the overall hydrophilicity of the fabricated films. At 5 min deposition time and 20 bi-layers the contact angles reach the values of the pure crosslinkers or even exceed it in the case of the PEI ($64.2^\circ \pm 9^\circ$ vs $57.3^\circ \pm 4.3^\circ$). This



Fig. 8. Water contact angles for the crosslinked films.

fact could be attributed to the reducing properties of PEI [60].

3.4. Film thickness analysis

The essentiality of ease of control of the thickness of the active layers cannot be understated in optimising device performances.

The thickness characterizations results show a strong linear correlation between film thickness and the respective number of bilayers at each of the immersion times for both sets of crosslinked films (Fig. 9).

It is important to highlight that due to the thin thickness of the 1 bilayer films, especially those deposited at 1 min immersion time, it was necessary to fabricate them on a silicon wafer, as the roughness of the glass slides was overly and therefore it was not possible to have an accurate thickness measure for those specific samples.

Displayed in Fig. 9 are the thickness results of the two sets of crosslinked films at both immersion times and different bilayer cycles. The results are very repeatable and 1 bilayer thin films at 1 min immersion are very close to the resolution of the equipment.

A general linear trend due to the additional material accumulation as the immersion time and the number of bilayers increases is evident. Nevertheless, for the PEI-crosslinked films the thickness magnitude is much higher than that of the PPD thin films (one order of magnitude) as it can be seen in Fig. 9. For instance, the PPD crosslinked films at 1 min immersion time the thickness rises from 3 nm to 21 nm as the number of

bi-layers increases from 1 to 20 bilayers, while it increases from 6 nm to 29 nm when the immersion time is increased to 5 min. These values are relatively close to the theoretical expected step increase of 1.5 nm per bi-layer [58].

On the other hand, PEI crosslinked films thickness increases is from 5 nm to 92 nm (1 min dipping) and from 13.9 nm to 330 nm (5 min immersion time). Theoretically, since PEI is a polymer and therefore with varying chain lengths, the expected step increase for the PEI crosslinked films cannot be predicted with absolute certainty [61]. In both cases however a strong linear progression with the increasing number of bi-layers is observed.

The varying magnitude of increase in film thickness regarding the two crosslinkers is mainly due to the differences in the sizes of the crosslinkers, as PPD is a much smaller molecule while PEI is a bigger polymer with long branched chains and thus resulting in higher thickness as the number of bi-layers increases [61]. This further supports the claim that the thickness of the crosslinked films is majorly due to vertical inter layer crosslinking as evidenced by the fact that the bigger the crosslinker the higher the increase in film thickness magnitude.

The immersion time also has a significant impact on the thickness of the obtained films. In the case of PEI, increasing the immersion time from 1 min to 5 min results in films three times thicker and between 1.5 and 2 times for PPD-crosslinked films. As such, selection of the

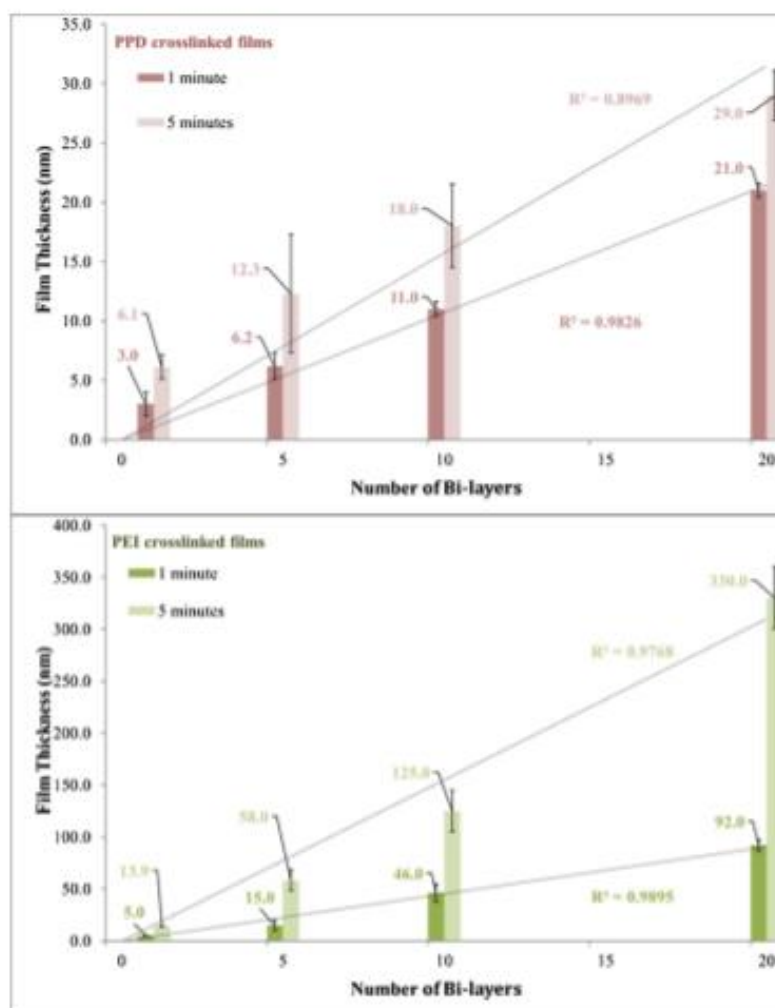


Fig. 9. Thickness measurements of the cross-linked thin films.

interlayer crosslinker and the deposition parameters is key to fine-tuning and modification of the thickness of dip-assisted layer by layer assembled thin films.

The importance of the study is on the fact that the GO films can be easily fine-tuned to specific characteristics required in particular industrial operations. This makes the fabrication process economically efficient and viable. Furthermore, the successful fabrication of the different crosslinked thin films on glass slides highlights that various substrates including porous ones can be employed and as such the films can have different applications ranging from sensors to separation membranes and not solely in lab scale research applications. The study verifies the significance of both inter and intra layer crosslinking in altering the significant properties of GO based thin films. This further opens a possibility for the use of other different sized crosslinkers and polymers in fine tuning significant thin film characteristics via the dip-assisted layer-by-layer-assembly.

4. Conclusions

In summation it was successfully demonstrated that crosslinked GO films with step-controlled thickness and hydrophilicity could be fabricated in a facile manner by means of dip-assisted layer-by-layer assembly. Good film homogeneity was also achieved. The thickness was successfully controlled through the use of different sized crosslinkers and operating conditions of the dip-assisted layer-by-layer method; the immersion time and the number of assembly cycles. It was observed that different crosslinkers have different impact on thickness progression as both the number of bi-layers and immersion time increase. This is advocated to the differences in size and nature of the crosslinkers entailed. Interpolation to fabrication operating conditions to obtain a specific characteristic can be thus be easily carried out.

- [48] J.I. Paredes, S. Villar-Baíl, A. Martínez-Alonso, J.M.D. Tascón, Graphene oxide dispersions in organic solvents *graphene*, *Langmuir* 24 (2008) 10560–10564, <https://doi.org/10.1021/la801744a>.
- [49] X. Li, M. Huang, Y. Yang, Synthesis and Characterization Of O-Phenylene diamine and Xylylene Copolymers 42 (2001).
- [51] N.P.G. Jewson, *Guide to the Complete Interpretation of Infrared Spectra of Organic Structures*, John Wiley and Sons Ltd, Baffins Lane, Chichester, West Sussex, 1994.
- [52] R.A. Heacock, L. Marion, The infrared spectra of secondary amines and their salts, *Can. J. Chem.* 34 (2011) 1782–1795.
- [53] A.P. Cleaves, E.E. Hylar, The infra-red absorption spectrum of Methylamine Vapor, *J. Chem. Phys.* 7 (1939) 563–569.
- [54] R.M. Silverstein, P.X. Webster, D.J. Kimble, *Identification of Organic Compounds (Spectrometric Identification of Organic Compounds*, 4th Ed), 4th ed., Wiley, New York, 1981.
- [55] J. Li, X. Zeng, T. Ren, E. van der Heide, The preparation of graphene oxide and its derivatives and their application in bio-tribological systems, *Lubricants* 2 (2014) 137–161, <https://doi.org/10.3390/lubricants2030137>.
- [56] S. Dai, Z. Xu, M. Zhu, Y. Qian, C. Wang, Detection of *p*-phenylenediamine based on a glassy carbon electrode modified with nitrogen doped graphene, *Int. J. Electrochem. Sci.* 10 (2015) 7063–7072.
- [57] L. Zhao, H. Zhang, N. Flood, D. Hai, J. Hee, Q. Li, H. Sun, P. Li, Preparation of graphene oxide / polyethyleneimine layer-by-layer assembled film for enhanced hydrogen barrier property, *Compos. Part B Eng.* 92 (2016) 252–258, <https://doi.org/10.1016/j.compositesb.2016.02.037>.
- [58] Y. Lee, S.H. Min, M. Gu, Y.K. Jung, W. Lee, J.U. Lee, D.G. Seo, B.S. Kim, Layer-by-Layer assembly for graphene-based multilayer nanocomposites: synthesis and applications, *Chem. Mater.* 27 (2015) 3785–3796, <https://doi.org/10.1021/acs.chemmater.5b00491>.
- [59] W.S. Hwang, C.H. Tsou, M. De Guzman, Q.F. An, Y.L. Liu, Y.M. Zhang, C.C. Hu, K.R. Lee, J.Y. Lai, Cross-linking with diamine monomers to prepare composite graphene oxide-framework membranes with varying d-spacing, *Chem. Mater.* 26 (2014) 2983–2990, <https://doi.org/10.1021/cm500787z>.
- [60] H. Liu, K. Tapan, N.H. Kim, B.-C. Koo, J.H. Lee, In situ synthesis of the reduced graphene oxide-polyethyleneimine composite and its gas barrier properties, *J. Mater. Chem. A* 1 (2013) 3739–3746, <https://doi.org/10.1039/C3TA01128J>.
- [61] C.N. Lange, M.V. Druão, M.V. Pires, I.P. Grudziński, Linear and branched PEIs (Polyethyleneimines) and their property space, *Int. J. Mol. Sci.* 17 (2016), <https://doi.org/10.3390/ijms17040955>.



Contents lists available at ScienceDirect

Journal of Hazardous Materials

journal homepage: www.elsevier.com/locate/jhazmat

Enhanced covalent p-phenylenediamine crosslinked graphene oxide membranes: Towards superior contaminant removal from wastewaters and improved membrane reusability

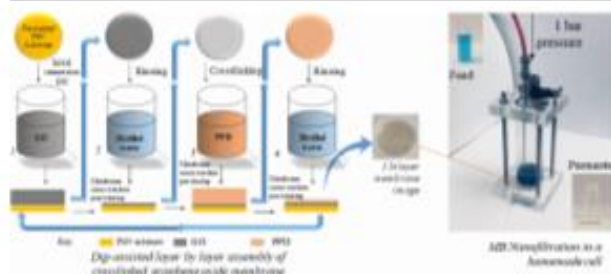


Vepika Kandjou^a, Ana M. Perez-Mas^a, B. Acevedo^a, M. Hernaez^a, Andrew G. Mayes^b, Sonia Melendi-Espina^{a,*}

^a Engineering Faculty of Science, University of East Anglia, Norwich, UK

^b School of Chemistry, Faculty of Science, University of East Anglia, Norwich, UK

GRAPHICAL ABSTRACT



ARTICLE INFO

Keywords:

Graphene oxide
Dip coating
Layer-by-layer
Crosslinker
Rejection
Methylene blue

ABSTRACT

The increasing depletion of freshwater necessitates the re-use and purification of wastewaters. Among the existing separation membrane materials, graphene oxide (GO) is a promising candidate, owing to its tunable physicochemical properties. However, the widening of GO membranes pore gap in aqueous environments is a major limitation. Crosslinking agents can be incorporated to alleviate this problem. This study describes a comparative analysis of uncrosslinked and p-Phenylenediamine (PPD) crosslinked GO membranes' water purification performance. Dip-coating and dip-assisted layer-by-layer methods were used to fabricate the uncrosslinked and crosslinked membranes respectively. The covalent interaction between GO and PPD was confirmed by Fourier Transform Infra-Red and X-ray Photoelectron Spectroscopy. The excellent membrane topographical continuity and intactness was assessed by means of Scanning Electron Microscopy, while water contact angle measurements were undertaken to evaluate and confirm membrane hydrophilicity. The improvement impact of the crosslinker was manifested on the enhancement of the stability and performance of the membranes during nanofiltration tests of aqueous solutions of methylene blue in a homemade nanofiltration cell operated at 1 bar.

* Corresponding author.

E-mail address: s.melendi-espina@uea.ac.uk (S. Melendi-Espina).

<https://doi.org/10.1016/j.jhazmat.2019.120840>

Received 13 February 2019; Received in revised form 1 May 2019; Accepted 26 June 2019

Available online 28 June 2019

0304-3894/ © 2019 Elsevier B.V. All rights reserved.

1. Introduction

The modern world is currently facing an impending global water crisis, which is fueled by the changing climate, global population increase and the depletion of underground water aquifers [1]. The World Health Organization highlighted that 1.1 billion people lack access to improved drinking water supply [2]. This evidently calls for the re-use of both domestic and industrial waters via improved purification methods and durable materials. From adsorption, distillation to nanofiltration, different water purification methods have been deployed depending on the nature and size of the particulates being separated [3–5]. Among these different purification methods, nanofiltration offers an advantage of having high rejection rates for smaller sized particulates at high flux rates and lower energy consumption relative to energy intensive separation techniques like reverse osmosis [6]. Conventional polymers like polyamide, polysulfone and poly(ethersulfone) are amongst the most used membranes materials in nanofiltration, but the lack of resistance to corrosion and durability of the membranes is a major limitation [7]. Membrane susceptibility to fouling, which shortens their lifespan, has also been a major limitation to most separation membrane materials [8].

Carbon materials have attracted much attention as potential candidates to overcome these issues. Carbon nanotubes (CNTs) have been explored in nanofiltration and their intrinsic mechanical stability and flexibility suggest that they should be ideal nanofiltration membrane materials [9]. Majumder et al. reported a high water flux of several orders higher than the predicted hydrodynamic flow using CNTs [10]. However, their relatively high cost, complexity in fabricating vertically aligned CNTs and large-scale production challenges mean that the use of CNTs in nanofiltration is not feasible now [11,12].

Graphene, with its high mechanical strength evidenced by a Young's modulus of 1 TPa, 2-dimensionality, high specific surface area and insusceptibility to fouling, is an ideal next generation nanofiltration membrane material [13–15]. Although it is a model membrane material due to its outstanding properties, scaling up the production of a defect free, one atom thick large area graphene is extremely challenging [16,17]. Furthermore, scalable formation of sub-nanometer pores on pristine graphene membrane for nanofiltration is a cost-intensive process [18–20].

Fortunately, GO, a derivative of graphene with protruding oxygenated functional groups, has emerged as a reasonable graphene substitute pertaining to separation membrane applications [21,22]. Initial experiments by Nair et al. have paved a way for the use of GO as a separation membrane precursor in water purification [23]. GO can be fabricated cost effectively and therefore can be easily up-scaled to mass production [24,25]. Furthermore, its possession of oxygenated functional groups enhances its hydrophilicity, limiting membranes' fouling susceptibility [26–29]. This further adds to the materials' chemical activity the ability to be covalently interconnected to molecular compounds which further enhances the properties of fabricated hybrid GO membranes [30–32].

The major drawback to the use of solely GO in membrane separation is the lack of membrane stability during nanofiltration [33]. It has been discovered that GO membranes tend to swell during water purification [33,34]. This is mostly advocated to the enlargement of the interlayer gap because of the accumulation of water molecules onto the oxygenated functional groups, consequently leading to reduced membrane rejection over time [22]. Several attempts have been made to try to alleviate this major problem. For instance, Abraham et al. used an epoxy encapsulate to physically confine the pore gap of GO membranes [35]. The major limitation to the physical confinement method employed is that scale-up for production of such membranes is a great challenge [35]. Zhang et al. explored covalent crosslinking of GO membranes using ethylenediamine as a crosslinker and the vacuum filtration fabrication method [36]. However, higher GO loading is used and difficulty in controlling membrane thickness relative to layer-by-

layer assembly is a limitation for the vacuum filtration method [37]. Elsewhere, attempts to fabricate nanofiltration layer-by-layer assembled membranes have been made [38–40], however, a comparative investigation of the impact of multilayers of sub-nanometer sized covalent based crosslinked GO membranes via dip-assisted layer-by-layer assembly has not been explored to the authors current knowledge.

Consequently, this study aimed at the enhancement of membrane stability and separation abilities of GO membranes through the introduction of a small, subnanometer-sized covalent crosslinker, on a dip-assisted layer-by-layer basis. This should bond adjacent layers of GO plates together, thus stabilizing the structure during membrane operation. Two sets of GO based membranes were fabricated, uncrosslinked and crosslinked with *p*-phenylenediamine (PPD). Dip coating method for the uncrosslinked membranes and dip-assisted layer by layer assembly were the fabrication methods explored for the crosslinked membranes in this study.

The explored membrane fabrication methods offer an added advantage of fabrication of continuous membranes with controlled thickness and low material load [38–40]. Simplicity in operation, together with cost effectiveness are also key benefits of these fabrication methods [40]. The fabrication methods, especially dip-assisted layer-by-layer, offers firmer interconnection between the GO and crosslinker layers, thus avoiding the swelling and enlargement of GO interflake gaps that is a common problem for GO membranes in aqueous environments [37].

The study also addressed the influence of number of layers and bi-layers on the water purification capabilities of the membranes.

2. Materials and methods

2.1. Materials

GO powder was purchased from Graphenea (Spain). The membranes were supported by poly(acrylonitrile) (PAN) filter substrates with 0.2 μm pore size and 47 mm diameter from Sterlitech Corporation (USA).

The crosslinker, *p*-phenylenediamine (PPD, product code P6001), polyethyleneimine (PEI, product code 03,880), potassium hydroxide powder (KOH) and methylene blue (MB, product code M9140) were all purchased from Sigma Aldrich (UK). A bath type sonicator (Fisherbrand FB1505, Elmasonic S30 H) enhanced the dispersion of the GO water suspensions and the membranes were fabricated with a rotary dip-coater device (Nadotech Innovations, Spain).

2.2. Crosslinked and uncrosslinked membrane fabrication

2.2.1. Pre-treatment of poly (acrylonitrile) (PAN) substrates

The 0.2 μm pore sized fibrous PAN substrates were first hydroxylated via immersion in 1 M KOH for 30 min at 70°C. This was done to enhance a negative charge via the conversion of the nitriles in the PAN substrates to carboxylic groups [39,41,42]. Subsequently, the substrates were rinsed with distilled water and dried prior to immersion in a positively charged 2.0 mg/ml PEI solution for 5 min. PEI conferred a positive charge onto the hydroxylated PAN substrates [42]. The positively charged substrates were then rinsed in distilled water to remove excess unattached PEI and then dried prior to membrane fabrication.

2.2.2. Dip-coating and dip-assisted layer-by-layer assembly

Prior to membrane fabrication, 0.5 mg/ml of GO aqueous dispersion was prepared and sonicated for 2 h to enhance the individuality and dispersion of the GO sheets in water. To analyse the impact of the crosslinker on the performance and stability of the GO membrane, two types of membranes were fabricated. One was the uncrosslinked GO membranes, fabricated via dip-coating method where, following pre-treatment, the PAN substrates were immersed in 0.5 mg/ml GO dispersion solution in a vertical orientation with rinsing and drying

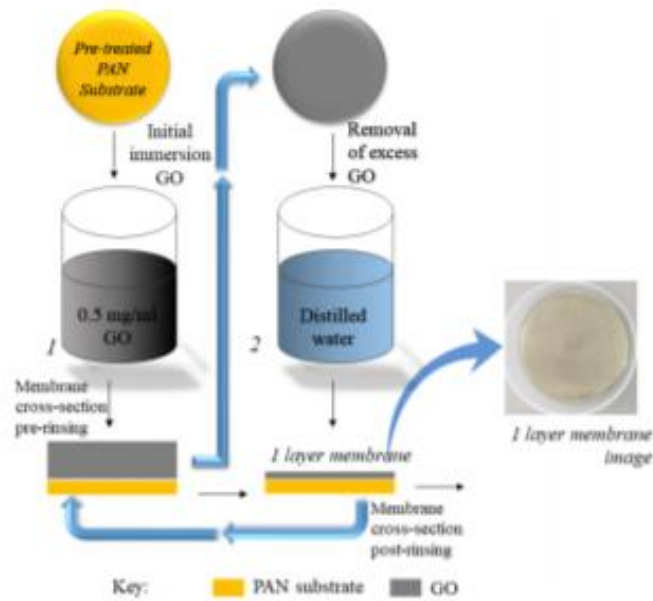


Fig. 1. Dip-coating schematic (fabrication of uncrosslinked membranes).

between cycles (Fig. 1). This was done using 5 min immersion time and membranes with 1 and 5 assembly cycles were fabricated.

In the crosslinked membranes, PPD was introduced onto the membranes via dip-assisted layer-by-layer assembly. This was done on an alternating basis with GO, with rinsing and drying after each immersion in GO or PPD (Fig. 2). The main basis of this layer-by-layer fabrication was an epoxy ring opening reaction between the amines in PPD and the epoxy group in GO (Fig. 3) [31,43], where a hydroxyl group and a secondary amine are generated. This leaves the other amine group in PPD to interconnect with a subsequent GO sheet in the next assembly.

Subsequently, 1 and 5 bi-layers were assembled using 5 min immersion time.

2.3. GO and PPD covalent bonding

A crucial step in this study was to verify the GO-PPD covalent bonding via a chemical reaction at the designated reaction time. Following the preparation of a 0.5 mg/ml of aqueous GO suspension and 2.0 mg/ml of aqueous PPD solution, both were reacted for 5 min (which was the membrane fabrication immersion time). The reaction time was controlled by a pH switch through the addition of 97% purity sulphuric acid (H_2SO_4 , Sigma Aldrich, product code: 07,208) to the reacting mixture, which resulted in the protonation of the reacting entities and hence rendering them unreactive after the addition of the acid [44–46]. The reacted entities were then centrifuged (Bio-Fuge

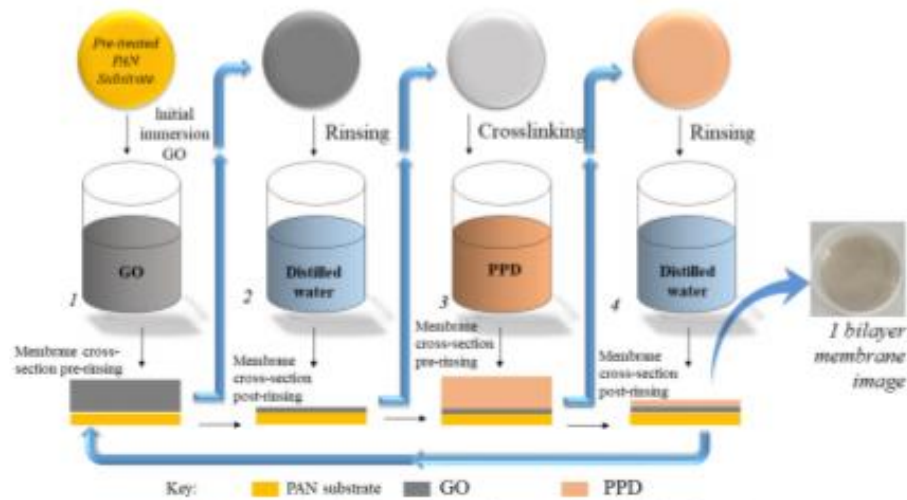


Fig. 2. Dip-assisted layer-by-layer schematic (fabrication of crosslinked membranes).

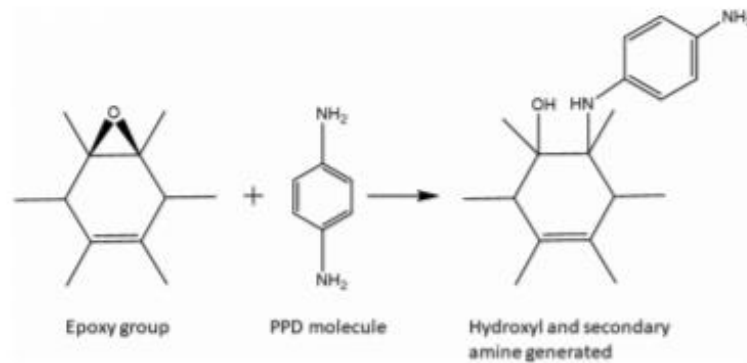


Fig. 3. Epoxy ring opening reaction between GO and PPD.

Primo Heraeus Centrifuge) at 1000 rpm for 10 min to collect the centrifuge residue for FTIR and XPS characterizations. The centrifugation was done with rinsing three times with distilled water to remove the excess unreacted entities.

The presence of notable functional groups in GO, PPD and reacted entity were determined by FTIR and XPS. An attenuated total reflectance unit (ATR) equipped PerkinElmer Spectrometer was used for the FTIR analysis while a Kratos Ultra-DLD XPS System (K-Alpha⁺) was used for the XPS characterizations.

2.4. Contact angle measurements

As it proved impossible to measure the water contact angles on hydrophilic porous PAN substrates due to permeation of pure water through the membranes, uncrosslinked and crosslinked films were similarly fabricated on non-porous silicon-based glass slide substrates to measure the relative water contact angles of the thin films. This was similarly done at 5 min immersion time and 1 and 5 layers and bilayers.

To enhance the reliability of the results, an average of 8 contact angle measurements was taken, noting down the standard deviation in error bars. Several pure water drops were introduced to the films in different positions from two different fabrication sets of the same film type.

The water contact angle measurements were subsequently recorded with a DMK 318F03 camera and the angles were processed by image j software (1.50i/Java 1.6.0) (Public Domain, BSD-2).

2.5. Membrane performance tests

2.5.1. Nanofiltration setup

Following the fabrication of both crosslinked and uncrosslinked membranes, the membrane performance was evaluated with a 10 mg/l aqueous solution of MB. The tests were carried out at room temperature in a 330 cm³ dead end homemade filtration cell constructed from poly (methyl methacrylate) (Fig. 4), where the membrane was supported by a porous sintered polyethylene disc with an effective area of 13.20 cm² and an operation pressure of 1 bar. The cell was sealed with neoprene gaskets.

To enhance the reliability of the results, three membranes of the same type were fabricated and subsequent standard deviation of the nanofiltration results were noted for both the flux and rejection results.

The overall membrane performance was determined through calculation of the permeation flux (F) across the membrane. This was determined from the total permeate volume collected (V) per unit time (t) and membrane effective area (A) (Eq 1).

$$F = V/(At) \text{ Eq (1)}$$

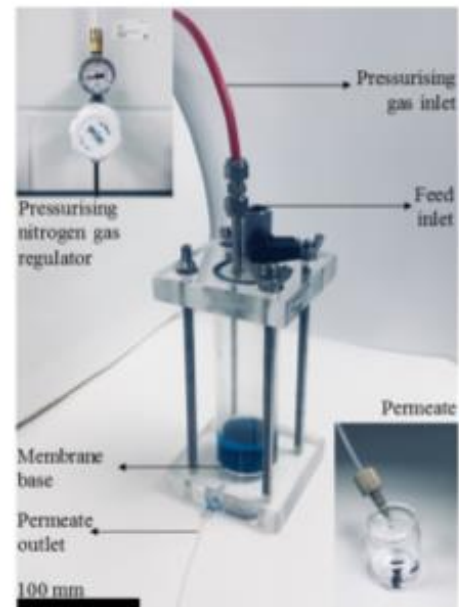


Fig. 4. Homemade nanofiltration cell unit in operation.

2.5.2. Methylene blue calibration line

The membrane rejection, on the other hand, was determined by UV-vis characterization of the permeate solutions relative to the feed solution. A calibration line relating MB concentrations with absorbance was then established (Eq. 2) in order to have a concentration based MB rejection, as follows:

$$\text{Absorbance (a.u)} = 0.1897 \text{ MB concentration (mg/l)} \quad (2)$$

$$R^2 = 0.9971$$

Percentage rejection [R (%)] was then calculated using Eq. (3). Where C_p is the permeate concentration and C_f the feed concentration.

$$R(\%) = \left(1 - \frac{C_p}{C_f}\right) 100 \quad (3)$$

2.6. Continuity of uncrosslinked and crosslinked membranes

The surface coverage and continuity of the fabricated membranes was analysed by a JEOL JSM – 5900 Scanning Electron Microscope, before and after the nanofiltration experiments. Prior to characterization, the membranes were coated with gold using a CC7640 Quorum Technologies Gold Coater.

3. Results and discussions

3.1. Proof of covalent bonding between GO and PPD

The significance of the FTIR characterizations was to verify the presence of the notable functional groups in the reacting entity, these being the epoxide in GO and the amine groups in PPD. These are essential for covalent crosslinking of both via an epoxy ring opening reaction as stated previously. A covalent –C–N– bond between GO and PPD is expected following an epoxy ring opening reaction [47,48].

The loss of the doublet band near 3400 cm^{-1} in the PPD spectrum is evidence for the interconnection of the PPD and GO where the primary amine (1°) in PPD converted to a secondary amine (2°) [47] and a new C–N bond was formed and it is assigned by the stretch at around 1250 cm^{-1} [49] (Fig. 5). The IR spectra also show a small but distinct band at around 1500 cm^{-1} , corresponding with N–H bend [50]. This is present in the reference PPD spectrum (very strong) and it is clearly visible in the reacted entity. However, it is notably absent in the GO spectrum. The appearance of this band corresponds with an evident reduction in the signal at 1060 cm^{-1} , which can be attributable to epoxy C–O bonds [43,51,52]. This is in agreement with the XPS results, which show a clear decrease of C(epoxy) (Table 1).

Wide-scan spectra in the binding energy range of approximately 0–1000 eV were obtained to identify the elements present on the surfaces of the GO and the GO-PPD reacted entity to further support the covalent cross-linking.

High resolution spectra were obtained and the carbon and nitrogen spectra were fitted. Five peaks emerged at different binding energies (BE) when the C1 s peak was curve fitted, which correspond to C graphitic (BE = 284.3–284.4 eV), C–O in the epoxy bond (BE = 285.6–285.7 eV), C=O in the carbonyl bond (BE = 286.9–287.0), the peak at around 288.9 assigned to the carboxyl bond as well as the $\pi\text{-}\pi^*$ shake-up signal (290.8 eV) typical for sp^2 -hybridized carbon. The N(1 s) peak was also curve-fitted, emerging five peaks, assigned to N6 from N-pyridine like structures (BE = 398.8–

Table 1

Surface chemistry of GO and GO-PPD reacted entity.

	GO	GO-PPD reacted 5 min
C 1 s (at.%)	71.2	67.5
O 1 s (at.%)	27.4	29.9
S 1 s (at.%)	1.3	1.6
N 1 s (at.%)	—	1.0
Cp2 (%)	54.8	45.7
Cp3 (%)	3.7	6.2
C(epoxy) (%)	37.1	25.7
C = O (%)	1.2	15.7
COOH (%)	3.2	6.3
$\pi\text{-}\pi^*$ (%)	0.0	0.5
N6 (%)	—	17.6
NC (%)	—	26.4
N5 (%)	—	6.7
NQ (%)	—	39.0
N-X (%)	—	10.3

398.4 eV), NC from amides/amines or lactams (BE = 399.9–399.5 eV), N5 from N-pyrrolic (BE = 400.6–400.0 eV), NQ from N-quaternary (BE = 401.8–400.9) and the peak at around 405–402 eV assigned to the nitrogen oxides as Pyridine N-Oxide (N-X).

XPS characterizations show a small introduction of nitrogen into material that is completely absent in the starting GO (Table 1). Of this nitrogen, significant signal corresponds to amines/amides. In this case, it relates with the presence of secondary amines due to the epoxy ring opening. Formation of amides is heavily disfavored under the aqueous reaction conditions used, since it is a condensation reaction. Normally acid activation chemistry is required (e.g. as acid chlorides, active esters or similar) to achieve such reactions and even then there is a competitive reaction with water as active nucleophile. Unlike the amide formation reaction, nucleophilic attack of epoxy groups to generate secondary amines is a reaction that readily occurs under mild aqueous conditions. Indeed, such reactions are routinely used to couple proteins to epoxy-activated polymeric supports for instance. Additionally, if this nitrogen corresponded to amides, there would be a concomitant reduction in COOH signal, but this is the opposite of what the XPS indicates, showing significant increase in COOH.

Of the N present, a large proportion is quaternized/charged. This can be explained through the acid treatment of the material to stop the reaction, which would leave secondary amines charged, but would have no effect on any amides present, since they do not ionize under these conditions. This is a further evidence of amine formation.

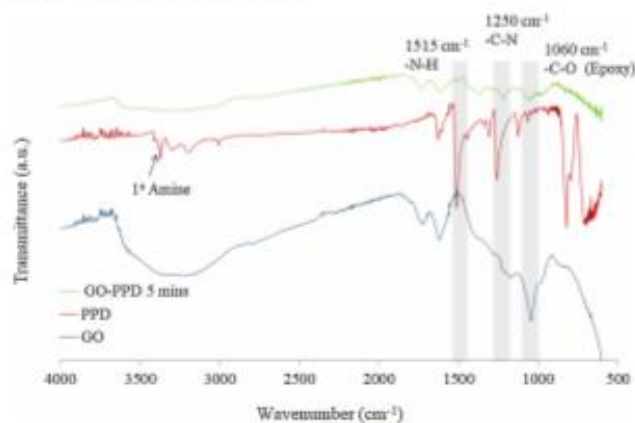


Fig. 5. FTIR characterization of GO, PPD and GO-PPD reacted entity.

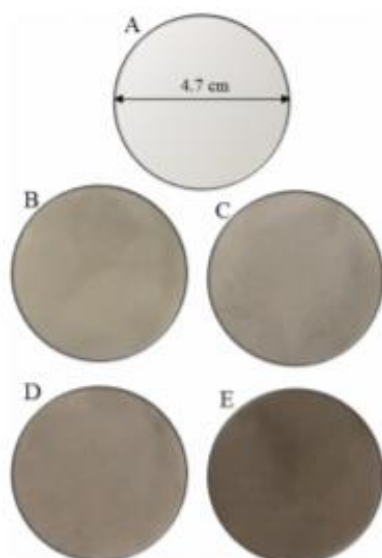


Fig. 6. Photographic images of the fabricated membranes (pre-nanofiltration). A: Uncoated PAN substrate; B: Uncrosslinked membrane 1 bilayer; C: Crosslinked membrane 1 bilayer; D: Uncrosslinked membrane 5 layers; E: Crosslinked membranes 5 bilayers.

3.2. Membrane continuity analysis

The uniformity of coverage of the fabricated membranes is necessary to prove successful membrane fabrication onto the PAN support substrates. To an extent, the characterizations were carried out to give detailed information on the stability and intactness of the fabricated membranes, both before and after nanofiltration tests (the latter shown in Fig. 12, after performing the rejection analysis).

Fig. 6 shows that there is good coverage for both membrane types from the very first bi-layer. This can be seen further in detail in the subsequent SEM images shown in Fig. 7. The membrane coverage increases, as the number of assembly cycles increases from 1 cycle to 5 cycles for both crosslinked and uncrosslinked membranes. This is because of the increase in material accumulation as the number of assembly cycles increases [47]. The coverage is significant for the closing of the fibrous pore gaps in the plain PAN substrates as this gives a good sieving potential for the separation performance of the fabricated membranes [39,53]. The ability to enhance proper membrane pore size is therefore dependent on the number of dip coating and dip-assisted layer by layer assembly cycles in this regard [54].

3.3. Hydrophilicity analysis

The hydrophilicity of the membranes is a significant characteristic in water purification since the more hydrophilic the membranes are, the less they are susceptible to fouling [27]. Relatively, the crosslinked membranes have lower hydrophilicity compared to the uncrosslinked ones. This is due to the hydrophobic nature of the PPD crosslinker [55,56]. For the crosslinked membranes, the water contact angle increased from 53.2° to 59.7° with an increase in the number of bi-layers (Fig. 8) owing to bigger accumulation of the hydrophobic crosslinker. However, a decrease in the contact angle for the uncrosslinked membranes from 39.2° to 35.2° was observed as the number of layers increased from 1 to 5 due to increased accumulation of the hydrophilic GO. Overall, both crosslinked and uncrosslinked membranes are

relatively very hydrophilic as they show low water contact angles and ease permeation of water [57].

3.4. Membrane performance results analysis

3.4.1. Rejection analysis

The fabricated membranes were tested in a lab-scale nanofiltration device to study their performance on the removal of MB. Permeates after passing through each fabricated membrane are displayed in Fig. 9, where the decrease in coloration, which symbolizes the removal of MB, is evident.

Across the two membrane types, MB rejection increases with the assembly cycles (Fig. 10). The average MB rejection increased from 20.4% to 99.8% for the crosslinked membranes as the number of bi-layers increased from 1 to 5. Comparatively, the uncrosslinked membranes showed a similar trend, as the GO layers increased from 1 to 5 the rejection increased from 5.1% to 87.4%. It is also evident that the performance of the membranes improved with the addition of the crosslinker. This is indirect evidence that the crosslinker holds the GO nanosheets together through the -C-N- covalent bonds [58] and thus maintains the pore gap in the sub-nanometer range even when wetting occurs.

3.4.2. Flux analysis

The flux decreases as the number of assembly cycles increases for both crosslinked and uncrosslinked membranes (Fig. 11). A sharp decrease in flux from the plain PAN to the coated membranes is observed. This is evidence for substrate pore size reduction via GO coverage. Crosslinking also results in decrease in flux, as for similar number of assembly cycles the crosslinked membranes display a lower flux in comparison with the uncrosslinked ones. For instance, 1 layer of uncrosslinked GO on the membrane had a flux of 18.7 L m⁻² h⁻¹ while it was 6.2 L m⁻² h⁻¹ for the crosslinked one. However, at larger assembly cycles a smaller decrease in flux of only 0.2 L m⁻² h⁻¹ was observed (2.0 vs 1.8 L m⁻² h⁻¹).

The decrease in flux with the number of assembly cycles is hypothesized to be due to the increase in membrane compactness due to material accumulation. The lengthening of the tortuous path as the number of assembly cycles increases is also significant for the reduction in permeation flux [37]. A likely factor for the observed flux difference between crosslinked and uncrosslinked membranes is that crosslinking maintains a smaller pore-gap, hence the lower flux, while for the uncrosslinked membranes, wetting resulted in enlarged membrane pores and therefore increased flux [33].

Elsewhere, lower fluxes at 10 times higher operation pressure than the one used in this study have been reported; for instance, Aba et al reported a lower flux in the range of 0.58 to 0.60 L m⁻² h⁻¹ on the separation of organic dyes at an operation pressure of 10 bars [59]. Thus given the lower pressure of only 1 bar used and the relatively high flux achieved in this study, the significance of the results of this study is apparent.

The molecular size of an individual MB (anhydrous basis) molecule is about 1 nm (13.84 Å) [60,61]. It is smaller than most textile dyes like remazol yellow [60,62]. These are therefore significant results for the separation of almost all textile dyes and they can be refined further to separate even smaller entities including divalent salts. The ease of fabrication of the membranes, very low GO loading, cost effectiveness and their stability is a step forward in the purification of dye contaminated waters.

3.5. Membrane separation mechanism, operation longevity and reusability

To understand the separation mechanism and operation longevity of the fabricated membranes, the overtime separation of the best performing membrane (PPD crosslinked 5 bi-layers) was analyzed. Continuous operation of the membrane for more than 120 h at 1 bar

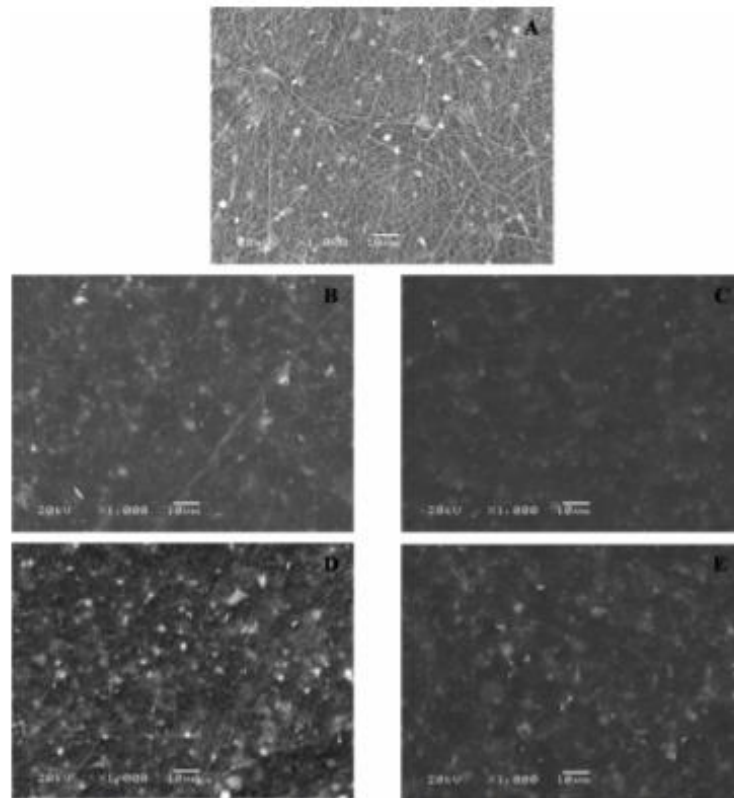


Fig. 7. SEM images of the fabricated membranes (pre-nanofiltration). A: Uncoated PAN substrate; B: Uncrosslinked membrane 1 layer; C: Crosslinked membrane 1 bilayer; D: Uncrosslinked membrane 5 layers; E: Crosslinked membranes 5 bilayers.

showed no decrease in membrane selective separation abilities, however the flux across the membrane considerably diminishes over time (Table 2). The maintenance of a constant rejection throughout the experiment leads to the conclusion that the mechanism at hand is mainly

a selective permeation based separation instead of a selective binding based separation [63-67].

The separation mechanism was further evaluated increasing the feed concentration to 125 and 250 mg/l and it was observed that the

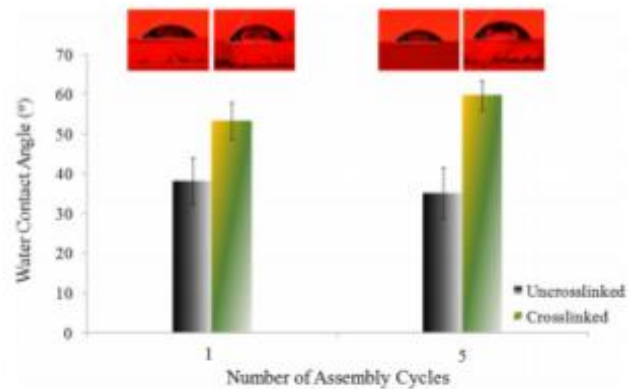


Fig. 8. Water contact angles of the fabricated coatings.

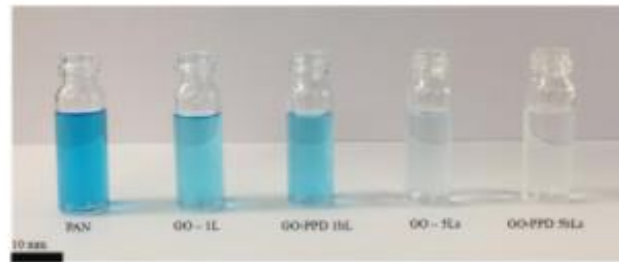


Fig. 9. Nanofiltration permeates of each membrane.

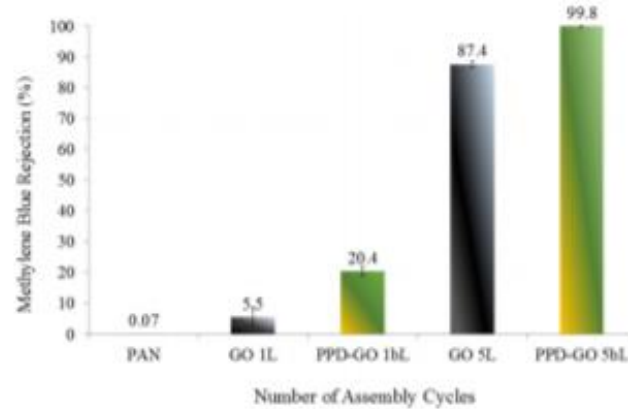


Fig. 10. MB Rejection with respect to increase in the number of layers and bi-layers including plain PAN substrate.

permeation flux at the high feed concentration decreases drastically at prolonged membrane operation and as the feed concentration increases (Table 3). This might be attributable to the increased initial adsorption of MB onto the GO membranes via electrostatic attractions between the negatively charged oxygenated functional groups in GO and the positively charged nitrogen containing groups in MB [68]. However, the level of carboxylate functional groups in GO is relatively low, so

saturation of these sites would occur quite rapidly, even at low MB concentrations. Very importantly, the presence of aromatic rings in GO and PPD from the membrane and MB also gives rise to $\pi-\pi$ interactions, which are likely to enhance the adsorption of MB onto the membranes in the initial operation stages of the permeation tests [69–72]. Such interactions are strong under aqueous conditions. This in turn narrows the permeation path significantly and thus resulting in a

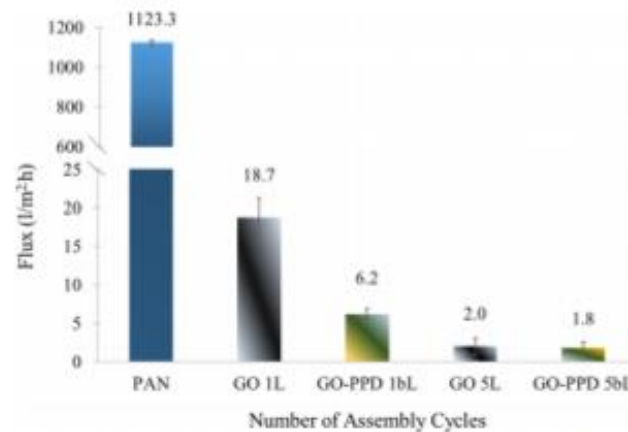


Fig. 11. Permeation flux with respect to increase in the number of layers and bi-layers including plain PAN substrate.

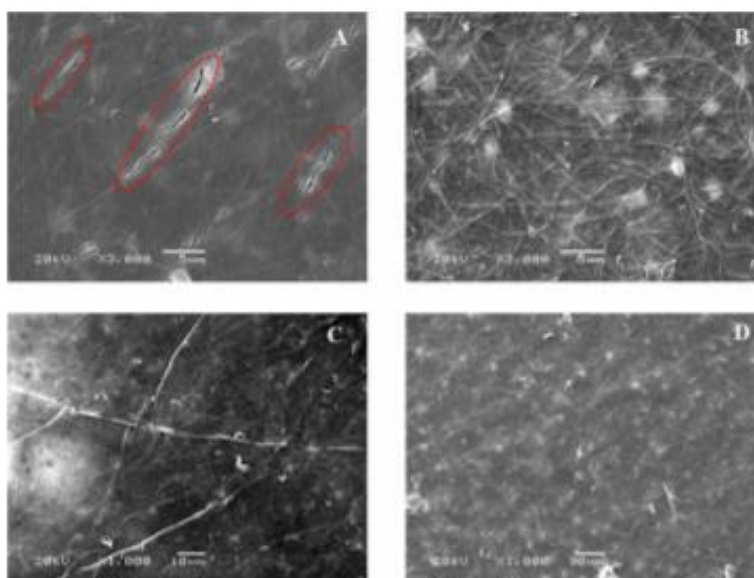


Fig. 12. SEM images of the fabricated membranes (post-nanofiltration). A: Uncrosslinked membrane 1 layer; B: Crosslinked membrane 1 bilayer; C: Uncrosslinked membrane 5 layers; D: Crosslinked membrane 5 bilayers.

Table 2
Membrane separation rejection for the 5 bi-layers crosslinked membrane at prolonged operation hours (working pressure 1 bar) and 10 mg/l MB.

Operation time (h)	MB rejection (%)	Permeation flux ($Lm^{-2} h^{-1}$)
10	99.8	1.81
20	100	1.47
45	100	0.85
70	100	0.63
108	100	0.41
121	100	0.36

Table 3
Relation between increasing feed concentration and membrane performance at lower and higher operation times (5 bi-layers crosslinked membrane).

Feed concentration (mg/l)	MB rejection (%) after		Permeation flux ($Lm^{-2} h^{-1}$) after	
	3 h	20 h	3 h	20 h
10	99.8	100	1.81	1.47
125	98.3	100	0.81	0.43
250	96.7	98.1	0.23	0.07

decreased flux across the membrane and high MB rejection at prolonged membrane operation.

The reusability of the membranes was achieved in a facile manner through the rinsing of the 5 bilayers crosslinked membrane after operation in a 15% (v/v) ethanol aqueous solution for 15 min. This resulted in the removal of attached MB giving the membranes good operation efficiency post initial use and confirming that MB was adsorbed onto the membrane. It was found out that the nanofiltration performance of the membranes post membrane rinsing was recovered almost to the initial performance, accomplishing a flux of $1.74 Lm^{-2} h^{-1}$ (Initial flux = $1.81 Lm^{-2} h^{-1}$) and a rejection of 99.2%. Five cycles of post clogging rinsing of the membranes were performed so the values provided are the average of all the series. Given the more than 120 h

operation longevity of the membranes per cycle before complete clogging and the excellent performance recovery, authors believe that the longevity and reusability of the membranes is thus highly feasible.

The longevity of the membranes paves a way for the implementation of these membranes in water purification. This modification of GO via crosslinking offers a myriad of opportunities for the use of these membrane in other separations. Potentially, this makes GO membranes potential alternatives to the current commercial thin-film membranes like polyamide taking into account the low pressure used in this study.

3.6. Membrane stability

Stability is also a significant membrane characteristic as it governs the re-usability and longevity of the membranes. For that reason, to investigate the integrity of the fabricated membranes, SEM characterizations were also carried out after the nanofiltration experiments and once the membranes were dried. Images are shown in Fig. 12.

Images evidently indicate that the uncrosslinked membranes tend to have micrometer-sized cracks as they dry up. This can be promoted by the consolidation of GO nanosheets as the solvent leaves the dispersion during drying [73]. No cracks could be spotted on the crosslinked membranes, demonstrating the influence of the crosslinker on the intactness of the GO-PPD membranes. This is likely a significant factor influencing the observed membrane performance difference between crosslinked and uncrosslinked membranes.

The membrane stability was further investigated through the fabrication of crosslinked and uncrosslinked membranes through the use of a pressure-assisted filtration method. For the uncrosslinked membranes, a 15 ml solution of 0.5 mg/ml of GO was filtered through PAN substrates using the homemade nanofiltration cell at a pressure of 3 bars. The crosslinked membranes, on the other hand, were fabricated by first reacting the GO and PPD solution and then filtrating the reacted entities in the same device at the same pressure. The fabricated membranes were then dried for 24 h to observe their stability over time under a dry environment (Fig. 13).

Similar results regarding membrane stability were observed.

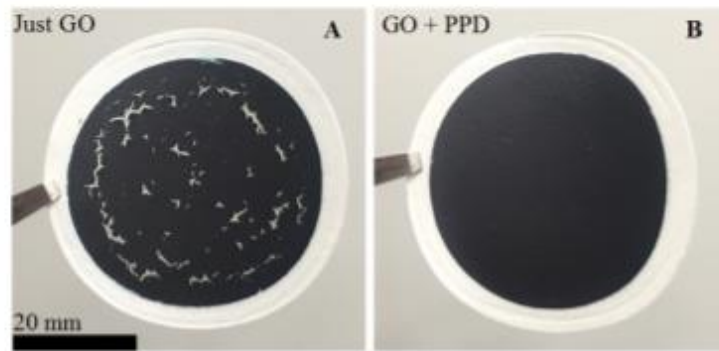


Fig. 13. Pressure assisted fabricated membranes after drying. A: uncrosslinked membrane; B: PPD-crosslinked membrane.

Uncrosslinked membranes tend to break and shrink after 24 h of drying. This phenomenon was ascribed to the drying related shrinkage of the membranes [68,73]. This further supports the observed micro cracking in dip-coated membranes. The higher material loading in this case results in evident visible cracks and the role of the crosslinker in alleviating the drying induced cracking is evident.

The disentanglement of the uncrosslinked membranes in comparison to the crosslinked membranes can be clearly observed. This validates the previous observation that crosslinking does not only enhance membrane rejection performance but also their stability, longevity, reusability and intactness of GO membranes.

4. Conclusions

In summary, uncrosslinked and PPD crosslinked GO membranes were successfully fabricated using dip-coating and dip-assisted layer by layer fabrication methods. The membrane performance in water purification was proven through the separation of MB via a homemade nanofiltration cell. The rejection increases as the number of assembly cycles increases for both membrane types. Better performance was observed for the crosslinked membranes relative to the uncrosslinked at similar assembly cycles. Through this study, the significance of covalent crosslinking was demonstrated, it was not only manifested in nanofiltration performance but also in enhanced stability and membrane intactness over time. A relatively high flux at an economical 1 bar driving pressure and excellent removal of MB (up to ~100%) was achieved for the crosslinked membranes and the stability and durability of layer by layer GO membranes was enhanced. The best performing crosslinked membranes also showed good operation longevity at the low operating pressure as they could be operated continuously for more than 120 h with no reduction in dye rejection. The good membrane reusability achieved also enhances the possibility of the use of covalent based crosslinkers in the fabrication of GO based membranes. The membranes can potentially be used for separation of other organic dyes, bacteria and other microbes; they can also be modified further for other significant separations like desalination.

Acknowledgments

Special thanks the Botswana Government's Ministry of Tertiary Education and Scientific Research and the Top Achievers Scholarship Programme for offering a Scholarship (100159844RA2 - TR. 163,096) that aided the carrying out of this work.

References

- [1] P.H. Gleick, *Water in Crisis: A Guide to the World's Freshwater Resources*, Oxford University Press, 1993.
- [2] World Health Organization, Meeting the MDG Drinking Water and Sanitation, the Urban and Rural Challenge of the Decade, Geneva (2007).
- [3] E. Dutta, S. Da, Smart responsive materials for water purification: an overview, *J. Mater. Chem. A Mater. Energy Environ.* 5 (2017) 22095–22112.
- [4] S. Babal, T.A. Kurian, Low-cost adsorbents for heavy metals uptake from contaminated water: a review, *J. Hazard. Mater.* 97 (2003) 219–243.
- [5] F. Fu, Q. Wang, Removal of heavy metal ions from wastewater: a review, *J. Environ. Manage.* 92 (2011) 407–418.
- [6] H.K. Shon, S. Phuntsho, D.S. Chandhary, S. Vignowaran, J. Cho, Nanofiltration for water and wastewater treatment - A mini review, *Desal. Water Treat. Technol.* 6 (2012) 47–53.
- [7] R.J. Peterson, Composite reverse osmosis and nanofiltration membranes, *J. Membr. Sci.* 83 (1993) 81–136.
- [8] L. Braeken, K. Binnon, B. Van Der Bruggen, C. Vandecastelle, Modeling of the adsorption of organic compounds on polymeric nanofiltration membranes in solutions containing two compounds, *ChemPhysChem* 6 (2005) 1806–1812.
- [9] L.F. Dumée, K. Saeed, J. Schütz, N. Fara, C. Hrynck, S. Hawkins, M. Druke, S. Grey, Characterization and evaluation of carbon nanotube bucky-Paper membranes for direct contact membrane distillation, *J. Membr. Sci.* 351 (2010) 36–45.
- [10] M. Majumdar, S. Chopra, R.J. Hindle, Mass transport through carbon nanotube membranes in three different regimes: ionic diffusion and gas and liquid flow, *ACS Nano* 5 (2011) 3867–3877.
- [11] M. Yu, H.H. Pao, J.L. Falconer, R.D. Noble, High density, vertically-aligned carbon nanotube membranes, *Nano Lett.* 9 (2009) 225–229.
- [12] S. Kim, J.R. Joo, H. Choi, D.S. Shin, E. Mamed, Scalable fabrication of carbon nanotube/polymer nanocomposite membranes for high flux gas transport, *Nano Lett.* 7 (2007) 2806–2811.
- [13] A. Geim, K. Novoselov, The rise of graphene, *Nat. Mater.* 3 (2007) 183–191.
- [14] A. Boretti, S. Al-Zubaidy, M. Vackovikova, M. Al-Ahri, S. Cavallaro, S. Mikhalovskiy, Outlook for graphene-based desalination membranes, *Npj Clean Water* 1 (2018) article number 5.
- [15] Y. Han, Z. Xu, C. Guo, Ultrathin graphene nanofiltration membrane for water purification, *Adv. Funct. Mater.* 23 (2013) 3695–3700.
- [16] J.R. Werber, C. Ong, M. Elimelech, Materials for next-generation desalination and water purification membranes, *Nat. Mater.* 1 (2016) 16018.
- [17] S.P. Surwade, S.N. Seirmen, I.V. Vlassiouk, R.R. Unocic, G.M. Veith, S. Dai, S.M. Mahurin, Water desalination using nanoporous single-layer graphene, *Nat. Nanotechnol.* 10 (2015) 459–464.
- [18] K.S. Novoselov, A.K. Geim, S.V. Morozov, D. Jiang, Y. Zhang, S.V. Dubonos, I.V. Geigerinov, A.A. Firsov, Electric field effect in atomically thin carbon films, *Science* 306 (2004) 666–669.
- [19] C.J. Bazzo, J.A. Golovchenko, Atom-by-atom nucleation and growth of graphene nanoropes, *Proc. Natl. Acad. Sci.* 109 (2012) 5953–5957.
- [20] S.C. O'Brien, M.K.H. Bouffar, J.C. Adams, Y. Song, J. Kang, T. Lassi, M. Ajah, K. Karim, Selective ionic transport through tunable subnanometer pores in single-layer graphene membranes, *Nano Lett.* 3 (2014) 1234–1241.
- [21] R.R. Joshi, P. Carbon, F.C. Wang, V.G. Kravets, A.K. Geim, R.R. Nair, Precision and ultrafast molecular oxide membranes, *Science* 343 (2014) 752–755.
- [22] R.R. Joshi, S. Alcantarap, M. Yushitama, V. Sahajwalla, Y. Nishino, Graphene oxide: The new membrane material, *Appl. Mater. Today* 1 (2015) 1–12.
- [23] R. Nair, H. Wu, A.V. Jayaram, V. Gopirajoo, A. Geim, Unimpeded permeation of water, *Science* 325 (2012) 442–445.
- [24] K.H. Lee, B. Lee, S. Hwang, J. Lee, H. Cheong, O. Kwon, K. Shin, N.H. Hur, Large-scale production of highly conductive reduced graphene oxide sheets by a solvent-free low temperature reduction, *Carbon* 69 (2014) 327–335.
- [25] S. Abdulmuttalib, H. Angharizadeh, H. Kim, Fast and fully-scalable synthesis

- of reduced graphene oxide. *Sci. Rep.* 5 (2015) 1–7.
- [26] L. Jin, Z. Wang, S. Zheng, B. Mi, Polyamide-crosslinked graphene oxide membrane for forward osmosis. *J. Membr. Sci.* 545 (2018) 11–18.
- [27] M. Hu, S. Zheng, B. Mi, Organic fouling of graphene oxide membranes and its implications for membrane fouling control in engineered osmosis. *Environ. Sci. Technol.* 50 (2016) 685–693.
- [28] C. Zhao, X. Su, J. Chen, G. Wang, F. Yang, Highly effective antifouling performance of PVDF/graphene oxide composite membrane as membrane bioreactor (MBR) system. *Desalination* 340 (2014) 59–66.
- [29] H.R. Chae, J. Lee, C.H. Lee, L.C. Kim, P.K. Park, Graphene oxide-embedded thin-film composite reverse osmosis membrane with high flux, anti-biofouling, and chlorine resistance. *J. Membr. Sci.* 483 (2015) 128–135.
- [30] A. Lert, H. Hu, M. Foster, J. Klimowski, Structure of graphite oxide revisited. *J. Phys. Chem. B* 102 (1998) 4477–4482.
- [31] I.A. Vaccari, C. Spasini, F. Rizzo, A. Bianci, C. Milardi-Meyon, Chemical reactivity of graphene oxide towards amines elucidated by solid-state NMR. *Nanoscale* 8 (2016) 13714–13721.
- [32] D. Dreyer, S. Park, C. Bielawski, R. Ruoff, The chemistry of graphene oxide. *Eur. Soc. Chem.* 39 (2010) 228–240.
- [33] S. Zheng, Q. Tu, J.J. Urban, S. Li, B. Mi, Swelling of graphene oxide membranes in aqueous solution: Characterization of interlayer spacing and insight into water transport mechanisms. *ACS Nano* 11 (2017) 6440–6450.
- [34] Y. Mo, S. Zhao, Y. Shen, Cation-dependent structural instability of graphene oxide membranes and its effect on membrane separation performance. *Desalination* 309 (2016) 40–46.
- [35] J. Alkhalaf, K.S. Yoon, C.D. Williams, E. Guzman-Guerrero, Y. Su, C.Y. Charin, J. Dai, E. Prost, S.J. Leigh, I.V. Grigorieva, F. Carbone, A.E. Geier, R.E. Nair, Tunable sieving of ions using graphene oxide membranes. *Nat. Nanotechnol.* 12 (2017) 546–550.
- [36] Y. Zhang, S. Zhang, T.J. Chung, Nanometric graphene oxide framework membranes with enhanced heavy metal removal via nanofiltration. *Environ. Sci. Technol.* 49 (2015) 10235–10242.
- [37] M. Hu, B. Mi, Layer-by-layer assembly of graphene oxide membranes via electrostatic interaction. *J. Membr. Sci.* 469 (2014) 80–87.
- [38] J.J. Richardson, J. Cai, M. Björnmaln, J.A. Braungart, H. Björn, F. Caruso, Innovation in layer-by-layer assembly. *Chem. Rev.* 116 (2016) 1482B–1496F.
- [39] Q. Nan, F. Li, B. Cao, Fabrication of positively charged nanofiltration membrane via the layer-by-layer assembly of graphene oxide and polythiolenamine for desalination. *Appl. Surf. Sci.* 387 (2016) 521–528.
- [40] W. Choi, J. Choi, J. Bang, J.H. Lee, Layer-by-layer assembly of graphene oxide nanosheets on polyamide membranes for durable reverse-osmosis application. *ACS Appl. Mater. Interfaces* 5 (2013) 12510–12519.
- [41] O. Saeki, Homogeneous hydrolysis of polyacrylonitrile by potassium hydroxide. *Eur. Polym. J.* 26 (1990) 9–13.
- [42] M. Jassal, S. Bhawanick, S. Sangupta, P.K. Patra, D.I. Walker, Hydrolyzed polyacrylonitrile electrospun ion-exchange fibers. *Environ. Eng. Sci.* 31 (2014) 288–296.
- [43] X. Liu, N. Wei, K. Wang, Y. Zheng, Layer-by-layer self-assembled graphene multi-layer films via covalent bonds for supercapacitor electrodes. *Int. J. Nanomater. Nanotechnol. Nanomed.* 5 (2015) article number 14.
- [44] M.I. Vorkhovsky, A. Jasaitis, M.I. Vorkhovskaya, J.E. Morgan, M. Wikstrom, Protein immobilization by cytochrome c oxidase. *Nature* 400 (1999) 480–483.
- [45] M. Frummi, R. Tai-verod, J. Ethar, I. Willner, Electrochemically-stimulated pH changes: A route to control chemical reactivity. *J. Am. Chem. Soc.* 132 (2010) 1–3.
- [46] Z. Abdalgataw, I.M. Abdalgataw, V.N. Emirov, Effect of temperature and pressure on the thermal conductivity of sandstone. *Int. J. Rock Mech. Min. Sci.* (1997) 46 (2009) 1055–1071.
- [47] M.M. Sh, C.Y. Yan, Layer-by-layer (LBL) assembly of graphene with *p*-phenylenediamine (PPD) spacer for high performance supercapacitive applications. *RSC Adv.* 4 (2014) 19908–19915.
- [48] M.B. Azevêdo, C.E. Corcoso, A. Ghel, M. Maggio, A. Maffrand, G. Guerra, Graphene oxide as a catalyst for ring opening reactions in amine crosslinking of epoxy resins. *RSC Adv.* 6 (2016) 23858–23865.
- [49] R.M. Silverstein, F.X. Webster, D.J. Kiemle, *Identification of Organic Compounds (Spectrometric Identification of Organic Compounds)*, 4th ed, Wiley, New York, 1981.
- [50] N.P.G. Swegen, *Guide to Complete Interpretation of Infrared Spectra of Organic Structures*, Wiley and Sons Ltd, Chichester, 1994.
- [51] C. Fontarria-Lucas, A. Lopez-Pinedo de, D. Lopez-Gonzalez, M. Corvino-Rojas, R. Martín-Aranda, Study of oxygen containing groups in a series of graphite oxides: physical and Chemical Characterization. *Carbon* 33 (1995) 1585–1592.
- [52] J.L. Paredes, A. Marin, J.M.D. Tascón, Graphene oxide dispersions in organic solvents. *Langmuir* 24 (2008) 10560–10564.
- [53] Y. Wei, Y. Zhang, X. Guo, Z. Ma, X. Wang, C. Guo, Multilayered graphene oxide membrane for water treatment: A Review. *Carbon* 139 (2018) 964–981.
- [54] W.R. Bowen, J.S. WeiSun, Modelling the performance of membrane nanofiltration-critical assessment and model development. *Chem. Eng. Sci.* 57 (2002) 1121–1137.
- [55] A. Caspi, H. Kuzowolka, M. Góssic, *p*-Phenyl-ethylenediamine and its dihydrolic: Two-dimensional isomorphism and mechanism of the dehydrolysis process, and N-H–N and N-H– π interactions. *Acta Crystallogr. Sect. C Cryst. Struct. Commun.* 66 (2010) 128–132.
- [56] A.J. Wu, X.D. Li, J. Yang, J.H. Yan, Synthesis and characterization of a plasma carbon aerosol coated sponge for recyclable and efficient separation and adsorption. *RSC Adv.* 7 (2017) 9303–9308.
- [57] F. Benise, S. Hulger, J. Tobias, *Surface Design: Applications in Nanoscience and Nanotechnology*, Wiley-VCH, 2009.
- [58] W.S. Huang, et al., Cross-linking with diamine monomers to prepare composite graphene oxide-framework membranes with varying *d*-spacing. *Chem. Mater.* 26 (2014) 2983–2990.
- [59] N.F.D. Abu, J.V. Chong, B. Wang, C. Mattetti, E. Li, Graphene oxide membranes on osseous hollow fibers - microstructural stability and nanofiltration performance. *J. Membr. Sci.* 484 (2015) 87–94.
- [60] J. de, S. Maanda, et al., Kinetic and calorimetric study of the adsorption of dyes on mesoporous activated carbon prepared from coconut air dust. *J. Colloid Interface Sci.* 298 (2006) 515–522.
- [61] M. Os, D.E. Lorbe, M. Hassan, G.A. Petrosians, Cellular and molecular actions of methylene blue in the nervous system. *Med. Res. Rev.* 31 (2012) 93–117.
- [62] M.J.S. Dewar, E.G. Zwickich, E.F. Healy, J.J.F. Stewart, Development and use of quantum mechanical molecular models. 76. AM1: a new general purpose quantum mechanical molecular model. *J. Am. Chem. Soc.* 107 (1985) 3902–3909.
- [63] D. Qiao, J. Sun, Y. Li, X. Yang, X. Wang, Z. Wang, L. Xia, Highly enhanced adsorption of orange red onto graphene oxide/chitosan fibers by wet chemical etching of silica nanoparticles. *Chem. Eng. J.* 245 (2014) 99–106.
- [64] L. Chen, Y. Li, S. Hu, J. Sun, D. Qiao, X. Yang, Q. Ji, Z. Wang, D. Wang, Y. Xia, Removal of methylene blue from water by cellulose/graphene oxide fibers. *J. Exp. Nanosci.* 11 (2016) 1156–1170.
- [65] Q. Ling, Z. Xiaohua, Y. Wenrong, W. Yuli, S. George, L. Dan, Covalent integration of chemically converted graphene sheets in water and potential application for nanofiltration. *Chem. Commun. (Camb.)* 47 (2011) 5810–5812.
- [66] M. Hu, B. Mi, Enabling graphene oxide nanosheets as water separation membranes. *Environ. Sci. Technol.* 47 (2013) 3715–3723.
- [67] K. Vikar, W. Wilfried, U. Mathias, Molecularly imprinted composite membranes for selective binding of diameteryn from aqueous solutions. *Desalination* 149 (2002) 323–326.
- [68] W. Peng, H. Li, Y. Liu, S. Song, Adsorption of methylene blue on graphene oxide prepared from amorphous graphite: Effects of pH and foreign ions. *J. Mol. Liq.* 221 (2016) 82–87.
- [69] S. Yang, S. Chen, Y. Chang, A. Guo, Y. Liu, H. Wang, Removal of methylene blue from aqueous solution by graphene oxide. *J. of Col. and Interface Sci.* 359 (2011) 24–29.
- [70] L. Ai, C. Zhang, Z. Chen, Removal of methylene blue from aqueous solution by a adsorbent synthesized graphene/magnetic composite. *J. of Hazardous Mat.* 192 (2011) 1515–1524.
- [71] M. Yuan, S. Tong, S. Zhao, C. Jia, Adsorption of polycyclic aromatic hydrocarbons from water using petroleum coke-derived porous carbon. *J. Haz. Mat.* 181 (2010) 1115–1120.
- [72] D. Barredo, A.M. Pérez-Mas, A. Silvestro-Albero, M.E. Casco, S. Budio, C. Herber, E.A. Miller, C. Blanco, R. Santamaría, J. Silvestro-Albero, F. Rodríguez-Reinos, Unusual flexibility of mesoporous pitch-derived carbon materials: An approach to the synthesis of graphene. *Carbon* 113 (2017) 539–545.
- [73] W.P. Lau, A.P. Booth, Why Do Drying Films Crack? *Langmuir* 20 (2004) 9885–9888.